VOLUME 124 NUMBER 3

THE ASTROPHYSICAL JOURNAL

AN INTERNATIONAL REVIEW OF SPECTROSCOPY AND ASTRONOMICAL PHYSICS

NOVEMBER 1956

THE MAGNETIC VARIABLE HD 71866 . . . . *Horace W. Babcock* 489
RADIAL VELOCITIES OF NINE S-TYPE STARS . . . *P. C. Keenan and R. G. Teske* 499
THE RADIAL VELOCITIES OF RHO PUPPIS . . . . *O. Struve, J. Sahade, and V. Zebergs* 504
THE TRIPLE SYSTEM LAMBDA TAURI . . . . *E. G. Ebbighausen and O. Struve* 507
THE DISTRIBUTION OF LATE M-TYPE STARS ALONG THE GALACTIC EQUATOR
J. J. Nassau, V. M. Blanco, and D. M. Cameron 522
NEW MEMBERS OF THE ASSOCIATION VI CYGNI . . . . *D. H. Schulte* 530
OBSERVATIONAL CONSEQUENCES OF O STAR FORMATION . *Malcolm P. Savedoff* 533
PHOTOELECTRIC K AND L SHELL ABSORPTION COEFFICIENTS FOR HIGHLY IONIZED ATOMS . . . . *S. A. Moszkowski and Roland E. Meyerott* 537
INFLUENCE OF COLLISIONS UPON POPULATION OF HYPERFINE STATES IN HYDROGEN . . . . *Edward M. Purcell and George B. Field* 542
ABSORPTION COEFFICIENTS FOR FREE-FREE TRANSITIONS IN A HYDROGEN PLASMA . . . . *Jay M. Berger* 550
RADIATION BY PLASMA OSCILLATIONS . . . . *George B. Field* 555
HYDROMAGNETIC OSCILLATIONS OF A FLUID SPHERE WITH INTERNAL MOTIONS . . . . *S. Chandrasekhar* 571
LYMAN-ALPHA INTENSITY AND SOLAR LIMB DARKENING FROM ROCKET SPECTROGRAMS . . . . *S. C. Miller, Jr., R. Mercure, and William A. Rense* 580
LYMAN-α AND THE STRUCTURE OF THE SOLAR CHROMOSPHERE
R. G. Athay and R. N. Thomas 586
MOTIONS OF PROMINENCES . . . . . *Malcolm Correll, Martha Hazen, and John Bahng* 597
SYNCHROTRON RADIATION IN THE SUN'S RADIO SPECTRUM
U. E. Kruse, L. Marshall, and J. R. Platt 601
INADEQUACY OF RECOMBINATION AS SOURCE OF RADIATION FROM METEORIC TRAINS . . . . *Allan F. Cook and Gerald S. Hawkins* 605
THE IMPACT OF LARGE METEORITES . . . . *J. J. Gilvarry and J. E. Hill* 610
DIAMONDS, METEORITES, AND THE ORIGIN OF THE SOLAR SYSTEM
Harold C. Urey 623
NOTE ON THE HIGH RELIEF OF THE LUNAR MARIA . . . . . *E. R. DuFresne* 638
ON THE MOTIONS OF STARS IN AN ELLIPSOIDAL STELLAR SYSTEM
George Contopoulos 643
AN F/2 CASSEGRAIN CAMERA . . . . *A. B. Meinel* 652
ON THE POSSIBLE PRESENCE OF He^3 IN THE MAGNETIC STAR 21 AQUILAE
E. Margaret Burbidge and G. R. Burbidge 655
NOTES
21-CM Line Emission from the Coma Cluster . . . . *David S. Heeschen* 660
Excitation in Nebulae: Electron-Hydrogen Inelastic Collisions in a Radiative H II Region . . . . *Joseph W. Chamberlain* 662
On Rohrlich's Discussion of the Calcium XV Problem . . . . . . *David Layzer* 664
A Note on the Color-Magnitude Array of the White Dwarfs. I. . . *D. L. Harris III* 665
ABSTRACTS OF ASTROPHYSICAL JOURNAL SUPPLEMENT SERIES
Studies of Extremely Young Clusters. I. NGC 2264 . . . . . . *Merle F. Walker* 668
Photometric, Polarization, and Spectrographic Observations of O and B Stars
W. A. Hiltner 669
INDEXES 671

THE UNIVERSITY OF CHICAGO PRESS
CHICAGO, ILLINOIS, U.S.A.

November 1956 Vol. 124, No. 3

THE ASTROPHYSICAL JOURNAL

AN INTERNATIONAL REVIEW OF SPECTROSCOPY AND ASTRONOMICAL PHYSICS

Founded in 1895 by George E. Hale and James E. Keeler

Published in Collaboration with the American Astronomical Society

S. CHANDRASEKHAR
Managing Editor

A. BLAAUW
Associate Editor

Yerkes Observatory of the University of Chicago

EDITORIAL BOARD

HAROLD F. WEAVER (1956-60)
Berkeley Astronomical Department
University of California

MARTIN SCHWARZSCHILD (1954-58)
Princeton University Observatory

LEO GOLDBERG (1955-59)
The Observatory of the University of Michigan

HORACE W. BABCOCK (1953-57)
Mount Wilson Observatory of the Carnegie Institution of Washington

G. HERZBERG (1952-56)
National Research Council, Ottawa

The Astrophysical Journal is published bimonthly by the University of Chicago at the University of Chicago Press, 5750 Ellis Avenue, Chicago 37, Illinois, during January, March, May, July, September, and November. ¶Two volumes are published per year, one beginning with the January issue and the other beginning with the July issue. On all orders from the United States and its possessions the subscription price is $7.50 per volume or $15.00 per year; the price of single copies is $3.50. ¶On all orders from Canada the subscription price is $8.00 per volume or $16.00 per year; the price of single copies is $3.65. On all orders from all other countries the subscription price is $8.25 per volume or $16.50 per year; the price of single copies is $3.75. (Orders for service of less than a volume will be charged at the single-copy rate.) ¶Subscriptions are payable in advance. Please make all remittances payable to The University of Chicago Press, in United States currency or its equivalent by postal or express money orders or bank drafts. (Exception: members of The American Astronomical Society must send their subscriptions and remittances to the Treasurer of the Society.)

The following is an authorized agent:

For the British Commonwealth, except North America and Australasia: The Cambridge University Press, Bentley House, 200 Euston Road, London, N.W. 1, England. Prices of yearly subscriptions and of single copies may be had on application.

Claims for missing numbers should be made within the month following the regular month of publication. The publishers expect to supply missing numbers free only when losses have been sustained in transit, and when the reserve stock will permit.

Business correspondence should be addressed to The University of Chicago Press, Chicago 37, Illinois.

Communications for the editors and manuscripts should be addressed to: S. Chandrasekhar, Editor of THE ASTROPHYSICAL JOURNAL, Yerkes Observatory, Williams Bay, Wisconsin.

Line drawings and photographs should be made by the author, and all marginal notes such as co-ordinates, wave lengths, etc., should be included in the cuts. It will not be possible to set up such material in type.

One copy of the corrected galley proof should be returned as soon as possible to the editor, Yerkes Observatory, Williams Bay, Wisconsin. Authors should take notice that the manuscript will not be sent to them with the proof.

The cable address is "Observatory, Williamsbay, Wisconsin."

The articles in this journal are indexed in the *International Index to Periodicals*, New York, N.Y.

Applications for permission to quote from this journal should be addressed to The University of Chicago Press, and will be freely granted.

Microfilms of complete journal volumes are available to regular subscribers only and may be obtained at the end of the year. Orders and inquiries should be addressed to University Microfilms, 313 North First Street, Ann Arbor, Michigan.

Notice to subscribers: If you change your address, please notify us and your local postmaster immediately.

Entered as second-class matter, July 31, 1895, at the Post-Office at Chicago, Ill., under the Act of March 3, 1879.

Acceptance for mailing at special rate of postage provided for in United States Postal Act of October 3, 1917, Section 1103, amended February 28, 1925.

Copyright 1956 by the University of Chicago.

[PRINTED IN U.S.A.]

THE ASTROPHYSICAL JOURNAL

AN INTERNATIONAL REVIEW OF SPECTROSCOPY AND
ASTRONOMICAL PHYSICS

VOLUME 124 NOVEMBER 1956 NUMBER 3

THE MAGNETIC VARIABLE HD 71866

Horace W. Babcock
Mount Wilson and Palomar Observatories
Carnegie Institution of Washington, California Institute of Technology

Received June 14, 1956

ABSTRACT

Sixty-one spectrograms made with the differential analyzer for the Zeeman effect have been measured in a study of the magnetic variations of this peculiar A-type star. The strong magnetic field ($H_{\mathrm{eff}} = 2$ kilogauss; $H_p = 6$ kilogauss) shows nearly symmetrical reversals of polarity in a period of about 6.8 days that is probably slightly irregular; irregularities in amplitude also occur. The lines of Eu II undergo moderate variations in intensity in phase with the magnetic variations, but the spectrum variability is of much lower degree than that of HD 125248. Velocity measurements yield only random fluctuations within a range of several kilometers per second, without definite evidence for harmonic variations. The star may be classed along with a^2 CVn, HD 153882, and HD 125248 as one of a small group of regularly reversing magnetic variables of large and nearly equal amplitude, all of which have periods of about 1 week. The crossover effect on the line profiles in polarized light is unusually prominent for Fe I but is much less so for lines of ionized elements. On the reasonable assumption that the visibility of the effect is near maximum owing to a matching of the Zeeman displacements by Doppler displacements for two hypothetical areas of opposite magnetic polarity, the matching velocity is derived from several lines of Fe I; it is about 5 km/sec. On the "rotator model" this leads to a v_e (axial rotation) of 3.5 km/sec, whereas an A0 star with a period of axial rotation of 6.8 days should have $v_e = 16$ km/sec. Furthermore, the line widths in HD 71866, by direct measurement, are appreciably narrower than would be indicated by the rotator model.

According to the *Henry Draper Catalogue*, the star HD 71866 has a peculiar A-type spectrum, in which the Si II lines λ 4128 and λ 4131 are unusually strong. Along with many other stars so listed, its spectrum was examined with the coudé spectrograph of the 100-inch telescope, using the differential analyzer for circular polarization, in order to test its suitability for measurements of the Zeeman effect. Plates taken at 10 A/mm in 1949 showed that the spectrum is indeed an excellent example of a peculiar A type. It is rich in unusually sharp lines of the metals, having half-widths of about $\frac{1}{4}$ A. Measurements show that Zeeman broadening is one of the principal contributors to these widths. Lines of Fe I, Fe II, and Ti II are numerous, and peculiarities characteristic of the magnetic stars are seen in the prominent lines of Cr I, Cr II, Eu II, and Gd II. Lines of Ca II are weak and sharp, and on my plates the lines of Si II are quite weak. The spectrum has a general similarity to that of HD 125248, the most obvious difference being that, whereas the latter is perhaps the most striking example of a spectrum variable star, with large periodic antiphase variations of the lines of the rare-earth elements and of chromium, the degree of spectrum variability in HD 71866 is slight. Only after several plates had been taken, was it found that there is, in fact, a systematic variation in the intensities of the lines of Eu II. According to Provin's (1953) photoelectric studies, the star shows a possible light-variation of small amplitude.

Several spectrograms made with the analyzer showed that the star has a strong magnetic field that undergoes reversal of polarity from time to time. Thereafter it was observed as regularly as possible with the 100-inch and 200-inch telescopes. A dispersion of 10 A/mm was employed for twenty-three of the plates, while the remaining thirty-nine had a dispersion of 4.5 A/mm. A list of observations, with Julian day and the measured value of the effective magnetic-field intensity, H_e, is given in Table 1. For most plates the determination of H_e rests on measures of differential Zeeman displacements for thirty to fifty spectrum lines, according to the method outlined previously (Babcock 1947; Babcock and Cowling 1953). The results are expressed in terms of the effective field intensity instead of the computed polar field intensity, H_p, that was used in earlier papers. The relationship is $H_e = 0.303\ H_p$, where H_e is simply the intensity of a purely longitudinal uniform magnetic field that would yield the observed displacements. The reason for the change is that the formula for H_p was derived (Babcock 1947; Schwarzschild 1950; Stibbs 1950) on the assumption that the field of the star is that of a regular dipole, similar to that of a uniformly magnetized sphere; but there is growing evidence, partly from solar observations (Babcock and Babcock 1955) and partly from theoretical studies, that a simple field like a regular dipole probably cannot predominate over the integrated effect of more intense and numerous local photospheric fields. The reference here is not to spots like sunspots, which, because of their low temperature and relative darkness, contribute little in integrated light, but rather to more or less extended magnetic regions like the bipolar magnetic (BM) and unipolar magnetic (UM) regions observed on the sun. The relative contributions of the general or polar magnetic field and of the local magnetic M regions remain to be evaluated. Also the larger problem of developing a satisfactory model to explain the complex spectroscopic phenomena of the magnetically variable stars is yet to be solved.

The effective field intensity is based on the simple formula for the Zeeman effect:

$$\Delta\bar{\nu} = 4.67 \times 10^{-5}\, H_e\ \mathrm{cm}^{-1}\ .$$

The practical formula used in this paper is

$$H_e = 52.8 \left(\frac{4500}{\lambda}\right)^2 F\, (\Delta s)\ z^{-1}\ \text{gauss}\ ,$$

where F is the dispersion in angstroms per millimeter, z is the weighted mean displacement of the σ components of the Zeeman pattern of the lines as compared to the normal triplet, and Δs is the measured displacement in microns between the line images in the right-handed and left-handed polarized spectra.

At a declination of +40°, the phase shift of elliptically polarized light upon reflection from the coudé flat mirror is appreciable, so that, as is usual for stars at declinations north of +10°, the phase-shifting compensator was used. This had been calibrated empirically for various declinations by tests with artificial circularly polarized light in the 200-inch telescope. Since the phase shift introduced by the oblique reflection from the thin aluminum coats of the coudé mirrors of the two telescopes is to some extent dependent upon the age and condition of the aluminum, there is some uncertainty as to the precision with which the phase shift is compensated. It is unlikely, however, that relative differences greater than 10 per cent could have been introduced into the measured values of the field intensity in this way.

TABLE 1

MAGNETIC OBSERVATIONS OF HD 71866

	Plate No.	J. D. 2430000+	Epoch	H_e (Gauss)	Eu II Int.	Cross-over
Ce	5539x	2957.82	-0.011	+215	1	+
	5568x	2984.72	+3.945	- 45	2	+
	5600x	3010.70	7.766		1	
	6214x	3378.76	61.899		1	
	7870x	4105.69	168.814	-1210	1	
	8643x	4411.66	213.815	-1480	2	
Pb	867	4467.76	222.066	+325	2	+
	936	4527.68	230.879	-2185	2	
	943	4528.68	231.026		2	
	949	4530.69	231.322	+1875	3	
	950	4531.68	231.467	+990	1	
	1245	4706.92	257.241	+1190	3	
	1251	4707.92	257.388	+1700	2	
Ce	9034x	4728.89	260.472	+270	1	
	9038x	4729.87	260.616	-1155	1	
	9043x	4730.90	260.768	-1570	2	
	9048x	4731.94	260.921	-1360	2	
	9051x	4732.91	261.063	+260	2	+
Pb	1335	4765.85	265.908	-1290	2	
	1340	4768.81	266.344	+1800	2	
Ce	9091x	4792.78	269.869	-1650	2	
	9077x	4793.85	270.026	+910	2	+
	9104	4794.82	270.198	+1910	3	
	9111x	4795.73	270.303	+2320	3	
	9120x	4796.85	270.468	-1130	1	-
Pb	1396	4815.68	273.237	+1350	3	
	1404	4816.66	273.381	+1590	2	-
	1448	4845.67	277.648	-1520	2	
	1454	4846.64	277.791	-1820	2	
	1459	4847.66	277.941	-1460	1	+
	1466	4848.68	278.091	+1520	2	+
Ce	9513x	5059.97	309.167	+1840	3	
	9517	5060.94	309.309	+2150	3	
	9521x	5061.98	309.462	+1370	1	
Pb	1871	5084.99	312.846	-1950	2	
	1891	5116.91	317.541	-630	1	-
	1898	5119.96	317.990	-790	1	+
	1902	5120.86	318.122	+1810	2	
	1908	5121.85	318.268	+1940	3	
Pc	1918x	5141.80	321.202	+940	3	
Pb	1922	5142.80	321.349	+1660	2	
Pb	1926	5143.72	321.484	+1020	1	-
	1932	5144.79	321.642	-1350	1	
	1937	5145.78	321.787	-1370	2	
Ce	9699	5168.76	325.167	+1960	3	
	9701	5169.77	325.316	+2060	3	
	9728x	5178.81	326.645	-1060	1	
	9730x	5179.66	326.770	-1190	2	
	9735x	5180.71	326.925	-450	2	+
	9736x	5181.70	327.070	+1030	2	
	9769	5206.72	330.750	-1290	2	
	9773	5207.72	330.897			
	9777x	5209.70	331.188	+1470	3	
	9779	5210.71	331.337	+2470	3	
Pb	2064	5226.69	333.687	-1870	1	
	2402	5470.92	369.607	-1250	1	
	2404	5471.88	369.748	-1270	2	
	2431	5523.71	377.372	+1510	2	
	2504	5556.69	382.222	+2080	3	
	2511	5557.69	382.369	+1860	2	
	2517	5558.70	382.518	+715	1	-

x: dispersion 10 A/mm; all other 4.5 A/mm.

MAGNETIC VARIATIONS

Figure 1 shows the magnetic variations observed in HD 71866 as represented by the elements

$$\text{Positive crossover} = \text{JD } 2432957.90 + 6.79916E\,.$$

Positive crossover, as the name implies, is taken to be the time at which H_e equals zero in passing from negative to positive values. It appears that there are real deviations from true periodicity, which are particularly evident near the crossover phases. For this reason the period is meaningful only to four significant figures and is perhaps best indicated by the statement that $\langle P\rangle$ lies between 6.798 and 6.800 days. It is interesting to note that in the cepheid **X** Cygni similar irregularities, of the order of 10 per cent of the period, have been found by R. Kraft (unpublished).

In plotting the points of Figure 1, no attempt has been made to distinguish between the results from spectrograms of 10 and of 4.5 A/mm dispersion, for which the internal probable errors are in the vicinity of ± 110 and ± 80 gauss, respectively. A comparison between the results from the plates of different dispersion showed little or no evidence of a systematic difference in the derived field intensity.

A smooth curve has been drawn in Figure 1 to represent the mean magnetic variations. There are apparent deviations from a sine-curve, and, more important, the larger deviations of the individual points from the mean curve, as regards both amplitude and phase, must be significant. Prior to the observations of the last cycle (382) listed in Table 1, the twelve points near the positive peak of the magnetic curve of Figure 1 appeared to define a deep and rather sharp notch between double maxima. One of the last points (Pb 2504), however, spoils the notch; whether this is the result of some random deviation from regularity or whether the notch is meaningless is open to question. It is interesting to note that the mean magnetic curve for the 5.5-day magnetic variable α^2 Canum Venaticorum (Babcock and Burd 1952) also has a dip centered on the phase of maximum intensity of the rare-earth lines, although for this star the dip is much shallower and broader. As was pointed out earlier, deviations from true periodicity are apparent in HD 71866 near the crossover phases, and non-uniform amplitudes from cycle to cycle appear well established between phases 0.6 and 0.9. Such irregularities, which are here superimposed on the main magnetic cycle, may well be of the same kind as those prevailing in HD 133029 (Babcock and Burd 1951), which appears to be completely irregular.

In reducing the measurements of the spectrograms, the magnetic-field intensity indicated by the various elements was derived separately, in addition to the mean results obtained from all elements taken together. Significant deviations from the mean H_e appear to occur for Fe I, Fe II, and Cr II, which are represented on the various plates, on the average, by about eleven, eight, and six lines, respectively. These results are indicated by the three lower curves in Figure 1, where the light broken lines join the points derived from individual plates and the heavy smoothed line has been drawn in to suggest the mean variation. A certain similarity in shape, but with a progressive difference in phase, is noted for the three curves, of which that for Cr II has the greatest amplitude. It is felt that some of the deviations of individual points from the mean curve are greater than can reasonably be attributed to errors of measurement and that they probably reflect the changing pattern of "hydromagnetic fine structure" in the atmosphere of the star.

ANOMALOUS FIELD INTENSITIES

It was noticed that certain lines, especially some of Fe I, exhibited abnormally large Zeeman displacements. To illustrate this effect, eight unblended lines in multiplet No. 152 of Fe I were measured and reduced separately on plates Pb 1908, 2504, and 2511,

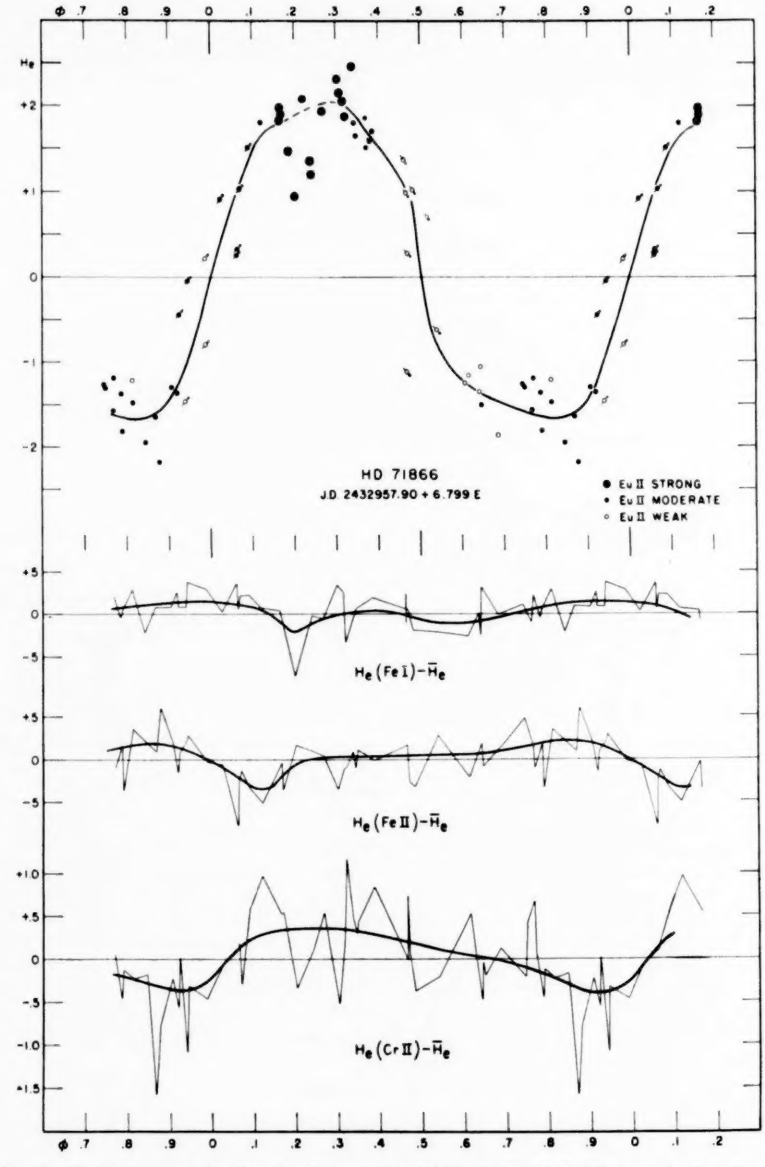

FIG. 1.—In the upper section the effective magnetic-field intensity, H_e, in kilogauss, is plotted against phase. Each point represents the result from one spectrogram. The curve is intended only to represent the mean variation, for the deviations of the individual points, which have probable errors of about ± 0.1 kilogauss, are believed to result largely from intrinsic hydromagnetic fluctuations at the stellar surface. Small arrows indicate the presence and sign of the crossover effect. Large dots indicate that the lines of Eu II are strong; small dots, of moderate intensity; open circles, weak. The lower curves are self-explanatory.

for which the mean H_e derived from lines of all elements averaged together was +1940, +2080, and +1860 gauss, respectively. Table 2 lists the wave lengths and z-values of the lines and for each line the mean H_e derived from the three plates.

The line Fe I 4233.608 yields a magnetic-field intensity about twice as great as the other lines, although all have about the same equivalent width; the same line also appears to be more sensitive than most as an indicator of the crossover effect when the mean field is near zero. The reason for this anomaly is unknown.

LINE-INTENSITY VARIATIONS

Information on the intensity variation of the lines of Eu II is also presented in the upper curve of Figure 1, where the large dots indicate that the Eu II lines, according to eye-estimates, are exceptionally strong. This condition occurs between phases 0.15 and 0.34, even though a wide range of magnetic intensity (+940 to +2470) is found. A secondary, but weaker, maximum in the intensity of the Eu II lines occurs near the negative maximum in the magnetic curve (*small dots*). These lines are weakest near the crossover phases (*open circles*). Lines of Gd II undergo intensity variations similar to those of Eu II, but no other spectrum variations have been noticed.

TABLE 2

MEASURES OF LINES OF Fe I IN MULTIPLET NO. 152

λ	z	H_e (gauss)	Matching Velocity (km/sec)	λ	z	H_e (gauss)	Matching Velocity (km/sec)
4191.436	1.28	2960	4.4	4260.479	1.62	2700	5.2
4210.352	3.05	1710	6.2	4271.159	1.43	1660	2.8
4233.608	1.53	4400	7.9	4299.242	1.50	1760	3.1
4235.942	1.68	1980	3.9				
4250.125	1.46	1810	3.1	Mean	....	2370	4.6

RADIAL VELOCITIES

Velocities of the elements were also derived from the measurements. These velocities showed an essentially random dispersion within the range 25–33 km/sec. The dispersion appeared to be noticeably greater than would be expected for such a sharp-line star and greater than the dispersion of the individual observations about the velocity-curves derived earlier for α^2 CVn (Babcock and Burd 1952), even though the line widths are some 40 per cent wider in the latter star and the errors of measurements are presumably greater. This velocity dispersion, together with the rather low degree of spectrum variation, suggests that a relatively disorganized form of hydromagnetic turbulence prevails in HD 71866 as compared to α^2 CVn. The possibility that the principal variation in the period of 6.8 days is a co-ordinated form of hydromagnetic cycle is not to be excluded, however.

THE CROSSOVER EFFECT

The crossover effect, first described in the spectrum of HD 125248 (Babcock 1951), is more pronounced in HD 71866 than in any other star yet investigated, although it is clearly seen also in α^2 CVn, HD 153882, and 78 Virginis. (The appearance of this effect in 78 Vir is especially noteworthy, since this star shows a fluctuating magnetic field, probably irregular, and always of the same polarity.) The crossover effect appears as a difference in sharpness of the profiles of most of the spectrum lines when the right-handed polarized spectrum is compared with the left-handed; it occurs at and near the phases

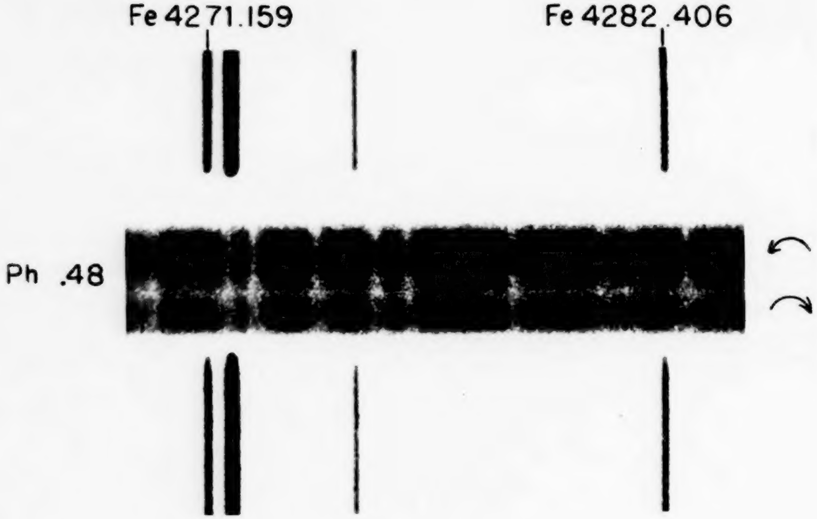

FIG. 2a

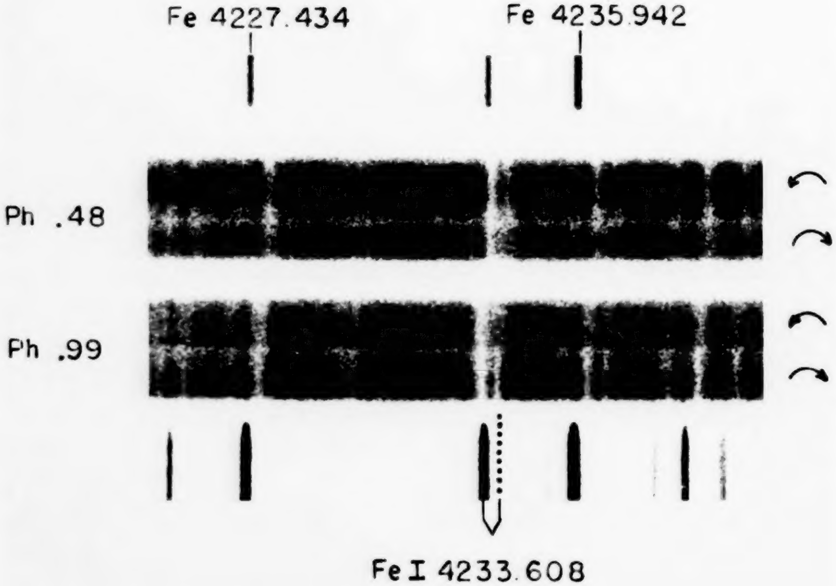

FIG. 2b

FIG. 2.—Crossover effect in the spectrum of HD 71866. (*a*) The stellar spectrum, photographed with the differential analyzer in front of the slit, is in two strips, corresponding to left-handed and right-handed polarization as indicated. Note that the lines are sharper in the upper strip. (*b*) Two spectra made with the differential analyzer at phases 0.48 and 0.99 show the crossover effect prominently but with opposite sign. At these phases the field indicated by the directly measured Zeeman displacements is near zero. The crossover effect is inconspicuous for the strong line λ 4233.167 of Fe II, but it is particularly obvious for the adjacent line λ 4233.608 of neutral iron.

when the mean magnetic curve is passing through zero. In one spectrum the lines tend to be broad and shallow; in the other, sharp and deep. But the effect is selective, being much more obvious on some lines than on others (Fig. *2a*, *b*). The spectrograms of HD 71866 that show the effect are indicated by arrows through the points of Figure 1.

The only suggestion that has yet been put forward to account for the crossover effect is that the absorption lines may be considered to arise in two regions or sets of regions, A and B, in the atmosphere of the star and that these regions are characterized by magnetic fields of opposite effective polarity. The peculiarities in the line profiles then result from a combination of Zeeman and Doppler effects that arises when both sets of regions A and B are visible and when a differential radial velocity prevails between them. It would then be expected that the selective nature of the effect for different lines would depend upon the Zeeman patterns of the lines in relation to the field intensity and the differential radial velocity. In general, lines particularly sensitive to the Zeeman effect might be expected to exhibit the crossover effect to the most pronounced degree. Lines having Zeeman patterns with widespread σ components but without an exaggerated spread of components within the σ groups would be favored. To test this hypothesis, eye-estimates of the degree of the crossover effect according to the scale 0, 1, 2, 3, 4, were made for thirty-two lines of Fe I and Fe II on one plate (Pb 1896). The estimated degree of the effect was then plotted against the z-value of the line. The degree of correlation was low, but it appeared that the three lines having z-values of 2.0 or greater all showed a high degree of visibility of the crossover effect. All of the lines of Fe I showed some evidence of the effect, whereas six of the ten lines of Fe II seemed to show none.

One line that appears to be extremely sensitive to the crossover effect is Fe I 4233.608, which has the Zeeman pattern (0.00, 1.00) 1.00, 2.00, 3.00, computed from the Lande g formula. The pattern observed in the laboratory (Weeks 1944) is essentially identical to the computed pattern. According to Russell's rule, the weighted mean position of the σ components (which we call the z-value) is 1.50 Lorentz units from the undisturbed position. Another line also very sensitive to the crossover effect and of about the same moderate equivalent width in HD 71866 is Fe I 4210.352 (0.00), 3.00, which belongs to the same multiplet. If our working hypothesis is correct, we may expect that, for a line having a Zeeman pattern like λ 4233.608, the magnetic-field intensity and the differential velocity prevailing temporarily between the areas A and B are such as to yield the maximum degree of sharpness for the "sharp" profile. When the effective magnetic-field intensity is known, the matching differential velocity may be computed directly. In Figure 3 the Zeeman patterns (0.00, 1.00) 1.00, 2.00, 3.00, for A and B are offset by the Doppler shift corresponding to Δv. The adjacent Zeeman components of the patterns are separated by one Lorentz unit, which in a magnetic field of 4400 gauss is equivalent to 0.037 A. The value 4400 gauss is adopted here, as it is the effective field indicated by the line under discussion, when H_e is at maximum, even though the mean H_e derived from all lines is only about 2000 gauss. If, as in the diagram, the velocity is adjusted to obtain exact coincidence of the three σ components having the same sign of polarization, the Doppler displacement will equal four Lorentz units, or 0.147 A. This corresponds to a velocity difference of 10.4 km/sec. However, maximum sharpness of the "sharp" profile may result if, instead of matching the centers of the σ groups of components their "centers of gravity" specified by the z-values ($z = 1.53$) are matched. This yields a velocity of 7.9 km/sec.

In a similar way I have computed the matching velocity difference for seven other lines of Fe I, all in multiplet No. 152 and all of approximately the same equivalent width. These lines show the crossover effect apparently to about the maximum possible degree; i.e., it is difficult to imagine that the "sharp" profile could become appreciably sharper for any field strength. The results are tabulated in the last column of Table 2. The mean matching velocity is about 5 km/sec.

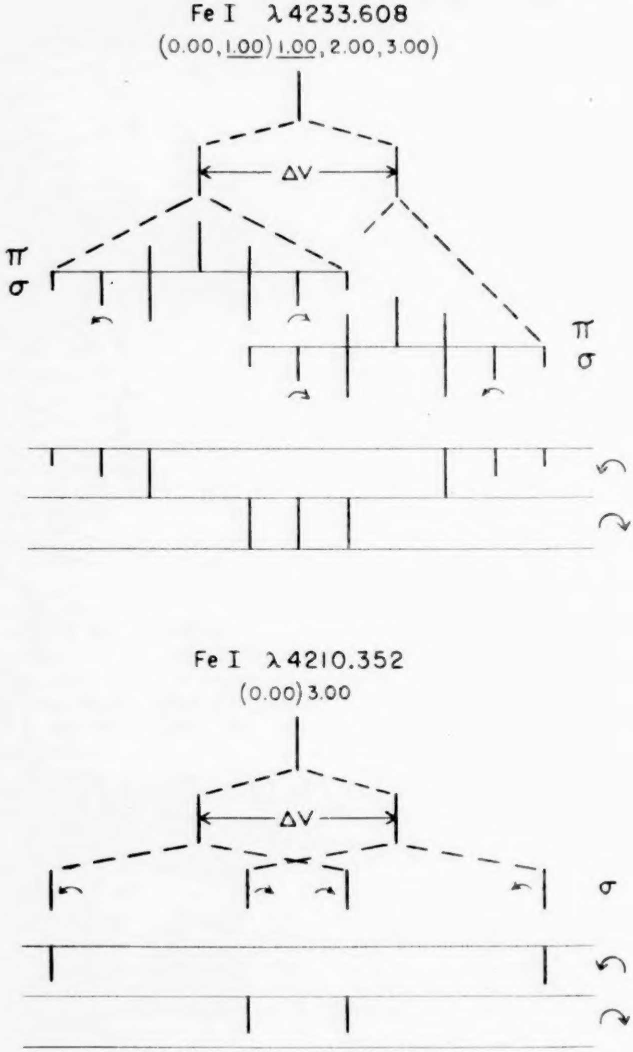

Fig. 3.—Diagrams illustrating the development of the crossover effect. The line is first split by the Doppler effect, corresponding to a differential velocity, Δv, between two areas on the star. If the two areas have longitudinal magnetic fields of opposite polarity, the lines are further split into their Zeeman patterns. The σ components are sorted out by the differential analyzer according to their sign of circular polarization, leading to a "broad" and a "sharp" profile in the two strips. If the field is not strictly longitudinal, the π components appear in both strips of the spectrum. In general, there occurs considerable overlapping of the profiles represented by the "lines" in the diagrams.

REMARKS ON INTERPRETATION

The crossover effect provides evidence bearing on the interpretation of stars showing periodically reversing magnetic fields. Ever since the reversing field of HD 125248 was discovered, it has been recognized that the simplest qualitative explanation was that stars of this kind (we may now include α^2 CVn, HD 71866, and HD 153882) are oblique rotators, in which the magnetic axis is inclined to the axis of rotation at a large angle approaching 90°, and that the axial rotation of the rigidly rotating dipolar star in the appropriate period (6.8 days for HD 71866) presents alternately the two sides of the star, showing opposite magnetic polarity, usually with associated spectroscopic anomalies. But when detailed analyses of the data have been attempted on the basis of the rotator model, certain discrepancies have appeared that argued against the acceptance of the model. An alternative interpretation of the magnetically variable stars requires a hydromagnetic cycle, related in kind to the 22-year magnetic cycle of the sun but of vastly greater amplitude and shorter period. A discussion of the specific and the statistical data pertaining to these alternative models would be out of place here, so the present discussion will be limited almost entirely to the interpretation of the crossover effect in HD 71866 as it applies to the rotator.

On the oblique rotator model for HD 71866 we first note that the sign of the crossover effect is correct; i.e., the region of magnetic polarity that is becoming more prominent shows a velocity of approach relative to the region of opposite polarity. This relationship holds as well in the three other regularly reversing stars mentioned earlier. The matching of Doppler and Zeeman displacements in a given magnetic field to yield maximum visibility of the crossover effect resulted, for the lines listed in Table 2, in a mean differential velocity of about 5 km/sec. We overlook the fact that, for a dipolar star viewed at an inclination of 90° to the magnetic axis, the effective field intensity of the magnetic polar regions (and the matching velocity) would be appreciably reduced below the value measured at maximum. The relationship of the matching velocity of 5 km/sec to v_e, the equatorial velocity of rotation of the star, depends upon the distribution of the magnetic areas and upon the degree of darkening at the limb. It seems a reasonable assumption that, at the crossover phases, our hypothetical areas A and B are on the stellar equator, on opposite sides of the central meridian, and effectively about 0.7 R from the center of the disk. On these assumptions, $v_e = 3.5$ km/sec. But if $R = 2\,R_\odot$, as is usual for a star of type A0, a period of 6.8 days for axial rotation leads directly to $v_e = 16$ km/sec. The discrepancy is sufficient to raise serious doubts regarding the suitability of the rotator model or about the validity of the interpretation of the crossover effect.

There appears to exist a further discrepancy with respect to line widths, for a star with v_e of 16 km/sec and high axial inclination should exhibit rotational broadening of the lines amounting to about 0.46 A. Yet measurement directly on the spectrograms yields line widths of about 0.26 A, not all of which can be attributed to stellar rotation.

One of the peculiar features of the crossover effect is that it is so obvious. The sharpness of the "sharp" profiles of some lines suggests that they are remarkably free from contamination by the π components of the Zeeman pattern; yet contributions from the π components should be quite appreciable from all areas of the stellar surface where the field vector makes an appreciable angle with the line of sight. It is noteworthy, also, that no doubling of the "broad" profiles has been detected. Further, there appears to be no adequate explanation of the observation that the crossover effect is much more prominent for lines of Fe I than for lines of Fe II and also that the effect is barely seen on lines of Ca II and Mg II. In part the discrepancy may lie in the greater total intensity of the lines of the ionized elements, with the result that, because of saturation of the stronger components of the Zeeman pattern in absorption, the weaker components, including the π components, gain in prominence.

Additional items requiring further attention in regard to their bearing on models of magnetically reversing stars are as follows:

1. A patchy distribution of elements such as Fe I, which shows the crossover effect so prominently, and Eu II, which varies in total absorption, would lead, on the rotator model, to harmonic velocity-curves with amplitudes approaching a rather large fraction of v_e (16 km/sec). There is no firm evidence from the velocity measurements to support this. Especially for Fe I, there is no evidence of systematic variation of velocity as a function of phase other than that inferred from the crossover effect.
2. Some elements, especially Cr II and Mn II, occasionally give H_e at considerable variance to $\langle H_e \rangle$.
3. Superposed on the principal (roughly sinusoidal) curve of magnetic variation there appear to be random fluctuations in the magnetic amplitudes and some randomness in phase, especially near crossover. These effects support the view that intrinsic hydromagnetic fluctuations are taking place at the surface of the star.

Much of the observational evidence bearing on the development of a model can best be brought out in a discussion of the magnetic stars as a group; it is hoped that this can be taken up in a subsequent paper.

I am grateful to Miss Sylvia Burd and to Mrs. A. J. Deutsch for their painstaking measurement of the spectrograms.

REFERENCES

Babcock, H. W. 1947, *Ap. J.*, **105**, 105.
———. 1951, *ibid.*, **114**, 1.
Babcock, H. W., and Babcock, H. D. 1955, *Ap. J.*, **121**, 349.
Babcock, H. W., and Burd, S. 1951, *Pub. A.S.P.*, **63**, 81.
———. 1952, *Ap. J.*, **116**, 8.
Babcock, H. W., and Cowling, T. G. 1953, *M.N.*, **113**, 357.
Provin, S. 1953, *Ap. J.*, **118**, 489.
Schwarzschild, M. 1950, *Ap. J.*, **112**, 222.
Stibbs, D. W. N. 1950, *M.N.*, **110**, 395.
Weeks, D. W. 1944, *Trans. Amer. Phil. Soc.*, N.S., **34**, 181.

RADIAL VELOCITIES OF NINE S-TYPE STARS*

P. C. Keenan and R. G. Teske
Perkins Observatory
Received July 5, 1956

ABSTRACT

Coudé spectrograms taken at Mount Wilson in the red region of the spectrum were measured to give radial velocities of nine S-type irregular or semiregular variable stars of small amplitude. Fourteen stars of this group now have measured velocities, and their mean peculiar radial velocity is about 27 km/sec. Their motions are consistent with those of other red giants rather than with the slower speeds of supergiants.

Comparisons of proper motions and radial velocities of long-period variables having spectra of type Se have indicated that their mean absolute magnitudes are about the same ($\langle M_v \rangle_{av} \approx -1$) as those of the main body of long-period variables of types M5e and later (Wilson and Merrill 1942; Keenan 1955). About half the S-type stars, however, either have approximately constant light or belong to the semiregular or irregular groups of variables. These stars, which we shall call the "small-amplitude variables" of type S, are known to differ from the long-period variables in their spatial distribution. It is important, therefore, that this group should be studied independently in respect to the motions of the member stars.

The *General Catalogue of Stellar Radial Velocities* (Wilson 1953) lists radial velocities for only five S-type stars of the small-amplitude group. The scarcity of data is due to the faintness and redness of these stars. Their average color index is about 1.4 mag., and only four of those known in the northern sky have apparent visual magnitudes brighter than 8. A further consequence of the difficulty of observation is that most of the published determinations were based on spectrograms of rather small scale. This is reflected in the low weights (quality d) assigned to several of the catalogue values (Table 1).

In planning the present program, it was decided that the red region of the spectrum offers the best prospect for reaching fairly faint red stars with sufficient dispersion to allow accurate measurements of line displacements. The observations were carried out with the 32-inch camera of the coudé spectrograph of the Mount Wilson 100-inch telescope. When used with the excellent Babcock 46B grating, this camera gives a scale of 20 A/mm in the first order. After experiments with several emulsions it was concluded that maximum speed for most S-type stars was given by the Eastman 103*a*-F(3) emulsion. With this plate a spectrum 0.32 mm wide and well exposed over the range from 6100 to 6800 A could be obtained for a star with $m_v = 9$ in about 5 hours.

The observational data for the S-star program are given in Table 2. For the few exposures taken on emulsions other than 103*a*-F the plates used are identified in the notes to the table. Mean internal errors of each plate are listed after the measured velocities.

Since the red region has not been extensively used in measuring radial velocities, except for Sanford's work on the carbon stars (1944), the enlargements of Figure 1 have been made in order to show the character of that part of the spectrum of cool stars. The most obvious fact brought out by the illustration is that more lines are available for measurement in a strong S-type spectrum than in one of fairly late-type M. Although only the strongest lines and bands have been marked in the figure, it is apparent that molecular absorption, due chiefly to titanium oxide, weakens nearly all the lines in the red part of the M-type spectrum. The effect is particularly striking for the group of very

---

* The research reported in this paper was supported by a grant to the Ohio State University by the National Science Foundation.

strong lines of Ca I (note λ 6718). This absorption becomes serious for types M4 and later. On the other hand, although the zirconium oxide bands are very intense in the cooler S-type stars (including AD Cyg), they are still narrow enough to leave some fairly transparent windows, notably near 6100, 6450, and 6700 A. Another advantage possessed by the S spectra is that several of the metals which seem to be more abundant in stars of that type have very strong low-level lines in the red. Examples of neutral lines of zirconium, yttrium, lanthanum, and lithium[1] can be seen in Figure 1.

The number of lines actually measured on each plate depended upon the relative strength of the S and M characteristics in that particular star. The density of the plate was also a factor, for on the lighter exposures it was possible to measure only those lines

TABLE 1

PUBLISHED RADIAL VELOCITIES FOR SMALL-AMPLITUDE S-TYPE VARIABLES

Star	*HD*	*BD*	m_v	V_r	Quality
BS 1105.......	22649	+62°597	5.3	−22.0	b
WX Cam.....	....	....	12.2–13.0	−82	d
V 679 Oph....	172804	+ 6°3898	9.0– 9.3	−51	d
AD Cyg......	195665	+32°3850	8.5– 9.5	− 1	d
π^1 Gru........	212087	CD −46°14292	5.8– 6.4	−19.6	b*
BS 8714.......	216672	+16°4833	6.5	+11.1	b

* The velocity of π^1 Gru was measured by Feast (1953) from a number of prismatic spectrograms with dispersions of 30 or 50 A/mm at Hγ. Although the probable error of the mean was not published, a quality of b in Wilson's notation appears appropriate.

TABLE 2

OBSERVATIONS WITH 100-INCH COUDÉ SPECTROGRAPH, TYPE S

Star	R.A. 1950	Dec. 1950	m_v	Date	U.T.	Plate (Ce)	V_r	No. of Lines
BD+24°620......	4^h02^m6	+24°36′	9.1:	Nov. 5, 1954	7:20	9496	−23.9±0.6	18
HD 34738........	5 16.6	−22 16	8.8	Dec. 5, 1954	6:34	9547	+61.7±0.8	15
HD 35155........	5 19.9	− 8 43	7.0	Feb. 7, 1953	3:43	8660*	+80.5±0.8	33
				Jan. 4, 1955	6:44	9588*	+76.7±0.5	19
				Feb. 2, 1955	3:43	9638	+68.5±1.4	10
HD 49368........	6 45.7	+ 5 36	8.3:	Nov. 5, 1954	11:38	9497	+48.4±0.8	23
				Nov. 8, 1954	7:42	9505	+48.5±0.7	22
HD 58881........	7 24.7	−11 37	9.0	Feb. 4, 1955	6:44	9644	− 2.0±0.6	17
SU Mon (HD 62164)......	7 39.9	−10 46	8.4:	Feb. 24, 1953	5:53	8667†	+51.7±0.7	36
			8.2:	Dec. 5, 1954	9:46	9548	+45.6±0.6	18
HD 63733........	7 47.5	−18 53	8.5	Feb. 6, 1955	6:39	9650	+ 3.9±0.5	21
HD 64332........	7 50.6	−11 30	8.1	Jan. 4, 1955	9:29	9589	− 1.5±1.2	11
AD Cyg (HD 195665)......	20 29.6	+32 24	8.6:	Nov. 8, 1954	4:30	9504	+ 3.8±0.8	13

* HD 35155—Ce 8660 on 103a-G; Ce 9588 on 1-N (sensitized in NH_3).

† SU Mon—Ce 8667 on 103a-G.

---

[1] The figure illustrates the significant fact that Li 6708 is consistently enhanced in type S, but not to the extreme degree found in a few carbon stars, notably WZ Cas (McKellar 1941, 1944) and WX Cyg (Sanford 1944).

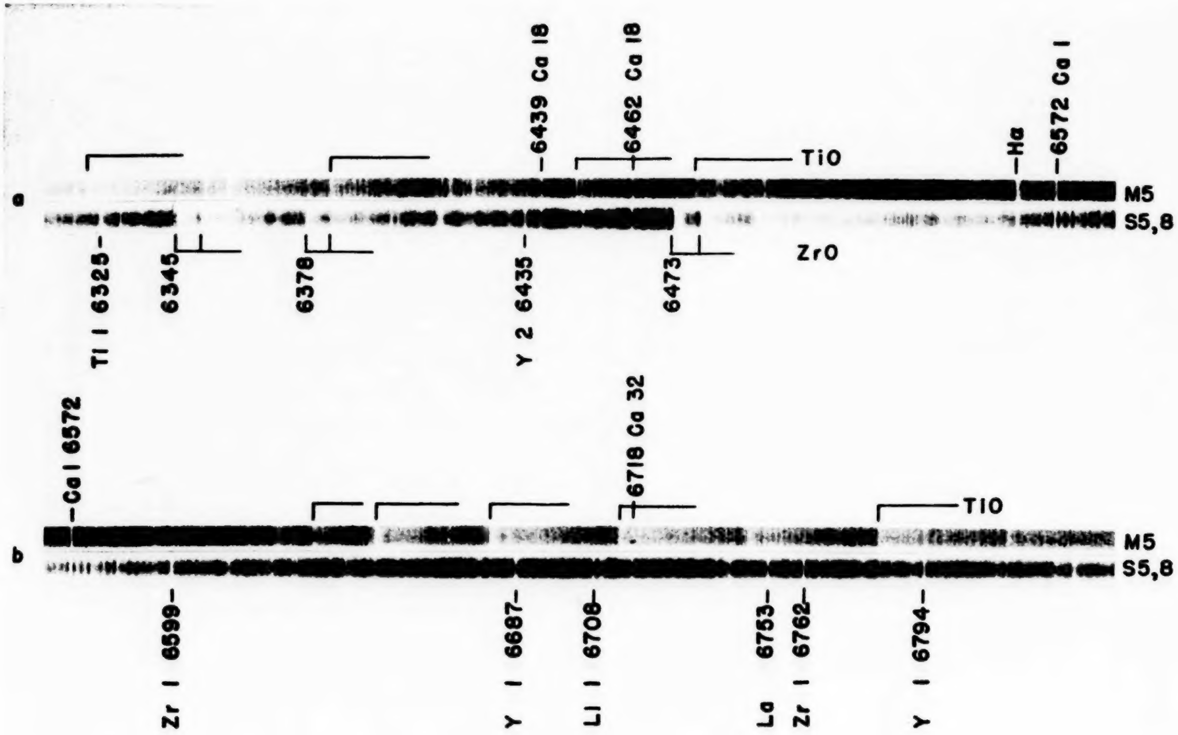

Fig. 1.—Coudé spectra of the standard M5 giant 56 Leo (*a*) and the S-type star AD Cyg (*b*). Emulsion, 103*a*-F(3)

which lay outside the regions of strong band absorption. For these reasons the numbers of lines used, as given in the ninth column of Table 2, vary considerably.

The internal mean errors in Table 2 are satisfactorily small, averaging ±0.8 km/sec. The absolute errors must be considerably larger, but the results for the few stars for which comparisons could be made between two plates of this program (HD 35155, HD 49368, and SU Mon) or with a published velocity (AD Cyg) are in good agreement, with the one exception of HD 35155. The 1953 plate of this star (green region) gave a velocity 12.0 km/sec higher than the 1955 (red region) plate. Since there was available an additional 1955 spectrogram, Ce 9588, of the near-infrared spectrum of this star (1-N emulsion), this plate was measured also. Although its quality was not so good as that of the other two, nineteen lines distributed over the range from 7460 to 8470 A gave a mean of +76.7 km/sec with very little scatter. This intermediate value agrees better with the 1953 result than with the one from the other 1955 plate taken about a month later and leaves uncertain the question of whether there is a real variation in the velocity of HD 35155.

TABLE 3

OBSERVATIONS OF M-TYPE STARS WITH KNOWN VELOCITIES

STAR	TYPE	DATE	CATALOGUE		OBSERVED		$V_{\mathrm{obs}} - V_{\mathrm{cat}}$	NO. OF LINES
			V_r (km/sec)	Quality	V_r (km/sec)	M.E. (km/sec)		
BS 46.....	M3 III	Jan. 1, 1955	−1.7	b	−0.2	±0.4	+1.5	24
α Cet.....	M2 III	Nov. 7, 1954	−25.9	a	−27.4	± .5	−1.5	25
4 o′ Ori....	M3 S	Nov. 7, 1954	−6.9	a	−10.8	± .5	−3.9	11
119 Tau...	M2 *Ib*	Jan. 26, 1953	+22.5	a	+22.4	± .4	−0.1	21
π Aur.....	M3 II	Nov. 1, 1955*	+0.9	a	+0.2	± .8	−0.7	15
β Peg....	M2+II–III	Nov. 5, 1954	+8.7	a	+7.4	±0.6	−1.3	21

* π Aur—emulsion 103*a*-D (λ 5400 and λ 6100 regions).

As an independent check on the reliability of velocities measured in the red, spectrograms of six bright stars had been taken on the same observing program at Mount Wilson. Velocities measured on these plates are compared in Table 3 with the values from the *General Catalogue of Stellar Radial Velocities* (Wilson 1953). These stars are all of type M3 or earlier, and hence the titanium oxide bands were not strong enough seriously to affect the measurements in the red. The average difference, $V_{\mathrm{obs}} - V_{\mathrm{cat}}$, is −1.0 km/sec. This suggests that our measurements systematically give velocities too negative by about 1 km/sec, but the value of the small corrections is not well enough established by these few stars to make it worthwhile at present to change the velocities in Table 2.

The known radial velocities of S-type stars are brought together in Table 4. A quality of b was assigned to our values, since that was the measure of quality adopted in the *General Catalogue of Stellar Radial Velocities* for velocities based on a single coudé plate of medium dispersion. In addition to V_r, the measured velocity with respect to the sun, Table 4 gives in the tenth column the velocity, V'_r, corrected for the solar motion:

$$V'_r = V_r + V_{\odot} \cos \lambda ,$$

where the value $V_{\odot} = 15.5$ km/sec and the co-ordinates of the solar apex were taken from the solution by Vyssotsky and Janssen (1951) for the solar motion with respect to the local standard of rest.

The total sample of fourteen S-type small-amplitude variables with measured radial velocities is still pitifully small. For most of these stars proper motions are available only from the Yale catalogues, and these motions are, on the average, about equal to their probable errors, around 0".010. Consequently, it appears necessary to wait until longer time intervals improve the accuracy of proper motions before a significant comparison of these with the radial motions can be made.[2] There are, however, three points that can be tentatively made now about the motions of our group of stars.

1. The fact that the proper motions of even the eighth-magnitude S-type stars are quite small is further evidence that these stars are not appreciably less luminous than normal red giants.

2. If the S stars were supergiants, the contribution due to differential galactic rotation should be a considerable fraction of the total radial velocity for the stars on our program. If M_v were -3, an eighth-magnitude star should show a maximum increment of about 20 km/sec, the actual amount depending upon the values adopted for Oort's constant (*A*), and interstellar absorption. Since the factor $\cos^2 b \sin 2 (l - l_0)$ in the Oort equation exceeds 0.7 for most of the stars in Table 4, we tried plotting V'_r against this factor but found no well-defined correlation even for the stars fainter than the seventh magnitude. This is easily seen by inspection of the table; stars such as HD 58881 and SU Mon, situated in directions only a few degrees apart, differ in radial velocity by nearly 50 km/sec. Only WX Cam, which is the faintest star included and has a poorly determined velocity of -85 km/sec derived from two small-scale spectrograms, stands out as obviously likely to possess a considerable rotational component in its observed motion.

TABLE 4

ADOPTED VELOCITIES OF SMALL-AMPLITUDE VARIABLES OF TYPE S

Star	*HD*	Type	R.A. 1950	Dec. 1950	Galactic Long.	Galactic Lat.	m_v	V_r	V'_r	Quality
BS 1105	22649	S5, 3	3h37m8	+63°03'	108°	+ 7°	5.3	−22.0	−22.8	b
WX Cam	....	S5, 8	3 45.3	+53 03	115	0	10–11:	−82	−85	d
BD+24°620	....	S4, 2	4 02.6	+24 36	137	−19	9.1:	−23.9	−33.6	b
Vys 3	34738	S4, 5	5 16.6	−22 16	192	−28	8.8:	+61.7	+46.3	b
	35155	S4, 1	5 19.9	− 8 43	178	−22	7.0:	+75: (Var.?)	+60:	b:
	49368	S5, 1	6 45.7	+ 5 36	175	+ 3	8.3:	+48.4	+35.0	a
	58881	S3, 9	7 24.7	−11 37	195	+ 4	9.0	− 2.0	−15.9	b
SU Mon	62164	S3, 6	7 39.9	−10 46	196	+ 7	7.7–9.0	+48.6	+35.2	b
	63733	S3.5, 2	7 47.5	−18 53	204	+ 6	8.5	+ 3.9	− 9.6	b
	64332	S6, 2	7 50.6	−11 30	198	+ 9	8.1	− 1.5	−14.6	b
V 679 Oph	172804	S4.5, 8	18 39.5	+ 6 45	5	+ 4	9.0–9.3	−51	−36.4	d
AD Cyg	195665	S5, 8	20 29.6	+32 24	41	− 5	8.5–9.5	+ 2.8	+15.1	b
π' Gru	212087	S5.7:	22 19.7	−46 12	317	−56	5.8–6.4	−19.6	−20.0	b
BS 8714	216672	S5, 1	22 52.1	+16 40	56	−38	6.5	+11.1	+15.7	b

3. The evidence of the last section suggests that the mean value of $|V'_r|$ should be a fairly good measure of the average peculiar velocity in one co-ordinate for the stars in this group. We find $\langle |V'_r| \rangle = 28.6$ km/sec for the fourteen stars, with weights 1 for quality b and ¼ for quality d. If WX Cam is omitted, $\langle |V'_r| \rangle = 27.2$ km/sec.

Although these rough figures do not warrant extended discussion, the mean peculiar radial velocity for the group can be taken as not far from 25–30 km/sec. This confirms the conclusion that most, at least, of the S stars are moving more slowly than stars of the high-velocity, population II group of G and K giants. On the other hand, their speeds are more consistent with those of late-type giants in general than with the slower motions of supergiants (cf. Wilson 1951).

---

[2] We are indebted to Dr. A. N. Vyssotsky for good advice on this point.

We should like to express appreciation to Dr. I. S. Bowen and the Observatory Committee of the Mount Wilson and Palomar Observatories for permitting one of us (P. C. K.) to obtain these spectrograms as a guest investigator. The generous co-operation of many members of the staff at both Pasadena and Mount Wilson helped greatly in the carrying-out of the program.

REFERENCES

Feast, M. W. 1953, *M.N.*, **113**, 510.
Keenan, P. C. 1955, *Ap. J.*, **120**, 484; *Perkins Obs. Contr.*, Ser. 1, No. 39.
McKellar, A. 1941, *Observatory*, **64**, 4.
———. 1944, *J.R.A.S. Canada*, **38**, 237.
Merrill, P. W. 1934, *Ap. J.*, **79**, 183; *Mt. W. Contr.*, No. 486.
Sanford, R. F. 1944, *Ap. J.*, **99**, 145; *Mt. W. Contr.*, No. 689.
———. 1947, *Pub. A.S.P.*, **59**, 333.
Vyssotsky, A. N., and Janssen, E. M. 1951, *A.J.*, **56**, 58; *Pub. McCormick Obs.*, Vol. **11**, Part 3.
Wilson, R. E. 1941, *Ap. J.*, **93**, 212; *Mt. W. Contr.*, No. 643.
———. 1953, *General Catalogue of Stellar Radial Velocities* ("Carnegie Institution of Washington Publications," No. 601).
Wilson, R. E., and Merrill, P. W. 1942, *Ap. J.*, **95**, 248; *Mt. W. Contr.*, No. 658.

THE RADIAL VELOCITIES OF RHO PUPPIS*

O. STRUVE, J. SAHADE† AND V. ZEBERGS,
Berkeley Astronomical Department, University of California

Received June 12, 1956

ABSTRACT

Radial velocities of ρ Puppis have been derived from 42 coudé spectrograms secured at Mount Wilson with a dispersion of about 4.5 A/mm. The results are represented by a period of about 0.1409 day and yield a value of $2K$ of about 10 km/sec and an average velocity of about +46 km/sec.

Rho Puppis ($\alpha = 8^h05^m38^s$, $\delta = -24°10'.4$, 1955.0) was announced long ago by Campbell (Reese 1903; Campbell and Moore 1928) as a star of variable radial velocity, and this result was confirmed at the Cape Observatory by Spencer Jones (1928). But, only recently, photoelectric observations by Eggen (1956*a*) disclosed that ρ Puppis is also variable in light and that the period is a short one—nearly $3\frac{1}{2}$ hours. The authors had the privilege of reading Eggen's paper in manuscript, and spectrographic observations of the star were undertaken immediately afterward. They were secured on five nights in March, April, and May, 1956, at the coudé focus of the 100-inch telescope of the Mount Wilson Observatory, with a dispersion of about 4.5 A/mm.

TABLE 1

LIST OF STAR LINES

Wave Length	Element	Wave Length	Element	Wave Length	Element
4215.52	Sr II	4254.35	Cr I	4312.86	Ti II
4219.36	Fe I	4271.16	Fe I	4352.74	Fe I
4246.83	Sc II	4271.76	Fe I	4375.93	Fe I
4247.43	Fe I	4274.80	Cr I	4395.03	Ti II
4250.12	Fe I	4282.41	Fe I	4404.75	Fe I
4250.79	Fe I	4283.01	Ca I		

A spectral type F6 II has been assigned to ρ Pup by Bidelman (1951), with the remark that "the *Ca* II lines are rather weak for the type given," and the star is particularly interesting because it seems to belong to the δ Scuti sequence of pulsating stars (Eggen 1956*a*) or perhaps to the dwarf cepheid sequence (Struve 1955), of which very few members are known. The star has been studied spectrophotometrically by Greenstein (1948).

All the spectrograms—forty-two in number—were measured for radial velocity by Mrs. Zebergs. The stellar lines used are listed in Table 1, and the radial velocities obtained from each plate appear in Table 2. The velocities on each night are plotted in Figure 1, and Figure 2 shows a combined plot of all five nights by using a period of 0.1409 day. This value for the period was derived from our material and agrees very well with the one derived by Eggen (1956*b*) by combining his photometric observations with the available spectrographic results from Lick and Cape, namely, 0.141050 day. Our phases have been computed from the time of maximum velocity at JD 2435560.756.

---

* The observational material used in this paper was obtained by O. Struve and J. Sahade as guest investigators at the Mount Wilson Observatory.

† John Simon Guggenheim Fellow.

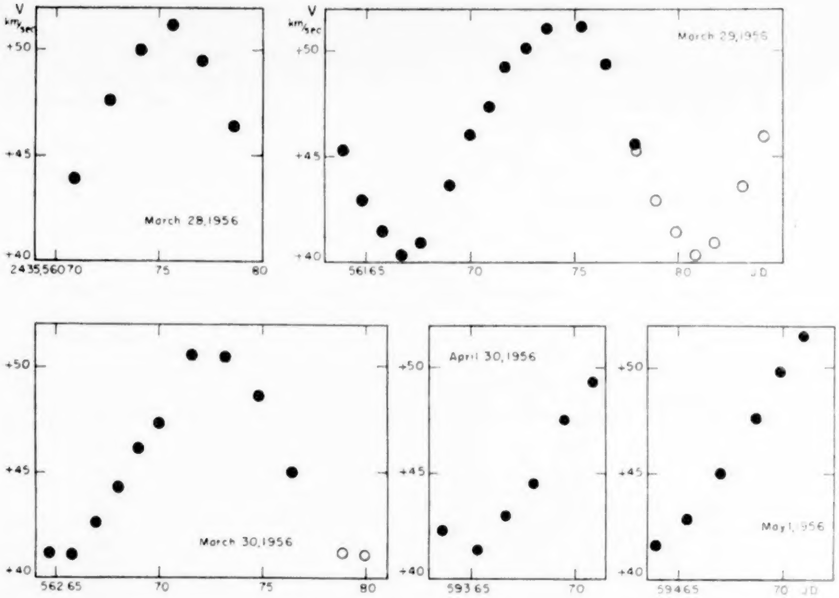

FIG. 1.—Radial velocities of ρ Puppis

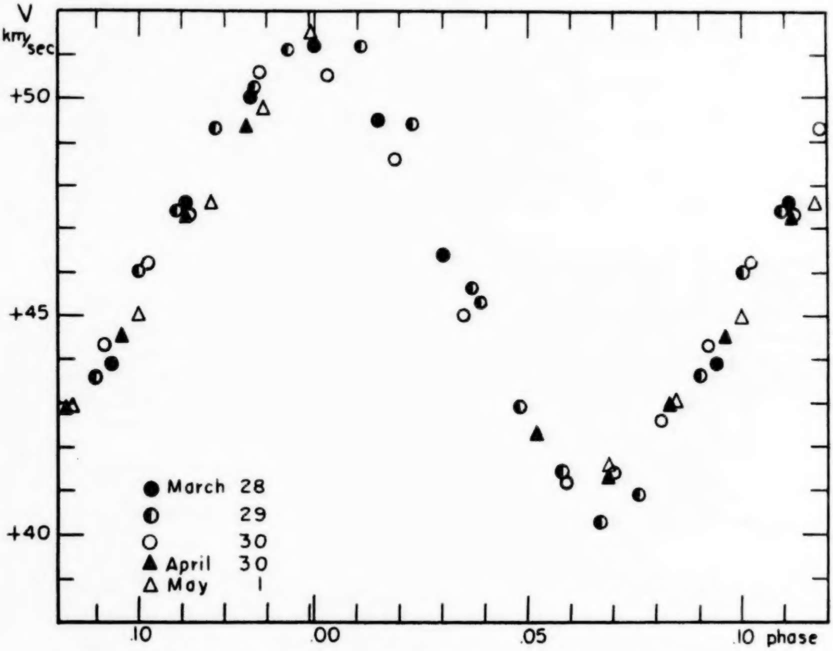

FIG. 2.—Combined plot of the radial velocities of ρ Puppis

Our material suggests that we are probably dealing with a constant velocity-curve, but the number of cycles covered by our plates is too small for a definite conclusion. The value of $2K$ is about 10 km/sec, and the mean velocity is +46 km/sec, in agreement with the early Lick and Cape data.

The combination of Eggen's and our data indicates that in ρ Pup maximum brightness falls about 0.02 day later than the minimum radial velocity. No spectral changes have been detected on our plates.

TABLE 2

RADIAL VELOCITIES OF ρ PUPPIS

JD	v (km/sec)	Phase* (Fraction of Day)	JD	v (km/sec)	Phase* (Fraction of Day)
2435000+			2435000+		
560.709	+43.9	0.094	562.658	+41.1	0.070
.726	47.6	.111	.669	42.6	.081
.741	50.0	.126	.680	44.3	.092
.756	51.2	.000	.690	46.2	.102
.771	49.5	.015	.700	47.3	.112
.786	46.4	.030	.716	50.6	.128
561.639	45.3	.038	.732	50.5	.003
.648	42.9	.047	.748	48.6	.019
.658	41.4	.057	.764	45.0	.035
.667	40.3	.066	593.636	42.3	.050
.676	40.9	.075	.653	41.4	.067
.690	43.6	.089	.667	43.0	.081
.700	46.0	.099	.680	44.5	.094
.709	47.4	.108	.695	47.5	.109
.718	49.3	.117	.709	49.3	.123
.727	50.2	.126	594.639	41.6	.067
.737	51.1	.136	.654	42.9	.082
.753	51.2	.010	.670	45.0	.098
.765	49.4	.022	.687	47.6	.115
.779	45.6	.036	.699	49.8	.127
562.647	41.2	0.059	.710	51.5	0.138

* $P = 0.1409$ day; T_0 = JD 2435560.756.

REFERENCES

Bidelman, W. P. 1951, *Ap. J.*, **113**, 304.
Campbell, W. W., and Moore, J. H. 1928, *Lick Obs. Pub.*, **16**, 124.
Eggen, O. J. 1956*a*, *Pub. A.S.P.*, **68**, 238.
———. 1956*b*, private communication.
Greenstein, J. L. 1948, *Ap. J.*, **107**, 151.
Reese, H. M. 1903, *Lick Obs. Bull.*, **2**, 29.
Spencer Jones, H. 1928, *Cape Ann.*, **10**, Part 8, 1928.
Struve, O. 1955, *Sky and Telescope*, **14**, 461.

THE TRIPLE SYSTEM LAMBDA TAURI*

E. G. Ebbighausen and O. Struve
Department of Physics, University of Oregon, and Berkeley Astronomical
Department, University of California

Received May 2, 1956; revised June 8, 1956

ABSTRACT

The spectroscopic elements of the eclipsing binary λ Tauri are examined by a rediscussion of the published results from Potsdam (1901–1902), Allegheny (1906–1916), and Michigan (1923–1925) and the measurements by the authors of spectrograms from Victoria (1935–1939) and Mount Wilson and Lick (1952–1955). The main problem of the apparent change in period of the third body, as suggested by the Allegheny and Michigan results, is resolved: a period of 33.025 days satisfies the residuals from the 4-day orbit for all series of spectrograms. The behavior of the differences between the H- and He-line velocities is discussed, a rough value of 4.0 is derived for the mass ratio of the eclipsing pair, and some remarks are made concerning the photometric data.

I. INTRODUCTION

Variations in the light of λ Tauri were discovered in 1848, and it became the third star to be recognized as an eclipsing binary. The spectrum is of type B3, the period of the eclipsing pair is almost 4 days, the visual magnitude varies from 3.7 to 4.2 during primary eclipse, and a well-marked secondary minimum is present, with a depth of a little more than 0.1 mag. Although five spectrograms had been secured by Belopolsky (1898) in 1897 and twenty-three by Hartmann at Potsdam in the season 1901–1902 (von Aretin 1913), the first extenisve investigation of λ Tauri was made by Schlesinger (1916*a*, *b*) at Allegheny with spectrograms taken there in the interval 1906–1916. He found for the eclipsing pair that K was 58 km/sec and the eccentricity less than 0.1. In addition, he observed that the residuals from the calculated velocity-curve were larger than would ordinarily be expected; from these residuals he concluded that the systemic velocity of the eclipsing pair is variable, with an amplitude of 10.4 km/sec in a period of 34.6 days. This variation he ascribed to the presence of a third body.

In the two seasons 1915–1917 Stebbins (1920) at the Washburn Observatory obtained two extensive series of photoelectric observations, from which he obtained a light-curve showing that the eclipse is partial. He derived the photometric elements and the following formula for the times of primary minima:

$$\text{Primary minimum} = \text{JD } 2421506.850 + 3^{d}952952E\,.$$

This formula has been used throughout the present investigation, and Stebbins' period seems to satisfy all series of observations.

During the two seasons 1923–1925 McLaughlin (1937) at Michigan obtained a number of spectrograms of λ Tauri for the specific purpose of examining the rotation effect. The number of his spectrograms and their distribution in phase did not allow the calculation of the orbital elements. Instead, McLaughlin revised Schlesinger's orbit by omitting the spectrograms taken during primary eclipse and found only a small change in the new elements. With the aid of this new orbit, McLaughlin computed the residuals for his own velocities and found that they could not be satisfied by Schlesinger's period of 34.6 days but by one close to 30.0 days. This new period did not satisfy the Allegheny residuals.

---

* This investigation was supported in part by the Research Corporation in the form of a travel grant to Mr. Ebbighausen and by the Graduate Research Fund of the University of Oregon. The new material was obtained by the authors as guest investigators at the Mount Wilson and Lick Observatories.

This conclusion raised the possibility that the period of the third body was actually variable. λ Tauri is distinguished by the fact that the ratio (about 8) of the longer period to the shorter period is the smallest for any triple system. For Algol the ratio is about 250. Hence for λ Tauri the third body must be rather close to the eclipsing pair, giving rise to the possibility of measurable perturbations. It should be remarked that this change in period is very large and therefore quite unlikely. The present investigation was undertaken to determine the period of the longer oscillation.

II. SUMMARY OF THE SPECTROSCOPIC DATA

Although Belopolsky had obtained five spectrograms of λ Tauri in 1897, they were not used because of their small number. The following four groups have been extensively treated.

TABLE 1

RADIAL VELOCITIES OF λ TAURI, POTSDAM

JD 2415000+	Phase 4-Day Period (days)	v (km/sec)	Residual (km/sec)	Phase 33.025-Day Period (days)
689.49	1.39	−26	+ 1	1.4
690.44	2.34	+52	+ 7	2.3
712.39	0.57	−19	− 4	24.3
716.31	0.54	− 8	+ 4	28.2
761.23	1.98	+14	− 3	7.1
764.32	1.11	−34	+ 1	10.2
766.33	3.12	+61	− 7	12.2
785.40	2.43	+60	+ 9	31.3
787.36	0.44	− 4	+ 1	0.2
791.21	0.33	− 7	−10	4.0
797.38	2.55	+46	−11	10.2
814.22	3.58	+66	+11	27.0
814.24	3.60	+65	+11	27.0
815.31	0.72	−12	+12	28.1
820.29	1.74	− 8	− 5	0.1
821.25	2.70	+66	+ 3	1.1
823.26	0.76	−32	− 6	3.1
849.28	3.06	+66	− 2	29.1

a) Potsdam

Twenty-three spectrograms with a dispersion of 27 A/mm at Hγ were obtained by Hartmann at Potsdam in the 1901–1902 season and were discussed by von Aretin in an extensive paper, most of which is devoted to a photometric study. Four of these plates obtained during primary eclipse and one of low quality were omitted. Since von Aretin gave the wave lengths of both the iron comparison and the star lines, it was seen that both sets were systematically in error by the same amount, and therefore his individual line velocities needed no systematic correction. Although he used an elaborate weighting system with weights varying from zero to 10, these were ignored, and all line velocities were given equal weights. In forming the plate means, the line velocities for Mg II 4481 and H–Hε were omitted. The data are given in Table 1.

b) Allegheny

A total of one hundred and thirty-three spectrograms was obtained by Schlesinger and his co-workers at Allegheny in several seasons: 1906–1907 (5, 4), 1907–1908 (80, 67), 1911–1912 (8, 6), 1913–1914 (33, 26), and 1915–1916 (7, 5). Each season is followed by two numbers in parentheses, the total number of spectrograms in that season and the number taken outside primary eclipse. The total number outside eclipse is one hundred and eight. The dispersion was 40 A/mm at Hγ.

Since the stellar wave lengths are now know with a higher degree of accuracy than in 1916, it was felt desirable to remeasure all the spectrograms. Through the generosity of Dr. N. E. Wagman, director of the Allegheny Observatory, all the spectrograms were sent to the University of Oregon, where they were measured and reduced. The results are in Table 2.

c) Michigan

In the two seasons 1923–1925 McLaughlin secured a number of spectrograms for the purpose mentioned in the introduction. Forty-seven of these velocities obtained outside eclipse were used in this investigation. The residuals only are given in Table 3. The dispersion of the spectra was 40 A/mm at Hγ.

d) Victoria

Through the courtesy of Mr. R. M. Petrie, director of the Dominion Astrophysical Observatory, a number of spectrograms taken at Victoria were made available to us. They were measured at the University of Oregon. Of these, thirty-six were taken outside primary eclipse and are discussed here. The spectrograms were obtained in the four seasons 1935–1939. Most of the spectrograms have a dispersion of 11 A/mm at Hγ and the remainder 15 A/mm and 30 A/mm. Table 4 contains a list of the data.

e) Mount Wilson and Lick

In the three seasons 1952–1955 both authors were at various times guest investigators at Mount Wilson, where a total of three hundred and fifty spectrograms was obtained with the 60-inch reflector. The dispersion is 36 A/mm at Hγ. All spectrograms were secured on eighteen nights and the great majority on twelve nights. Since a large number of plates was secured on most nights, the Mount Wilson velocities were grouped into normal points. The average number of spectrograms per normal point is about five, with a range from four to six, and with only one from two velocities. The number of normals is sixty-eight. Four spectrograms were taken at the Lick Observatory, two on each of two nights, and they bring the total of normal points to seventy. The data are given in Table 5. In the column of residuals the values given are the mean residuals for all the normal points on one night. A group of normal points made in this way is referred to later on as a "supernormal."

Tables 1–5 give all the data used in this investigation. The table headings depend somewhat on the material. Tables 1, 2, 4, and 5 give the Julian Day of the observation or of the normal point, the phase in the 4-day orbit with Stebbins' period, the plate or normal-point velocity reduced to the sun, the residual from the 4-day orbit (described in the next section), and the phase of the residual, using the period 33.025 days and the reference point JD 2415688.1. The latter is, to the tenth of a day, the time of the primary minimum just preceding von Aretin's first observation as calculated from Stebbins' formula.

III. COMPUTATION OF THE ELEMENTS

For each group of data an orbit was calculated without the long-period variation, and from these elements the residuals were obtained. With the exception of von Aretin's data, the velocities were distributed quite uniformly in time with respect to phase in the longer period, and hence the foregoing procedure was justified. The distribution of the Mount Wilson–Lick data is not so good as might be desired.

TABLE 2

RADIAL VELOCITIES OF λ TAURI, ALLEGHENY

JD	Phase 4-Day Period (days)	v (km/sec)	Residual (km/sec)	Phase 33.025-Day Period (days)
2417000+				
523.762	1.494	−36	−14	19.3
523.785	1.517	−25	− 5	19.3
595.651	2.226	+38	+ 2	25.2
606.677	1.393	−34	− 6	3.2
831.878	1.275	−30	+ 3	30.2
831.918	1.315	−28	+ 3	30.2
851.830	1.464	−40	−16	17.1
851.865	1.499	−19	+ 3	17.2
854.818	0.499	−17	+ 4	20.1
854.856	0.538	−15	+10	20.2
855.856	1.538	− 6	+13	21.2
863.726	1.502	−13	+ 8	29.0
863.774	1.550	+ 2	+20	29.1
863.826	1.602	0	+15	29.1
865.775	3.551	+57	+ 6	31.1
865.821	3.597	+55	+ 7	31.1
866.795	0.618	−25	+ 4	32.1
866.824	0.647	−19	+11	32.1
867.722	1.546	−20	− 2	0.0
867.785	1.609	−14	0	0.1
869.722	3.546	+62	+11	2.0
888.697	2.757	+78	+12	21.0
888.742	2.802	+80	+13	21.0
888.792	2.852	+81	+13	21.1
890.649	0.756	−27	+ 8	22.9
891.660	1.767	+ 7	+ 9	24.0
891.710	1.817	+21	+19	24.0
891.738	1.845	+15	+11	24.0
891.789	1.896	+21	+13	24.1
892.671	2.778	+86	+19	25.0
892.719	2.826	+77	+ 9	25.0
892.763	2.870	+77	+ 8	25.1
896.688	2.842	+79	+11	29.0
896.727	2.882	+74	+ 5	29.0
896.761	2.915	+67	− 3	29.1
908.635	2.930	+68	− 2	7.8
908.705	3.000	+55	−15	7.9
916.614	3.003	+70	0	15.8
916.693	3.082	+57	−13	15.9
918.631	1.067	−38	0	17.8
936.647	3.271	+58	− 7	2.8
936.686	3.310	+59	− 5	2.9
941.587	0.305	−24	−16	7.8
941.616	0.334	−29	−19	7.8
942.735	1.453	−44	−20	8.9
944.565	3.282	+47	−18	10.8
946.531	1.295	−40	− 8	12.7
946.582	1.346	−41	−11	12.8
947.535	2.299	+30	−11	13.7
947.572	2.336	+24	−20	13.8
950.538	1.349	−25	+ 5	16.7
951.565	2.376	+40	− 7	17.8
951.600	2.411	+37	−12	17.8
955.695	2.552	+58	+ 1	21.9
955.735	2.592	+59	− 1	21.9

TABLE 2—*Continued*

JD	Phase 4-Day Period (days)	v (km/sec)	Residual (km/sec)	Phase 33.025-Day Period (days)
2407000+				
959.574	2.478	+55	+ 2	25.8
959.616	2.520	+67	+11	25.8
960.534	3.438	+76	+18	26.7
960.570	3.474	+74	+18	26.8
981.594	0.780	−37	− 1	14.8
981.641	0.826	−48	−11	14.8
2418000+				
010.548	2.060	+18	− 4	10.6
010.587	2.099	+24	− 1	10.7
011.504	3.016	+64	− 6	11.6
011.527	3.039	+67	− 3	11.6
013.503	1.061	−56	−18	13.6
013.524	1.082	−50	−12	13.6
013.547	1.105	−47	− 9	13.6
013.572	1.130	−47	−10	13.7
022.561	2.213	+41	+ 6	22.7
2419000+				
367.788	3.444	+53	− 4	13.9
376.756	0.553	− 9	+17	22.9
377.704	1.501	−16	+ 5	23.8
384.692	0.584	−18	+ 9	30.8
409.671	1.843	+11	+ 7	22.8
418.556	2.821	+60	− 8	31.7
2420000+				
072.815	0.892	−22	+16	25.4
074.733	2.810	+80	+12	27.3
077.763	1.887	+ 2	− 6	30.4
086.703	2.922	+65	− 5	6.3
092.732	1.045	−42	− 4	12.3
093.735	2.048	+10	−11	13.3
113.694	2.241	+36	− 1	0.2
114.692	3.239	+63	− 3	1.2
116.762	1.357	−24	+ 5	3.3
117.740	2.335	+33	−11	4.2
121.727	2.368	+44	− 2	8.3
129.562	2.297	+34	− 7	16.1
146.618	3.540	+36	−15	0.1
165.551	2.707	+66	+ 2	19.1
169.548	2.751	+69	+ 3	23.0
173.603	2.852	+87	+19	27.1
176.540	1.836	+13	+10	30.0
183.583	0.972	−43	− 4	4.1
188.514	1.950	+ 8	− 5	9.0
189.526	2.960	+54	−16	10.0
191.524	1.006	−51	−12	12.0
203.523	1.145	−16	+21	24.0
204.510	2.132	+39	+11	25.0
205.506	3.128	+77	+ 8	26.0
207.508	1.177	−29	+ 7	28.0
212.517	2.233	+26	−10	0.0
853.681	3.026	+59	−11	13.7
885.579	3.298	+45	−19	12.6
887.602	1.368	−29	0	14.6
901.567	3.474	+71	+15	28.6
915.527	1.620	−24	−11	9.4

The elements were computed by the Russell-Wilsing method (Russell 1902). Although this method is not generally used by investigators of the orbits of spectroscopic binaries, it has many advantages over the least-squares method developed by Schlesinger. In brief, the Russell-Wilsing method consists in the Fourier expansion into a series of sines and cosines of the usual formula for radial velocity resulting from orbital motion. For eccentricities up to about 0.3 the series can be limited to terms in the single and double angle. The constant term plus the four coefficients of the sines and cosines number five and are the unknowns. The constant term is the systemic velocity, and the other four unknowns are simply related to the orbital elements. The computations of the summations in the normal equations are quite straightforward. It should be noted that this is not a method for obtaining differential corrections to assumed elements. The principal advantage is that the separation of e and ω is done without the ambiguity inherent in Schlesinger's method. A useful feature of the method is that a secondary oscillation can be introduced into the observation equation by the addition of further terms, but this is possible only if the secondary period is known.

TABLE 3

RADIAL VELOCITIES OF λ TAURI, MICHIGAN

JD	Phase 4-Day Period (days)	Residual (km/sec)	Phase 33.025-Day Period (days)	JD	Phase 4-Day Period (days)	Residual (km/sec)	Phase 33.025-Day Period (days)
2423000+				2424000+			
743.692	3.431	+ 8	30.5	023.914	2.987	− 9	13.5
770.817	2.884	+ 9	24.6	023.924	2.997	− 4	13.5
770.832	2.899	− 6	24.6	025.911	1.032	+ 4	15.5
770.840	2.907	+20	24.6	025.926	1.047	+ 4	15.5
770.858	2.925	+12	24.7	025.937	1.058	+ 4	15.5
782.705	2.913	+ 5	3.5	026.914	2.035	−16	16.5
782.724	2.932	0	3.5	026.924	2.045	− 9	16.5
782.736	2.944	−16	3.5	027.935	3.056	+10	17.5
786.607	2.861	− 8	7.4	027.945	3.066	− 2	17.5
785.635	2.889	− 9	7.4	031.911	3.079	− 2	21.5
786.660	2.914	−12	7.5	031.926	3.094	+11	21.5
808.742	1.277	+ 3	29.5	033.928	1.143	+ 9	23.5
808.767	1.302	− 9	29.6	033.943	1.158	+ 5	23.5
824.690	1.411	+14	12.4	064.846	0.440	+ 5	21.4
861.881	2.823	− 2	16.6	073.766	1.454	− 3	30.4
2424000+				078.798	2.534	− 6	2.3
014.898	1.876	− 5	4.5	080.807	0.590	− 4	4.3
014.911	1.889	− 1	4.5	081.715	1.498	−19	5.2
014.924	1.902	− 5	4.5	084.858	0.688	− 4	8.4
015.894	2.872	− 2	5.5	085.821	1.651	−21	9.3
015.906	2.884	− 2	5.5	092.784	0.709	+ 7	16.3
015.917	2.895	− 6	5.5	121.689	1.943	− 3	12.2
019.902	2.927	−15	9.5	134.677	3.072	+11	25.2
019.917	2.942	− 3	9.5	157.663	2.339	− 1	15.2

Table 6 is a summary of the elements derived from each group. The Michigan and Victoria velocities were combined into one solution, since the data in each case were not sufficient for a good orbit determination. Actually, separate determinations were made but only to derive the systemic velocity. The two values differed by 2 km/sec, and this was added to all Victoria velocities before they were incorporated into the solution. Figure 1 is a plot of the velocity-curve derived for the Mount Wilson–Lick data. The individual normal points have been corrected for the long-period variation. The mean errors have been estimated. Within the limits of these errors, there appears to be no significant change in the elements with time and, hence, no apparent perturbation in these elements caused by the third body.

IV. THE TREATMENT OF THE RESIDUALS

It will be recalled from the introduction that Schlesinger obtained a period of 34.6 days for the Allegheny residuals, and McLaughlin a period of 30.0 days from his own data. Neither period would satisfy the other set of residuals. Furthermore, neither of these periods will satisfy the Michigan-Victoria or the Mount Wilson-Lick residuals. A period of 30.3 days shows a periodicity for all four groups of residuals taken separately, but no value close to this will give an integral number of periods between all groups.

TABLE 4

RADIAL VELOCITIES OF λ TAURI, VICTORIA

JD	Phase 4-Day Period (days)	v (km/sec)	Residual (km/sec)	Phase 33.025-Day Period (days)
2428000+				
048.010	2.978	+62	− 7	8.5
049.990	1.005	−47	− 6	10.5
067.939	3.142	+76	+ 7	28.4
070.917	2.170	+37	+ 5	31.4
077.940	1.288	−44	−14	5.4
105.888	1.566	− 8	+ 4	0.4
110.805	2.530	+51	− 4	5.3
112.980	0.752	−48	− 8	7.5
126.762	2.676	+78	+17	21.3
140.854	0.957	−39	+ 2	2.4
150.850	3.046	+61	− 8	12.4
196.646	1.403	− 8	+16	25.1
200.639	1.443	− 9	+12	29.1
431.040	2.574	+67	+10	28.3
434.903	2.484	+53	+ 1	32.2
438.990	2.618	+54	− 5	3.3
448.894	0.665	−30	+ 7	13.2
457.972	1.836	+16	+ 8	22.3
459.027	2.891	+79	+11	23.3
461.898	1.810	+17	+11	26.2
462.878	2.790	+81	+16	27.2
474.811	2.865	+65	− 1	6.0
493.745	2.035	+37	+14	24.9
496.956	1.293	−22	+ 8	28.2
497.783	2.120	+34	+ 5	29.0
504.731	1.162	−34	+ 2	2.9
510.847	3.325	+52	−12	9.0
539.705	0.557	−38	− 5	4.9
778.982	2.654	+57	− 3	13.0
785.028	0.795	−36	+ 5	19.0
793.969	1.830	+13	+ 6	28.0
804.994	0.998	−46	− 5	6.0
805.022	1.026	−57	−17	6.0
868.801	1.560	−14	− 1	3.7
2429000+				
196.924:	1.587	−10	+ 1	1.6
295.619	1.456	−23	− 3	1.2

TABLE 5

RADIAL VELOCITIES OF λ TAURI, MOUNT WILSON AND LICK

JD	Phase 4-Day Period (days)	v (km/sec)	Residual (km/sec)	Phase 33.025-Day Period (days)
2434000+				
326.740	0.473	−29.7	−11.3	12.6
.796	0.532	−32.6		
.849	0.582	−35.3		
.893	0.626	−44.4		
.945	0.678	−46.9		
327.733	1.466	−30.3	− 1.6	13.6
.772	1.505	−27.2		
.813	1.546	−20.9		
.853	1.586	−17.1		
.888	1.621	−13.4		
.953	1.686	− 7.1		
350.853	0.868	−40.8	+ 2.0	3.6
351.902	1.917	+ 1.5	− 9.7	4.7
408.618	3.288	+72.5	+ 4.0	28.4
.654	3.324	+74.6		
.695	3.365	+73.2		
.728	3.398	+72.9		
409.616	0.333	+ 0.3	+ 7.6	29.4
.664	0.381	− 0.7		
.714	0.431	− 5.4		
.755	0.472	− 7.9		
410.638	1.355	−28.0	+ 5.1	30.3
674.780	0.652	−24.8	+ 7.1	30.3
.818	0.690	−33.1		
.910	0.782	−34.2		
.968	0.840	−28.4		
703.723	1.925	+25.9	+11.3	26.3
.773	1.975	+19.9		
.816	2.018	+31.9		
.887	2.089	+38.3		
.936	2.138	+40.6		
704.654	2.856	+71.1	+ 5.7	27.2
2435000+				
056.704	3.093	+69.8	− 4.3	16.0
.735	3.124	+66.2		
.764	3.153	+63.6		
.792	3.181	+65.8		
059.720	2.157	+24.4	− 2.0	19.1
.765	2.202	+30.0		
.802	2.239	+32.2		
.840	2.278	+35.3		
.881	2.318	+37.0		
.924	2.361	+40.5		
.966	2.403	+48.2		
060.007	2.445	+46.5		

TABLE 5—*Continued*

JD	Phase 4-Day Period (days)	v (km/sec)	Residual (km/sec)	Phase 33.025-Day Period (days)
2435000+				
139.676	3.049	+74.8	+ 6.7	32.9
.705	3.078	+76.6		
.738	3.111	+83.6		
.776	3.149	+73.2		
141.616	1.036	−44.9	− 0.8	1.9
.654	1.074	−43.0		
.691	1.111	−43.6		
.728	1.148	−44.7		
.770	1.190	−43.4		
142.603	2.023	+14.3	− 3.9	2.9
.625	2.045	+12.9		
.652	2.072	+20.5		
.682	2.102	+23.8		
.712	2.132	+26.7		
.744	2.164	+22.3		
.777	2.197	+32.8		
143.606	3.026	+62.7	− 5.1	3.9
.634	3.054	+67.8		
.661	3.081	+62.8		
.690	3.110	+69.0		
.722	3.142	+63.4		
.744	3.164	+65.9		
.763	3.183	+66.8		
.781	3.201	+64.3		
017.007	2.923	+65.0	− 2.3	9.3
036.798	2.951	+83.6	+15.6	29.1

TABLE 6

ORBITAL ELEMENTS OF THE ECLIPSING PAIR

Source	Mean Date	K_1 (km/sec)	e_1	γ (km/sec)
Potsdam	1902.0	59.1±2.0	0.08±0.05	+20.6±2.0
Allegheny	1910.0	54.4±1.0	.02± .03	+16.2±1.2
Michigan-Victoria	1924.5 (1929.8) 1936.8	55.1±1.0	.08± .03	+17.4±1.5
Mt. Wilson–Lick	1954.2	57.3±1.0	0.12±0.03	+17.8±1.0

After a number of trials a period of 33.025 ± 0.002 days was found which would properly satisfy all the groups. The evidence for this period is seen in Figures 2*a* and 2*b*. The former is a plot, obtained in two ways, of the residuals from von Aretin's data. The upper plot is of the residuals from our orbit, using von Aretin's velocities, and the lower of the residuals from our determination of the Allegheny orbit. Both plots show that there is a maximum around phase 25 days.

Figure 2*b* consists of three plots, one each for the Allegheny, Michigan-Victoria, and Mount Wilson–Lick residuals. The phases are calculated for the same period and zero point as for the Potsdam data. For each set of data a least-squares solution was made for the best sine-curve. This implies that we have adopted an eccentricity of zero for the third body, which is all that can be done, considering the scatter of the residuals. The resulting curve is shown on each of the three plots. Reading from top to bottom, the amplitudes are 11.6, 8.6, and 8.7 km/sec. The phase of maximum velocity is indicated on each curve by a short vertical line. The computed values are, respectively, 26.0, 24.7, and 26.7 days. Within the accuracy of determination, the agreement is considered to be good, and these phases also agree with the maximum from von Aretin's data. There has been no change in period, and our value of 33.025 ± 0.002 days satisfies all the data.

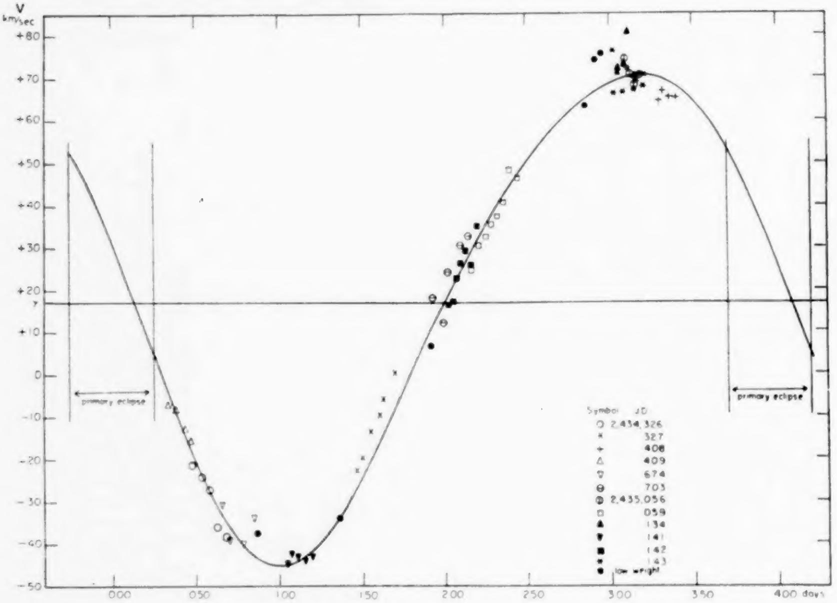

FIG. 1.—Velocity-curve of λ Tauri from Mount Wilson and Lick observations

V. THE DIFFERENCES BETWEEN THE HYDROGEN AND HELIUM VELOCITIES

During the course of the measurements it became apparent that there was a systematic difference between the hydrogen and helium velocities. These differences were ignored in the formation of the velocity for a single spectrogram, where the simple mean was always taken from the individual line velocities. However, if we separate the hydrogen- and helium-line velocities, we find that the differences are dependent on the phase

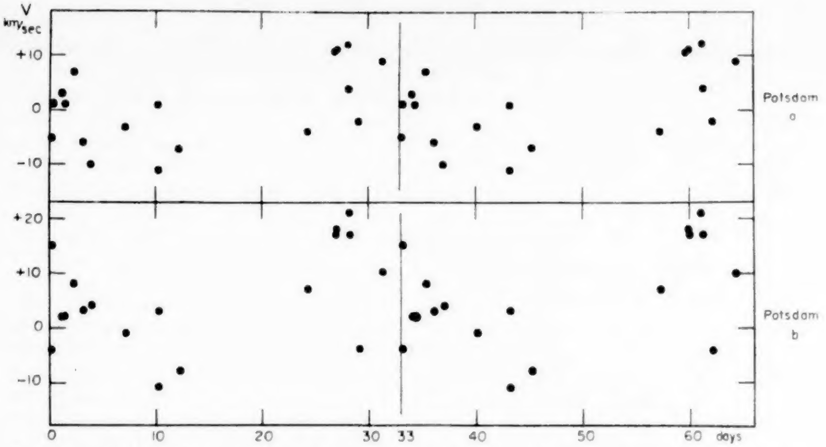

FIG. 2*a*.—Velocity residuals from the Potsdam observations plotted against the period of 33.025 days

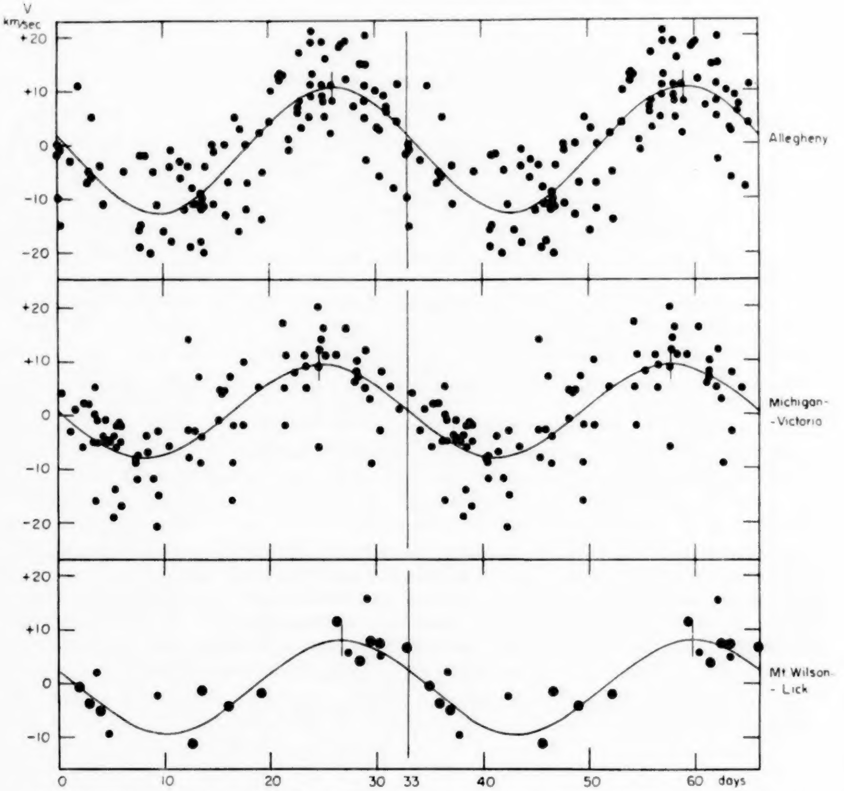

FIG. 2*b*.—Velocity residuals from Allegheny, Michigan-Victoria, and Mount Wilson–Lick observations plotted against the period of 33.025 days.

in the 4-day orbit. Table 7 lists these differences for the supernormals according to phase for the Mount Wilson data. The errors are mean errors.

In the first half of the period, when the bright star is approaching, all the differences are positive, and at least three are statistically significant; while in the latter half, when the star is receding, the values are both positive and negative and generally small, except at phase 2.30 days. The orbital elements, ignoring the long-period variation, are given in Table 8 for the separate velocities of hydrogen plus helium, hydrogen, and helium.

TABLE 7

HYDROGEN MINUS HELIUM DIFFERENCES FOR MOUNT WILSON DATA

Mean Phase (days)	H−He (km/sec)	Mean Phase (days)	H−He (km/sec)	Mean Phase (days)	H−He (km/sec)
0.40	$+12.5\pm1.7$	1.57	$+9.5\pm2.1$	3.10	$+5.4\pm2.5$
0.58	$+10.8\pm1.0$	2.03	$+0.5\pm2.7$	3.12	$+2.4\pm1.1$
0.74	$+5.2\pm2.5$	2.10	-3.0 ± 1.5	3.14	-3.4 ± 1.1
1.11	$+3.1\pm1.6$	2.30	-12.9 ± 1.8	3.34	-1.9 ± 0.7

TABLE 8

SEPARATE ORBITAL ELEMENTS FOR HYDROGEN PLUS HELIUM, HYDROGEN, AND HELIUM

	K_1 (km/sec)	e_1	γ (km/sec)
H+He	57.3	0.12	+17.8
H	55.3	.17	+20.2
He	59.1	0.08	+15.8

TABLE 9

HYDROGEN MINUS HELIUM DIFFERENCES FOR ALLEGHENY AND MOUNT WILSON (KM/SEC)

	$v<(\gamma-20)$	$v=(\gamma\pm20)$	$v>(\gamma+20)$
Allegheny	$+7.8\pm1.5$	-3.0 ± 3.0	-5.1 ± 1.8
Mount Wilson	$+7.7\pm0.9$	-1.3 ± 1.9	-1.7 ± 1.4

This same trend is seen in the Allegheny and Victoria data. The necessary information was not available for the Michigan velocities. Because the data are not so extensive as for Mount Wilson, the Allegheny differences were divided into three groups: $v < (\gamma - 20)$, $v = (\gamma \pm 20)$, and $v > (\gamma + 20)$. Table 9 gives these differences for both Allegheny and Mount Wilson. For the more limited Victoria data, the differences were collected into two groups—below and above the systemic velocity. The results are

$$\mathrm{H} - \mathrm{He} = +3.1 \pm 1.8 \text{ km/sec for } v < \gamma \,,$$

$$\mathrm{H} - \mathrm{He} = -4.3 \pm 1.5 \text{ km/sec for } v > \gamma \,.$$

If the helium velocities give a true picture of the orbital motion, then it would appear that, when the bright star is approaching, hydrogen is streaming into the front surface of the star. When it is receding, the effect is much less pronounced. The large negative residual at phase 2.30 days suggests that the proposed streaming might be erratic at times. It should be stated that on the Mount Wilson spectrograms the hydrogen lines are asymmetrical in the sense that the wing of the line which extends from the position of deepest absorption to the normal, or unshifted, position of the line is the broadest. The effect is what would be produced by the fainter lines of a secondary component. Schlesinger made the same observation, except that he stated that this was also true for the helium lines. This latter is not obvious from the Mount Wilson spectrograms. Evidence for the spectrum of the secondary component will be given in the next section.

In view of the differences in the orbital elements from the hydrogen plus helium, hydrogen, and helium velocities, it was felt desirable to make a determination of the elements with only the Mg II 4481 velocities. Its velocity was never included in the mean plate velocities. Of the 350 Mount Wilson spectrograms, this line could be measured on 167 spectrograms. All are on spectrograms taken on 13 nights. The measures were grouped into thirteen means, and the number of measures in each mean varied from five to twenty-seven. Weighted and unweighted solutions were made for the orbital elements, with little difference between them. The results are $\gamma = +21$ km/sec, $K_1 = 67$ km/sec, and $e = 0.26$. In spite of the small amount of data, the value of K_1 seems to be significantly larger than that for hydrogen plus helium, hydrogen, and helium, but e is poorly determined and of little weight.

VI. THE SATELLITE LINES AND THE MASS RATIO

Although Schlesinger reports no lines due to the secondary component, McLaughlin measured numerous "satellite lines" on spectrograms of the same dispersion. His report of their behavior suggests that some of the strong lines are accompanied on the red and violet sides by faint lines, such that the violet line always has a velocity about 200 km/sec less than the strong line and the red satellite gives a velocity about 200 km/sec greater than the strong line. This gives rise to three velocity-curves: one derived from the strong lines, a second one from the red satellites displaced upward by 200 km/sec, and the third below that of the strong lines by 200 km/sec. All three velocity-curves are in phase with one another. The physical explanation of this result is obscure.

Neither the Allegheny nor the Mount Wilson spectrograms show any secondary lines. However, a number of the Victoria spectrograms, most of which are of high quality and high dispersion, show faint lines accompanying the strong lines. In almost every case these lines are too faint to be measured. However, on eleven Victoria spectrograms. Mg II 4481 is clearly double, with one component about three times as strong as the other. Five of these spectrograms were taken in the phase interval 0.0–2.0 days when the star is approaching, and six in the other half of the cycle when the bright star is receding. All these plates are concentrated around the times of maximum velocity of approach or recession. On all five spectra taken when the bright star is approaching, the stronger component of Mg II 4481 is on the violet side of the fainter component, and the reverse is true for the other six. This is clear evidence that the fainter component arises from the secondary star in the eclipsing system. The separations in kilometers per second between the components of Mg II 4481 are listed in Table 10. The resultant mass ratio of the brighter star to the fainter one is $m_1/m_2 = 4.0$. Admittedly, this is a rough determination, but it is not without value. The fact that the fainter component of Mg II 4481 is present probably means that the spectrum of the eclipsing star at primary minimum is of type late B or early A. This secondary spectrum would account for the asymmetry of the strong lines.

VII. SOME REMARKS ON THE PHOTOMETRIC DATA

The mass functions of the two orbits and the values of $a \sin i$ have not been significantly changed by our new results. We may, therefore, use McLaughlin's results, which are listed in the "Fifth Catalogue of Spectroscopic Binaries" by J. H. Moore and F. J. Neubauer:

$$f_1(m) = 0.072\ \odot, \quad \text{4-day orbit;}$$

$$f_2(m) = 0.0020\ \odot, \quad \text{30-day orbit;}$$

$$a_1 \sin i_1 = 3.037 \times 10^6\ \text{km}, \quad \text{4-day orbit;}$$

$$a_2 \sin i_2 = 3.540 \times 10^6\ \text{km}, \quad \text{30-day orbit.}$$

It is at once apparent that any attempt to reveal the presence of the third body by means of a periodic displacement of the time of primary minimum due to light-time can hardly succeed, since the light-time is only about 10 seconds.

TABLE 10

SEPARATION OF Mg II 4481 COMPONENTS

JD	Phase in Days (4.0-Day Period)	Separation (km/sec)	m_1/m_2	JD	Phase in Days (4.0-Day Period)	Separation (km/sec)	m_1/m_2
2428000+				2428000+			
049.990	1.00	+272	3.4	419.980	3.37	−213	3.2
067.939	3.14	−272	4.1	462.878	2.79	−246	4.3
077.940	1.29	+250	3.6	504.731	1.16	+253	3.0
126.762	2.68	−230	4.5	2429000+			
140.854	0.96	+253	3.1	225.830	2.82	−248	4.3
196.646	1.40	+282	4.8	288.699	2.44	−219	6.3

It is of interest that the values of $a_1 \sin i_1$ and $a_2 \sin i_2$ are so nearly alike. Since the close pair—both components of which are visible in the spectrum—shows eclipses, we may assume that i_1 is close to 90°. The distant star is invisible, and i_2 is unknown. But if the orbits are co-planar, or nearly so, then the mass ratio $(m_1 + m_2)/m_3$ must be large, perhaps of the order of 10, in order to remove the third body to a sufficiently great distance from the pair 1-2. Otherwise, there would be appreciable perturbations. This suggests that star 3 has a mass of the order of that of the sun or somewhat less; the masses of the components of the close pair are given by the mass function,

$$\frac{m_2^3}{(m_1 + m_2)^2} \sin^3 i = \frac{m_2}{(1 + \alpha)^2} = 0.072\odot\,,$$

where $\alpha = m_1/m_2 = 4.0$. Thus $m_2 = 1.8\ \odot$ and $m_1 = 7.2\ \odot$. Even if i_1 is slightly smaller than 90° (Stebbins gives $i_1 = 78°$), the total mass of the close pair is probably about 10 $\odot$. For the pair (1 + 2)-3 we have the expression

$$\frac{m_3^3}{(10 + m_3)^2} \sin^3 i_2 = 0.002\odot\,.$$

Assuming co-planar orbits, $\sin^3 i_2 = 1$. Hence $m_3 = 0.7\ \odot$. But if $i_2 < 90°$, the mass m_3 may well be equal to 1 $\odot$. It is thus entirely reasonable to conclude that m_3 is relatively distant from the close pair.

If i_2 is very much smaller than $90°$ and m_3 is considerably larger than $1\,\odot$, its distance from the close pair becomes unreasonably small, in view of the absence of perturbations. It is thus probable that the two orbits are approximately co-planar and that the triple star in this respect is similar to the solar system.

The only photoelectric light-curve of this eclipsing binary which is known to the authors is that of Stebbins. The primary minimum is quite sharp, with a depth of about 0.5 mag., and the well-marked secondary minimum has a depth slightly greater than 0.1 mag. The light-curve shows a continuous change in light between the two minima, and the eclipse is partial.

Starting with von Aretin, attempts have been made to show a periodic shift in the time of primary minimum. Hellerich (1922) gives the formula for the time of primary minimum as follows:

$$\mathrm{JD}\ \underset{\pm 100}{2399607.5383} + \underset{\pm 34}{3\overset{d}{.}9529452E} - \underset{\pm 87}{0\overset{d}{.}0255} \sin(0.2637E + \underset{\pm 20}{59\overset{\circ}{.}1}).$$

The figures given under the equations are mean errors. Most of the data used in deriving the formula were visual observations. The amplitude seems to be barely significant. The amplitude of the oscillation is 37 minutes, and the period is 14.9 years. If this oscillation is due to apsidal motion, then the eccentricity of the orbit must be about 0.02, which, although rather smaller than most of our determinations, is not unreasonable in view of the precision of Hellerich's amplitude and the precision of our own determinations.

One other investigation of interest here is that of Nikonov (1938). He redetermined the basic period and obtained 3.9529507 days, very close to Stebbins' value. From this it would appear that there has probably been no significant change in this period.

Mr. Ebbighausen wishes to express his thanks to Dr. D. H. Menzel, director of the Harvard College Observatory, for the hospitality offered him during the academic year 1955–1956 when he was a Visiting Fellow in General Education at Harvard University under the auspices of the Carnegie Foundation.

REFERENCES

Aretin, E. F. von. 1913, *Göttingen Astr. Mitt.*, **15**, 1.
Belopolsky, A. 1898, *A.N.*, **145**, 281.
Hellerich, J. 1922, *A.N.*, **216**, 97.
McLaughlin, Dean B. 1937, *Pub. U. Michigan*, **6**, 3.
Nikonov, V. B. 1938, *Bul. Abastumanskaia Astr. Obs.*, **2**, 29.
Russell, H. N. 1902, *Ap. J.*, **15**, 254.
Schlesinger, F. 1916*a*, *Pub. Allegheny Obs.*, **3**, 23.
———. 1916*b*, *ibid.*, p. 167.
Stebbins, J. 1920, *Ap. J.*, **51**, 193.

THE DISTRIBUTION OF LATE M-TYPE STARS ALONG THE GALACTIC EQUATOR

J. J. Nassau, V. M. Blanco, and D. M. Cameron
Warner and Swasey Observatory of the Case Institute of Technology

Received June 8, 1956

ABSTRACT

An extension of the infrared survey of M5 and later stars in the Milky Way is given. The previous survey was confined to a zone 4° wide centered at the galactic equator. The present investigation extends it to a zone 12° wide. In the new areas surveyed, the surface distribution of 4953 stars of type M5 or later shows a gradual diminution in their number as the anticenter of the Galaxy is approached. A similar distribution was obtained for the 941 stars of class M7 and later. The average number of late M stars per square degree in the zone 12° wide is 2.9. In the direction of the anticenter the corresponding number is 1.5. A catalogue of all the late M-type *BD* stars is given.

INTRODUCTION

This report deals with an extension of the survey of the late M-type stars along the galactic equator from $l = 333°$ to $l = 201°$. The previous investigation (Nassau and Blanco 1954*b*) was confined to a zone 4° wide, centered at the galactic equator, while the present extends it to a zone 12° wide. Carbon and S-type stars and suspected M supergiants which were considered in the previous survey are not included. They will be discussed later. The two catalogues of *BD* stars given here, together with a similar catalogue for the central zone already published, furnish complete spectral data of *BD* M5 and later stars in the galactic zones surveyed. It should be recalled in this connection that many of the late M-type stars are variable with variable spectra; hence it is not possible to claim completeness.

DATA

To cover the additional area of the sky, two sets of overlapping plates were taken. The plates of zone *a* were centered at $b = +4°$, and those of zone *b* at galactic latitude of $-4°$. Each of these zones is approximately 4° wide. The distance between centers of plates for each zone was $3\overset{\circ}{.}5$, and, since their diameter is $5\overset{\circ}{.}2$, a complete coverage with generous overlaps was obtained for the two zones.

As in the previous survey, the 2° objective prism was used. All exposures, with the exception of regions of declination of $-10°$ or less, were of 5 minutes' duration. The estimated limiting infrared magnitude of the survey is about 10.2. The complete 12°-wide zone was also covered by plates taken with the 4° objective prism and with a basic exposure of 10 minutes. On each of these plates two additional short exposures were taken to permit the classification of the brighter stars. As a rule, these plates reach M stars somewhat fainter than 10.2 infrared mag.

THE DISTRIBUTION OF THE LATE M STARS

All stars of spectral classes M5–M10 were marked on the 2° objective-prism plates. The total numbers for the two zones are given in Table 1. In deriving these figures the actual counts were adjusted for the effects of overlapping plates. Since the distribution in longitude for the two zones was found to be about the same, Figure 1 shows a combined distribution. A gradual diminution in the number of M stars as the anticenter of the Galaxy is approached is apparent. Discontinuities, however, exist which are usually associated with known obscurations. Similar results were obtained for the M stars of the central zone as were pointed out in the previous paper. For the sake of completeness, the stars of the three zones are combined and their distribution shown in Figure 2. The number of late M stars in the central zone is given in Table 1.

The classification of M-type stars from infrared objective-prism spectra is based on Mount Wilson Standards (Adams, Joy, and Humason 1926) and has proved satisfactory for classes M0 through M6 (Nassau and van Albada 1949). The progressive strengthening of the titanium oxide bands provides the criteria. However, the classification of very late M stars, M7 and later, has been found unsatisfactory for several reasons. A system of classification for these late-type stars has been proposed by Cameron and Nassau

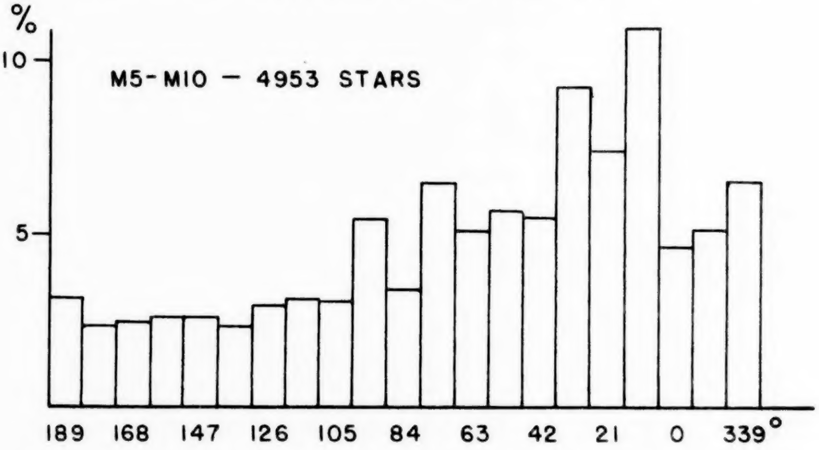

FIG. 1.—The distribution of M5–M10 stars for zones *a* and *b* combined. Each interval includes 10°.5 in longitude.

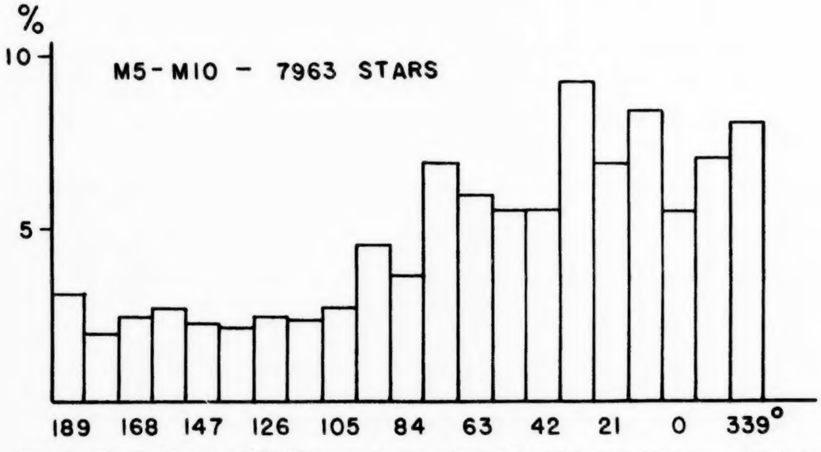

FIG. 2.—The distribution of M5–M10 stars for the galactic belt of 12° width. Each interval includes 10°.5 in longitude.

(1955) which is based primarily on the progressive strengthening of the vanadium oxide bands. The stars of class M7 begin to show these bands, and they increase in strength with later classes. These very late M stars have been given a distinct marking, as they were detected in zones *a* and *b*. Table 1 gives the number of such stars contained in each of the two zones. The published data (Nassau and Blanco 1954*b*) for the central zone (the M7–M10 stars are called "M's with VO" in the Nassau and Blanco paper) cannot be compared with the numbers of the outer zones, as the classification of the very late M stars did not follow the same system. For this reason the distribution in longitude given in Figure 3 includes only the stars of zones *a* and *b*. No marked difference from that of all the M5–M10 stars is apparent. That is, the gradual decrease in number of stars as the direction of the anticenter is approached is shown. It is interesting to compare the numbers of M stars found near the galactic plane with those observed in the direction of the galactic poles. An unpublished study by W. Wehlau of a region covering 300 square degrees in the vicinity of the north galactic pole shows a total of eleven stars of type M5 or later brighter than the limiting magnitude of the Milky Way plates. Long-exposure plates taken within this region indicate that this number does not increase with distance. Seven of these stars are *BD* objects and are within a limiting distance of 1 kpc from the galactic plane. These figures strengthen the hypothesis that the giant M stars have a disklike distribution in the Galaxy. The average number of late M stars per square degree in the zone 12° wide is 2.9. In the direction of the anticenter the corresponding number is 1.5.

TABLE 1

NUMBER OF STARS IN THE ZONES

	Zone *a*	Zone *b*	Central Zone		Zone *a*	Zone *b*	Central Zone
M5–M10....	2319	2634	3010	M7–M10...	446	495	....

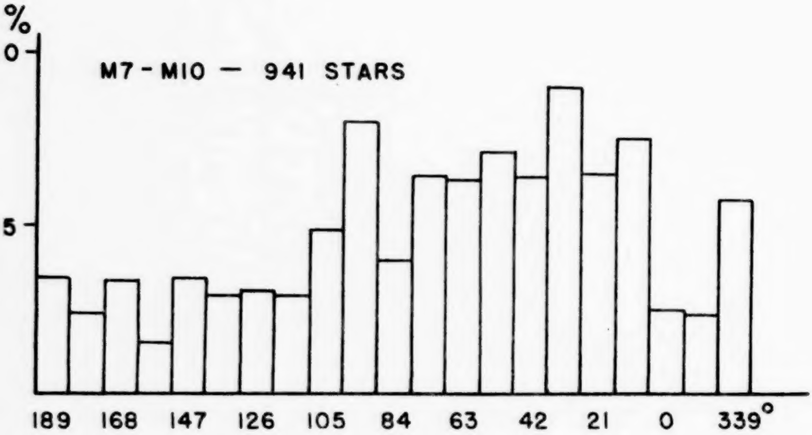

FIG. 3.—The distribution of M7–M10 stars for zones *a* and *b* combined. Each interval includes 10°.5 in longitude.

TABLE 2

LATE M-TYPE BD STARS - ZONE a

No.	B.D.		1900				m	Sp	l	b	Remarks
1	+65°	179	1^h	$\overset{m}{27.8}$	+65°	17′	8.8	M6	95°	+4°	
2	+64	208	1	32.0	+65	01	8.9	M6	95	4	
3	+63	312	2	10.6	+63	25	9.5	M6	100	3	
4	+65	267	2	24.1	+66	03	9.4	M5	100	6	
5	+62	461	2	38.8	+62	35	9.4	M7	103	4	CQ Cas, I
6	+57	756	3	47.9	+57	23	9.1	M6	113	4	
7	+48	1136	4	36.8	+48	34	9.5	M6	125	3	431
8	+51	980	4	43.1	+52	04	8.6	M5:	123	6	
9	+45	1002	4	48.4	+45	57	9.5	M6	128	3	
10	+42	1180	5	01.8	+42	27	8.8	M6	132	3	
11	+39	1225	5	08.3	+40	01	8.8	M5	135	2	UZ Aur, M4, I
12	+42	1239	5	11.1	+42	41	6.0	M5:	133	4	524
13	+40	1250	5	12.9	+40	53	8.8	M5	135	3	
14	+44	1187	5	15.3	+44	34	9.5	M6	133	6	
15	+38	1168	5	22.1	+38	58	9.5	M6.5	137	4	AD Aur, M6, I
16	+32	1050	5	30.8	+32	15	9.2	M5	144	1	
17	+37	1300	5	37.3	+37	57	9.5	M5	140	6	
18	+27	933	5	52.5	+27	50	9.5	M5:	150	3	
19	+29	1068	5	53.8	+29	14	9.5	M5	149	4	BO Aur, SR
20	+25	1097	5	57.7	+25	05	9.0	M5	153	3	
21	+25	1112	5	59.5	+25	53	9.3	M5	153	4	
22	+26	1101	6	03.1	+26	33	9.5	M6.5	152	5	
23	+22	1199	6	03.9	+22	59	9.5	M5	156	3	
24	+26	1131	6	06.1	+26	22	9.5	M5.5	153	5	
25	+17	1187	6	09.7	+17	47	9.0	M5	161	2	
26	+21	1185	6	12.2	+21	08	9.5	M5.5	158	4	
27	+17	1236	6	19.4	+17	04	9.5	M7	163	4	GN Ori, M
28	+15	1236	6	27.4	+15	54	9.0	M6.5	164	5	
29	+14	1350	6	30.2	+14	16	9.4	M5	166	5	DY Gem, M, SR
30	+13	1349	6	33.6	+13	29	9.5	M6	167	5	
31	+ 6	1377	6	40.5	+06	32	9.3	M5	174	3	
32	+12	1305	6	43.6	+12	18	9.1	M6.5	170	7	FK Gem, M7, I
33	+ 4	1476	6	46.7	+ 4	53	7.9	M6.5	176	4	SX Mon, M6, SR?
34	+ 0	1689	6	49.0	+ 0	55	9.4	M6.5	180	2	898, L
35	+ 3	1452	6	49.1	+ 3	01	9.2	M6	178	3	
36	- 1	1503	6	56.2	- 2	01	9.5	M5	184	3	
37	+ 0	1814	7	03.2	+ 0	13	9.4	M5.5	183	5	
38	- 3	1772	7	05.3	- 3	38	9.9	M5:	186	4	
39	- 6	1977	7	07.0	- 6	46	9.5	M5	189	3	
40	- 3	1800	7	08.8	- 3	47	9.0	M6.5	187	5	
41	-10	1983	7	14.6	-10	44	8.9	M6	194	2	
42	-12	1936	7	19.1	-12	57	9.4	M5	196	2	
43	- 7	1946	7	20.4	- 7	42	9.8	M5.5	192	5	1042, M
44	- 8	1913	7	21.6	- 8	43	9.5	M6	193	5	1047, L?
45	- 9	2060	7	23.0	- 9	22	9.4	M5	193	5	
46	- 7	4569	18	04.9	- 7	23	9.5	M7	349	4	
47	- 2	4585	18	12.1	- 2	30	9.7	M6.5:	355	5	
48	+ 6	3849	18	30.1	+ 6	59	9.5	M6	5	5	V851 Oph, M4, SR
49	+ 8	3780	18	33.7	+ 8	44	8.6	M9	7	5	X Oph, M6e, M
50	+ 9	3809	18	35.3	+ 9	53	8.0	M6	8	+6	101752, M5e

TABLE 2

LATE M-TYPE BD STARS - ZONE a (Cont'd.)

No.	B.D.		1900				m	Sp	l	b	Remarks
51	+ 8°	3835	18^h	40.9^m	+ 8°	38′	9.0	M5	8°	+4°	T Aql, M5, I ?
52	15	3579	18	44.8	15	48	9.5	M5:	15	7	
53	11	3649	18	48.2	11	34	9.5	M5:	11	4	VW Aql, M5, I
54	16	3696	18	56.0	16	51	9.5	M5	17	4	
55	20	4027	18	58.6	20	34	9.5	M7	20	6	
56	22	3659	19	15.2	22	51	9.3	M6	24	3	
57	22	3660	19	15.3	22	23	7.7	M6:	24	3	
58	30	3564	19	22.8	30	35	9.1	M6	32	6	
59	33	3507	19	31.3	33	35	7.5	M6:	35	5	
60	33	3546	19	36.0	33	41	9.3	M5	36	5	
61	35	3810	19	44.3	35	10	9.4	M5p	38	4	
62	37	3622	19	45.5	37	07	9.4	M6.5	40	5	
63	36	3812	19	56.8	36	52	9.0	M5	41	3	
64	39	3997	19	57.2	39	54	9.3	M6.5	43	4	AH Cyg, M5, SR
65	40	4001	20	00.9	40	09	9.5	M7	44	4	GN Cyg, M5, SR
66	43	3490	20	03.7	43	24	9.4	M5	47	5	
67	40	4065	20	09.7	40	31	9.4	M5	45	3	
68	46	2892	20	12.8	46	36	9.5	M5	51	6	
69	47	3096	20	21.0	47	24	9.3	M5	52	5	
70	46	2998	20	35.7	46	28	9.5	M5	53	3	
71	50	3186	20	41.9	50	35	9.5	M6	57	4	
72	50	3217	20	48.9	50	55	9.4	M6	58	4	
73	54	2511	21	15.2	54	51	9.5	M6.5	63	4	
74	54	2517	21	16.7	55	02	7.2	M6:	64	4	
75	64	1710	22	42.1	65	13	9.5	M6	78	6	
76	+63	1954	23	10.6	+63	40	9.5	M6.5	80	+3	

TABLE 2a

BD STARS WITH A LATE M COMPANION - ZONE a

No.	B.D.		1900				m	Sp	l	b
1	+20°	1365	6^h	12.9^m	+20°	06′	9.5	M7	159	+3
2	-17	4970	17	51.9	-17	07	9.2	M6	21	2
3	+11	3631	18	45.8	+11	16	9.5	M6	10	4
4	+ 9	3922	18	50.0	+ 9	46	9.5	M5	10	2
5	+38	3762	19	44.6	+38	35	9.5	M8	41	+6

Notes: 20° 1365 - M star 15" east of blue star; -17° 4970 - M star about 20" of arc south of blue star; 11° 3631 - M star 10" west of blue star; 9° 3922 - M star 17" north-west of blue star; 38° 3762 - M star 20" south-east of blue star.

TABLE 3

LATE M-TYPE BD STARS - ZONE b

No.	B.D.		1900				m	Sp	1	b	Remarks
1	$+58^\circ$	127	0^h	46.4^m	$+59^\circ$	11′	8.8	M6	91°	-3°	
2	+55	224	0	55.0	+56	05	9.1	M6	92	6	
3	+56	194	1	00.4	+57	02	9.5	M5	93	5	
4	+56	229	1	09.1	+56	50	9.5	M5	94	5	
5	+57	237	1	12.0	+57	16	7.0	M6:	94	5	
6	+51	629	2	40.9	+51	54	8.5	M6	108	6	
7	+53	580	2	45.2	+53	37	8.9	M5	108	4	
8	+54	622	2	49.6	+54	15	9.2	M6.5	108	3	ER Per, M8, SR
9	+48	928	3	22.1	+48	24	9.5	M6	116	5	
10	+48	986	3	37.9	+48	41	9.5	M5	118	4	
11	+44	806	3	45.6	+44	47	9.5	M8	121	6	
12	+42	898	4	01.4	+42	09	9.3	M6.5	125	6	
13	+41	824	4	04.0	+41	57	8.5	M5	126	6	SW Per, M5, SR
14	+42	935	4	11.1	+42	29	9.3	M5	126	4	
15	+40	933	4	13.2	+40	50	9.2	M6.5	127	5	
16	+41	871	4	20.1	+41	18	9.5	M5	128	4	
17	+39	1046	4	34.6	+40	00	9.5	M6	131	3	HO Per, M7, I
18	+40	1022	4	34.7	+40	18	9.5	M6	131	3	
19	+32	890	5	00.9	+32	47	9.1	M5	140	3	
20	+30	786	5	01.1	+30	39	9.0	M5	142	4	
21	+24	815	5	13.0	+24	40	9.5	M6.5	148	6	532
22	+21	912	5	32.1	+21	50	9.0	M5	153	4	
23	+18	915	5	36.1	+18	29	9.0	M5	156	5	DY Tau, M2, I
24	+21	940	5	36.5	+21	58	9.5	M6	153	3	
25	+18	984	5	44.6	+18	54	9.4	M5	157	3	BD star is double, M star has smaller R.A.
26	+10	979	5	56.1	+10	55	9.5	M7	165	4	DP Ori, M6, I?
27	+10	1005	6	00.9	+10	10	9.4	M6	166	4	
28	+11	1028	6	01.7	+11	49	9.1	M5	165	3	
29	+ 5	1113	6	04.0	+ 5	18	9.4	M6	171	5	
30	+ 2	1196	6	15.8	+ 2	37	7.8	M5:	175	4	
31	- 2	1581	6	17.8	- 2	09	var	M8	179	6	V Mon, M5e, M
32	- 2	1596	6	20.0	- 2	55	9.1	M5:	180	6	
33	- 5	1699	6	30.9	- 5	18	9.2	M6.5:	184	4	GL Mon, Mc, SR
34	-14	1681	6	56.0	-14	12	9.8	M6.5	194	3	RV CMa, M6, I
35	-16	1709	6	56.7	-16	59	9.7	M5:	196	4	
36	-20	4986	18	00.6	-20	23	9.0	M5	337	1	
37	-21	4940	18	12.3	-21	37	9.6	M6	338	4	
38	-12	5123	18	32.5	-12	27	9.9	M6.5	348	4	
39	- 5	4748	18	40.4	- 5	42	9.6	M5	355	3	4355
40	- 2	4786	18	50.9	- 2	45	9.8	M5	359	4	
41	+ 2	3825	19	08.9	+ 2	27	8.8	M6	6	5	V842, Aql, M7, I
42	+ 8	4051	19	15.6	+ 9	02	9.5	M6.5	12	4	
43	+ 9	4142	19	27.7	+ 9	48	9.1	M5	14	6	
44	+15	3891	19	34.3	+15	30	9.2	M5	20	4	
45	+15	3937	19	42.1	+15	47	9.5	M6	21	6	V830 Aql, M2, I
46	+21	3966	19	49.8	+21	22	9.2	M5	27	4	
47	+25	4035	19	53.1	+25	27	9.5	M6	31	3	
48	+32	3852	20	27.7	+32	12	9.0	M6:	41	5	AI Cyg, M5, I
49	+35	4211	20	37.0	+36	00	9.5	M5	45	4	
50	+36	4211	20	40.1	+36	31	9.0	M6:	46	-4	

TABLE 3

LATE M-TYPE BD STARS - ZONE b (Cont'd.)

No.	B.D.		1900				m	Sp	l	b	Remarks
51	+36°	4272	20^h	$46^m.6$	+36°	42′	8.6	M6:	47°	-5°	
52	37	4101	20	50.7	37	55	8.9	M5	48	5	
53	43	3790	20	58.6	44	01	9.5	M5	54	2	V354,Cyg, M6, SR
54	39	4457	21	05.6	39	57	9.1	M5:	52	6	
55	43	3827	21	07.2	43	46	9.5	M6	55	3	V579 Cyg, M5, I
56	45	3483	21	13.8	45	17	9.4	M6	56	3	V590 Cyg, M5, I
57	46	3338	21	25.9	46	31	9.4	M5	59	4	
58	45	3583	21	29.5	46	02	9.5	M6	59	4	
59	47	3563	21	45.2	47	29	9.5	M6	62	5	
60	45	3700	21	47.2	46	08	9.4	M6	61	6	
61	47	3658	21	57.3	48	04	9.4	M6.5	64	6	
62	48	3582	21	58.0	48	15	9.4	M7	64	6	GY Cyg, M3, I
63	50	3571	22	03.7	50	29	9.0	M6	66	4	
64	51	3283	22	08.2	51	44	8.8	M5:	67	4	
65	+55	3011	23	40.0	+55	55	8.6	M5	82	-5	

TABLE 3a

BD STARS WITH A LATE M COMPANION - ZONE b

No.	B.D,		1900				m	Sp	l	b
1	- 8°	4755	18^h	$48^m.8$	- 8°	15′	9.7	M6	6°	-6°
2	+ 8	4090	19	20.2	+ 8	49	9.4	M6:	13	5
3	+15	3890	19	34.3	+15	57	9.3	M7	20	4
4	+22	3840	19	48.2	+22	12	8.0	M6.5	27	4
5	+51	3348	22	17.5	+51	18	9.2	M6.5	68	5
6	+52	3237	22	28.4	+52	43	8.7	M6.5:	71	-4

Notes: -8° 4755 - Three stars within 20" of arc; 8° 4090 - M and A star are 10" apart, M star south of A star; 15° 3890 - M and A star are 15" apart; 22° 3840 - M star about 15" south of A star; 51° 3348 - M star is 8" west of blue star; 52° 3237 - M star is about 8" south-west of blue star.

Since a great percentage of stars of classes M7 and later are either long-period variables or Mira type (Cameron and Nassau 1956), their distribution in the Milky Way is of considerable interest. For this reason, particular attention was paid to the possible clusterings of these stars. In the 12°-wide galactic zone no apparent clusterings were in evidence. In addition, a region which extended to galactic latitude ±18° was examined. It was in the form of a rectangle at longitude 6°.5 containing 385 square degrees (see Fig. 4, Nassau and Blanco 1954*b*). The uniform surface distribution of stars of class M5 and later did not differ from that of M7–M10 stars.

A list of bright late M stars in the central zone has been published by Nassau and Blanco (1954*a*). It included 121 *BD* stars and 263 non-*BD* stars. Tables 2 and 3 give a similar list for the *BD* stars in zones *a* and *b*, respectively. The spectral classes were secured from 4° spectral plates, and they were classified on the basis of the system proposed by Cameron and Nassau (1955). The description of the columns in these tables is as follows: Column 1, the Warner and Swasey Observatory number of the star; column 2, the *BD* number; columns 3 and 4, the co-ordinates for the epoch of 1900; column 5, the *BD* magnitudes; column 6, the spectral class secured from our plates; columns 7 and 8, the galactic co-ordinates; and column 9, under "Remarks" the known variables are indicated. The variable-star designation, spectral class, and type of variability are obtained from the *General Catalogue of Variable Stars* (Kukarkin and Parenago 1948) and its supplements. The notations used for type of variability are the same as given by Nassau and Blanco (1954*a*). When a number alone or a number followed by type of variability or spectral class is given, the number refers to the *Catalogue of Stars Suspected of Being Variable* (Kukarkin, Parenago, Efremov, and Kolorov 1951). Table 2*a* gives the *BD* stars in zone *a* which have late M companions. Similar data are given for zone *b* in Table 3*a*.

REFERENCES

Adams, W. S., Joy, A. H., and Humason, M. L. 1926, *Ap. J.*, **64**, 225.

Cameron, D. M., and Nassau, J. J. 1955, *Ap. J.*, **122**, 177.

———. 1956, *ibid.*, **124**, 346.

Kukarkin, B. V., and Parenago, P. P. 1948, *General Catalogue of Variable Stars* (Moscow: Academy of Sciences U.S.S.R.).

Kukarkin, B. V., Parenago, P. P., Efremov, U. E., and Kolorov, P. N. 1951, *Catalogue of Stars Suspected of Being Variable* (Moscow: Academy of Sciences U.S.S.R.).

Nassau, J. J., and Blanco, V. M. 1954*a*, *Ap. J.*, **120**, 118.

———. 1954*b*, *ibid.*, p. 464.

Nassau, J. J., and van Albada, G. B. 1949, *Ap. J.*, **109**, 391.

NEW MEMBERS OF THE ASSOCIATION VI CYGNI*

D. H. SCHULTE
Yerkes Observatory

Received May 11, 1956

ABSTRACT

Further observations of the heavily obscured O-association VI Cygni have been made with the 82-inch McDonald Observatory reflector; photoelectric and spectroscopic results confirm the previous suspicion that a number of fainter stars are early-type members of this association. Some rather long-exposure plates of the region are here presented, showing stars of fainter limiting magnitudes; these plates were taken by the use of low-dispersion, slitless-spectrograph techniques and show the same effect of interstellar reddening as was seen with low-dispersion, objective-prism plates.

INTRODUCTION

The O-association VI Cygni, discovered by Münch and Morgan (1953), is an interesting one, largely because of the very high values of interstellar absorption displayed by its members. Johnson and Morgan (1954) found values of the total absorption to be as high as 6 or 7 mag. for the eleven members which were easily accessible to spectroscopic observations, and more recently Morgan, Johnson, and Roman (1954) discussed the extreme amount of reddening in star No. 12, another obvious member of early type of the association. The interstellar complexity of this region may be emphasized by the fact that the center of VI Cygni is at $\alpha = 20^h32^m$, $\delta = +41^\circ$ (1950), while $\alpha = 20^h27^m \pm 3^m$, $\delta = 40^\circ.5 \pm 1^\circ$ (1950) is the position given by Piddington and Minnett (1952) for the center of the extended radio source Cygnus X. Baade and Minkowski (1954), in their investigation concerning the optical identification of radio sources, found in this region no peculiar emission nebulosities that were similar to those associated with the Cassiopeia and Cygnus A sources, but they do not rule out the possibility that such a nebulosity might be optically obscured. The very high obscuration in this association, with its consequently high selective absorption/wave-length gradient, makes the process of using very low-dispersion objective-prism spectra to find reddened early-type members a quite efficient one. Morgan, Meinel, and Johnson (1954) used a 2-inch $f/4$ Schmidt camera with an objective prism giving spectra (unwidened) about 100–200 μ in length; in this way they published a finding list of seven probable members of early type. A later paper (Schulte 1956) discussed the use of a 6-inch, $f/16$ objective-prism, Newtonian reflector combination. Most of the Morgan-Meinel-Johnson stars seemed to be confirmed with this program; in addition, it was possible, from plates made in good seeing conditions, to identify nine additional suspected members, some of which seemed to be as much as 1 mag. (visual) fainter than the previous group of seven; contributing factors to this fainter limit were the reduction in the sky background and the smaller effect of plate graininess on the variation in shape of individual spectral images. It was with the last two groups of stars mentioned that the 82-inch observations were primarily concerned.

THE OBSERVATIONS

Photoelectric measurements were made on the nights of September 9–10 and 17–18, 1955, with the 82-inch McDonald reflector. The Harris Cassegrain photometer was used, refrigerated with dry ice. Extinction coefficients were determined for each night from two cluster standards; star No. 9 was picked as the red standard, and the anonymous star between Nos. 14 and 17 was used for the blue standard. The extinction coefficients did not vary appreciably for the two nights. To convert the natural colors C_{y0} and C_{u0} to $(B - V)$ and $(U - B)$ colors, two primary standards from the list of Johnson and

---

* *Contributions of the McDonald Observatory*, No. 270.

Harris (1954), 10 Lacertae and HR 8832, were observed. The results of the photometry are summarized in Table 1. These stars are plotted on the two-color diagram of Figure 1. The main-sequence and yellow giant stars are all taken from the list of one hundred and eight photometric standard stars of Harris and Johnson (1954). The other stars are all in Cygnus: the open circles are the seven stars discussed by Johnson and Morgan as reddened O5–O7 stars in the Cygnus rift. The half-filled circles are all stars in VI Cygni—Nos. 1, 2, 3, 4, 6, 8D, and 10 (*bottom halves filled*) and the stars in Table 1 (*top halves filled*). Of the newly investigated stars, it will be seen that Nos. 14–17 fall near the region in the diagram of the known VI Cygni members having spectral types from O5 to B1. An exception is No. 13, which from the photoelectric data would seem to be a main-sequence star near spectral class K. The 80 per cent ratio of successful selection of early-type stars to the total number is therefore as good as it was hoped the method would yield.

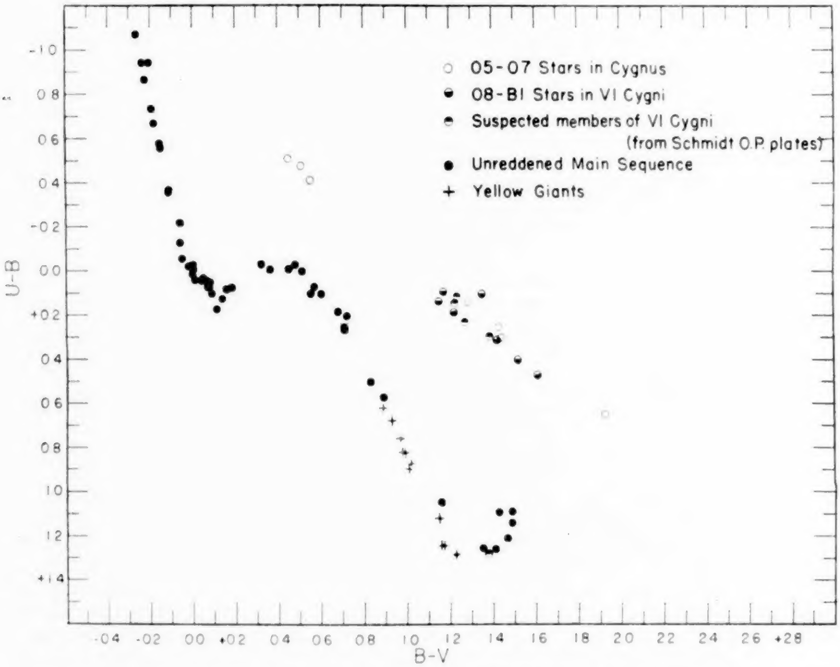

FIG. 1.—Two-color diagram of unreddened standard stars and of stars in Cygnus region

It is intended to obtain spectroscopic data on the foregoing stars in the future. During the interval in the observing period that the Cassegrain spectrograph was attached to the 82-inch, it was possible to obtain a spectrogram of star No. 22, on a moonless night, using the 110-mm camera and a 103*a*-O plate. This star was selected because it was felt to be the most questionable member of the group of ten found from the 6-inch Newtonian survey, being apparently located in a very much obscured region of the association. An exposure of $3^{h}40^{m}$, with the spectrum widened only a very small amount, allowed the detection of a strong λ 4430 interstellar band and the hydrogen lines in absorption. Star No. 22 therefore seems to be definitely involved in the association and of type A0 or earlier.

TABLE 1

MAGNITUDES AND COLORS

Star VI Cyg No.	V	$(B-V)$	$(U-B)$	Star VI Cyg No.	V	$(B-V)$	$(U-B)$
13	10.51	+1.38	+1.28	16	10.93	+1.22	+0.13
14	11.55	+1.27	+0.23	17	11.71	+1.40	+0.30
15	11.20	+1.23	+0.12				

A set of plates was taken of both the central and the surrounding regions, using the Meinel Cassegrain reduction camera. This camera will be described by Meinel in a forthcoming paper; in brief, it is a field-lens–collimator-camera arrangement, operating on a slitless-spectrograph principle; when used for direct photography at the Cassegrain focus of the 82-inch, a field of 20′ of arc and a speed of $f/2$ are obtained. Dispersing elements and glass or interference filters can be placed in the parallel beam. In the present case a glass prism having an angle of 5° was used; this gave spectral images of all the stars in the field, about 0.8 mm in length, with 103*a*-E plates. The images have relative dimensions comparable to those in the earlier low-dispersion studies. Figures 2 and 3 are intended to show the comparability of the 82-inch plates with the previous observations; Figure 2 is a 1-minute exposure of the region east of No. 8; it can be compared with Figure 3 of the previous paper (Schulte 1956). Figure 3 is also a 1-minute exposure, centered on star No. 10. This can be compared with Figure 4 of the previous paper; the limiting magnitude is about the same (in Fig. 2 of the present paper, star No. 11 is correctly identified; in the first paper, through an oversight, it was erroneously listed as a new member, No. 28). Figure 4 is a 10-minute exposure of the same region as Figure 2; the dispersion is in the opposite direction. Finally, a 30-minute plate of the central region, surrounding the quadruple star No. 8, is shown in Figures 5 and 6. From the last three figures, it is seen that, with an increase of exposure times, there is an increase in the percentage of stars having spectral images similar to those of the brighter members. The approximate magnitudes seem compatible with the idea that perhaps early-type main-sequence members are being encountered. It appears unlikely that they are foreground objects, because of the clustering tendency shown by some of them—for instance, those near star No. 22 and, to a lesser extent, near star No. 8. Confirmation of this hypothesis, however, would be extremely difficult with conventional techniques; pulse-counting photometry and image-tube spectroscopy will probably be necessary.

I wish to express my thanks to Drs. A. B. Meinel and W. W. Morgan for their encouragement of this work, and to Messrs. J. C. Golson and M. E. Krebs for their help with the observations.

REFERENCES

Baade, W., and Minkowski, R. 1954, *Ap. J.*, **119**, 215.
Johnson, H. L., and Harris, D. L. 1954, *Ap. J.*, **120**, 196.
Johnson, H. L., and Morgan, W. W. 1953, *Ap. J.*, **118**, 161.
———. 1955, *ibid.*, **122**, 142.
Morgan, W. W., Johnson, H. L., and Roman, Nancy G. 1954, *Pub. A.S.P.*, **66**, 85.
Morgan, W. W., Meinel, A. B., and Johnson, Hugh M. 1954, *Ap. J.*, **120**, 506.
Münch, Luis, and Morgan, W. W. 1953, *Ap. J.*, **118**, 161.
Piddington, J. H., and Minnett, H. C. 1952, *Australian J. Sci. Res.*, *A*, **5**, 17.
Schulte, D. H. 1956, *Ap. J.*, **123**, 250.

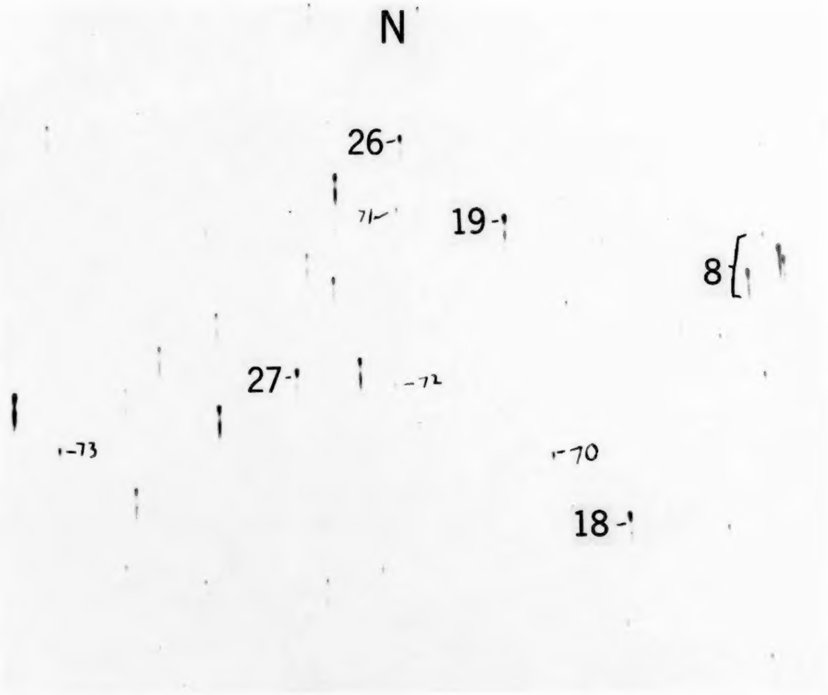

FIG. 2.—Low-dispersion slitless spectrogram of region near center of VI Cygni, taken with the 82-inch telescope; exposure time was 1 minute with 103*a*-E plate. Red is toward the top. In all these illustrations, stars with designations larger than 30 are newly suspected reddened early-type members; the others refer to the previous investigations. The unusual appearance of No. 19 is due to the presence of a fainter star directly south of it.

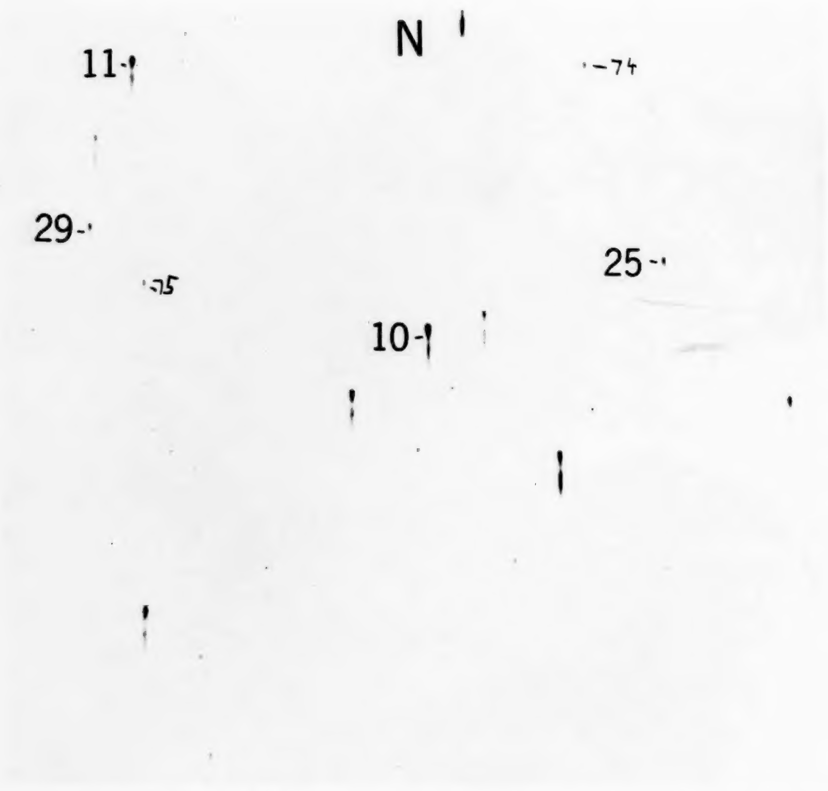
N
11
-74
29
25
75
10

FIG. 3.—One-minute exposure centered on the O9.5 I*a* star No. 10. Red is toward the top. No. 11 is an O6f star.

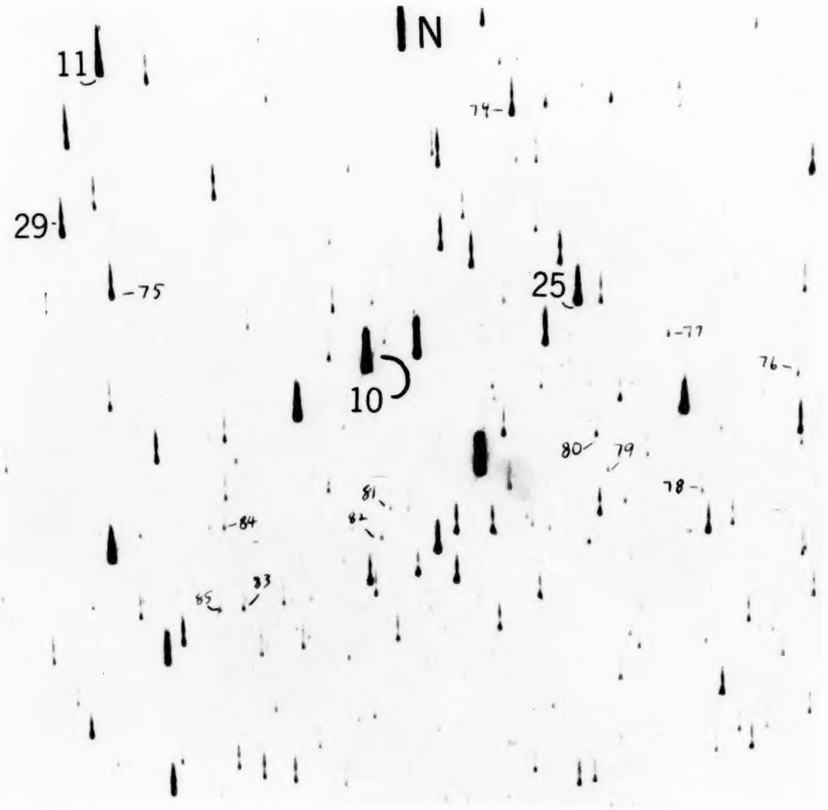
N
11
74
29
75
25
77
76
10
80
79
78
81
82
84
83
85

FIG. 4.—Ten-minute exposure of same region as Fig. 3; red is toward the bottom

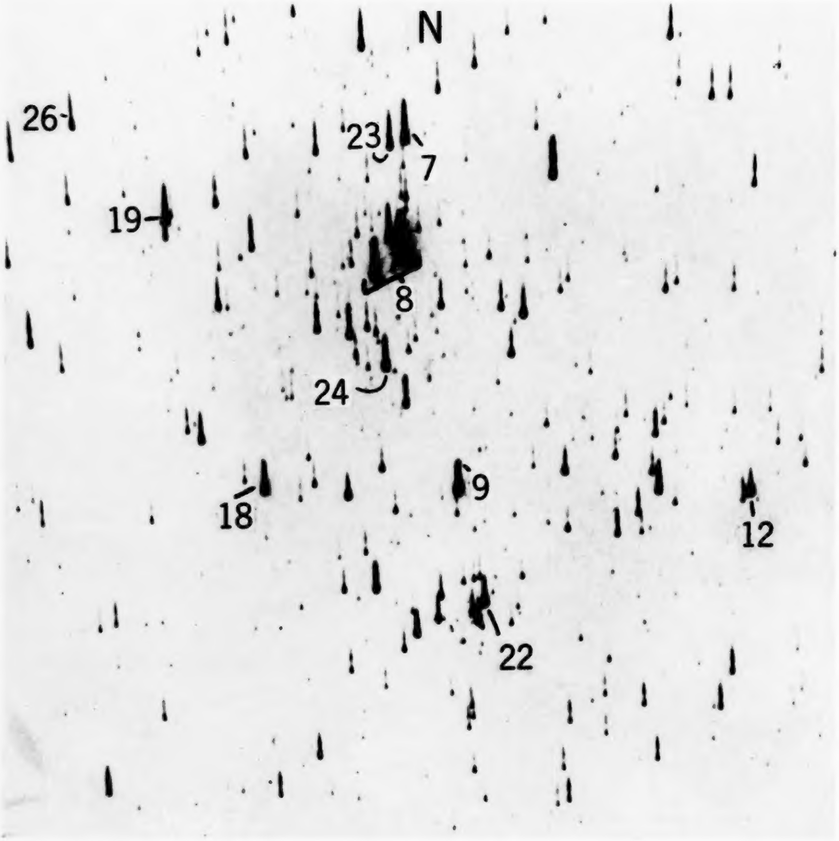
N
26
23
7
19
8
24
18
9
12
22

FIG. 5.—Central part of the association, 30-minute exposure. Only the previously discussed stars are marked. Red is toward the bottom.

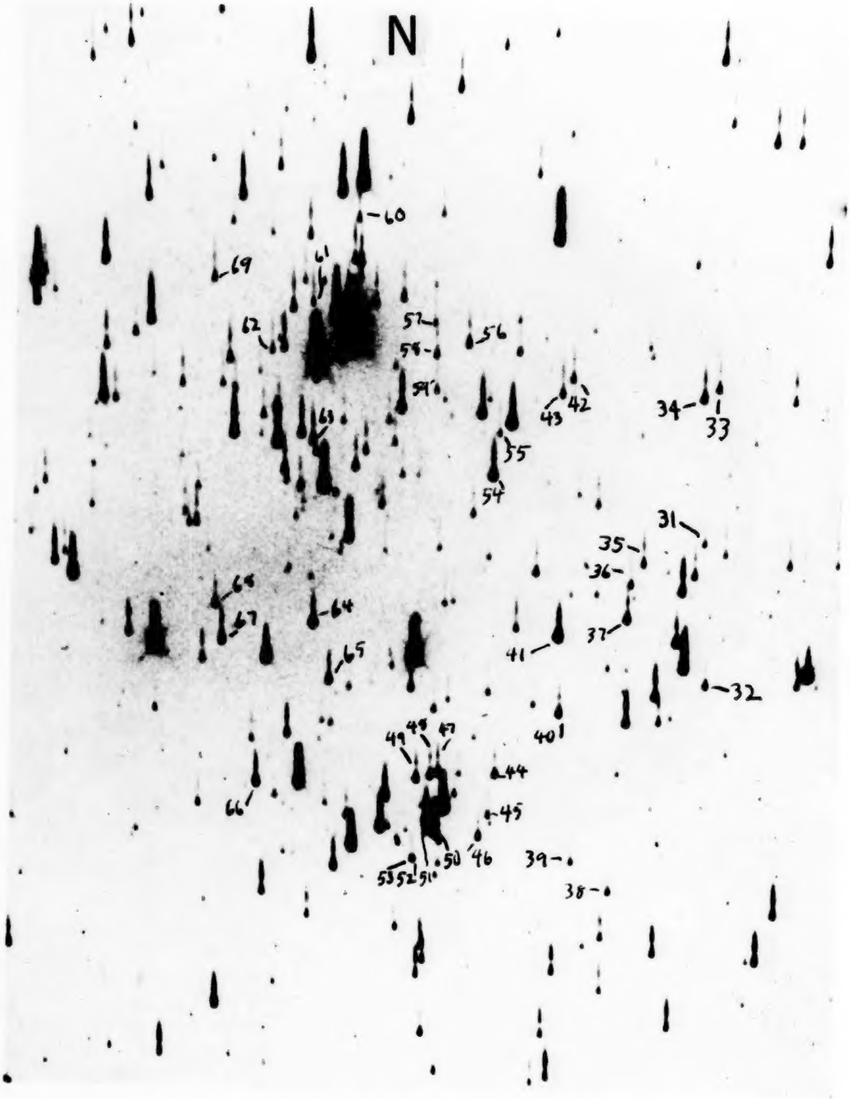
N
60
61
69
62
57
56
58
59
42
43
34
33
63
55
54
31
35
36
68
64
67
37
41
65
32
40
49
48
47
44
66
45
46
39
50
53
52
51
38

FIG. 6.—Same plate as Fig. 5. New probable members are marked

OBSERVATIONAL CONSEQUENCES OF O STAR FORMATION

MALCOLM P. SAVEDOFF
Institute of Optics and Physics Department, University of Rochester

Received July 16, 1956

ABSTRACT

Observations of an expanding hydrogen shell in Orion are interpreted as a shell resulting from an expanding H II region. This assumption is consistent with an age of 1.9×10^6 years and an original $O_{7.5}$ star with $M_v = -5.00$. It is suggested that the dense regions observed in Orion are part of this shell and are the site of star formation. The tremendous kinetic energy of the shell, 10^{50} ergs, whatever its mechanism of formation, is a possible source for most of the kinetic energy in the interstellar material. A predicted brightness distribution for H II regions is given.

Recent radio observations of the Orion region by T. K. Menon (1956) show that the neutral hydrogen is both expanding and rotating. In this paper I shall apply the model of the expanding H II region (Savedoff and Greene 1955), referred to as "Paper I," on the assumption that the expansion observed is that of the compressed shell surrounding the H II region. An approximate version of the model of Paper I will be used to compute pertinent parameters.

The assumed history of events in the Orion region may be briefly described as the consequence of the birth and death of an O star in a large neutral hydrogen cloud. If the O star becomes luminous rapidly, an ionized hydrogen region is formed about it in which the gas pressure is several hundred times that in the neutral cloud. The ionized gas expands, producing a compressed region of neutral hydrogen, which is, in turn, separated from the undisturbed neutral hydrogen by a shock wave. It is suggested that radiative processes are sufficiently rapid to result in the temperature of the compressed gas being essentially unchanged from that in the surrounding gas. Secondary star formation is supposed to occur in the compressed region; most of the O and B stars of the Orion aggregate are considered to be of this second generation.

We may summarize the results of Paper I with the approximations suggested by Table 3 therein as follows:

a) The initial velocity of expansion, w_{so}, is $(2T_{II}/T_I)^{1/2}c$, where T_I and T_{II} are the temperatures in the neutral and ionized hydrogen regions, respectively, and c is the isothermal sound velocity in the neutral hydrogen region. We shall assume $w_{so} = (200)^{1/2}c = 14$ km/sec, for $T_I = 10^2$ ° K and $T_{II} = 10^4$ ° K.

b) The velocity of expansion is almost $w_s = w_{so}(R/R_0)^{-3/4}$, where R_0 is the radius of the Strömgren sphere for the undisturbed density.

c) The density of the compressed region and the ionized region is almost proportional to $R^{-3/2}$.

d) Although some of the compressed region is later ionized, for most of the expansion the compressed region grows in mass; in fact, $M_s = n_0 m_H(R^3 - R^{3/2}R_0^{3/2})$.

Menon (1956) outlines the optical properties of the Orion region as well as the radio observations. Of greatest interest to us is the great Hα arc of Barnard (1895), which appears as an elliptical ring of approximately 120 pc in diameter at 450 pc. This object is associated by Menon with a region producing double-line profiles in the neutral hydrogen observations at +11 and −13 km/sec relative to the local standard of rest in that vicinity. This corresponds to an expansion with a velocity w_s of about 10 km/sec. The intensity of the emission in 21 cm is estimated by Menon to be equivalent to 10^5 solar masses. The center of Barnard's ring is near the point of closest approach of the three high-velocity supergiants AE Aurigae, μ Columbae, and 53 Arietis (Blaauw and Morgan 1954; Blaauw 1956). This approach occurred approximately 2.6×10^6 years ago.

One suggestion, due to Öpik (1953), is that this ring may result from a supernova explosion. The original high-velocity gases of the supernova collide inelastically with the surrounding interstellar medium and accelerate large masses of gas. In this process momentum is conserved. For 10^5 solar masses, the momentum of the supernova outburst is estimated as 10^6 suns km/sec. The expansion rate of the Crab suggests an initial expansion velocity of 2×10^3 km/sec and hence that our supernova was approximately 500 solar masses. This is unlikely, as the really violent supernovae seem to be associated with Baade's population II, while the Orion phenomena show low space velocity; further, it is now believed that few population II objects are even 2 solar masses in weight. The less violent population I supernovae would undoubtedly show lower expansion velocities and need even larger masses. I believe the supernova hypothesis may be discarded.

TABLE 1

PRIMARY PARAMETERS

Initial shell velocity	w_{s0}	14 km/sec	Observed radius	R_s	60 pc
Observed shell velocity	w_s	10 km/sec	Observed mass	M	10^5 solar masses
Distance	d	450 pc			

TABLE 2

DERIVED PARAMETERS

Expansion ratio	R/R_0	1.57
Original radius	R_0	38 pc
Original mean density	n_{H_0}	4.6 cm^{-3}
Luminosity parameter	$R_0 n_{H_0}^{2/3}$	105 pc cm$^{-9/2}$
Original star	Assumed $O_{7.5}$	$M_v = -5.0$ $M_{bol} = -9.0$
Original emission measure	$n_{H_0}^2 R_0$	800 pc/cm^6
Present emission measure	$n_{H_0}^2 R_0 (R_0/R)^2$	324 pc/cm^6
Age of shell		1.9×10^6 years
Gravitational contraction scale		5×10^2 years
Thermonuclear scale		1.6×10^6 years
Kinetic energy of shell		10^{50} ergs
Equivalent rate of energy production		6.9×10^{-28} erg/cm^3/sec

If we now apply the model of Paper I, we take as our primary data the observed mass, radius, and rate of expansion of the arc. In addition, we introduce the estimated initial expansion velocity. These are summarized in Table 1. In Table 2 we collect the derived parameters. Here we use the approximations collected earlier. The original radius of the ionized hydrogen region is found from approximation *b* (see above), which relates radius and expansion velocity. The density may be found from relation *d*. With these numbers we compute Strömgren's parameters $R_0 n_H^{2/3}$ and $n_H^2 R_0$, which measure the luminosity of the star and the brightness of the H II region, respectively. We have used the recent luminosity calibration of Johnson and Hiltner (1956) and Table 7 of Strömgren (1948) to estimate the spectral class and luminosity of the original star. The time for gravitational contraction is estimated from the theoretical models of Henyey *et al.* (1955) for Sirius, assuming that the time for gravitational contraction is proportional to the main-sequence luminosity. The time for thermonuclear burnup is taken as an extrapolation from the data of R. S. Kushwaha (unpublished), assuming $M_{bol} = -9.00$. A mass-luminosity law, $L \propto M^{3.5}$, was assumed.

At present only two of these numbers appear exceptional. The age of the arc seems short compared to the Blaauw-Morgan data. Certainly, both this result and the Blaauw-Morgan age are consistent with the remark by Johnson and Hiltner that stars of approximately B8 and A0 have reached the main sequence; hence most of the stars were formed approximately 2×10^6 years ago.

At a mean density $n_H = 10$, the time of free fall from the periphery to the center under purely gravitational forces is about 7×10^6 years. The simultaneous appearance of over one hundred O and B stars under these circumstances seems rather remarkable. For the estimated density in the compressed shell this time of free fall, for $n_H = 500$, is only 1×10^6 years. For a star of 10 solar masses, the radius of the region containing this mass is about 0.40 pc. Since one would assume that the collapse is subsonic at about 1000° K, we may estimate a time of collapse exceeding 1.3×10^5 years. This permits simultaneous formation of large aggregates. Incidentally, the density in the compressed shell is comparable with that measured in the Orion Nebula.

This model fails in three respects. First, the emission measure in the evolved H II region today should be of the order of 324, if the O star still supported it. It is presumed that this would be observable. Second, we offer no explanation for the current emission from the arc. Since the recombination time in the H II region is estimated as 8×10^4 years, it is difficult to produce the dense compressed shell and an ionized ring simultaneously. Finally, the extreme velocities of AE Aurigae, μ Columbae, and 53 Arietis, namely, 127, 127, and 60 km/sec, require some additional mechanism. Kahn's analysis (1954) of the Spitzer-Oort mechanism (1955) indicates that it is rather unlikely that this agency could explain such exceptionally high velocities.

One should note the tremendous injection of kinetic energy into the interstellar medium produced by this object. We have estimated that at present the total kinetic energy is about 10^{50} ergs. If we assume that one such object occurs per million years within a cylinder, radius 500 pc and 200 pc high, we obtain a mean energy-production rate of 6.9×10^{-28} erg/cm³/sec. This is to be compared with the cosmic-ray energy loss of 10^{-26} erg/cm³/sec estimated by Morrison, Olbert, and Rossi (1954). Kahn (1953) estimated that the energy loss by inelastic collisions between clouds is about $3 \times 10^{-27} n_H$ erg/cm³/sec or 10^{-26} erg/cm³/sec.

If one assumes that both the brightness of the initial star and the density of the medium are unique, then the model predicts a dependence of the emission measure on time and hence a frequency distribution. The frequency distribution will be proportional to the reciprocal of the time derivative of the emission measure. It then follows from Paper I, equations (18′), (8), and (20), on differentiation with L constant, that

$$P(e)\,de = \frac{7}{8e_0}\left(\frac{e_0}{e}\right)^{15/8} de .$$

Here e and e_0 are the present and original emission measures, respectively. In unresolved emission regions the brightness in Hα will be nearly independent of time and proportional only to L.

In summary, one is led to believe that the Orion region was a fairly amorphous neutral hydrogen cloud some 2×10^6 years ago. Since then an initial star with an average luminosity sufficient to burn it out in 1.8×10^6 years appeared, evolved, and burned out, leaving a dense compressed shell within which a second generation of stars is formed. In this second generation the Orion Nebula is the brightest emission nebula in the sky; accordingly, it should be the most ephemeral. For this object R_0/w_{s0} is about 7×10^4 years. This agrees with Parenago's (1953) suggestion that 10^4 years is a significant period in the history of the Trapezium, while in our original generation the appropriate time scale was one hundred times longer. It is not surprising that there are so few regions as bright as the Orion Nebula.

One may hope that eventually our knowledge of distances in the Orion region will become sufficiently precise that a study of radial distance from the center of Barnard's ring versus velocity will be feasible. Unfortunately, this would require a precision exceeding 0.2 mag. in modulus measurement.

I would like to express my gratitude to T. K. Menon for making the final interpretation of his measures available prior to publication. This work was largely supported by the National Science Foundation.

REFERENCES

Blaauw, A. 1956, *Scient. Amer.*, **194**, 36.
Blaauw, A., and Morgan, W. W. 1954, *Ap. J.*, **119**, 625.
Henyey, L. G., LeLevier, R., and Levée, R. D. 1955, *Pub. A.S.P.*, **67**, 154.
Johnson, H. L., and Hiltner, W. A. 1956, *Ap. J.*, **123**, 267.
Kahn, F. D. 1954, *B.A.N.*, **12**, 187.
———. 1955, *Gas Dynamics of Cosmic Clouds* ("I.A.U. Symposium Series," Symposium No. 2 [Amsterdam: North Holland Publishing Co.), chap. xii, p. 60.
Menon, T. K. 1956, unpublished.
Morrison, P., Olbert, S., and Rossi, B. 1954, *Phys. Rev.*, **94**, 440.
Öpik, E. J. 1953, *Irish A.J.*, **2**, 219.
Oort, J. H., and Spitzer, L. 1955, *Ap. J.*, **121**, 6.
Savedoff, M. P., and Greene, J. 1955, *Ap. J.*, **122**, 477.
Strömgren, B. 1948, *Ap. J.*, **108**, 242.

PHOTOELECTRIC K AND L SHELL ABSORPTION COEFFICIENTS FOR HIGHLY IONIZED ATOMS*

S. A. MOSZKOWSKI† AND ROLAND E. MEYEROTT‡
University of California, Los Angeles, California, and RAND
Corporation, Santa Monica, California

Received June 8, 1956

ABSTRACT

The effect of electron screening on the photoelectric absorption coefficients averaged over the K and L shells of ions has been computed from the work of Meyerott. The average absorption coefficient is less sensitive to screening effects. In some cases the average absorption coefficient can be expressed in terms of effective screening constants.

I. INTRODUCTION

It is of importance for certain problems to be able to estimate accurate values of the photoelectric dipole absorption coefficients for atoms and ions. To do this, one must have some detailed knowledge of atomic wave functions, in order to take screening properly into account. Such calculations have been made by one of us (Meyerott 1954; hereafter referred to as "REM"), and the results given in that paper enable one to compute the effect of electron screening on each individual transition. These screening corrections vary rapidly with frequency and have been computed for only four points, making interpolation difficult. It turns out that the screening effect, when averaged over a complete shell, varies more slowly with frequency and can be interpolated more reliably from the data given in REM than can those for the individual transitions. This result is similar to the situation that exists for the pure coulomb case, where the frequency cubed *times* the mass absorption coefficient averaged over a complete shell is a slowly varying function of the frequency, i.e., the Gaunt factors vary slowly with frequency.

The present paper deals only with the absorption coefficients averaged over subshells for the K and L shells of atoms and ions. In Section II the absorption coefficient is expressed in terms of an effective charge which is evaluated with the use of coefficients given in REM. The effective charge is also expressed in terms of an effective screening constant which is useful in certain limiting cases. In Section III a comparison is made between the various methods of computation, and their reliability is discussed.

II. CALCULATIONS

a) The Effective Charge

The average absorption coefficient μ_n for electrons in a shell of principal quantum number n (1 or 2) can be written in the usual form,

$$\mu_n = 4\pi^2 \alpha \frac{a_0^2 N_0 \rho}{A} \frac{N_n}{3} \frac{\nu}{Z^4} (I_n^\eta)^2 , \qquad (1)$$

where

α = Fine-structure constant, ρ = Density,
a_0 = Bohr radius for hydrogen, A = Atomic weight,
N_0 = Avogadro's number, ν = Frequency in Rydbergs.

---

* The work involved in this study was sponsored entirely by the U.S. Atomic Energy Commission.

† Consultant, RAND Corporation, Santa Monica, California.

‡ Now at Lockheed Missile Systems Division, Palo Alto, California.

The I^η_n are defined in terms of the radial integrals given in REM, by

$$I^\eta_k = I^{\eta p}_{1s}\,, \tag{2a}$$

$$(I^\eta_L)^2 = \tfrac{1}{4}\,(I^{\eta p}_{2s})^2 + \tfrac{1}{4}\,(I^{\eta s}_{2p})^2 + \tfrac{1}{2}\,(I^{\eta d}_{2p})^2\,. \tag{2b}$$

The absorption coefficient may also be expressed by an effective charge Z^e_n, averaged over all subshells, g^η_n, and a Gaunt factor (Chandrasekhar 1939; Menzel and Pekeris 1936),

$$\mu_n = 4\pi^2 \alpha a_0^2 N_0 \frac{16}{\pi 3^{3/2}} \frac{\rho}{A} \frac{N_n}{n^5} \frac{(Z^e_n)^4}{\nu^3}\, g^\eta_n\,. \tag{3}$$

The quantity η is the kinetic energy of ejected electrons in the absence of external screening in units $Z^2e^2/2a_0$. It is related to ν by[1]

$$\nu = Z^2\eta + \frac{(Z^i_n)^2}{n^2}\,. \tag{4}$$

Here in equation (4) Z^i_n is taken to be (Mayer 1947)

$$Z^i_K = Z - 0.625\,(N_K - 1)\,, \tag{5a}$$

$$Z^i_L = Z - 0.938 N_K - 0.690\,(N_L - 1)\,, \tag{5b}$$

representing the effect of screening by the electrons (interior to that making the transition) on the ionization energy.

By substitution of the well-known expression for the Gaunt factor in equation (3) and comparing with equation (1), we find that the effective screening constants are simply related to the dipole matrix elements by the following (apart from small correction terms):

$$\frac{Z^e_n}{Z} = \frac{\eta + (1/n^2)(Z^i_n/Z)^2}{\eta + (1/n^2)} \left(\frac{I^\eta_n}{{}^H I^\eta_n}\right)^{1/2}, \tag{6}$$

where ${}^H I$ denotes the radial integral for a hydrogenic atom.

The assumption has been made that exactly 25 per cent of the L electrons are in the 2s subshell, even though this number may not be an integer. The radial integrals have been calculated previously as power series in $1/Z$. Numerical values of the coefficients are given in REM. The second term of equation (6) may also be expanded as a power series in $1/Z$. The results can, after some minor approximations,[2] be written as follows:

$$\left(\frac{I^\eta_K}{{}^H I^\eta_K}\right)^{1/2} = 1 + \frac{1}{Z}(N_K - 1)\, b^K_K + \frac{1}{Z^2}(N_K - 1)^2 b^K_{KK}\,, \tag{7a}$$

$$\begin{aligned}\left(\frac{I^\eta_L}{{}^H I^\eta_L}\right)^{1/2} = 1 &+ \frac{1}{Z}\,[N_K b^L_K + (N_L - 1)\, b^L_L] \\ &+ \frac{1}{Z^2}\,[N_K^2 b^L_{KK} + 2N_K(N_L - 1)\, b^L_{KL} + (N_L - 1)^2 b^L_{LL}]\,.\end{aligned} \tag{7b}$$

---

[1] In Meyerott (1954), ν in eq. (24) is in units of Z^2 Rydbergs instead of Rydbergs.

[2] Terms of order $1/Z^3$ and also small correction terms which involve differences between ΔI's and are independent of N_L are neglected.

In REM, absorption for L electrons when the K and L shells are filled was discussed in some detail. For this case equation (7*b*) becomes:

$$\left(\frac{I_{\mathrm{L}}^{\eta}}{{}^{H}I_{\mathrm{L}}^{\eta}}\right)^{1/2} = 1 + \frac{C_1^{\mathrm{L}}}{Z} + \frac{C_2^{\mathrm{L}}}{Z^2}. \tag{8}$$

Values of the *b* and *C* coefficients are given in Table 1.

TABLE 1

VALUES OF *b* AND *C* COEFFICIENTS (EQS. [7], [8])

η	$b_{\mathrm{K}}^{\mathrm{K}}$	$b_{\mathrm{KK}}^{\mathrm{K}}$	$b_{\mathrm{K}}^{\mathrm{L}}$	$b_{\mathrm{L}}^{\mathrm{L}}$	$b_{\mathrm{KK}}^{\mathrm{L}}$	$b_{\mathrm{KL}}^{\mathrm{L}}$	$b_{\mathrm{LL}}^{\mathrm{L}}$	C_1^{L}	C_2^{L}
0.00....	0.955	−0.554	+1.268	0.859	−0.774	−0.401	−0.274	+8.55	−27.76
0.25....	.682	− .215	+0.044	.453	+ .117	+ .226	+ .088	+3.26	+11.13
0.50....	.512	− .047	−0.213	.222	+ .161	+ .395	+ .241	+1.13	+23.50
1.00....	0.314	+0.106	−0.360	0.064	+0.180	+0.335	+0.212	−0.27	+20.53

TABLE 2*

EFFECTIVE SCREENING CONSTANTS

η	σ_{KK}^{e}	σ_{KL}^{e}	σ_{LL}^{e}	η	σ_{KK}^{e}	σ_{KL}^{e}	σ_{LL}^{e}
0.00.	0.295	0.608	0.521	1.00.	0.314	0.735	0.212
0.25.	.318	.894	.237				
0.50.	0.321	0.838	0.238	σ^s........	0.30	0.85	0.35

* To be used only if the number of bound electrons is much smaller than *Z*. Values of the Slater screening constants (Slater 1930), σ^s, are also listed for comparison.

b) *Effective Screening Constants*

For some cases the number of electrons may be sufficiently small compared to *Z* that *all* terms of order $1/Z^2$ can be ignored in equations (7) and (8). In this limiting case it is convenient to define effective screening constants σ^e. Here

$$Z^e = Z - \Sigma'_{n'} N_{n'} \sigma^e_{n'n} , \tag{9}$$

where Σ' denotes summation over all electrons except the one making the transition.

The effective screening constants are given in terms of previously defined quantities as follows:

$$\sigma^e_{\mathrm{KK}} = b_{\mathrm{K}}^{\mathrm{K}} - \frac{2\,(0.625)}{\eta + 1}, \tag{10a}$$

$$\sigma^e_{\mathrm{KL}} = b_{\mathrm{K}}^{\mathrm{L}} - \frac{1}{2}\,\frac{(0.938)}{\eta + \frac{1}{4}}, \tag{10b}$$

$$\sigma^e_{\mathrm{LL}} = b_{\mathrm{L}}^{\mathrm{L}} - \frac{1}{2}\,\frac{(0.690)}{\eta + \frac{1}{4}}. \tag{10c}$$

Numerical values of the effective screening constants are given in Table 2.

It is seen that the effective screening constants for absorption, on the average, are about the magnitude of the Slater screening constants, in agreement with the values suggested by Bethe (1933) and Hall (1936). They do show considerable variation with energy of ejected electron.

III. NUMERICAL EXAMPLE AND VALIDITY OF VARIOUS APPROXIMATIONS

Since the analytical details which show the approximate equivalence of the computing methods used in REM and the present paper have been omitted, we include a numerical example which indicates the reliability of the present method. In Table 3 the quantity $\nu^3\mu/\rho$ for the L shell of copper ($Z = 29$) as found in REM is compared with that computed by the present method. It can be seen that the differences are small and probably not significant, in view of the errors inherent in the method of that paper.

TABLE 3

COMPARISON OF ABSORPTION COEFFICIENTS CALCULATED USING PRESENT METHOD WITH VALUES OBTAINED PREVIOUSLY

($Z = 29$; $N_K = 2$; $N_L = 8$)

η	ν_{Rydbergs}	$\nu^3\mu_L/\rho\times 10^{-9}$ (Present Paper)	$\nu^3\mu_L/\rho\times 10^{-9}$ (REM)	η	ν_{Rydbergs}	$\nu^3\mu_L/\rho\times 10^{-9}$ (Present Paper)	$\nu^3\mu_L/\rho\times 10^{-9}$ (REM)
0.00	124	3.60	3.60	0.50	545	9.70	9.63
0.25	334	8.31	8.26	1.00	965	10.49	10.22

TABLE 4

VALUES OF $Z - Z^e$ FOR SEVERAL CONFIGURATIONS CALCULATED USING METHOD OF SECTION II*a* AND FROM SCREENING CONSTANTS OF SECTION II*b*

η	$(Z-Z^e)_K$		$(Z-Z^e)_L$					
	$Z=13$, $N_K=2$, $N_L=0$		$Z=29$, $N_K=2$, $N_L=1$		$Z=29$, $N_K=2$, $N_L=4$		$Z=29$, $N_K=2$, $N_L=8$	
	Sec. II*a*	Sec. II*b*	Sec. II*a*	Sec. II*b*	Sec. II*a*	Sec. II*b*	Sec. II*a*	Sec. II*b*
0.00	0.295	0.394	1.216	1.508	2.78	3.81	4.86	7.37
0.25	.318	.360	1.788	1.720	2.50	2.29	3.45	3.03
0.50	.321	.337	1.676	1.595	2.39	2.00	3.34	2.28
1.00	0.314	0.304	1.470	1.401	2.11	1.75	2.95	1.97
$Z-Z^s$	0.30	....	1.70	....	2.75	....	4.15	....

In order to evaluate the reliability of the effective screening constant approximation in computing the effective charge, we show examples of the effective charge computed correctly and that using the effective screening constant approximation. In Table 4 are shown the values of the effective charge computed by the two methods for $Z = 13$, K-shell absorption, and $Z = 29$, L-shell absorption, for various numbers of screening electrons. The differences between the two methods reflect the importance of N^2/Z^2 terms. One can readily observe the breakdown of the screening constant approximation as the number of screening electrons increases. In Table 4 the effective charge $Z - Z^s$, computed by Slater's screening constants, is shown for comparison.

In conclusion, it is possible to fit photoelectric K and L shell absorption coefficients fairly well by the method of Section II*a*. A suggested criterion for the applicability of this method is

$$N_K + N_L < \tfrac{1}{3}Z \,.$$

REFERENCES

Bethe, H. 1933, *Handb. d. Phys.* (Berlin: Julius Springer), Vol. **24,** No. 1, chap. iii.

Chandresekhar, S. 1939, *An Introduction to the Study of Stellar Structure* (Chicago: University of Chicago Press), p. 262.

Hall, H. 1936, *Rev. Mod. Phys.*, **8,** 358.

Mayer, H. 1947, Los Alamos Scientific Report LADC-464 (unpublished).

Menzel, D. H., and Pekeris, C. L. 1936, *M.N.*, **96,** 177.

Meyerott, R. E. 1954, *Phys. Rev.*, **95,** 72.

Slater, J. C. 1930, *Phys. Rev.*, **36,** 57.

INFLUENCE OF COLLISIONS UPON POPULATION OF HYPERFINE STATES IN HYDROGEN

EDWARD M. PURCELL AND GEORGE B. FIELD*
Harvard University and Harvard College Observatory

Received June 14, 1956

ABSTRACT

In a collision between two hydrogen atoms in their ground states, the electron spins may exchange. Such exchanges affect the relative populations of the hyperfine levels and are therefore important in determining the rate of 21-cm transitions in an assembly of atoms undergoing collision. A cross-section is computed for electron exchange over a range of gas kinetic temperatures, and the competition between collisions and radiation in establishing the hyperfine populations is analyzed. The results are applied to typical situations encountered in 21-cm radio astronomy.

INTRODUCTION

The intensity of emission or absorption by atomic hydrogen at the 21-cm resonance depends on the populations of the two levels into which the ground state of the atom is split by the hyperfine interaction. It is convenient to describe the relative occupation of these levels by a "spin temperature," T_S, defined by the relation

$$\frac{n_1}{n_0}=3\exp-\frac{\hbar\omega}{kT_S}, \qquad (1)$$

in which n_1 and n_0 are, respectively, the populations of the upper ($F = 1$) and lower ($F = 0$) levels and $\hbar\omega$ is the energy difference. If we observe with a radio telescope an extended, homogeneous, optically thick hydrogen source, the power received per unit band width will be simply kT_S. The spin temperature of the source in other situations is not so directly accessible. In the limiting case of low opacity and negligible background radiation, the observed emission intensity will be practically independent of T_S, so long as T_S is much greater than $\hbar\omega/k$. In that case the power received is determined simply by the probability of spontaneous emission and the number of hydrogen atoms (nearly three-fourths of which are in the upper level) in a column of unit cross-section extending through the source. But in any case the degree of opacity of a given source depends on T_S, among other factors. All this is well known (Wild 1952) and is repeated here only to recall the role of the level occupations, or the spin temperature, in the interpretation of 21-cm observations. This note is concerned with processes which, in typical astrophysical situations, may establish the level occupations and hence the spin temperature.

In an earlier publication (Ewen and Purcell 1951) the effect of atomic collisions was estimated and was asserted to be the dominant effect in determining T_S in the galactic H I regions then observed. The conclusion was, as it turns out, correct, but the reason was wrong; for the most important process at work during collisions had been overlooked, one which may be called "spin exchange." Its importance was pointed out in a private communication by V. F. Weisskopf and N. F. Ramsey. Subsequent calculations by the senior author yielded an approximate cross-section for the process.

A closely related question had arisen in the laboratory experiments of Wittke and Dicke (1956), who developed the theory of the effect for their purposes, along slightly different lines. They have provided us with much help and illumination; indeed, the conclusions presented here are to a considerable extent the result of a common effort.

---

* Junior Fellow, Society of Fellows.

EXCHANGE COLLISIONS

We are interested in this question: A hydrogen atom in a given hyperfine state, say $F = 1$, collides with a random hydrogen atom; what is the probability that the first atom will be left after the collision in the state $F = 0$? One interaction which occurs during a collision is the direct magnetic interaction of the electron spins. The energy of such an interaction is, in order of magnitude, β^2/d^3, β being the Bohr magneton and d the distance between the two electrons. If we take $d = 10^{-8}$ cm as representative of the situation during a collision, the duration of which is some 10^{-13} sec, we may estimate the probability that a hyperfine transition is induced. It is (interaction energy × duration/$\hbar$)^2, or roughly 10^{-4}. This crude estimate could be refined, but there is no point in doing so, for the spin-exchange process, which we shall now discuss, is so much more effective in all circumstances.

The collision of two hydrogen atoms presents us, temporarily, with a hydrogen molecule, in the structure of which electron exchange plays a prominent part. Speaking very loosely, we may say that the atoms exchange electron spins at a rate given by $(V_t - V_s)/\hbar$, where $V_t - V_s$ is the difference in energy between the triplet electronic state of the molecule and the singlet electronic state. If the collision is close enough and lasts long enough for the exchange to occur several times, the chance that a given proton will leave the collision with its electron in a new orientation is simply $\frac{1}{2}$. In some fraction of these cases the orientation of the new direction of the electron spin, relative to that of the proton spin, will be such that the atom is in a hyperfine state different from its state prior to the collision.

The argument can be developed rigorously along these lines, following Wittke and Dicke. Consider a system of two atoms whose state before the collision is specified, so far as all spin co-ordinates are concerned, by the four quantum numbers F_1, m_1, F_2, m_2, appropriate to isolated atoms individually in well-defined hyperfine states. To treat the collision, write the spin function of the initial state (F_1, m_1, F_2, m_2) as a linear combination of molecular spin functions which have been properly symmetrized with respect to electron co-ordinates. (The nuclear spin co-ordinates need not be so treated.) Our initial spin state for the separated atoms is then expressed as a superposition of singlet and triplet electronic spin states of the molecule, multiplied by the nuclear spin functions. The effect of a collision can now be described precisely: it brings about a relative phase shift, ϕ_{ts}, between the amplitude of the singlet component and the amplitudes of the triplet components of the electron spin function; so that when we revert to a representation in terms of our original spin functions, we find, in general, a mixture of several (F_1, m_1, F_2, m_2) states, not merely the pure state we began with. The decisive quantity is therefore

$$\phi_{ts} = \int dt \, \frac{V_t - V_s}{\hbar}, \tag{2}$$

where V_t is the energy of the triplet ("repulsive") electronic state, V_s is the energy of the singlet ("attractive") state, and the integration extends over the whole duration of the collision.

The matrices which transform the representation in the manner described have been given by Wittke and Dicke. Our problem is simpler than theirs in several respects: we need not worry about a correlation in phase among spin functions for different atoms which can arise in their experiments through the coupling to the radio-frequency field in their cavity; we are interested only in the probability of transitions from $F = 0$ to $F = 1$ and vice versa, and we need not sort out the m-substates of $F = 1$, which remain degenerate under all conditions of interest to us. Because of this, the only result we shall need can be deduced from one simple case.

Let the spin functions for an atom consisting of electron (1) and proton (1) be $a(1)\alpha(1)$, $[a(1)\beta(1) + b(1)\alpha(1)]/\sqrt{2}$, $b(1)\beta(1)$, and $[a(1)\beta(1) - b(1)\,\alpha(1)]/\sqrt{2}$, where a and b are normalized spin functions for a proton and α and β are normalized spin functions for an electron. Suppose that atom (1) is initially in one of the $F = 1$ states, say $\alpha(1)a(1)$. It meets in collision an arbitrary second atom. The nuclear spin of this atom is not correlated with that of atom (1); hence the spin of electron (2) is directed at random; this would be true even if the quantum number F_2 were specified (though not, of course, if we further specified m_2). We may, therefore, write for the spin functions of the unpolarized electron (2), $[\alpha(2)e^{i\gamma} + \beta(2)]/\sqrt{2}$; and the nature of its nuclear spin function $S(2)$ is irrelevant. The factor $e^{i\gamma}$, a particular value of which would imply more about the spin of electron (2) than we may specify, is introduced explicitly to show that it does not affect the final result. The entire spin function, prior to collision, may now be written

$$\psi_{\text{before}} = 2^{-1/2} a(1)\,\alpha(1)\,[\alpha(2)\,e^{i\gamma} + \beta(2)]\,S(2)\,. \tag{3}$$

This is readily expanded in symmetrical and antisymmetrical electronic spin functions:

$$\begin{aligned}\psi_{\text{before}} = 2^{-3/2} a(1)\,S(2)\,\{2\alpha(1)\,\alpha(2)\,e^{i\gamma} &+ [\alpha(1)\,\beta(2) + \beta(1)\,\alpha(2)] \\ &+ [\alpha(1)\,\beta(2) - \beta(1)\,\alpha(2)]\}\,.\end{aligned} \tag{4}$$

With the symmetrical parts is associated the phase factor $\exp(-iV_t t/\hbar)$ and with the antisymmetrical component, $\exp(-iV_s t/\hbar)$. Hence, apart from an irrelevant common phase factor, the spin function after collision is

$$\begin{aligned}\psi_{\text{after}} = 2^{-3/2} a(1)\,S(2)\,\{2\alpha(1)\,\alpha(2)\,e^{i\gamma} &+ [\alpha(1)\,\beta(2) + \beta(1)\,\alpha(2)] \\ &+ e^{i\phi_{ts}}[\alpha(1)\,\beta(2) - \beta(1)\,\alpha(2)]\}\,,\end{aligned} \tag{5}$$

with ϕ_{ts} given by equation (2). From this we easily compute the probability that atom (1) is in the state $F = 0$, with spin function $[a(1)\beta(1) - b(1)\alpha(1)]/\sqrt{2}$ after the collision; it is $|1 - e^{i\phi_{ts}}|^2/16$, or $\frac{1}{4}\sin^2(\phi_{ts}/2)$.

We define a *strong* collision as one for which $\phi_{ts} \gg 1$. For such collisions as a class the average value of $\sin^2(\phi_{ts}/2)$ will be $\frac{1}{2}$. We therefore conclude that an atom in the state $F = 1$, which experiences a strong collision with an arbitrary atom of the gas, has a chance of $\frac{1}{8}$ of departing the collision in the state $F = 0$. This probability we call W_{10}. It is clearly necessary that the converse probability, W_{01}, that is, the probability that an atom initially in $F = 0$ will leave a strong collision in $F = 1$, be $\frac{3}{8}$.

It is worth noting that the conclusion reached here is independent of the prior state of the collision partner; in other words, the probability that a selected atom in its next strong collision will be thrown into the other hyperfine state is independent of the relative occupation of the two states in the gas as a whole. However, W_{10} may depend on the gas kinetic temperature, T_K. Indeed, it must, because the ratio of the upward to the downward probability has, by detailed balancing, the value appropriate to thermal equilibrium with only collisions acting, namely, $3\exp(-\hbar\omega/kT_K)$. Detailed examination of the collisions with the kinetic and spin co-ordinates given full and equal treatment would necessarily yield probabilities biased in favor of downward transitions. In our case the bias is relatively small because $\hbar\omega/kT_K$ is a small quantity for all temperatures of interest ($\hbar\omega/k = 0.068°$ K). We may therefore use

$$\begin{aligned} W_{10} &= W\,, \\ W_{01} &= 3W\exp\left(-\frac{\hbar\omega}{kT_K}\right), \end{aligned} \tag{6}$$

and take W to be $\frac{1}{8}$. The error in so doing (of order $\hbar\omega/kT_K$) resides entirely in W and can cause, at worst, a wholly negligible error in the net transition rate. The *ratio* of upward to downward probability is given correctly by equations (6), although, of course, to the accuracy we require, the Boltzmann factor can be replaced by $(1 - \hbar\omega/kT_K)$.

Finally, to quiet any misgivings about the preservation of an atom's identity through a collision, we remark that all interactions involving the nuclear spin, including the hyperfine interaction itself, are, in fact, weak compared to ($\hbar$/collision duration), so that the orientation of the proton spin is an admissible label. The same argument justifies our brusque treatment of the nuclear spin co-ordinates in the calculation.

CROSS-SECTIONS

In the picture of the collision outlined previously, we may view the colliding pair as being in a mixture of space-symmetric and space-antisymmetric electronic states. Each state evolves independently of the other, and a phase shift ϕ_{ts} develops between the two. It is clear that in the development of the symmetric state, which is attractive, closer distances of approach will be involved for given initial conditions than in the development of the antisymmetric. The phase shift will thus arise chiefly from the behavior of the symmetric state. We need consider, therefore, only what happens in a "symmetric collision."

We shall treat the kinematics of the collision classically, justifying this approximation later by showing that, over most of the range of interest, the angular momentums involved are fairly large. The internuclear force for a given instantaneous nuclear separation will be assumed to be that appropriate to the same configuration at rest. That is, we shall work in the usual adiabatic approximation.

We shall concentrate our attention on strong collisions at the outset. If no angular momentum were involved, all collisions would be strong in the sense that the attractive force would bring the atoms together until the repulsive core of the molecular potential began to act, thus conducting them through a region of large exchange energy. Such a collision would result in a phase shift of hundreds of radians. The centrifugal barrier prevents this from happening in many cases, however. Consider the motion of a pair of atoms in center-of-mass co-ordinates. Let E be the energy of one of the atoms at infinity, where it moves in a trajectory specified by the impact parameter r_0 (measured to the center of the mass). The atom will be repelled by a centrifugal barrier Er_0^2/r^2. Only when r_0 is small enough will the atom surmount the barrier and proceed on to the repulsive core. If r_0 is too big, the atom is repelled by the centrifugal barrier and never reaches the region of large exchange energy. Evidently, there is a critical value of r_0 (a function of E), dividing strong from not-strong collisions. With the critical r_0, the atom arrives at the top of the potential barrier with zero velocity. The strong collision cross-section σ for the energy E is then $4\pi r_0^2$. In actual computations, $r_0(E)$ is computed parametrically through its dependence on r_1, the turning-point radius. If $S(r) = d(\log V)/2d(\log r)$, with V the potential per atom, then $E = V(r_1)[1 + S(r_1)]$ and $r_0^2 = r_1^2 S(r_1)/[1 + S(r_1)]$.

Values of $V(r)$ for r between $2a_0$ and $6a_0$ (nuclear separations between $4a_0$ and $12a_0$) were taken from Hirschfelder, Curtiss, and Bird (1954). Two additional points at $r = 6.5a_0$ and $7a_0$ were computed with the formulae of Pauling and Beach (1935) recommended by Hirschfelder *et al.* (The latter authors review various experimental curves, exchange and variational calculations, and van der Waals' calculations and select a "most likely potential" for both symmetric and antisymmetric cases.)

The calculated r_0 varies only slowly with E, a behavior which reflects the steepness of $V(r)$. It is not hard to take this variation into account for a gas having a Maxwellian velocity distribution. We use an equation adapted from Jeans (1925):

$$\bar{\sigma} = \int^{\infty} \sigma(u)\, u\, e^{-u} du\,; \qquad u = \frac{2E}{kT_K}. \tag{7}$$

If $\sigma(E)$ were given by a power law $\sigma \sim E^{-\mu}$, the effective cross-section appropriate to the kinetic temperature T_K, $\bar{\sigma}\ (T_K)$, would be found as follows:

$$\bar{\sigma}(T_K) = \sigma(E^*) = 4\pi r_0^2(E^*)\ , \tag{8}$$

with

$$E^* = \tfrac{1}{2}kT_K[\Gamma(2-\mu)]^{-1/\mu}\ .$$

Our results are fairly well represented by $\mu = 0.27$. Inserting this value into equation (8) gives $E^* = 0.70\,kT_K$. That is, we get the correct strong-collision rate in a Maxwellian gas at T_K by finding the r_0 that corresponds to $E = 0.70\,kT_K$ and using $4\pi r_0^2$ as a "hard sphere" cross-section in the Maxwellian formula,

$$\nu = \sqrt{2}n\bar{\sigma}\left(\frac{8kT_K}{\pi M}\right)^{1/2}. \tag{9}$$

The errors in this procedure due to imprecision in the power law and the assumption of the same power law for the tails of the velocity distribution were investigated and found to be no more than a few per cent.

TABLE 1

STRONG-COLLISION CROSS-SECTION AS FUNCTION OF KINETIC TEMPERATURE

T_K (° K)	$\bar{\sigma}$ (10^{-15} cm^2)	Angular Momentum ($\hbar$)	y/n	T_K (° K)	$\bar{\sigma}$ (10^{-15} cm^2)	Angular Momentum ($\hbar$)	y/n
1	19.6	1.4	1200	300	4.42	11	16
3	13.7	2.0	490	1000	3.45	17	6.7
10	9.50	3.0	190	3000	2.62	26	3.3
30	7.42	4.5	85	10000	1.90	40	1.3
100	5.65	7.4	35				

The effective cross-section for strong collisions thus computed is given in Table 1 for various kinetic temperatures. At 1° K the cross-section $\bar{\sigma}$ is more than two hundred times πa_0^2. It decreases slowly with rising gas temperature, varying approximately as $T_K^{-0.27}$, as already noted. It is perhaps worth remarking that the cross-section for ordinary gas collisions between hydrogen atoms (that is, the cross-section for momentum transfer) is likewise large, being, in fact, not much different from the cross-section given in Table 1. This should be borne in mind when one is considering transport properties of interstellar or intergalactic H I gas.

The third column of the table gives the angular momentum, in units of $\hbar$, of a typical collision. This provides some justification for our classical treatment of the impact. Note that at the lowest temperatures the angular momenta are *not* very large; the accuracy of our results there is uncertain.

It remains to examine the contribution of collisions which are not strong. Consider the value of ϕ_{ts}: evidently, as we increase r_0 from its critical value at the energy E, we reach a point where $\phi_{ts} = \pi$. An exchange is likely in the *intermediate region* between $\phi_{ts} = \infty$ and $\phi_{ts} = \pi$, and so its area should be added to the strong-collision cross-section. Beyond the point where $\phi_{ts} = \pi$, ϕ_{ts} will decrease uniformly outward, implying a rather small probability, $\frac{1}{8}\sin^2(\phi_{ts}/2)$, of exchange. This *region of weak collisions* will contribute something to the total cross-section if the annular areas weighted by the exchange probability are summed. Closer examination shows that both these effects become considerable above $T_K = 1000°$, so that the strong-collision approximation is not accurate above that temperature.

The deviation from the critical r_0 for which $\phi_{ts} = \pi$ depends very sensitively on the critical impact parameter itself, and thus the contribution of the intermediate region will drop very sharply as r_0 is increased. However, it amounts to 10 per cent of the strong-collision cross-section at $r_0 = 1.66 \times 10^{-8}$ cm, which corresponds to 1000°. At that radius the contribution of weak collisions of the same energy is 25 per cent, falling exponentially as r_0 is increased. We conclude that the strong-collision approximation breaks down for $T_K = 1000°$. The cross-sections for 3000° and 10000° are therefore in error by an uncertain amount. On the other hand, we may be sure that they are *less* than the 1000° value of 3.45×10^{-15} cm², since in a higher-energy collision the phase shifts will be less for every impact parameter.

APPLICATIONS

In view of the effectiveness of the hydrogen-hydrogen collisions and the rarity of collisions of any other sort in the interstellar medium, the only collision process we shall need to consider is the spin exchange examined earlier. To be sure, a similar spin exchange could occur between a hydrogen atom and a free electron, but this would assume relative importance only in an H I region containing electrons with more than a few per cent of the hydrogen abundance—an unlikely state of affairs.

Radiative processes may be of two types—radio-frequency and optical. The latter, notably absorption of Lyman radiation, can excite atoms in the singlet ground state, whereupon they re-emit and land on the triplet. For 21-cm processes the radiation intensity is important; for Lyman transitions the spectral gradient over the 1420-megacycle interval is important also. Wouthuysen (1952) has considered this effect for trapped Lyman-α radiation and has shown that the color temperature of such radiation will approach the kinetic temperature of the gas. It now seems likely, however, that Lyman radiation processes will be unimportant in interstellar space, owing to the large effective opacity of the dust for the highly scattered Lyman-α (van de Hulst, Muller, and Oort 1954). We shall confine our attention here to radio-frequency transitions. We want to examine the competition between exchange collisions and radiation in establishing the spin temperature.

Let P_{10} be the probability per second that an atom in the triplet state will go to the singlet as a result of a collision; it is equal to $\nu/8$, with ν the collision rate previously given in equation (9). The probability of the inverse process is, then, $3P_{10} \exp(-\hbar\omega/kT_K)$. The equation of equilibrium is

$$n_1\left(P_{10} + A_{10} + A_{10}\frac{\lambda^2}{2\hbar\omega} I\right) = 3n_0\left[P_{10}\exp\left(-\frac{\hbar\omega}{kT_K}\right) + A_{10}\frac{\lambda^2}{2\hbar\omega_K} I\right]. \tag{10}$$

Here λ and ω refer to 21 cm, and I is the specific intensity of 21-cm background radiation. By "background radiation" we mean the 21-cm radiation of any origin whatever, incident on the region in question. Usually this background radiation will not be isotropic, so we must understand I to mean an average taken over all directions of incidence. We define in terms of I a radiation temperature, T_R, by the relation

$$I = \frac{2\hbar\omega}{\lambda^2}\left[\exp\left(\frac{\hbar\omega}{kT_R}\right) - 1\right]^{-1}. \tag{11}$$

No matter what the source of the radiation is, T_R is the temperature to which the spin populations of atoms exposed to this radiation would adjust in the absence of competing mechanisms. If it happens that the T_R so defined is large compared to $\hbar\omega/k$, it coincides with the brightness temperature, T_B, usually defined in radio astronomy by

$$I = \frac{2kT_B}{\lambda^2}. \tag{12}$$

It follows from equations (1), (10), and (11) that

$$e^{-\hbar\omega/kT_S} = \frac{P_{10}\, e^{-\hbar\omega/kT_K}\,(e^{\hbar\omega/kT_R} - 1) + A_{10}}{(P_{10} + A_{10})\,(e^{\hbar\omega/kT_R} - 1) + A_{10}}. \tag{13}$$

Usually, both kT_K and kT_R will be large compared to $\hbar\omega$. We may be sure that kT_S will then be large compared to $\hbar\omega$ also, since T_S will necessarily lie between T_K and T_R. Making the appropriate approximations in equation (13), we obtain the simpler relation,

$$T_S = \frac{y}{1+y}\, T_K + \frac{1}{1+y}\, T_R, \tag{14}$$

where we have introduced the abbreviation

$$y = \frac{\hbar\omega P_{10}}{kT_K A_{10}}. \tag{15}$$

The dependence of the parameter y on the density of atoms n, the kinetic temperature T_K, and the strong-collision cross-section $\bar{\sigma}$ is shown explicitly in equation (16):

$$y = \frac{\hbar\omega}{2kA_{10}} \left(\frac{k}{\pi M}\right)^{1/2} n\bar{\sigma} T_K^{-1/2}. \tag{16}$$

Since $\bar{\sigma} \sim T_K^{-0.27}$ approximately, y varies as $T_K^{-0.77}$. It expresses the effectiveness of collisions relative to that of radiation processes in establishing the spin temperature. In the last column of Table 1 the values of y/n for various T_K are given. Here $A_{10} = 2.85 \times 10^{-15}$ sec^{-1} was used (Wild 1952). To employ equation (14), then, we multiply n by the y/n from Table 1 and insert the result in equation (14).

The statement that collisions are most important in the standard galactic interstellar H I situation (Shklovsky 1949; Ewen and Purcell 1951; Wild 1952) follows if we recognize that T_R, even at the galactic center, is only about 10°. For then, at densities comparable with unity and practically all kinetic temperatures, y is large, and collisions dominate. For example, if we take $T_K = 100°$ K, $n = 1$ cm^{-3}, and $T_R = 10°$ K, y is 35, and T_S differs from T_K by only 2.5° K. If n were as small as 0.01 cm^{-3}, on the other hand, T_S would fall to 33° K, illustrating the importance of spontaneous emission at low densities. Care should therefore be exercised in interpreting weak absorption lines in terms of total numbers of atoms. If the derived densities are low, on the basis of assumed kinetic temperatures, the spin temperature may differ considerably from T_K, and the derived densities should be re-examined.

There are particular conditions under which we might expect collisions to be unimportant relative to radiation. In the intergalactic medium, for example, y will be small for even the lowest kinetic temperatures, if the density is as low as has been suggested (10^{-4} cm^{-3}). Also, even in dense regions, the radiation temperature may reach such values as to make T_R dominant. For example, absorbing clouds in the near vicinity of a bright radio source should exhibit spin temperatures far from the kinetic temperature. It is easy to show that the apparent absorption $(T_{\text{cont}} - T_{\text{line}})/T_{\text{cont}} = (1 - e^{-\tau})(1 - T_S/T_R)$, where τ is the opacity of the absorbing layer. In the particular case of Lilley and McClain's (1956) observations of H I absorption in Cyg A, we may draw some interesting conclusions from a consideration of the effects of the continuum radiation on the spin temperature of the H I in front of the source. From the angular dimensions given by Baade and Minkowski (1954) and the continuum flux near 21 cm given by

Hagen, McClain, and Hepburn (1955), we estimate an average radiation density in the neighborhood of the source which corresponds to a radiation temperature T_R approximately equal to 1.0×10^5 ° K. On the other hand, if we take $n = 1\ \text{cm}^{-3}$ and $T_K = 100°$ for the H I, following Lilley and McClain, we find that $y = 35$. Thus the 2880° K contribution by the radiation term far outweighs that of 97° K by the collision term. The *direct* effect of increasing T_S is to increase the H I emission, thus reducing the apparent absorption, and is accounted for by the second term in the expression for the apparent absorption. Evidently, we may neglect the direct effect in the present case, since T_S/T_R is only $\frac{1}{36}$.

On the other hand, increasing T_S decreases the effective opacity in the ratio $h\omega/kT_S$ (Wild 1952). Thus the τ deduced by using our expression for the apparent absorption can be related to the number of absorbing atoms only if T_S is known. In fact, the number of absorbing atoms estimated from the apparent absorption will be proportional to T_S. Lilley and McClain adopted 100° K for the latter and derived $7 \times 10^7 \times A$ suns for the mass of absorbing H I, with A the absorbing area in square kiloparsecs. We have shown that T_S is, in fact, thirty times as great as they assumed, from which it follows that the mass estimate should be revised upward to $2.0 \times 10^9 \times A$ suns. The latter figure approaches the mass of H I in a typical spiral galaxy if the dimensions of the absorbing region are of the order of 10 kpc. That this should be so does not disagree with the radio dimensions of 10×40 kpc; or with Baade and Minkowski's characterization of the system as a giant one. It should be noted that the estimate of number of atoms absorbing the radiation from Cyg A is still sensitive to the density and temperature assumed for the H I. We conclude that in the case of Cyg A and in similar cases one needs to know something about the radiation density as well as something about the gas density and temperature in the cloud, in order to interpret absorption measurements properly in terms of numbers of atoms.

REFERENCES

Baade, W., and Minkowski, R. 1954, *Ap. J.*, **119**, 206.
Ewen, H. I., and Purcell, E. M. 1951, *Nature*, **168**, 356.
Hagen, J. P., McClain, E. F., and Hepburn, N. 1954, *Proc. I.R.E.*, **42**, 1811.
Hirschfelder, J. O., Curtiss, C. F., and Bird, R. B. 1954, *Molecular Theory of Gases and Liquids* (New York: John Wiley & Sons).
Hulst, H. C. van de, Muller, C. A., and Oort, J. H. 1954, *B.A.N.*, **12**, No. 452, 117.
Jeans, Sir J. 1925, *Dynamical Theory of Gases* (Cambridge: At the University Press), p. 36.
Lilley, A. E., and McClain, E. F. 1956, *Ap. J.*, **123**, 172.
Pauling, L., and Beach, J. Y. 1935, *Phys. Rev.*, **47**, 686.
Shklovsky, I. S. 1949, *Astr. J. U.S.S.R.*, **26**, 10.
Wild, J. P. 1952, *Ap. J.*, **115**, 206.
Wittke, J. P., and Dicke, R. H. 1956, *Phys. Rev.*, **103**, 620.
Wouthuysen, S. 1952, *Physica*, **18**, 75.

ABSORPTION COEFFICIENTS FOR FREE-FREE TRANSITIONS IN A HYDROGEN PLASMA

JAY M. BERGER*
Project Matterhorn, Forrestal Research Center, Princeton University

Received June 28, 1956

ABSTRACT

Absorption coefficients for free-free transitions in a dilute hydrogen plasma have been calculated numerically, making use of results obtained for Bremsstrahlung from Sommerfeld's exact treatment and from the Born approximation as modified by Elwert. Results were obtained for a range of temperatures from 0.5 to 100.0 ev and a range of wave lengths from 500 to 10000 A. These results, including Gaunt factors, are given in Table 1.

INTRODUCTION

We have performed numerical calculations of the free-free absorption coefficients for a dilute, completely ionized hydrogen plasma in thermal equilibrium, making use of the result obtained by Sommerfeld for the inverse process of Bremsstrahlung. Sommerfeld's result is exact, except that relativistic and retardation effects are neglected. Also, effects produced by high densities, considered by Kulsrud (1954) and Rudkjøbing (1955) in this connection, are ignored. The absorption coefficients have been calculated for a range of temperatures from 0.5 to 100.0 ev and for the optical wave lengths from 500 to 10000 A. These results have been compared to those obtained from Kramers' (1923) formula to obtain the average Gaunt factor. In addition, we have calculated the absorption coefficients obtained by making use of the Bremsstrahlung results from the non-relativistic Born approximation as modified by Elwert (1939). This last result, while still necessitating numerical calculation, is obtained much more easily than the exact results and, as will be seen, yields better agreement with the exact results than does Kramers' formula. All numerical calculations were done with the aid of the New York University A.E.C. computing facility UNIVAC.

The calculation and results for the total intensity of Bremsstrahlung, upon which the calculations described here are based, are reported elsewhere (Berger 1956). They are summarized briefly in the next section, where the calculation of the absorption coefficient is also described. The results we obtain here are presented in Table 1 and Figure 1 and are discussed in the last section.

THE CALCULATION

The basis of this calculation is the numerical results that have been obtained for the total intensity of electron Bremsstrahlung from the formula given by Sommerfeld and from the Born approximation as modified by Elwert. Sommerfeld's formula is

$$W_S = \frac{8\pi}{3}\frac{e^2}{c^3}\left(\frac{h}{m}\right)^2\left(\frac{Z}{a}\right)^2 \frac{d\nu}{(e^{2\pi|n_1|}-1)(1-e^{-2\pi|n_2|})}\frac{x_0}{k_1^2}\frac{d}{d x_0}\left|F(x_0)\right|^2, \qquad (1)$$

where

$$a = \frac{h^2}{m e^2}, \qquad k_1 = \frac{m v_1}{\hbar}, \qquad n_1 = \frac{Z}{i k_1 a}, \qquad x_0 = \frac{4 n_1 n_2}{(n_1 - n_2)^2},$$

$$F(x_0) = F(-n_1, -n_2, 1; x_0);$$

---

* Now at the I.B.M. Research Laboratory, Poughkeepsie, N.Y.

the subscript 1 refers to the incoming electron and the subscript 2 to the emergent electron; v is the electron velocity and Z the nuclear charge (unity in this calculation); m is the electron mass and e the electron charge; c is the velocity of light; h is Planck's constant; and $F(x_0)$ is the hypergeometric function. The total intensity from the Born approximation, as modified by Elwert, is given by

$$W_{BE} = \frac{4}{3\pi} \frac{(1 - e^{-2\pi|n_1|})}{(1 - e^{-2\pi|n_2|})} \frac{e^2}{c^3} \left(\frac{h}{m}\right)^2 \left(\frac{Z}{a}\right)^2 \frac{d\nu}{k_1 k_2} \ln(1 - x_0) , \tag{2}$$

in which W_S and W_{BE} represent the total radiated energy in ergs per frequency interval $d\nu$ per unit flux of electrons per proton and in which the integrations over all angles of emission of the final electron and photon have been performed. For the calculations to be described, about ten thousand cases of both W_S and W_{BE} were required, corresponding to two hundred incident electron energies in the range from 0.44 to 800.0 ev and fifty emergent electron energies per incident electron energy.

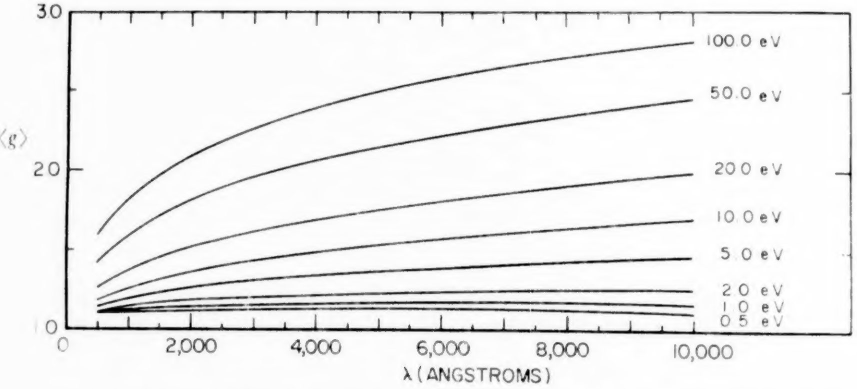

FIG. 1.—The average Gaunt factor, $\langle g \rangle = K_S/K_K$, plotted as a function of wave length for various temperatures between 0.5 and 100.0 ev.

The numerical calculations then proceed as follows: for each value of the incident electron energy, interpolations were performed on the emergent electron energies, using Aitken's (see Milne 1949) method, for that value corresponding to the desired wave length of emitted light. Ten-point interpolation was used, except for some cases in which only six points were used. The twenty wave lengths which were interpolated for are given by

$$\lambda = 500\,\text{A} + N \cdot 500\,\text{A}, \quad (N = 0, 1, 2, \ldots, 18, 19) . \tag{3}$$

The two hundred values of W for each wave length were then multiplied by the electron flux, corresponding to an electron density of 1/cc, and integrated over a Maxwell distribution for each temperature, using Simpson's rule, thus yielding the integrated intensity $I(\lambda, T)$. The temperatures used were T = 0.5, 1.0, 2.0, 5.0, 10.0, 20.0, 50.0, and 100.0 ev. Use was then made of detailed balancing in thermal equilibrium to obtain the absorption coefficient, K. That is,

$$I(\lambda, T) \left[1 + \frac{B}{A} \rho(\lambda, T) \right] = K \rho(\lambda, T) , \tag{4}$$

TABLE 1

ABSORPTION COEFFICIENTS AND GAUNT FACTORS

λ (A)		T(ev)							
		0.5	1.0	2.0	5.0	10.0	20.0	50.0	100.0
500	$K_S \times 10^{41}$	2.48	1.75	1.25	0.8167	0.5981	0.4480	0.3194	0.2547
	$K_{BE} \times 10^{41}$	2.47	1.74	1.25	0.8172	0.6021	0.4535	0.3246	0.2585
	$\langle g \rangle$	1.10	1.10	1.11	1.149	1.190	1.260	1.421	1.602
1000	$K_S \times 10^{40}$	2.00	1.43	1.03	0.6800	0.5090	0.3917	0.2887	0.2338
	$K_{BE} \times 10^{40}$	2.00	1.43	1.03	0.6910	0.5216	0.4034	0.2970	0.2392
	$\langle g \rangle$	1.11	1.12	1.14	1.196	1.266	1.377	1.605	1.839
1500	$K_S \times 10^{40}$	6.70	4.81	3.49	2.346	1.785	1.397	1.048	0.8540
	$K_{BE} \times 10^{40}$	6.77	4.87	3.55	2.419	1.856	1.457	1.086	0.8779
	$\langle g \rangle$	1.10	1.12	1.15	1.222	1.315	1.456	1.727	1.990
2000	$K_S \times 10^{39}$	1.63	1.19	0.862	0.5767	0.4402	0.3469	0.2622	0.2140
	$K_{BE} \times 10^{39}$	1.64	1.20	0.883	0.6010	0.4628	0.3650	0.2732	0.2207
	$\langle g \rangle$	1.13	1.17	1.199	1.267	1.368	1.525	1.823	2.105
2500	$K_S \times 10^{39}$	3.16	2.29	1.684	1.144	0.8825	0.7013	0.5335	0.4362
	$K_{BE} \times 10^{39}$	3.19	2.33	1.737	1.203	0.9360	0.7430	0.5580	0.4506
	$\langle g \rangle$	1.12	1.15	1.199	1.288	1.404	1.579	1.899	2.196
3000	$K_S \times 10^{39}$	5.455	3.958	2.916	2.004	1.558	1.247	0.9535	0.7802
	$K_{BE} \times 10^{39}$	5.543	4.058	3.035	2.128	1.666	1.329	1.000	0.8070
	$\langle g \rangle$	1.123	1.153	1.201	1.306	1.436	1.624	1.964	2.273
3500	$K_S \times 10^{39}$	8.664	6.292	4.652	3.225	2.524	2.030	1.557	1.275
	$K_{BE} \times 10^{39}$	8.843	6.493	4.878	3.451	2.717	2.173	1.637	1.320
	$\langle g \rangle$	1.123	1.154	1.207	1.323	1.464	1.666	2.021	2.339
4000	$K_S \times 10^{38}$	1.294	0.9411	0.6979	0.4872	0.3835	0.3098	0.2383	0.1950
	$K_{BE} \times 10^{38}$	1.329	0.9780	0.7374	0.5253	0.4153	0.3329	0.2510	0.2021
	$\langle g \rangle$	1.124	1.156	1.213	1.339	1.490	1.702	2.071	2.397
4500	$K_S \times 10^{38}$	1.841	1.341	0.9982	0.7015	0.5549	0.4498	0.3467	0.2837
	$K_{BE} \times 10^{38}$	1.901	1.403	1.062	0.7614	0.6039	0.4851	0.3657	0.2943
	$\langle g \rangle$	1.123	1.158	1.218	1.354	1.514	1.736	2.116	2.449
5000	$K_S \times 10^{38}$	2.525	1.843	1.375	0.9722	0.7723	0.6280	0.4848	0.3967
	$K_{BE} \times 10^{38}$	2.623	1.941	1.474	1.061	0.8446	0.6793	0.5121	0.4117
	$\langle g \rangle$	1.123	1.159	1.223	1.368	1.537	1.767	2.157	2.496
5500	$K_S \times 10^{38}$	3.361	2.457	1.838	1.396	1.042	0.8495	0.6567	0.5371
	$K_{BE} \times 10^{38}$	3.511	2.604	1.984	1.435	1.144	0.9212	0.6943	0.5577
	$\langle g \rangle$	1.123	1.162	1.229	1.381	1.558	1.796	2.195	2.539
6000	$K_S \times 10^{38}$	4.356	3.192	2.396	1.712	1.369	1.119	0.8661	0.7082
	$K_{BE} \times 10^{38}$	4.577	3.405	2.602	1.890	1.509	1.216	0.9167	0.7356
	$\langle g \rangle$	1.121	1.162	1.234	1.394	1.577	1.822	2.230	2.579
6500	$K_S \times 10^{38}$	5.542	4.067	3.060	2.195	1.762	1.442	1.117	0.9132
	$K_{BE} \times 10^{38}$	5.845	4.360	3.341	2.435	1.948	1.571	1.183	0.9490
	$\langle g \rangle$	1.122	1.165	1.239	1.406	1.596	1.848	2.263	2.615
7000	$K_S \times 10^{37}$	0.6930	0.5092	0.3839	0.2765	0.2225	0.1825	0.1414	0.1155
	$K_{BE} \times 10^{37}$	0.7334	0.5484	0.4213	0.3080	0.2468	0.1991	0.1499	0.1201
	$\langle g \rangle$	1.123	1.167	1.245	1.418	1.614	1.871	2.293	2.650

TABLE 1—*Continued*

λ (Å)		T(ev)							
		0.5	1.0	2.0	5.0	10.0	20.0	50.0	100.0
7500	$K_S \times 10^{37}$	0.8539	0.6280	0.4743	0.3429	0.2766	0.2272	0.1761	0.1438
	$K_{BE} \times 10^{37}$	0.9065	0.6792	0.5230	0.3834	0.3076	0.2482	0.1868	0.1495
	$\langle g \rangle$	1.125	1.170	1.250	1.429	1.631	1.894	2.322	2.682
8000	$K_S \times 10^{37}$	1.037	0.7640	0.5781	0.4193	0.3390	0.2788	0.2162	0.1765
	$K_{BE} \times 10^{37}$	1.105	0.8299	0.6405	0.4707	0.3780	0.3051	0.2295	0.1836
	$\langle g \rangle$	1.127	1.173	1.256	1.440	1.647	1.915	2.349	2.712
8500	$K_S \times 10^{37}$	1.246	0.9185	0.6964	0.5068	0.4106	0.3381	0.2622	0.2140
	$K_{BE} \times 10^{37}$	1.331	1.001	0.7748	0.5707	0.4588	0.3704	0.2784	0.2226
	$\langle g \rangle$	1.128	1.176	1.261	1.451	1.663	1.936	2.375	2.741
9000	$K_S \times 10^{37}$	1.480	1.092	0.8299	0.6058	0.4919	0.4054	0.3145	0.2565
	$K_{BE} \times 10^{37}$	1.586	1.196	0.9271	0.6844	0.5507	0.4446	0.3340	0.2669
	$\langle g \rangle$	1.129	1.179	1.266	1.461	1.678	1.956	2.399	2.768
9500	$K_S \times 10^{37}$	1.742	1.287	0.9799	0.7169	0.5829	0.4810	0.3733	0.3044
	$K_{BE} \times 10^{37}$	1.874	1.415	1.099	0.8129	0.6545	0.5285	0.3968	0.3169
	$\langle g \rangle$	1.130	1.181	1.271	1.470	1.691	1.973	2.422	2.793
10000	$K_S \times 10^{37}$	2.032	1.505	1.147	0.8414	0.6851	0.5658	0.4394	0.3582
	$K_{BE} \times 10^{37}$	2.194	1.660	1.291	0.9570	0.7710	0.6226	0.4673	0.3728
	$\langle g \rangle$	1.130	1.183	1.276	1.480	1.704	1.990	2.444	2.817

where A and B are the Einstein coefficients and $p(\lambda, T)$ is the intensity of black-body radiation, i.e.,

$$\frac{B}{A}=\frac{\lambda^3}{2hc}, \quad p(\lambda, T)=\frac{2hc}{\lambda^3}\,\frac{1}{\exp(hc/\lambda kT)-1},$$

where k is the Boltzmann constant. Re-expressing equation (4), we have

$$K=\frac{\lambda^3}{2hc}\exp\left(\frac{hc}{\lambda kT}\right) I(\lambda, T). \tag{5}$$

When W_S is used, we obtain the exact absorption coefficient, K_S, and with W_{BE} we obtain K_{BE}. Then K_S was compared to Kramers' result, K_K, which is

$$K_K=\frac{8}{3\sqrt{3}}\,\frac{Z^2h^2e^2}{m^4c^4}\,\lambda^3\left(\frac{m}{2\pi kT}\right)^{3/2} RkT, \tag{6}$$

where R is the Rydberg constant, thus obtaining $\langle g\rangle$ as

$$\langle g\rangle=\frac{K_S}{K_K}. \tag{7}$$

The units in which the absorption coefficients are expressed are square centimeters per electron per cubic centimeter per proton per cubic centimeter.

RESULTS

In Table 1 we present the numerical results of the calculations of the Sommerfeld absorption coefficient, K_S; the Born-Elwert absorption coefficient, K_{BE}; and the average Gaunt factor, $\langle g \rangle$, relating K_S and the Kramers absorption coefficient, K_K, for the various values of wave length and temperature. In addition, in Figure 1 we display $\langle g \rangle$ as a function of wave length for the different temperatures that were calculated.

In Table 1 the last significant figure is uncertain to about two parts for the short wave lengths and low temperatures. The accuracy increases along the main diagonal, yielding results to more significant figures, with about the same uncertainty for the last significant figures in the center of the table. For the longest wave lengths and highest temperatures, the results given may be considered as exact.

Examination of Table 1 yields two interesting points. The first is that $\langle g \rangle$ is seen to be roughly constant for the same value of $h\nu/kT$, in agreement with Kulsrud's results obtained at higher energies. The second point is that, while the Born-Elwert result gives better agreement than does Kramers' result for the points calculated, Kramers' result appears to be quite good if one extrapolates these results to the maximum of the Planck distribution for the various temperatures.

We are indebted to Professor Lyman Spitzer, Jr., for his aid and advice, to Dr. Phyllis Fox for her aid in programing the problem, and to Mrs. Frances Hirschkron for hand computations.

REFERENCES

Berger, J. 1956, *Phys. Rev.*, in press.
Elwert, G. 1939, *Ann. d. Phys.*, **34**, 178.
Kramers, H. A. 1923, *Phil. Mag.*, **46**, 836.
Kulsrud, R. 1954, *Ap. J.*, **119**, 386.
Milne, W. E. 1949, *Numerical Calculus* (Princeton, N.J.: Princeton University Press), p. 69.
Rudkjøbing, M. 1955, *Ann. d'ap.*, **18**, 11.
Sommerfeld, A. *Wellenmechanik* (New York: Frederick Ungar Publishing Co.), p. 527.

RADIATION BY PLASMA OSCILLATIONS

George B. Field*
Princeton University Observatory

Received February 3, 1956; revised April 26, 1956

ABSTRACT

In a homogeneous plasma having no static electric or magnetic fields the longitudinal plasma waves and the transverse electromagnetic waves are uncoupled. It is shown that in the presence of inhomogeneities they are coupled, leading to the possibility of radiation by plasma waves generated in astronomical sources. In particular, the radiation resulting from the incidence of a plasma wave on a density discontinuity is calculated. The modifications due to the presence of a static magnetic field are considered. The analysis is applied to a model of solar flare ejections having a density discontinuity; the calculated power greatly exceeds that observed for the solar radio outbursts by Wild and his collaborators. Thus there is hope that the same type of coupling, but with more realistic inhomogeneities, will provide power in the amount observed.

I. INTRODUCTION

Plasma oscillations were first studied in the laboratory by Tonks and Langmuir (1929); following them there has been a steady series of experimental papers devoted to the study of oscillations in gas discharges. However, little of the experimental work bears on the problem under discussion—the coupling of such oscillations to the radiation field. Therefore, we are forced to base the discussion on theoretical developments. The theory of plasma oscillations in a gas of vanishing temperature was given by Tonks and Langmuir in their 1929 paper; it is of merely historical interest that Lord Rayleigh had considered a closely related phenomenon in 1906, in connection with the theory of atomic spectra. Thomson and Thomson (1933) extended the analysis, with a minor error, to the case of non-vanishing temperature; Vlasov (1938) corrected the error. Landau (1946) discussed damping, as did Bohm and Gross (1949*a*, *b;* 1950), who also discussed mechanisms for exciting plasma oscillations.

Astronomical interest in plasma oscillations stems from the results of radio astronomy. On the elementary theory, plasma oscillations have a frequency called the "plasma frequency," which is related only to the electron density by the equation $\nu_p = 10^4 n^{1/2}$. Thus, if the observed radiations originated in plasma oscillations, there would have to be electron densities of the order of 10^8 cm^{-3}. As there are electron densities of this order in the solar corona, various writers, such as Shklovsky (1946), Martyn (1947), and Haeff (1948), have suggested that at least some of the solar radio-frequency radiation, particularly the outbursts observed by Wild and his collaborators (see Pawsey and Smerd, 1953, for a review), does, in fact, originate in plasma oscillations.

There are severe objections to this hypothesis, however. Ryle (1949) pointed out that the identity of the plasma frequency with the critical frequency for total reflection would prevent the escape of any radiation, even if it should be produced. Vlasov (1938) emphasized that, in addition, there was only weak coupling, if any, between the plasma oscillations and the radiation field; this idea was discussed also by Bhatnagar, Krook, and Menzel (1952). Qualitatively, the idea of weak coupling was the consensus at the London Conference on the Dynamics of Ionized Media (1951), but the need for quantitative treatment of the coupling problem was stressed there also.

It is the aim of the present paper to treat the coupling problem quantitatively, showing that under certain conditions the two objections mentioned previously may be overcome. These conditions are, roughly, the presence of density gradients and non-vanishing temperature.

---

* National Science Foundation Predoctoral Fellow, 1954–1955; now a Junior Fellow, Harvard Society of Fellows.

In Section II the longitudinal and transverse waves are treated together on a hydrodynamic model of the plasma; the coupling introduced by inhomogeneities and by a statis magnetic field is discussed. In Section III the discussion is specialized to the case of a density discontinuity with a magnetic field parallel to the boundary. On the assumption that such a model is appropriate, the analysis is applied to a solar flare ejection in Section IV.

II. COUPLING OF LONGITUDINAL AND TRANSVERSE WAVES

In a plasma there are generally two types of wave motion: the longitudinal, or irrotational, and the transverse, or solenoidal. We shall see that in the presence of inhomogeneities or static magnetic fields the two are coupled so that the independent modes are a mixture of each of these two types. But in a homogeneous field-free plasma, the independent modes are of the types mentioned and correspond to the usual designations, "plasma oscillations" and "electromagnetic waves," respectively. The two modes correspond physically to the two ways of maintaining an electric field. In the plasma oscillation the source of the field is accumulation of charge; in the electromagnetic wave, changing magnetic field is the source. It should be noted that the plasma oscillations do not propagate, but a simple extension of them to include the effects of electron pressure does indeed propagate. Thus plasma oscillations which include pressure effects are called "plasma waves"; in what follows, the terms for the longitudinal waves will be used interchangeably. In addition, "radiation" will refer to the transverse mode.

Ideally, the complete treatment of the coupling problem should include both magnetic field and inhomogeneity from the start. It is simpler to consider the effects separately. In fact, if attention is concentrated on a situation in which the plasma density is discontinuous, separate consideration of the two effects is adequate, the effect of a magnetic field being to modify the plasma wave in a uniform way before it is incident on the plasma boundary. Thus the discussion will first center on the effect of inhomogeneity, which may be called "gradient coupling." "Magnetic coupling" will then be considered.

a) Gradient Coupling

Consider a plasma of homogeneous temperature, T, and possibly inhomogeneous electron density, n_0. Because the ions are so heavy compared to the electrons, we may ignore their motions, regarding them as a fixed background which neutralizes the electron charge density in the steady state. Collisions can be ignored except in the most dense plasmas because the ratio of collision frequency to plasma frequency is proportional to the square root of the density; in the corona, the ratio is about 10^{-8} and thus completely negligible.

In order to develop a linear theory, we assume that perturbations in the electron density are small compared to the steady-state value and that electron velocities are small compared to that of light. In fact, there is evidence, to be discussed in Section IV, that the plasma waves in the solar flare ejections are somewhat non-linear, so the present considerations must be viewed as heuristic when applied to them. Finally, we shall set the static magnetic field equal to zero in considering the effects of inhomogeneities.

The equations which describe the plasma are Maxwell's equations, which relate the electromagnetic fields to the electron convection currents; the equation of force, relating accelerations to the fields and pressure gradient; the continuity equation for the electron current; and the relation between pressure and density perturbations. Owing to the smallness of collision effects, this may be taken as the adiabatic relation, just as in the case of sound waves when heat conduction is neglected. The appropriate value of $\gamma = (f + 2)/f$ is not $\frac{5}{3}$, as when collisions excite three degrees of freedom, but rather 3, which results when we realize that only one degree of freedom is excited by the field. Thus the relation between pressure and density perturbations is

$$p = \frac{\gamma p_0 n}{n_0} = 3kTn = mV^2 n, \tag{1}$$

where we have used the expression for the static pressure in terms of the root-mean-square electron velocity V and the electron mass m. If we insert this directly in place of the pressure, the complete linearized equations can be written thus:

$$\nabla \times \boldsymbol{E} = -\frac{1}{c}\frac{\partial \boldsymbol{H}}{\partial t}, \tag{2a}$$

$$\nabla \times \boldsymbol{H} = \frac{1}{c}\frac{\partial \boldsymbol{E}}{\partial t} - \frac{4\pi}{c} n_0 e \boldsymbol{v}, \tag{2b}$$

$$\frac{\partial \boldsymbol{v}}{\partial t} = -\frac{e}{m}\boldsymbol{E} - \frac{V^2}{n_0}\nabla n, \tag{2c}$$

$$\frac{\partial n}{\partial t} = -\nabla \cdot (n_0 \boldsymbol{v}), \tag{2d}$$

in which we have used Gaussian units. Equations (2) are four homogeneous equations for the fields $\boldsymbol{E}$ and $\boldsymbol{H}$, the electron velocity $\boldsymbol{v}$, and the electron density n. An equation for $\boldsymbol{E}$ alone can be obtained as follows: differentiate equation (2*b*) with respect to ct, substitute the time derivatives of $\boldsymbol{H}$ and $\boldsymbol{v}$ from equations (2*a*) and (2*c*), respectively, giving

$$-\nabla \times (\nabla \times \boldsymbol{E}) = \frac{1}{c^2}\left(\frac{\partial^2}{\partial t^2} + \frac{4\pi n_0 e^2}{m}\right)\boldsymbol{E} + \frac{V^2}{c^2} 4\pi e \nabla n. \tag{3}$$

The term in n may be eliminated by using Gauss's law, derivable from equations (2*b*) and (2*d*):

$$\nabla \cdot \boldsymbol{E} = -4\pi e n, \tag{4}$$

so that

$$\nabla n = -\frac{1}{4\pi e}\nabla(\nabla \cdot \boldsymbol{E}). \tag{5}$$

Thus

$$\nabla \times (\nabla \times \boldsymbol{E}) + \frac{1}{c^2}\left(\frac{\partial^2}{\partial t^2} + \omega_p^2\right)\boldsymbol{E} - \frac{V^2}{c^2}\nabla(\nabla \cdot \boldsymbol{E}) = 0, \tag{6}$$

where we have written

$$\omega_p^2 = \frac{4\pi n_0 e^2}{m} \tag{7}$$

and ω_p is the radian plasma frequency. We have therefore replaced the parameters n_0 and T, specifying the state of the plasma, by ω_p and $V = (3kT/m)^{1/2}$. Oscillating solutions are obtained by taking all quantities proportional to $\exp(-j\omega t)$, so that $\partial/\partial t \rightarrow -j\omega$. We introduce the vacuum wave number for the frequency ω, $\kappa_V = \omega/c$, and the quantity $\mu = (1 - \omega_p^2/\omega^2)^{1/2}$, so that equation (6) becomes

$$-\nabla \times (\nabla \times \boldsymbol{E}) + \kappa_V^2 \mu^2 \boldsymbol{E} + \frac{V^2}{c^2}\nabla(\nabla \cdot \boldsymbol{E}) = 0. \tag{8}$$

The splitting of $\boldsymbol{E}$ into longitudinal and transverse components proceeds as follows. Let

$$\boldsymbol{E} = \boldsymbol{E}_L + \boldsymbol{E}_T \ ,$$

where

$$\begin{aligned} \boldsymbol{\nabla} \times \boldsymbol{E}_L &= 0 \ , \\ \boldsymbol{\nabla} \cdot \boldsymbol{E}_T &= 0 \ . \end{aligned} \tag{9}$$

According to a theorem in vector analysis, a vector is specified by its curl and divergence, together with boundary conditions. Thus we must have equations for the quantities $\boldsymbol{\nabla} \cdot \boldsymbol{E}_L$ and $\boldsymbol{\nabla} \times \boldsymbol{E}_T$, which, together with definitions (9), will specify the vectors $\boldsymbol{E}_L$ and $\boldsymbol{E}_T$ by this theorem. If we use definitions (9), together with the expansion of the product of the curl operator with itself, we may write

$$\boldsymbol{\nabla} (\boldsymbol{\nabla} \cdot \boldsymbol{E}) = \boldsymbol{\nabla} (\boldsymbol{\nabla} \cdot \boldsymbol{E}_L) = + \boldsymbol{\nabla}^2 \boldsymbol{E}_L \ ,$$

and

$$\boldsymbol{\nabla} \times (\boldsymbol{\nabla} \times \boldsymbol{E}) = \boldsymbol{\nabla} \times (\boldsymbol{\nabla} \times \boldsymbol{E}_T) = - \boldsymbol{\nabla}^2 \boldsymbol{E}_T \ . \tag{10}$$

If we substitute these equations in equation (8), we have

$$(\boldsymbol{\nabla}^2 + \kappa_V^2 \mu^2) \boldsymbol{E}_T + \left(\frac{V^2}{c^2} \boldsymbol{\nabla}^2 + \kappa_V^2 \mu^2 \right) \boldsymbol{E}_L = 0 \ . \tag{11}$$

The required equations for the curl and divergence of $\boldsymbol{E}_T$ and $\boldsymbol{E}_L$, respectively, are obtained by applying the operators $\boldsymbol{\nabla} \times$ and $\boldsymbol{\nabla} \cdot$ to equation (11):

$$\begin{aligned} (\boldsymbol{\nabla}^2 + \kappa_V^2 \mu^2) \boldsymbol{\nabla} \times \boldsymbol{E}_T &= - \kappa_V^2 (\boldsymbol{\nabla} \mu^2) \times \boldsymbol{E} \ , \\ \left(\frac{V^2}{c^2} \boldsymbol{\nabla}^2 + \kappa_V^2 \mu^2 \right) \boldsymbol{\nabla} \cdot \boldsymbol{E}_L &= - \kappa_V^2 (\boldsymbol{\nabla} \mu^2) \cdot \boldsymbol{E} \ . \end{aligned} \tag{12}$$

In equation (12) the inhomogeneity is represented by the non-vanishing of the gradient of μ^2, which, in turn, implies a gradient of density according to the definition of μ^2 and of ω_p^2. The homogeneous case is represented by the vanishing of the gradient of μ^2. In order better to understand the inhomogeneous case, we shall first examine the homogeneous case. If we let $\boldsymbol{\nabla} \mu^2 = 0$ in equations (12) and look for plane-wave solutions proportional to $\exp(+j\boldsymbol{\kappa} \cdot \boldsymbol{r})$, so that $\boldsymbol{\nabla} \rightarrow +j\boldsymbol{\kappa}$, we find that

$$\begin{aligned} (-\kappa^2 + \kappa_V^2 \mu^2) \, j\boldsymbol{\kappa} \times \boldsymbol{E}_T &= 0 \ , \\ \left(-\frac{V^2}{c^2} \kappa^2 + \kappa_V^2 \mu^2 \right) j\boldsymbol{\kappa} \cdot \boldsymbol{E}_L &= 0 \ , \end{aligned} \tag{13}$$

while definitions (9) imply that

$$\boldsymbol{\kappa} \times \boldsymbol{E}_L = \boldsymbol{\kappa} \cdot \boldsymbol{E}_T = 0 \ , \tag{14}$$

so that $\boldsymbol{E}_L$ is along, and $\boldsymbol{E}_T$ is transverse to, $\boldsymbol{\kappa}$, giving rise to the terms "longitudinal" and "transverse" for the independent modes of equations (13). Since $\boldsymbol{\kappa} \cdot \boldsymbol{E}_L$ and $\boldsymbol{\kappa} \times \boldsymbol{E}_T$ vanish only if $\boldsymbol{E}_L$ and $\boldsymbol{E}_T$ do, there are non-trivial solutions to equations (13) if and only if

$$\kappa_L = \kappa_V \frac{\mu c}{V} \ , \tag{15a}$$

$$\kappa_T = \kappa_V \mu = \frac{V}{c} \kappa_L \ , \tag{15b}$$

where κ_L is the longitudinal wave number and κ_T is the transverse. Equations (15) are the so-called "dispersion relations" for the longitudinal and transverse waves, respectively; they express the wave numbers as functions of frequency. Alternatively, they give frequency as a function of wave number, and thus we may write the transverse wave number as a function of the longitudinal one at the same frequency, as in equation (15*b*).

Bearing in mind that we are concerned with both kinds of waves at a single frequency, we see that the dispersion relations (15) allow the calculation of group and phase velocity for both wave types. For the transverse waves, in particular, equation (15*b*) implies, if each side is divided into the frequency, that the transverse wave has a phase velocity $v_p = c/\mu$. What is the group velocity? It can be shown, using equation (15*b*), that it is given by $v_g = c\mu$. If the temperature vanishes, equation (15*b*) implies that μ does for any finite κ_L, and thus the group velocity for the transverse wave at the same frequency is zero. Now in the case of normal dispersion, such as we have here, the signal velocity is the group velocity. Hence, if radiation were generated by the plasma wave, it would propagate at zero velocity. This statement is the basis of Ryle's contention alluded to previously. It is seen that if V is not zero, however, the radiation associated with the plasma wave will travel with a velocity which is zero when the plasma wave is infinitely long; the velocity of sound if the plasma wave has a wave length equal to that of the radiation *in vacuo;* and the velocity of light for plasma waves shorter than the vacuum radiation waves by a factor equal to V/c. (We shall see in Sec. III, however, that waves shorter than the latter are not possible, so the upper limit of velocity for the associated radiation wave is, in fact, c.) Thus we see that Ryle's objection is not valid if the temperature of the plasma is not zero.

Now equation (15*b*) can be written

$$\omega^2 = \omega_p^2 + \kappa_L^2 V^2 = \omega_p^2 + \frac{3kT}{m}\kappa_L^2\,, \tag{16}$$

which checks the Vlasov dispersion relation for plasma waves (1938). It is seen that, when $V = 0$, the phase velocity of plasma waves of any length is infinite, so that an arbitrary disturbance simply oscillates at the plasma frequency with the same phase everywhere; hence the disturbance does not propagate. This is not the case when $V \neq 0$; therefore, the zero temperature effects are properly called "plasma oscillations," as they were historically, and those when $V \neq 0$, "plasma waves."

Returning to the question of coupling, it is clear from equations (12) that if $\nabla\mu^2 \neq 0$, there is coupling, in that any possible solutions will have both $\boldsymbol{E}_L$ and $\boldsymbol{E}_T$ non-vanishing. To see this, imagine that there existed a solution $\boldsymbol{E}_L$, with $\boldsymbol{E}_T = 0$. Then, excepting the particular case when the wave is propagating along the gradient, the right-hand side of the first of equations (12) will not vanish. As that equation is an inhomogeneous wave equation for $\nabla \times \boldsymbol{E}_T$, the right-hand side is a source of waves of $\nabla \times \boldsymbol{E}_T$, and thus $\boldsymbol{E}_T$ will not vanish. Thus the assumption of a pure mode is contradicted.

The foregoing proof suggests a method of attacking problems of gradient coupling if the gradient is small. If a plasma wave is given at the boundary of an inhomogeneous region, the second equation describes how it propagates into that region. The first equation shows that the generated transverse wave is of first order in the gradient and hence may be neglected on the right side of the second equation, which already contains the gradient. The solution for the plasma wave so obtained may be put into the right-hand side of the first equation, which is then solved as an inhomogeneous wave equation. This procedure is very involved in practice, however, owing to the vector nature of the equations.

Physically, the reason for the coupling is that the plasma waves are refracted by the density gradient, producing a bending of the lines of force and thus a curl. Thus if the plasma wave propagates along the gradient, there is no refraction and hence no coupling. It should be noted that $\nabla \times \boldsymbol{E}_T$ is just $+j\omega\boldsymbol{H}/c$; so the first equation states that the magnetic field of the generated transverse wave is normal to the plane defined by $\boldsymbol{\nabla}\mu^2$ and $\boldsymbol{\kappa}_L$, in a problem where $\boldsymbol{\nabla}\mu^2$ is constant in direction and $\boldsymbol{E}_L$ is initially a plane wave.

The mathematical difficulties in solving equations (12) are obviated if we consider $\boldsymbol{\nabla}\mu^2 = \infty$, that is, a discontinuity of density. Such a case will be treated in Section III, after we discuss the effect of a static magnetic field. Since we are going to treat the case of a discontinuity, however, the plasma will be homogeneous except along a plane, and we may restrict the discussion of magnetic effects to the homogeneous case. Thus we inquire how the plane-wave solutions in the homogeneous case are modified by a static magnetic field before they are incident on a discontinuity.

b) Magnetic Coupling

Gross (1951) and Schlüter (1952) have discussed the coupling introduced by a static magnetic field. The derivation is briefly as follows: as before, we consider a plasma characterized by ω_p and V, but we introduce a constant magnetic field, $\boldsymbol{H}_0$. The effect of this is to add a magnetic force $(-e/mc)(\boldsymbol{v} \times \boldsymbol{H}_0)$ to the right-hand side of the force equation (2*c*). If we carry out the eliminations as before, the analogue of equation (8) is

$$W\boldsymbol{E} = +\frac{\omega_p^2}{c^3}(\boldsymbol{v} \times \boldsymbol{H}_0)\,, \tag{17}$$

where W is the operator applied to $\boldsymbol{E}$ in equation (8). If the velocity is substituted from equation (2*b*) and the whole differentiated with respect to ct to eliminate $\boldsymbol{H}$ by equation (2*a*), the result is

$$W\boldsymbol{E} = j\frac{\omega_c}{\omega}(\boldsymbol{\nabla} \times [\boldsymbol{\nabla} \times \boldsymbol{E}] - \kappa_V^2\boldsymbol{E}) \times \boldsymbol{u}\,, \tag{18}$$

where we have put $\boldsymbol{H}_0 = H_0\boldsymbol{u}$ and $H_0 = mc\omega_c/e$, so that ω_c is the radian cyclotron frequency corresponding to the field strength H_0. As with the previous field-free homogeneous case, we may look for solutions with constant wave vector $\boldsymbol{\kappa} = \kappa\boldsymbol{n}$, so that $\boldsymbol{\nabla} \to -j\kappa\boldsymbol{n}$, where $\boldsymbol{n}$ is a unit vector in the direction of propagation. We now restrict attention to the case where $\boldsymbol{n}$ is normal to $\boldsymbol{u}$. As might be expected, the coupling effects are maximum for this case. Then we may define a transverse unit vector $\boldsymbol{t} = \boldsymbol{n} \times \boldsymbol{u}$, so that $(\boldsymbol{n}, \boldsymbol{u}, \boldsymbol{t})$ is a right-handed system. Equation (18) becomes

$$\kappa^2\boldsymbol{n} \times (\boldsymbol{n} \times \boldsymbol{E}) + \kappa_V^2\mu^2\boldsymbol{E} - \kappa^2\frac{V^2}{c^2}\boldsymbol{n}(\boldsymbol{n}\cdot\boldsymbol{E}) = j\frac{\omega_c}{\omega}(-\kappa^2\boldsymbol{n} \times [\boldsymbol{n} \times \boldsymbol{E}] - \kappa_V^2\boldsymbol{E}) \times \boldsymbol{u}\,. \tag{19}$$

We now introduce small English letters for their equivalents to stand for the non-dimensional quantities:

$$\frac{\kappa}{\kappa_V} = k\,; \qquad \frac{V}{c} = v\,; \qquad \frac{\omega}{\omega_p} = z\,; \qquad \frac{\omega_c}{\omega_p} = z_c\,. \tag{20}$$

Equation (19) is equivalent to three simultaneous equations for the components of $\boldsymbol{E}$:

$$(\mu^2 - k^2v^2)E_n = j\frac{z_c}{z}(1 - k^2)E_t\,, \tag{21a}$$

$$(\mu^2 - k^2)E_u = 0\,, \tag{21b}$$

$$(\mu^2 - k^2)E_t = -j\frac{z_c}{z}E_n\,. \tag{21c}$$

First we note that E_u is uncoupled and satisfies the usual transverse dispersion relation (15*b*), as is expected from the fact that the motions in this mode are parallel to the field and hence unaffected by it. On the other hand, E_n and E_t are coupled, and, since they become pure longitudinal and transverse waves, respectively, when $z_c = 0$, we may call them "quasi-longitudinal" and "quasi-transverse"; the subscripts L and T will refer to them in the following.

Let us consider the quasi-longitudinal waves. From equation (21*a*) E_L has the usual dispersion relation $\mu = v$ for the particular plasma wave number $k_L = 1$. In other words, if we specify that the plasma wave length equals the vacuum wave length, the magnetic field does not appear explicitly in the dispersion relation, and thus $k_L = 1$ is a particularly simple case to consider. Therefore, in the following we take $k_L = 1$.

Thus the dispersion relation is

$$\mu = k_L v = v \, , \tag{22}$$

and, using the definition of μ, this implies that the frequency is given by

$$z = (1 - v^2)^{-1/2} \, . \tag{23}$$

As stated, there is a small transverse field component associated with the plasma wave. We define its ratio to the longitudinal field to be jR; hence from equation (21*c*) it is seen that

$$\left(\frac{E_t}{E_n}\right)_L = jR = j z_c (1 - v^2)^{-1/2} \, . \tag{24}$$

Thus when v is small (as it will certainly be), R is approximately z_c, and z is about 1, for $k_L = 1$.

We now consider the transverse wave associated with the plasma wave described previously, that is, the one having the same frequency or, equivalently, the same μ $(=v)$. Now the existence of non-trivial solutions of equations (21*a*) and (21*c*) requires that the determinant of coefficients vanish:

$$v^2 (v^2 - k^2)(1 - k^2) - \frac{z_c^2}{z^2}(1 - k^2) = 0 \, . \tag{25}$$

Factoring out $(1 - k^2)$, the vanishing of which gives the plasma wave as above, the equation for k_T becomes

$$k_T^2 = v^2 - \frac{z_c^2}{v^2}(1 - v^2) \, . \tag{26}$$

We see that, for $z_c = 0$, relation (15*b*) is recovered; the effect of the field is to lengthen the transverse waves, making them infinitely long at a magnetic-field strength given by $z_c = v^2(1 - v^2)^{-1/2}$. In fact, we may define a parameter t such that, in terms of $t = (1 - v^2)^{1/2} z_c/v^2$, $k_T = v(1 - t^2)^{1/2}$. Thus for $t = 0, 1, \gg 1$, respectively, $k_T = v, 0, jvt$. Just as in the case of the plasma wave, we may write the ratio of longitudinal to transverse electric field, inverting the ratio so as to obtain again something proportional to z_c. From equation (21*a*) we obtain

$$\left(\frac{E_n}{E_t}\right)_T = jS = j \frac{z_c}{v^2}(1 - v^2)^{1/2} = jt \, . \tag{27}$$

c) *Energy Transport*

We may derive expressions for the energy flux by forming an expression which vanishes *in vacuo* from equations (2*a*) and (2*b*):

$$\nabla \cdot \left(\frac{c}{4\pi} \boldsymbol{E} \times \boldsymbol{H}\right) + \frac{\partial}{\partial t}\left(\frac{\boldsymbol{E}^2 + \boldsymbol{H}^2}{8\pi}\right) = e n_0 \boldsymbol{E} \cdot \boldsymbol{v} \, . \tag{28}$$

But from equation (2*c*) we have, using the expression for the divergence of a product of scalar and vector,

$$\frac{\partial}{\partial t}\left(\tfrac{1}{2}v^2\right) = -\frac{e}{m}\,\boldsymbol{v}\cdot\boldsymbol{E} - \frac{V^2}{n_0}\left[\boldsymbol{\nabla}\cdot(n\boldsymbol{v}) - n\boldsymbol{\nabla}\cdot\boldsymbol{v}\right]. \tag{29}$$

Notice that the possible addition of a magnetic-force term does not affect this result, since we have taken the scalar product with $\boldsymbol{v}$. From the continuity relation we can eliminate the $\boldsymbol{\nabla}\cdot\boldsymbol{v}$, so that the right-hand side of equation (28) can be written

$$e n_0 \boldsymbol{v}\cdot\boldsymbol{E} = -\frac{\partial}{\partial t}\left[n_0 \tfrac{1}{2} m v^2 + n_0 \tfrac{1}{2} m V^2 \left(\frac{n}{n_0}\right)^2\right] - \boldsymbol{\nabla}\cdot\left(m V^2 n \boldsymbol{v}\right), \tag{30}$$

and we have, finally,

$$\boldsymbol{\nabla}\cdot\left(\frac{c}{4\pi}\boldsymbol{E}\times\boldsymbol{H} + m V^2 n \boldsymbol{v}\right) + \frac{\partial}{\partial t}\left[\frac{E^2+H^2}{8\pi} + n_0 \tfrac{1}{2} m v^2 + n_0 \tfrac{1}{2} m V^2 \left(\frac{n}{n_0}\right)^2\right] = 0\,; \tag{31}$$

so that the energy flux, identified with the first term, is just the sum of the electromagnetic flux and the mechanical flux, the latter of which has the same form as for a sound wave. For sine waves the time derivative averages to zero, so the time-average flux vector is solenoidal; we speak of "conversion" from plasma-wave energy to electromagnetic energy if the contribution of the first term grows at the expense of the second term in the flux.

The general expression for the flux can be specialized to the case of sine waves of wave vector $\boldsymbol{\kappa} = \kappa \boldsymbol{n}$ and frequency ω. The quantities needed in equation (31) can all be expressed in terms of the dominant field quantities, that is to say, the longitudinal field in the plasma wave and the transverse field in the electromagnetic wave. For time-averaged flux in the two cases we get

$$\langle S_L \rangle = \frac{c}{4\pi} E_n^2 k_L \left(v^2 z^2 + R^2\right), \tag{32}$$

$$\langle S_T \rangle = \frac{c}{4\pi} E_t^2 k_T \left(1 + v^2 z^2 S^2\right), \tag{33}$$

where we mean root-mean-square values for the field quantities. Note, then, in each expression that there is the contribution of the dominant field and a contribution from the secondary fields induced by the static magnetic field.

We may use values for z, R, and S computed earlier for the case $k_L = 1$:

$$\begin{aligned} \langle S_L \rangle &= \frac{c}{4\pi} E_n^2 \left(v^2 + z_c^2\right)\left(1 - v^2\right)^{-1}, \\ \langle S_T \rangle &= \frac{c}{4\pi} E_t^2 \left(v^2 + z_c^2\right)\left(1 - l^2\right)^{1/2} v^{-1}. \end{aligned} \tag{34}$$

It is clear that the additional flux caused by the field in each case is $(z_c/v)^2$ times the main component.

III. APPLICATION: A DISCONTINUITY IN DENSITY

With the ideas developed in Section II, we may consider a particular case of inhomogeneity. Imagine that, as in Figure 1, there is a plasma of density n_0 and temperature T to the left of the plane $z = 0$ and a vacuum to the right. The physical nature of the boundary plane determines its efficiency for conversion of longitudinal energy in the plasma to transverse energy in the vacuum. We take the boundary to be such that any electrons incident on it are elastically reflected, which means that the normal component of $\boldsymbol{v}$ must vanish. Such a boundary might be realized in practice by a cloud of plasma expanding into a vacuum. In that case there is a transition region in which the electron density falls from n_0 to zero; the width of such a region is approximately the Debye length, $\lambda_D \simeq V/\nu_p$, in the plasma. To avoid damping, the plasma waves must be longer than the Debye length, and so such a boundary may be considered to be a discontinuity for such waves. The free boundary described will reflect electrons through the restoring forces exerted by the ions.

We take the magnetic field $\boldsymbol{H}_0$ to be parallel to the boundary, say in the y-direction: $\boldsymbol{H}_0 = H_0\boldsymbol{u} = H_0\boldsymbol{u}_y$. With the plasma properties thus given, we may apply the analysis of a homogeneous plasma with a static magnetic field developed in Section II*b*. The idea is to set up a possible system of plasma and electromagnetic waves in the plasma and in the vacuum and to connect their amplitudes by application of boundary conditions along the plane $z = 0$. Now we are interested in the case in which a plasma wave in the plasma gives rise to an electromagnetic wave in the vacuum. Therefore, we assume a quasi-longitudinal wave having wave vector $\boldsymbol{\kappa}_i = \kappa_L \boldsymbol{n}_i$ incident from the left and a transverse wave of wave vector $\boldsymbol{\kappa}_t = \kappa_T \boldsymbol{n}_t$ transmitted into the vacuum. In order to apply the analysis of the previous section, we must take $\boldsymbol{n}_i$ perpendicular to $\boldsymbol{u}_y$, that is, in the x-z plane.

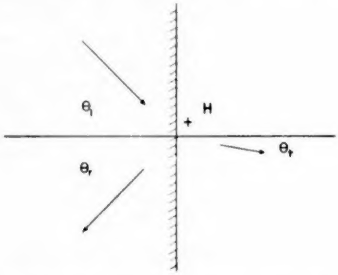

FIG. 1.—The plasma-vacuum boundary, showing incident, reflected, and transmitted waves for the case $k_L = \frac{1}{2}$, $\theta_i = 45°$. Arrows are proportional to wave lengths. The backward radiation wave is not shown, as it is evanescent.

Now equation (12) informs us that the magnetic field in the transverse wave is normal both to the gradient vector and to the longitudinal electric field in the plasma wave and hence is parallel to $\boldsymbol{u}_y$. To satisfy the boundary conditions, we must have three unknown quantities; the only possible other two besides the amplitude of the transmitted wave are those of a reflected plasma wave and an electromagnetic wave moving back from the boundary. We take their wave vectors to be $\boldsymbol{\kappa}_r = \kappa_L \boldsymbol{n}_r$ and $\boldsymbol{\kappa}_b = \kappa_T \boldsymbol{n}_b$, respectively. For the same reason as for the transmitted wave, the magnetic fields associated with these waves are parallel to $\boldsymbol{u}_y$. Thus the electric fields in each of the four waves all lie in the x-z plane.

The boundary conditions to be satisfied are

$$\begin{aligned} \boldsymbol{u}_z \cdot (\boldsymbol{E}_i + \boldsymbol{E}_r + \boldsymbol{E}_b - \boldsymbol{E}_t) &= 0 , \\ \boldsymbol{u}_z \times (\boldsymbol{E}_i + \boldsymbol{E}_r + \boldsymbol{E}_b - \boldsymbol{E}_t) &= 0 , \qquad (35) \\ \boldsymbol{u}_z \times (\boldsymbol{H}_i + \boldsymbol{H}_r + \boldsymbol{H}_b - \boldsymbol{H}_t) &= 0 . \end{aligned}$$

The continuity of tangential electric field and tangential magnetic field is true for all junctions of finite conductivity materials such as we have here. The continuity of the normal electric field is a direct result of our assumption that normal $\boldsymbol{v}$ vanishes, together with equation (2*b*). The usual law for the continuity of a normal magnetic field is here trivially satisfied by the polarizations of the incident and resulting waves, all of which are polarized with tangent magnetic vector.

Our object is to calculate a *conversion coefficient*, C, defined as the ratio of the normal flux in the transmitted wave to that in the incident wave. Such a coefficient will, in general, be a function of the plasma properties, κ_L and $\boldsymbol{n}_i$. As this function of five variables will be too difficult to discuss generally, certain specializations will be made here, considering particular or negligible values only of some of the variables.

In what follows we shall use the indices (i, r, b, t) to designate the incident and reflected plasma waves and the backward and transmitted electromagnetic waves, in that order; $\boldsymbol{n}_a$ will represent a unit propagation vector, and $\boldsymbol{t}_a = \boldsymbol{n}_a \times \boldsymbol{u}_y$. We shall let $\cos\theta_a \equiv c_a$, and $\sin\theta_a \equiv s_a$, where $\boldsymbol{a}$ is some index and θ_a is the angle between $\boldsymbol{n}_a$ and the normal to the boundary, always taken as less than 90°, as shown in Figure 1. Then we may write, for the various products of vectors occurring in equations (35),

$$
\begin{aligned}
\boldsymbol{u}_z \cdot \boldsymbol{n}_a &= c_{i,\,t}\,; \qquad - c_{r,\,b}\,, \\
\boldsymbol{u}_z \cdot \boldsymbol{t}_a &= s_{i,\,r,\,b,\,t}\,, \\
\boldsymbol{u}_z \times \boldsymbol{n}_a &= s_{i,\,r,\,b,\,t}\,(\boldsymbol{u}_y)\,, \\
\boldsymbol{u}_z \times \boldsymbol{t}_a &= c_{r,\,b}\,(\boldsymbol{u}_y)\,; \qquad - c_{i,\,t}\,(\boldsymbol{u}_y)\,.
\end{aligned}
\tag{36}
$$

The fields $\boldsymbol{E}$ and $\boldsymbol{H}$ in each mode may be expressed in terms of the dominant electric field for that mode, using the definitions of R and S given in equations (24) and (27), together with equation (2*a*):

$$
\begin{aligned}
\boldsymbol{E}_L &= E_n\,(\boldsymbol{n} + jR\boldsymbol{t})\,, \\
\boldsymbol{H}_L &= E_n\,(-\,jk_L R\boldsymbol{u})\,, \\
\boldsymbol{E}_T &= E_t\,(\boldsymbol{t} + jS\boldsymbol{n})\,, \\
\boldsymbol{H}_T &= E_t\,(-\,k_T\boldsymbol{u})\,.
\end{aligned}
\tag{37}
$$

Substitution of equations (36) and (37) into equations (35) yields

$$
\begin{aligned}
&e_r(-\,c_r + jR\,s_r) &&+ e_b\,(s_b - jS\,c_b) &&+ e_t\,(-\,s_t) &&= -\,c_i - jR\,s_i\,, \\
&e_r(s_r + jR\,c_r) &&+ e_b\,(c_b + jS\,s_b) &&+ e_t\,(c_t) &&= -\,s_i + jR\,c_i\,, \\
&e_r(-\,jRk_L) &&+ e_b\,(-\,k_T) &&+ e_t &&= jRk_L\,.
\end{aligned}
\tag{38}
$$

In these equations the amplitudes have been divided by the longitudinal component of the incident wave: $e_a \equiv E_{a(n \text{ or } t)}/E_{in}$. Thus in each case the field considered is the dominant one for that mode. The formal solution of equations (38) for the transmitted field is $e_t = D_t/D$, with

$$
D_t = \begin{vmatrix}
-\,c_i + jR\,s_i & s_b - jS\,c_b & -\,c_i - jR\,s_i \\
s_i + jR\,c_i & c_b + jS\,s_b & -\,s_i + jR\,c_i \\
-\,jRk_L & -\,k_T & jRk_L
\end{vmatrix}
\tag{39a}
$$

and

$$D = \begin{vmatrix} -c_i + jRs_i & s_b - jSc_b & -k_L s_i \\ s_i + jRc_i & c_b + jSs_b & c_t \\ -jRk_L & -k_T & 1 \end{vmatrix} . \tag{39b}$$

We have used Snell's laws for the equality of phase along the boundary to eliminate s_r, s_t, and s_b: $s_r = s_i$, $s_t = k_L s_i$, and $s_b = s_i k_L / k_T$. We shall leave the cosines for the time being.

Expression (39*a*) for D_t simplifies to

$$\frac{D_t}{2c_i} = \frac{s_b}{k_L} [R(R+S)k_L^2 + (1-R^2)k_T^2] - c_b jRk_L(1+RS) , \tag{40}$$

while that for D remains involved:

$$\begin{aligned} D = s_i c_t jRk_T\left[1 - \left(\frac{k_L}{k_T}\right)^2\right] + c_b c_t(-RSk_L) + s_i c_b jR\left(1 - k_L^2 + \frac{S}{R}\right) \\ + c_i c_t(-k_T) + s_i^2 \frac{k_L}{k_T}\left\{k_T^2\left[1 + \left(\frac{k_L}{k_T}\right)^2 RS\right] - 1 - RS\right\} \\ + c_i c_b(-1-RS) + c_i s_i\left(-jR\frac{k_L}{k_T}\right)\left(1 - k_T^2 + \frac{S}{R}\right). \end{aligned} \tag{41}$$

As stated before, further progress can be made only by eliminating some of the variable quantities of the foregoing solutions. For example, equation (41) shows that D depends in a complex way on the five quantities θ_i, k_L, v, z_c, and ω_p, since θ_t and θ_b depend on θ_i, k_L, and k_T through Snell's laws; whereas k_T depends on v and z_c through the dispersion relation specialized to $k_L = 1$ (eq. [26]). Also, R and S vary with v and z_c, according to equations (24) and (27), which again are specialized to the case $k_L = 1$.

The particular cases we shall consider are zero magnetic field, $z_c = 0$; and, with $z_c \neq 0$, equality of plasma wave length and vacuum wave length, $k_L = 1$. The dispersion relations and field ratios for these cases are given in Section II. It is readily shown that the case $k_L = 1$, or $\lambda_L = \lambda_V$, is physically reasonable in the corona, in the sense that the wave length is less than the dimensions of the radiating region and greater than the Debye length.

First we discuss the case $z_c = 0$. Then, according to equations (15*b*), (24), and (27),

$$k_T = vk_L , \quad R = 0 , \quad S = 0 ; \tag{42}$$

and when these are put into equations (40) and (41), we find that

$$\frac{D_t}{2c_i} = vk_L s_i , \tag{43}$$

$$D = -[s_i s_b(1 - k_L^2 v^2) + c_i c_b + k_L v c_i c_t] , \tag{44}$$

so that the transmitted field is

$$e_t = \frac{-2vk_L s_i c_i}{s_i s_b(1 - k_L^2 v^2) + c_i c_b + k_L v c_i c_t} . \tag{45}$$

If, on the other hand, we take $z_c \neq 0$ and $k_L = 1$, we may write, from equations (24), (26), and (27),

$$k_T = v\,(1 - t^2)^{1/2}\,, \qquad R = z_c\,(1 - v^2)^{-1/2}\,, \qquad S = z_c\,(1 - v^2)^{1/2}\,v^{-2} = t\,, \tag{46}$$

which leads to

$$\frac{D_t}{2\,v^2\,c_i} = s_b\left(1 + \frac{z_c^2}{v^2}\right)^2 - j\,c_b t\,(1 - v^2)^{-1}\left(1 + \frac{z_c^2}{v^2}\right) \tag{47}$$

and, if we remember that Snell's law gives $\theta_t = \theta_i$ for $k_L = 1$,

$$\begin{aligned} D = &- j\,s_b\,c_i t\left[1 + 2\,v^2\left(1 + \frac{z_c^2}{v^2}\right)\right] - c_i\,c_b\left(1 + 2\,\frac{z_c^2}{v^2}\right) + j\,s_i\,c_b t \\ &+ s_i\,s_b\left[1 - 2\,(1 - v^2)\left(1 + \frac{z_c^2}{v^2}\right)\right] - v\,(1 - t^2)^{1/2}\,. \end{aligned} \tag{48}$$

We have used the parameter $t = z_c(1 - v^2)^{1/2}\,v^{-2}$ to express the dependence on the static magnetic field. Clearly, we may ignore v^2 against unity in these expressions, since even in the very hot corona, for example, it is only 1/1800. In addition, we shall restrict attention to *weak* magnetic fields, defined by the relation

$$z_c \ll v\,. \tag{49}$$

Thus, with a plasma frequency of 100 megacycles, the analysis is restricted to fields less than 0.83 gauss. If such approximations are made, we find from equations (47) and (48) that

$$\frac{e_t}{2\,c_i v^2} \equiv l = \frac{j\,c_b t - s_b}{2\,v\,(1 - t^2)^{1/2} + [\,c_b + j t\,s_b\,]\,[\,c_i - v\,(1 - t^2)^{1/2}\,c_b\,]}\,, \tag{50}$$

which is a function of v and t.

With expressions (45) and (50) for the transmitted fields in the two cases, we may compute the conversion coefficient, C, previously defined. Using the equations of Section II*c*, we may write, ignoring v^2 and in the weak field approximation,

$$C = \frac{c_t}{c_i}\,\frac{S_t}{S_i} = \frac{c_t}{c_i}\,\frac{|\,e_t\,|^2}{k_L\,(R^2 + v^2 z^2)} \simeq 4\,c_i\,c_t\,v^2\,|\,l\,|^2 \qquad (k_L = 1,\ z_c \neq 0)\,, \tag{51}$$

$$\simeq \frac{c_t}{c_i}\,\frac{|\,e_t\,|^2}{k_L\,v^2} \qquad (k_L \neq 1,\ z_c = 0)\,. \tag{52}$$

Let us turn to equation (45). Though it is a complex function of θ_i, its general properties may be understood by an approximate analysis. First, we note that $k_L v$ is small compared to unity. This follows from the fact that $k_D = 1/vz$, where k_D is the Debye wave number, and that Landau (1946) showed that plasma waves shorter than the Debye length are heavily damped. Thus we may ignore $k_L v$. Now, as θ_i varies from 0 to $\pi/2$, s_b varies from 0 to $1/v$, becoming unity at the small angle given by $s_i = v$. Therefore, the term $c_i c_b$ in the denominator has a sharp zero at that angle, being large and real for smaller angles and large and imaginary for greater ones. Thus we consider three extreme cases: (I) $s_i \ll v$; (II) $s_i = v$; and (III) $s_i \gg v$:

$$\begin{aligned} \text{I:} \quad & e_t \simeq -2vk_L s_i , \\ \text{II:} \quad & e_t \simeq -2v \frac{k_L}{k_L+1} , \\ \text{III:} \quad & e_t \simeq 2jv^2 k_L c_i \exp(j\theta_i) . \end{aligned} \tag{53}$$

When these expressions are inserted into equation (52), we find, for the conversion coefficients,

$$\begin{aligned} \text{I:} \quad & s_i \ll v , \quad C = 4k_L s_i^2 ; \\ \text{II:} \quad & s_i = v , \quad C = \frac{4}{k_L}\left(\frac{k_L}{k_L+1}\right)^2 ; \\ \text{III:} \quad & s_i \gg v , \quad C = 4k_L v^2 c_i c_t . \end{aligned} \tag{54}$$

Proceeding to the case when $z_c \neq 0$, we consider two values of t to adjoin to the analysis when $t = 0$ given above. First take $t = 1$. Then, according to equation (46), $k_T = 0$, and l becomes

$$l = \frac{jc_b - s_b}{c_i(c_b + js_b)} = \frac{j}{c_i} . \tag{55}$$

On the other hand, if $t \gg 1$, $k_T \simeq jvt = jz_c(1 - v^2)^{1/2}v^{-1}$, which is small compared to unity by the weak-field assumption (49). We have

$$l = \frac{jc_b t - s_b}{(c_b + jts_b)(c_i - jvtc_b) + 2jvt} ; \tag{56}$$

and, since it can be shown that the absolute value of the first term in the denominator exceeds unity, this may be written, using the notation $s_b' = js_b$ and $t_b' = s_b'/c_b$,

$$l \simeq j \frac{t + t_b'}{1 + tt_b'} \frac{1}{c_i - jvtc_b} . \tag{57}$$

We have again used the weak-field assumption, $vt \ll 1$. From equations (55) and (57) we derive:

For $t = 1$:
$$|l|^2 = \frac{1}{c_i^2} , \tag{58a}$$

For $t \gg 1$:
$$|l|^2 \simeq \left|\frac{t + t_b'}{1 + tt_b'}\right|^2 \frac{1}{1 + (vt)^2} \simeq \left|\frac{t + t_b'}{1 + tt_b'}\right|^2 . \tag{58b}$$

Now, since $t_b' = s_b'/c_b = s_b'(1 + s_b'^2)^{-1/2}$, we see that $\max(t_b') = 1$, so that it may be ignored against (large) t in equation (58*b*). The behavior of the resulting function is this: it has a maximum equal to t^2 for $s_i = 0$ and drops to unity for angles $s_i \simeq vt$. With these considerations, we may derive C for the cases $t = 1$ and $t \gg 1$. Thus

For $t = 1$:
$$C = 4v^2 c_t \frac{1}{c_i} = 4v^2 \tag{59a}$$

For $t \gg 1$:
$$\begin{aligned} s_i \ll vt : \quad & C = 4v^2 t^2 \frac{1}{(1 + s_i/v)^2} , \\ s_i \gg vt : \quad & C = 4v^2 c_i c_t . \end{aligned} \tag{59b}$$

From equations (54) and (59) we see that the maximum conversion coefficients for the three cases considered are as follows:

$$z_c = 0, \qquad k_L \neq 1, \qquad C_m = \frac{4}{k_L}\left(\frac{k_L}{k_L + 1}\right)^2, \tag{60a}$$

$$z_c \neq 0, \qquad k_L = 1, \qquad t = 1 \qquad C_m = 4\,v^2\,, \tag{60b}$$

$$z_c \neq 0, \qquad k_L = 1, \qquad t \gg 1; \qquad C_m = 4\,v^2 t^2\,. \tag{60c}$$

It is clear that the maximum conversion coefficient attained in any of equations (60) is simply unity, as in equation (60*a*) when $k_L = 1$, corresponding to the other cases treated. Thus, if attention is directed to the case $k_L = 1$ throughout, it is seen that an increasing magnetic field at first suppresses conversion and then enhances it again to a value approaching unity (the behavior beyond that point is not given by the small-field analysis, which states $vt \ll 1$). Though it has not been demonstrated here, it seems likely that, for a given magnetic field, the maximum conversion is attained when $k_L = 1$, as in the case of a vanishing field. In that event, we must suppose the values for various magnetic fields will be diminished from those given, by either smaller or larger k_L. In conclusion, we reach the rather surprising result that, under special conditions, complete conversion occurs even with no magnetic field, so that it is impossible for a magnetic field to enhance conversion when these special conditions (wave-length matching) occur. In fact, the field inhibits conversion at first, attaining complete conversion again for a field given approximately by $\omega_c/\omega_p = V/c$, which gives 0.83 gauss for the corona at a plasma frequency of 100 megacycles.

It is rather to gain general insight into the coupling problem that the magnetic field has been introduced into the foregoing analysis. It develops, however, that, as concerns the application of the analysis to the solar outbursts made in Section IV, the needed data on the magnetic field, the value of which is critical, are meager. Rather, the only direct evidence on this point indicates that the field is weak; Wild reports (private communication) that the single type II outburst for which measures have been made over the whole frequency range showed no signs of polarization. It might therefore be useful to consider the case of vanishing static magnetic field.

The appropriate expressions for the conversion coefficient are given in equations (54). Since there is no obvious reason why any particular angle of incidence will be favored, we may consider an average coefficient, applicable to a uniform distribution of angles, calculated as the mean of equations (54) weighted according to the element of solid angle, $s_i \Delta\theta_i$. When this is done, it is seen that region I does not contribute significantly, while the contributions of regions II and III are each about equal to $4k_L v^2$ for small wave numbers k_L; for large wave numbers the contribution of region III remains, while that of region II becomes negligible. Thus a sufficiently accurate expression for the average conversion coefficient, valid over the whole range of possible wave numbers, is that of region III:

$$\langle C \rangle_{\theta_i} = 4 k_L v^2 = 4\,\frac{\lambda_V}{\lambda_L}\,\frac{3\,kT}{m\,c^2}\,. \tag{61}$$

IV. THE SOLAR TYPE II OUTBURSTS

Wild *et al.* (1954) have discussed observations of particularly intense solar radio-frequency emission which they call "outbursts of Type II." The question arises as to whether the mechanism of gradient coupling is sufficient to account for the observed intensities on a reasonable physical model, especially inasmuch as Wild and his collaborators have suggested that the radiation originates in plasma oscillations.

The model we shall adopt is that of a finite region in the corona having a sharp boundary. The density is non-vanishing on either side of the boundary, so that the picture of a plasma-vacuum interface will be only qualitatively correct. In addition, the boundary will not be absolutely sharp; the effects of this and of the finite density ratio are assumed to decrease the conversion coefficient from that given by equation (61) by some unknown efficiency factor, A. It is our goal to show that A has a reasonable value when theory and observations are compared. The whole region is supposed to be moving outward through the corona, in order to account for the observed frequency drifts. The motion of the region may be supposed to give rise to plasma waves in the space behind the boundary, in the region itself. These waves propagate at various angles against the boundary and, by gradient coupling, produce radiation which escapes.

The observational support for such a picture comes from radio and optical astronomy. It accounts for the sharp radio-frequency bands observed by Wild, and, if it is assumed that the plasma waves are so intense as to be non-linear, it explains the existence of a second harmonic with a slightly different spectral shape. If the velocity of outward movement is taken as 450 km/sec, on the average, the frequency drifts of ten recent outbursts can be understood. Optically, it is likely that the so-called "flare ejections" seen by Miss Dodson and her collaborators (1953) play the role of the moving region in this picture. The ejections are associated with flares, as are the outbursts, and travel with comparable speeds. A typical dimension on Miss Dodson's photographs appears to be of the order of 10^4 km, a figure checked by Kiepenheuer (1953) for similar optical events projected against the disk and not inconsistent with the band widths observed by Wild.

The region may be a stream of particles or a shock wave or both. In either case, there is reason to suppose that plasma waves will be generated. In the papers of Bohm and Gross (1949*b*), Haeff (1949), Blum, Denisse, and Steinberg (1951), and Sen (1954), mechanisms for excitation of plasma waves by streams or shocks are discussed. In what follows, it is assumed that the plasma waves exist, and we shall find a value of A which satisfies the observations.

Wild (private communication) gives the average energy radiated by an outburst of type II, integrated over frequency and time, as 10^{23} ergs. To compare with that, the foregoing picture gives an amount $E = A\langle C\rangle S_L D^2 t$, where D is the typical dimension quoted above, 10^4 km; t is the duration of a typical burst, say 10^3 sec; $\langle C\rangle$ is the conversion coefficient given by equation (61); and S_L is the energy flux in the plasma waves impinging on the boundary. This last is, of course, unknown, but an estimate of it may be found from the observed occurrence of the second harmonic. This possibility arises from the fact that if an oscillator diverges from linearity a reasonable amount, harmonics of the fundamental are required to describe the system. The harmonics fall off rapidly, however, if the departure from linearity is not too great. The fact that a second harmonic, but not higher, is detected may be taken as an indication that the oscillation is moderately non-linear. The theory of plasma oscillations shows (see Smerd 1955) that the condition for this is that the density perturbations approach the density of the quiescent medium in value. If we apply equation (4) to the plasma waves, assuming that they have wave number κ_L, the electric-field amplitude is thus

$$|E_L| = \frac{4\pi e n}{\kappa_L} = \frac{4\pi e n_0}{\kappa_L}. \tag{62}$$

Putting this into equation (32), with $R = 0$, and neglecting v^2 against unity, we get

$$S_L = |E_L|^2 k_L \frac{v^2 c}{4\pi} = \frac{3 n_0 c k T}{k_L}, \tag{63}$$

where c is the velocity of light and T is the coronal temperature. When this, together with equation (61), is combined to give the total radiated energy, we find a result which is independent of plasma wave length:

$$E = 12\, A\, v^2 n_0\, c k T\, D^2 t\,. \tag{64}$$

If we use $n_0 = 10^8$ cm^{-3} as an average value over the radiating region and $T = 10^6$ degrees, together with the resulting value of 1/43 for v, and $D = 10^4$ km, we find

$$E = 2.8 \times 10^{27} A \text{ ergs} . \tag{65}$$

This is to be compared with the observed value of 10^{23} ergs. It appears, therefore, that A is of the order of 310^{-5}—that is, an efficiency very low compared to that computed for the ideal case of a plasma-vacuum boundary of vanishing thickness will suffice to explain the observations. This result depends critically on the assumed energy flux for the plasma waves, here derived from the non-linearity.

It is hoped that a more complete theory, including the effects of finite boundary thickness and density ratio, will relate the parameter A to physically interesting quantities in the model and thus permit a stricter test. For example, a more exact theory might relate the intensity to boundary thickness, and this might become directly measurable from new observations.

The author appreciates the guidance offered in this work by Professor Lyman Spitzer, Jr.; his suggestions were always fruitful and his criticisms crucial. Discussions with Dr. J. P. Wild on the solar outbursts were most helpful. In addition, the author is indebted to the National Science Foundation, a fellowship from which has made this work possible.

REFERENCES

Bhatnagar, P. L., Krook, M., and Menzel, D. H. 1952, *Dynamics of Ionized Media* (Scientific Report No. 3 of the Solar Department of Harvard College Observatory) (Cambridge: The Observatory).

Blum, E. J., Denisse, J. F., and Steinberg, J. L. 1951, *C.R.*, **232**, 483.

Bohm, D., and Gross, E. P. 1949*a*, *Phys. Rev.*, **75**, 1851.

———. 1949*b*, *ibid.*, p. 1864.

———. 1950, *ibid.*, **79**, 992.

Dodson, H. W., Hedeman, E. R., and Chamberlain, J. 1953, *Ap. J.*, **117**, 66.

Gross, E. P. 1951, *Phys. Rev.*, **82**, 232.

Haeff, A. V. 1948, *Phys. Rev.*, **74**, 1532.

Kiepenheuer, K. O. 1953, "Solar Activity," in G. P. Kuiper (ed.), *The Sun* (Chicago: University of Chicago Press), chap. 6.

Landau, L. 1946, *J. Phys. U.S.S.R.*, **10**, 25.

London Conference on the Dynamics of Ionized Media. 1951, *Secretary's Report* (London: University College).

Martyn, D. F. 1947, *Nature*, **159**, 26.

Pawsey, J. L., and Smerd, S. F. 1953, "Solar Radio Emission," in G. P. Kuiper (ed.), *The Sun* (Chicago: University of Chicago Press), chap. 7.

Rayleigh, Lord. 1906, *Phil. Mag.*, ser. 6, **11**, 117.

Ryle, M. 1949, *Proc. Phys. Soc.*, **62**A, 483.

Schlüter, A. 1952, *Ann. d. Phys.*, ser. 6, **10**, 418.

Sen, H. K. 1954, *Australian J. Phys.*, **7**, 30.

Shklovsky, I. S. 1946, *Astr. J. U.S.S.R.*, **23**, 333.

Smerd, S. F. 1955, *Nature*, **175**, 297.

Thomson, J. J., and Thomson, G. P. 1933, *Conduction of Electricity through Gases* (3d ed.; Cambridge: At the University Press), Vol. **2**.

Tonks, L., and Langmuir, I. 1929, *Phys. Rev.*, **33**, 195.

Vlasov, A. 1938, *J. Exper. and Theoret. Phys. U.S.S.R.*, **8**, 291 (in Russian; reviewed in *Phys. Ber.*, **20**, Part 1, 409).

Wild, J. P., Murray, J. D., and Rowe, W. C. 1954, *Australian J. Phys.*, **7**, 439.

HYDROMAGNETIC OSCILLATIONS OF A FLUID SPHERE WITH INTERNAL MOTIONS*

S. CHANDRASEKHAR
University of Chicago

Received June 19, 1956

ABSTRACT

A stationary solution of the equations of hydromagnetics for an incompressible inviscid fluid of infinite electrical conductivity is given by $\boldsymbol{v} = \boldsymbol{H}/\sqrt{(4\pi\rho)}$, where $\boldsymbol{v}$ denotes the velocity, $\boldsymbol{H}$ the magnetic field, and ρ the density. The case is considered in which $\boldsymbol{v}$ and $\boldsymbol{H}$ have symmetry about an axis, and convenient forms for the equations governing axisymmetric oscillations about the stationary solution are obtained. These latter equations take their simplest forms when the initial magnetic field and fluid motions have no poloidal components. This case is considered in some detail.

I. INTRODUCTION

Since Babcock's discovery of the magnetic variables, the oscillations of a fluid sphere with a prevalent magnetic field have been the subject of investigations by several authors (Schwarzschild 1949; Gjellestad 1950, 1952; Cowling 1952, 1955; Ferraro and Memory 1952; Chandrasekhar and Limber 1954; Ferraro and Plumpton 1955). These investigations have been inconclusive, in part because of a lack of definiteness in characterizing the initial equilibrium configuration. The indefiniteness consists in the following: If one supposes, as has hitherto been customary in the subject, that the initial configuration is one of hydrostatic equilibrium, then there are immediate restrictions on the possible magnetic fields which can prevail. Thus, in media of uniform density, the assumption of hydrostatic equilibrium requires that the magnetic field, $\boldsymbol{H}$, which is present, be such that curl $\boldsymbol{H} \times \boldsymbol{H}$ is the gradient of a scalar function. In the investigations on hydromagnetic oscillations to which reference has been made, the restrictions on $\boldsymbol{H}$ arising from such considerations are not included; in particular, the magnetic fields which have been assumed to be present are generally incompatible with a spherical shape, which is also assumed (cf. Chandrasekhar and Fermi 1953, and several later investigations along the same lines). However, Chandrasekhar and Prendergast (1956) have recently characterized in an explicit way magnetic fields which have symmetry about an axis and which satisfy the requirements of hydrostatic equilibrium in media of uniform density; and Prendergast (1956*a*) has constructed a model which satisfies these requirements and is a true equilibrium configuration. Prendergast (1957) has also examined the periods of oscillation of his model by a variational method and related them to the condition for dynamical stability arising from the virial theorem (Chandrasekhar and Fermi 1953; Chandrasekhar and Limber 1954). Prendergast's investigations represent the first really self-consistent treatment of the hydromagnetic oscillations of a fluid sphere. Nevertheless, these latter investigations emphasize that if magnetic variability in nature is to be interpreted as variability about an initial state of static equilibrium, then the magnetic fields which prevail must be of very special kinds—a conclusion which is perhaps not altogether satisfying (cf. Chandrasekhar 1956*e*). One need not suffer these limitations if one does not restrict one's self (arbitrarily?) to static configurations with no internal motions. Thus, by assuming internal motions and sup-

---

* The research reported in this paper has been supported in part by the Geophysics Research Directorate of the Air Force Cambridge Research Center, Air Research and Development Command, under Contract AF 19(604)-299 with the University of Chicago.

posing that the velocity ($\boldsymbol{v}$) at each point is related to the magnetic field at that point by (cf. Chandrasekhar 1956*b*)

$$\boldsymbol{v}=\frac{\boldsymbol{H}}{\sqrt{(4\pi\rho)}}, \tag{1}$$

we can satisfy the equations of motion governing $\boldsymbol{v}$ and $\boldsymbol{H}$ identically; and we need not restrict $\boldsymbol{v}$ and $\boldsymbol{H}$ in any way except that they both be solenoidal. By thus relinquishing the condition of static equilibrium, we gain an enormous freedom in the choice of the possible magnetic fields. Indeed, this circumstance makes one wonder whether magnetic fields, when they occur on the cosmic scale, are not always accompanied by correlated motions. Regardless of one's views on this general matter, it is of interest that, in the framework of solution (1), we can construct a large class of non-static, but stationary, equilibrium configurations which have simple properties. It is the object of this paper to construct one such model and study its oscillations.

II. THE EQUATIONS OF THE PROBLEM

We shall restrict ourselves to magnetic fields and fluid motions which have symmetry about an axis. Convenient forms for the corresponding equations for $\boldsymbol{H}$ and $\boldsymbol{v}$ have recently been written and discussed (Chandrasekhar 1956*c;* this paper will be referred to hereafter as "Paper I"). We shall begin by quoting the relevant formulae.

Letting

$$\boldsymbol{h}=\frac{\boldsymbol{H}}{\sqrt{(4\pi\rho)}}, \tag{2}$$

we express $\boldsymbol{h}$ and $\boldsymbol{v}$ (following Lüst and Schlüter 1954) as superpositions of toroidal and poloidal fields in terms of four scalars P, T, U, and V in the following manner (Paper I, eqs. [15] and [16]):

$$\boldsymbol{h}=\mathbf{1}_z\times\boldsymbol{r}T+\operatorname{curl}(\mathbf{1}_z\times\boldsymbol{r}P) \tag{3}$$

and

$$\boldsymbol{v}=\mathbf{1}_z\times\boldsymbol{r}V+\operatorname{curl}(\mathbf{1}_z\times\boldsymbol{r}U), \tag{4}$$

where $\mathbf{1}_z$ is a unit vector in the z-direction (which is assumed to be the axis of symmetry). The equations governing P, T, U, and V, then, are (Paper I, eqs. [35]-[38])

$$\varpi^3\frac{\partial P}{\partial t}=-[\varpi^2P,\varpi^2U], \tag{5}$$

$$\varpi\frac{\partial T}{\partial t}=-[T,\varpi^2U]+[V,\varpi^2P], \tag{6}$$

$$\varpi^3\frac{\partial V}{\partial t}=-[\varpi^2V,\varpi^2U]+[\varpi^2T,\varpi^2P], \tag{7}$$

and

$$\varpi\Delta_5\frac{\partial U}{\partial t}=[\Delta_5P,\varpi^2P]-[\Delta_5U,\varpi^2U]+\varpi\frac{\partial}{\partial z}(T^2-V^2), \tag{8}$$

where, for the sake of brevity, we have used the notation

$$[f,g]=\frac{\partial(f,g)}{\partial(z,\varpi)}=\frac{\partial f}{\partial z}\frac{\partial g}{\partial\varpi}-\frac{\partial f}{\partial\varpi}\frac{\partial g}{\partial z}, \tag{9}$$

and Δ_5 denotes, as usual, the Laplacian operator for axisymmetric functions in five-dimensional Euclidean space.

a) The Stationary Solution

Equations (5)–(8) clearly admit the solutions

$$P = U = X(z, \varpi) \quad \text{(say)}$$

and

$$T = V = Y(z, \varpi) \quad \text{(say)} . \tag{10}$$

This represents a stationary solution of the equations of motion and corresponds under conditions of axisymmetry to solution (1), which the equations of hydromagnetics generally allow.

b) The Equations Governing the Oscillations about the Stationary Solution

It has been shown quite generally (Chandrasekhar 1956*b*) that solution (1) represents a stable solution of the basic equations. For a discussion of axisymmetric oscillations about the stationary solution (10), it will be convenient to have the general perturbation equations for the toroidal and the poloidal scalars.

Writing

$$P = X + P_1, \quad U = X + U_1, \quad T = Y + T_1, \quad \text{and} \quad V = Y + V_1 , \tag{11}$$

we readily find from equations (5)–(8) that the corresponding perturbation equations are

$$\varpi^3 \frac{\partial P_1}{\partial t} = - \, [\varpi^2\phi, \varpi^2 X] , \tag{12}$$

$$\varpi \frac{\partial T_1}{\partial t} = - \, [\psi, \varpi^2 X] + [Y, \varpi^2\phi] , \tag{13}$$

$$\varpi^3 \frac{\partial V_1}{\partial t} = + \, [\varpi^2\psi, \varpi^2 X] + [\varpi^2 Y, \varpi^2\phi] , \tag{14}$$

and

$$\varpi\Delta_5 \frac{\partial U_1}{\partial t} = [\Delta_5 X, \varpi^2\phi] + [\Delta_5\phi, \varpi^2 X] + 2\varpi \frac{\partial}{\partial z} Y\psi , \tag{15}$$

where we have used the abbreviations

$$\phi = P_1 - U_1 \quad \text{and} \quad \psi = T_1 - V_1 . \tag{16}$$

Rewriting equation (14) in the form

$$\varpi \frac{\partial V_1}{\partial t} = [\psi, \varpi^2 X] + [Y, \varpi^2\phi] - 2\varpi\psi \frac{\partial X}{\partial z} - 2\varpi Y \frac{\partial \phi}{\partial z} \tag{17}$$

and combining it with equation (13), we have

$$\varpi \frac{\partial \psi}{\partial t} = - \, 2 \, [\psi, \varpi^2 X] + 2\varpi Y \frac{\partial X}{\partial z} + 2\varpi Y \frac{\partial \phi}{\partial z} . \tag{18}$$

Similarly, by combining equations (12) and (15), we have

$$- \varpi\Delta_5 \frac{\partial \phi}{\partial t} = \varpi\Delta_5 \left\{ \frac{1}{\varpi^3} [\varpi^2\phi, \varpi^2 X] \right\} + [\Delta_5 X, \varpi^2\phi] + [\Delta_5\phi, \varpi^2 X] + 2\varpi \frac{\partial}{\partial z} Y\psi . \tag{19}$$

Equations (18) and (19) represent a pair of simultaneous equations for ϕ and ψ. Once these equations have been solved, equations (12) and (13) will complete the solution by determining P_1 and T_1 in terms of ϕ and ψ.

III. HYDROMAGNETIC OSCILLATIONS OF A FLUID SPHERE WITH TOROIDAL FIELDS AND ROTATIONAL MOTIONS ONLY

In this paper we shall restrict ourselves to a particularly simple case of the general equations of the preceding section. We shall suppose that in the stationary state the motions and the magnetic fields are purely toroidal, i.e.,

$$P = U = X = 0 . \tag{20}$$

Now the boundary conditions on a toroidal magnetic field are that it vanishes on the bounding sphere and is free of singularity at the origin. Thus

$$Y\ (= T = V) \quad \text{must vanish on} \quad r = R , \tag{21}$$

where R denotes the radius of the sphere. Accordingly, Y can be expressed as a linear combination of the fundamental toroidal functions (Chandrasekhar 1956*d*, eq. [36]; this paper will be referred to hereafter as "Paper II"):

$$T_{n,\,j} = \frac{J_{n+3/2}\,(\alpha_{j,\,n} r)}{r^{3/2}}\, C_n^{3/2}\,(\mu) , \tag{22}$$

where r is now measured in units of R; $\alpha_{j,\,n}$ is the jth zero of the Bessel function $J_{n+3/2}\,(x)$; and $C_n^{3/2}\,(\mu)$ denotes the Gegenbauer polynomial.

When $X = 0$, equations (18) and (19) reduce to

$$\frac{\partial \psi}{\partial t} = 2\,Y\,\frac{\partial \phi}{\partial z} \tag{23}$$

and

$$\Delta_5\,\frac{\partial \phi}{\partial t} = -\,2\,\frac{\partial}{\partial z}\,Y\psi , \tag{24}$$

while equations (12) and (13) become

$$\frac{\partial P_1}{\partial t} = 0 \tag{25}$$

and

$$\varpi\,\frac{\partial T_1}{\partial t} = [\,Y , \varpi^2\phi\,] . \tag{26}$$

From equation (25) it follows that

$$P_1 \equiv 0 . \tag{27}$$

Thus *during the oscillation no poloidal magnetic field will be generated; however, meridional motions, as well as rotational motions and toroidal magnetic fields, will be generated.*

Eliminating ψ between equations (23) and (24), we have

$$\Delta_5\,\frac{\partial^2 \phi}{\partial t^2} = -\,4\,\frac{\partial}{\partial z}\left(Y^2\,\frac{\partial \phi}{\partial z}\right). \tag{28}$$

Separating the time dependence by writing

$$\phi(z, \varpi) e^{i\sigma t} \quad \text{in place of} \quad \phi(z, \varpi, t) , \tag{29}$$

we obtain the equation

$$\sigma^2 \Delta_5 \phi = 4\,\frac{\partial}{\partial z}\left(Y^2\,\frac{\partial \phi}{\partial z}\right). \tag{30}$$

The boundary conditions which we should impose on ϕ can be inferred from equation (26). In spherical polar co-ordinates this equation is

$$\frac{\partial T_1}{\partial t} = e^{i\sigma t}\left\{\frac{1-\mu^2}{r^2}\,\frac{\partial}{\partial r}(r^2\phi)\,\frac{\partial Y}{\partial \mu} - \frac{\partial Y}{\partial r}\,\frac{\partial}{\partial \mu}\left[(1-\mu^2)\,\phi\right]\right\}. \tag{31}$$

Since T_1, like Y, must vanish on $r = 1$, it is clearly necessary that

$$\phi = 0 \quad \text{on} \quad r = 1\,. \tag{32}$$

Accordingly, we must seek solutions of equation (30) which vanish on $r = 1$ and are free of singularities at the origin. This is a characteristic value problem for σ^2.

a) The Variational Method

Let ϕ_j be a solution belonging to a characteristic value σ_j^2. Multiplying the equation governing ϕ_j by $\varpi^3\phi_k$ (belonging to σ_k^2) and integrating over the volume of the sphere, we have

$$\sigma_j^2\int\int\phi_k\Delta_5\phi_j\varpi^3 d\varpi\, dz = 4\int\int\phi_k\,\frac{\partial}{\partial z}\left(Y^2\,\frac{\partial\phi_j}{\partial z}\right)\varpi^3 d\varpi\, dz\,. \tag{33}$$

This equation can be rewritten in the form

$$\sigma_j^2\int\int\phi_k\left\{\frac{\partial}{\partial\varpi}\left(\varpi^3\,\frac{\partial\phi_j}{\partial\varpi}\right)+\varpi^3\,\frac{\partial^2\phi_j}{\partial z^2}\right\}d\varpi\, dz = 4\int\int\phi_k\,\frac{\partial}{\partial z}\left(Y^2\,\frac{\partial\phi_j}{\partial z}\right)\varpi^3 d\varpi\, dz\,. \tag{34}$$

Integrating by parts the integrals on both sides of this equation and remembering that ϕ vanishes on the boundary, we obtain

$$\sigma_j^2\int\int \operatorname{grad}\phi_j\cdot\operatorname{grad}\phi_k\varpi^3 d\varpi\, dz = 4\int\int Y^2\,\frac{\partial\phi_j}{\partial z}\,\frac{\partial\phi_k}{\partial z}\,\varpi^3 d\varpi\, dz\,. \tag{35}$$

From this equation it follows that

$$\int\int\operatorname{grad}\phi_j\cdot\operatorname{grad}\phi_k\varpi^3 d\varpi\, dz = 0 \qquad \text{if} \qquad j \neq k\,, \tag{36}$$

and, when $j = k$, we have (on further suppressing the subscripts)

$$\sigma^2 = \frac{4\int\int Y^2\,(\partial\phi/\partial z)^2\,\varpi^3 d\varpi\, dz}{\int\int|\operatorname{grad}\phi|^2\,\varpi^3 d\varpi\, dz}\,. \tag{37}$$

From equations (36) and (37) it is evident that the characteristic value problem associated with equations (30) and (32) is a self-adjoint one. Accordingly, equation (37) can be made the basis of a variational method for determining σ^2.

b) Case when Initial Magnetic Field and Fluid Motions Are Both Described by (0, 1) Toroidal Mode

We shall apply the formulae of the preceding section to the case when the magnetic field and the fluid motions in the initial stationary state both belong to the (0, 1) toroidal mode, i.e., when

$$Y = Y_0\,\frac{J_{3/2}\,(\alpha_{1,\,0}\, r)}{r^{3/2}}\,, \tag{38}$$

where Y_0 is a constant of the dimension sec $^{-1}$. To determine the corresponding lowest modes of oscillation, we expand ϕ in terms of the basic toroidal functions, $T_{n,\,j}$, and determine the coefficients in the expansion by minimizing the expression for σ^2 given by equation (37).

Thus, letting

$$\phi = \sum_{n,\,j} A_{n,\,j} T_{n,\,j} \tag{39}$$

and making use of the properties (Paper II, eqs. [32], [34], and [39])

$$\Delta_5 T_{n,\,j} = -\alpha^2_{j,\,n} T_{n,\,j} \tag{40}$$

and

$$\int_0^1 \int_{-1}^{+1} T_{n,\,j} T_{m,\,k} r^4 (1-\mu^2)\, d r\, d\mu = \frac{(n+1)(n+2)}{2n+3} [J'_{n+3/2}(\alpha_{j,\,n})]^2 \delta_{n,\,m} \delta_{j,\,k}\,, \tag{41}$$

we find that the denominator in the expression for σ^2 becomes

$$\int\!\!\int |\text{grad}\ \phi|^2 \varpi^3 d\varpi\, d z = -\int\!\!\int \phi \Delta_5 \phi \varpi^3 d\varpi\, d z$$

$$= \int_0^1 \int_{-1}^{+1} \Big(\sum_{n,\,j} A_{n,\,j} T_{n,\,j}\Big)\Big(\sum_{m,\,k} A_{m,\,k} \alpha^2_{k,\,m} T_{m,\,k}\Big) r^4 (1-\mu^2)\, d r\, d\mu \tag{42}$$

$$= \sum_{n,\,j} \frac{(n+1)(n+2)}{2n+3} [J'_{n+3/2}(\alpha_{j,\,n})]^2 \alpha^2_{j,\,n} A^2_{n,\,j}\,.$$

Considering, next, the numerator in equation (37), we first observe that the recurrence relations satisfied by the Gegenbauer polynomials (Paper II, eqs. [40] and [41]) and the Bessel functions enable us to write

$$\frac{\partial \phi}{\partial z} = \frac{1}{r^{5/2}} \sum_{n,\,j} A_{n,\,j} \big(F_{n,\,j} C^{3/2}_{n+1} + G_{n,\,j} C^{3/2}_{n-1}\big)\,, \tag{43}$$

where

$$\begin{aligned} F_{n,\,j} = \frac{n+1}{(2n+3)^2} \{ (\alpha_{j,\,n} r) [n J_{n+1/2}(\alpha_{j,\,n} r) - (n+3) J_{n+5/2}(\alpha_{j,\,n} r)] \\ - n(2n+3) J_{n+3/2}(\alpha_{j,\,n} r) \} \end{aligned} \tag{44}$$

and

$$\begin{aligned} G_{n,\,j} = \frac{n+2}{(2n+3)^2} \{ (\alpha_{j,\,n} r) [n J_{n+1/2}(\alpha_{j,\,n} r) - (n+3) J_{n+5/2}(\alpha_{j,\,n} r)] \\ + (n+3)(2n+3) J_{n+3/2}(\alpha_{j,\,n} r) \}\,. \end{aligned} \tag{45}$$

With $\partial\phi/\partial z$ given by equation (43), we have

$$\begin{aligned} 4 \int_0^1 \int_{-1}^{+1} Y^{-2} \Big(\frac{\partial \phi}{\partial z}\Big)^2 r^4 (1-\mu^2)\, d r\, d\mu = 4 Y_0^{-2} \int_0^1 \frac{d r}{r^4} [J_{3/2}(\alpha_{1,\,0} r)]^2 \\ \times \int_{-1}^{+1} d\mu\, (1-\mu^2) \Big\{ \sum_n C^{3/2}_n(\mu) \Big[\sum_j (A_{n-1,\,j} F_{n-1,\,j} + A_{n+1,\,j} G_{n+1,\,j})\Big]\Big\}^2. \end{aligned} \tag{46}$$

On making use of the orthogonality properties of the Gegenbauer polynomials (Paper II, eq. [34]), we can reduce the foregoing to the form

$$\begin{aligned} 4 \int_0^1 \int_{-1}^{+1} Y^{-2} \Big(\frac{\partial \phi}{\partial z}\Big)^2 r^4 (1-\mu^2)\, d r\, d\mu = 4 Y_0^{-2} \sum_n \frac{2(n+1)(n+2)}{2n+3} \\ \times \int_0^1 \frac{d r}{r^4} [J_{3/2}(\alpha_{1,\,0} r)]^2 \Big\{ \sum_j (A_{n-1,\,j} F_{n-1,\,j} + A_{n+1,\,j} G_{n+1,\,j}) \Big\}^2. \end{aligned} \tag{47}$$

From equation (47) it is clear that the solutions for ϕ which include in their expansions only the even, or only the odd, orders of the Gegenbauer polynomials fall into noncombining groups. The various modes of oscillation can therefore be classified as even or odd—a fact which could also have been inferred, directly, from equation (30).

For the form of ϕ assumed, the variational expression for σ^2 is given by the ratio of the quantities on the right-hand sides of equations (42) and (47). In practice one includes only a few terms in expansion (39) and minimizes the expression for σ^2 with respect to the $A_{n,j}$'s. The results, summarized in Tables 1 and 2, were derived in this manner.

TABLE 1

$\sigma^2/V_0^2 = S_0^2$ FOR THE LOWEST EVEN MODE

No.	Modes Included in the Variational Calculation	S_0^2	No.	Modes Included in the Variational Calculation	S_0^2
1	(0, 1) and (0, 2)	0.1461	5	(0, 1), (0, 2), (0, 3), and (0, 4)	0.0408
2	(0, 1), (0, 2), and (0, 3)	.07070	6	(0, 1), (0, 2), (0, 3), (0, 4), (2, 1), and (2, 2)	0.03842
3	(0, 1), (0, 2), (2, 1), and (2, 2)	.06980			
4	(0, 1), (0, 2), (0, 3), (2, 1), and (2, 2)	0.06223			

TABLE 2

$\sigma^2/V_0^2 = S_1^2$ FOR THE LOWEST ODD MODE

No.	Modes Included in the Variational Calculation	S_1^2
1	(1, 1) and (1, 2)	0.9697
2	(1, 1), (1, 2), and (1, 3)	0.5383

An inspection of Tables 1 and 2 shows that the sequence of trial functions used has not yet produced a satisfactory convergence toward the true characteristic values. This is also evident from the following list of the coefficients in the trial function (No. 6 in Table 1), including the modes (0, 1), (0, 2), (0, 3), (0, 4), (2, 1), and (2, 2), which minimizes the expression for σ^2:

$$A_{0,1} = 1;\ A_{0,2} = -0.93723;\ A_{0,3} = +0.52133;\ A_{0,4} = -0.16927;$$
$$A_{2,1} = -0.18525;\ \text{and}\ A_{2,2} = +0.0635\,. \tag{48}$$

This lack of convergence is somewhat surprising. It must originate in the basic equation's not being separable into the variables r and μ and in the problem's being so inextricably two-dimensional that it is impossible to approximate ϕ by a linear combination of the first few toroidal functions. A further fact which may be relevant in this connection is that equation (30) must change its character—hyperbolic or elliptic—within the unit sphere. This can be seen as follows:

Rewriting equation (30) in the form

$$\frac{\partial^2\phi}{\partial\varpi^2}+\left(1-4\,\frac{V^2}{\sigma^2}\right)\frac{\partial^2\phi}{\partial z^2}+\frac{3}{\varpi}\,\frac{\partial\phi}{\partial\varpi}-\frac{4}{\sigma^2}\,\frac{\partial\phi}{\partial z}\,\frac{\partial V^2}{\partial z}=0\,, \tag{49}$$

we observe that, since $V = 0$ on $r = 1$, the equation is certainly elliptic on and near the boundary. If it were elliptic throughout, then we could infer from the fundamental theorem on elliptic equations (cf. Courant and Hilbert 1937) that there exists no non-zero solution of equation (30) which vanishes on the boundary of the sphere. Hence a necessary condition for the existence of a solution of equation (30) which satisfies the boundary condition (32) is that σ^2 be less than V^2 in at least some parts of the unit sphere; in these parts the equation will be hyperbolic. Thus the equation must have this mixed character of being hyperbolic in some parts and elliptic in others.

Returning to the formula (cf. Tables 1 and 2)

$$\sigma^2 = V_0^2 S_1^2 , \tag{50}$$

we shall express V_0^2 in terms of more easily interpretable quantities: The magnetic energy, $\mathfrak{M}$, in the undisturbed sphere is given quite generally by

$$\mathfrak{M} = \tfrac{1}{2} \rho R^5 \int_0^1 \int_{-1}^{+1} \int_0^{2\pi} V^2 r^4 (1 - \mu^2)\, d r\, d\mu\, d\phi ; \tag{51}$$

and, for V of the chosen form (eq. [38]), we readily find that

$$\mathfrak{M} = \tfrac{2}{3} \pi \rho R^5 \,[J'_{3/2}(\alpha_{1,0})]^2 V_0^2 . \tag{52}$$

Defining $\langle H^2 \rangle_{\text{av}}$ by

$$\mathfrak{M} = \frac{\langle H^2 \rangle_{\text{av}}}{8\pi} \left(\tfrac{4}{3} \pi R^3\right) , \tag{53}$$

we can write

$$V_0^2 = \frac{V_A^2}{R^2} \,[J'_{3/2}(\alpha_{1,0})]^{-2} , \tag{54}$$

where V_A denotes the Alfvén velocity for the root-mean-square field. Inserting this expression for V_0^2 in equation (50), we obtain

$$\sigma^2 = S^2 \,[J'_{3/2}(\alpha_{1,0})]^{-2} \frac{V_A^2}{R^2} = 7.408 S^2 \frac{V_A^2}{R^2} . \tag{55}$$

Thus the period of oscillation, $2\pi/\sigma$, apart from a numerical factor, is given by the time taken for the Alfvén wave to travel once around the circumference of the sphere. For the lowest modes considered,

$$\sigma_0^2 < 0.28 \frac{V_A^2}{R^2} \quad \text{and} \quad \sigma_1^2 < 0.50 \frac{V_A^2}{R^2} . \tag{56}$$

IV. CONCLUDING REMARKS

This paper makes hardly more than a beginning in the study of hydromagnetic oscillations of models with internal motions. There are a great many problems in this general field which can be considered by the methods of this paper and whose solutions might be expected to contribute toward our understanding of hydromagnetic phenomena. While it is clearly premature to relate the results of this paper to particular aspects of known phenomena, it is perhaps worth pointing out that, by considering the hydromagnetic oscillations of a fluid sphere with rotational motions, we have removed a sharp distinction between the two models which have been proposed to interpret the magnetic variables—the model based on the oscillations of an initial static equilibrium configuration and the model based on a rotating star (cf. Deutsch 1956).

In conclusion I wish to express my thanks to Miss Donna Elbert for valuable assistance with the numerical calculations.

REFERENCES

Chandrasekhar, S. 1956*a*, *Proc. Nat. Acad. Sci.*, **42**, 1.
———. 1956*b*, *ibid.*, p. 273.
———. 1956*c*, *Ap. J.*, **124**, 232.
———. 1956*d*, *ibid.*, p. 244.
———. 1956*e*, *Proc. Nat. Acad. Sci.*, in press.
Chandrasekhar, S., and Fermi, E. 1953, *Ap. J.*, **118**, 116.
Chandrasekhar, S., and Limber, D. N. 1954, *Ap. J.*, **119**, 10.
Chandrasekhar, S., and Prendergast, K. H. 1956, *Proc. Nat. Acad. Sci.*, **42**, 5.
Courant, R., and Hilbert, D. 1937, *Methoden der mathematischen Physik*, **2** (Berlin: J. Springer), see particularly 274–275.
Cowling, T. G. 1952, *M.N.*, **112**, 527.
———. 1955, *Proc. R. Soc. London*, *A*, **233**, 319.
Deutsch, A. J. 1956, *Pub. A.S.P.*, **68**, 92.
Ferraro, V. C. A., and Memory, D. J. 1952, *M.N.*, **112**, 361.
Ferraro, V. C. A., and Plumpton, C. 1955, *Ap. J.*, **121**, 168.
Gjellestad, G. 1950, *Rept. Inst. Theoret. Ap.* (Oslo), No. 1.
———. 1952, *Ann. d'ap.*, **15**, 276.
Lüst, R., and Schlüter, A. 1954, *Zs. f. Ap.*, **34**, 263.
Prendergast, K. H. 1956*a*, *Ap. J.*, **123**, 498.
———. 1957, *ibid.*, in press.
Schwarzschild, M. 1949, *Ann. d'ap.*, **12**, 148.

LYMAN-ALPHA INTENSITY AND SOLAR LIMB DARKENING FROM ROCKET SPECTROGRAMS[*]

S. C. Miller, Jr., R. Mercure, and William A. Rense
University of Colorado, Boulder, Colorado

Received May 12, 1956; revised May 29, 1956

ABSTRACT

From recent rocket spectrograms the intensity of solar Lyman-α radiation has been measured to be 3.0 ergs/cm²/sec at 122 km, and the half-width about 0.8 A. Because of special features of the spectrograph design, it was possible to measure solar limb darkening in Lyman-α radiation. The averaged results indicate slight limb brightening, possibly because of an appreciable increase in intensity in Lyman-α radiation in the solar latitudes, which exhibited sunspot activity at the time of the flight.

INTRODUCTION

Three spectrograms of the sun in the ultraviolet were taken in a grating spectrograph flown in an Intermediate Aerobee at Holloman Air Base, New Mexico, on December 13, 1955. The grating, blazed for the Lyman-α region, had a radius of 39 cm, a constant of 6000 lines/cm, and was set at an angle of incidence of 49°.5. The slit was 12 μ by 0.5 cm. The film (Eastman 103-O-UV) was automatically pulled along the Rowland circle between exposures, winding into a light-tight cassette. The spectrograph was pointed continuously at the sun with an accuracy of 1 minute of arc by an electronic pointing control (Stacey, Stith, Nidey, and Pietenpol 1954; Nidey and Stacey 1956) developed and constructed at the Research Service Laboratories of the University of Colorado under Air Force sponsorship. Exposure times and average heights of the spectrograms were, respectively, 16.1 sec at 89 km, 7.5 sec at 105 km, and 31.4 sec at 122 km. The Lyman-α line and several other emission lines below 1900 A, along with the ultraviolet continuum and Fraunhofer lines at the longer wave lengths, were photographed. One objective of the flight was to study solar limb darkening in Lyman-α radiation. Therefore, the spectrograph was designed to be free of astigmatism at 1215.7 A. Instrument speed and absolute film response at 1215.7 A were also determined, enabling one to compute the intensity of the Lyman-α radiation for the three heights.

ELIMINATION OF ASTIGMATISM

In the following discussion "horizontal" will refer to the plane of the grating spectrograph (cutting the grating lines at right angles), and "vertical" will refer to a plane perpendicular to the former plane. The optical layout of the spectrograph is shown in Figure 1. Let α be the angle of incidence, β the angle of diffraction of the light with respect to the grating normal, and R the radius of curvature of the spherical concave grating. It will be assumed that the centers of the sun, slit, and gratings are on a straight line. The slit of the spectrograph is on the Rowland circle at the distance $r = R \cos \alpha$. Vertical fans of rays with the slit as source are not ordinarily focused at this same distance. Thus the image of the slit is astigmatic. However, vertical fans of rays have the sun, effectively at infinity, as source, since the diffraction effects of the slit occur only in the horizontal plane. For an infinitely distant source of a vertical fan of rays, the vertical and horizontal image distances are equal when

$$\frac{1}{\cos \beta} = \cos \alpha + \cos \beta \, . \tag{1}$$

---

[*] The research reported in this paper has been sponsored by the Geophysics Research Directorate of the Air Force Cambridge Research Center, Air Research and Development Command.

Another equation relating α and β is the diffraction equation (for first order):

$$\sin \alpha + \sin \beta = \frac{\lambda}{d}, \tag{2}$$

where λ is the wave length and d is the grating-line spacing. For $\lambda = 1215.7$ A (Lyman-α) and for $d = 1/6000$ cm, λ/d is 0.0729. With this value of λ/d, a solution for α and β is

$$\alpha = -49\overset{\circ}{.}5, \quad \beta = 43\overset{\circ}{.}0 .$$

Experimentally and theoretically, it was found that the focusing error was less than one-third of a minute of arc.

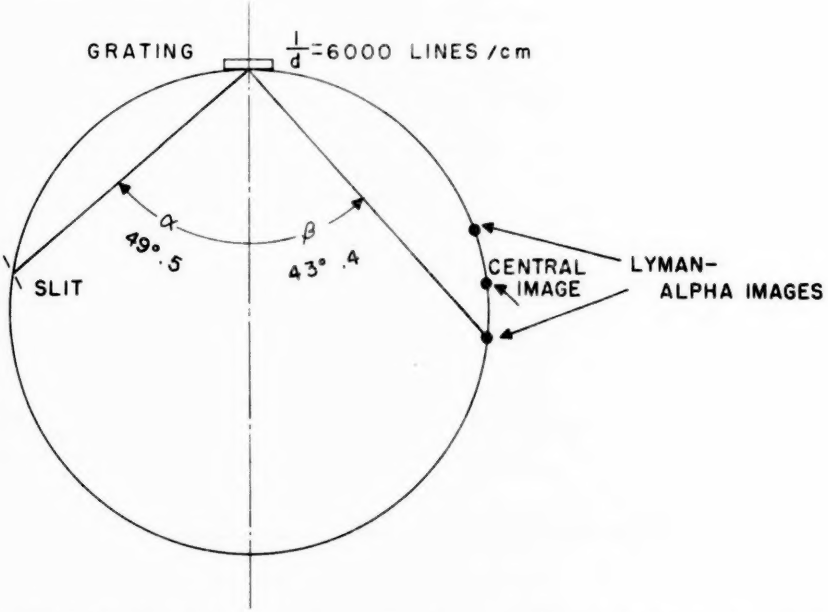

FIG. 1.—Sketch of the concave-grating spectrograph used to photograph the Lyman-α line without astigmatism.

ABSOLUTE INTENSITY AND LINE PROFILE

H- and D-curves for the actual rocket film were obtained after the flight in both Lyman-α light and white light. From these curves the effect of the scattered-light background (assumed to be white light) around the Lyman-α line could be eliminated. Densitometer tracings across the Lyman-α line were made for each spectrogram (Fig. 2). The intensity of any part of the profile could be found with respect to the white-light background by computations based on data from the H- and D-curves. In this way the relative intensities of the integrated line (or any part of the line) might be obtained. The results are indicated in the third column of Table 1.

It will be observed that the intensity is reduced by almost one-half in going from the 122-km height to the 89-km height, showing that an appreciable amount of molecular oxygen exists above 89 km. (Absorption by nitrogen is inappreciable at Lyman-α.) Computed amounts of molecular oxygen appear in column 4. The numbers were obtained by using the value (Watanabe, Inn, and Zelikoff 1953) of 0.27 cm^{-1} for the absorption coefficient of oxygen gas at 1215.7 A and by assuming negligible absorption at 122 km. The sun's zenith distance was 60° at the time of the flight. Theoretical values listed by Mitra (1951) are 1.0, 0.01, and 10^{-6} cm. Laboratory measurements of the energy in Lyman-α radiation required to produce a density of 0.5 yielded the result 0.63 $\text{erg}/\text{cm}^2 \pm 50$ per cent. The values of Lyman-α line absolute intensity given in column 5, therefore, have high probable errors but may be regarded as reliable to within a factor of about 2.

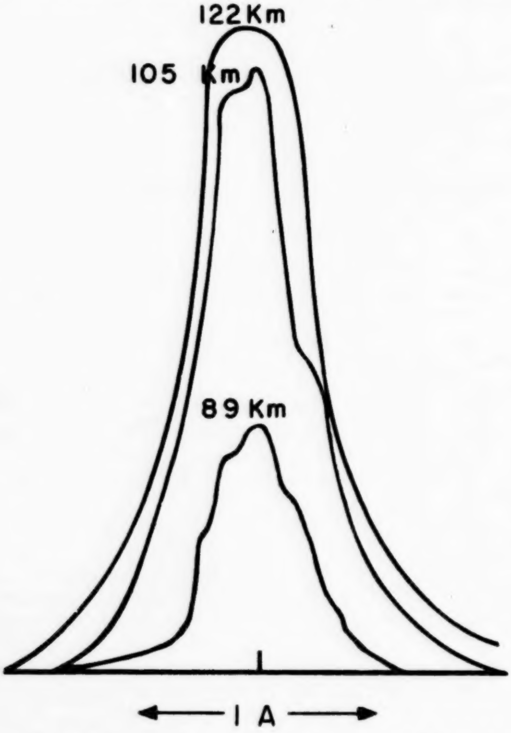

FIG. 2.—Lyman-α profiles uncorrected for film and instrumental effects, taken at three average heights. The density scale is arbitrary and different for each profile. Relative intensities are listed in Table 1.

The Lyman-α line profiles as revealed by microphotometer tracings, such as in Figure 2, include instrumental effects. Uncorrected half-widths determined from the tracings after these were changed to intensity versus wave-length curves are listed in column 6 of Table 1. The half-width of a laboratory-produced ultraviolet line at 1215.7 A for about the same density above background as on the rocket spectrograms was measured to be 0.5 A. The profiles in Figure 2 hint at structures in the line on both the short- and long-wave-length sides. That such a structure is not entirely instrumental is supported by a similar profile obtained from a spectrogram (Rense 1953) taken on December 12, 1952, with an instrument of higher dispersion and at an altitude of about 80 km. The line profile in Figure 2 is smoothest for the spectrogram taken at the highest altitude. The absorption of oxygen varies in the vicinity of 1215.7 A, and possibly some of the structure at the lower altitudes may be due to narrow oxygen absorption lines in this wave-length region.

The Lyman-α line intensity reported in this paper is not entirely in agreement with the results obtained from rockets by other observers. Photon-counter measurements (Friedman, Lichtman, and Byram 1951) have given a range of values from 0.1 to 3.5 ergs/cm^2/sec. Measurements of spectrograms (Rense 1953; Johnson, Purcell, Malitson, and Tousey 1955) have yielded values between 0.3 and 0.6 erg/cm^2/sec. Data from three recent flights (Byram, Chubb, Friedman, and Kupperion 1956), for which ionization-chamber detectors were used, all lead to an intensity greater than 2 ergs/cm^2/sec. Some of these results involve large probable errors. Others obtained at low altitudes may not have been corrected accurately for absorption by residual terrestrial molecular oxygen. Nevertheless, it appears that there is a real and significant time variation in the intensity of Lyman-α radiation. The results of the limb-darkening study in the next section of this paper bear out this conclusion.

TABLE 1

RESULTS OF ANALYSIS OF LYMAN-α LINE ON THREE SPECTROGRAMS TAKEN AT DIFFERENT ROCKET HEIGHTS

Exp. (sec) (1)	Av. Ht. (km) (2)	Rel. Int. (Total) (3)	Molecular Oxygen above Rocket (S.T.P.) (cm) (4)	Abs. Intensity (ergs/cm^2/sec) (5)	Half-width (A) (6)
16.1	89	0.58	1.0	1.7	0.74
7.5	105	0.86	0.3	2.6	.80
31.5	122	1.00	0	3.0	0.85

A half-width of about 0.75 A was obtained by one of the authors (Rense 1953) from a study of a spectrogram taken at 80 km. The resolving power in that case was superior to that for the present instrument, but the agreement with the results in Table 1 is excellent. Other observers (Johnson *et al.* 1955) have found a half-width smaller than 0.3 A.

LIMB DARKENING

To measure limb darkening, one must associate the intensity of points on the spectrum line with the intensity of corresponding regions of the sun's disk. The intensity at any point on the spectral line will be proportional to the integrated intensity over a horizontal line across the face of the sun, provided that the slit is long enough to avoid vignetting. A transformation must be made to find the actual intensity at a point on the sun as a function of the distance from the center of the sun. Assuming circular symmetry for the intensity on the sun's disk as seen from the earth, one writes, for the energy in an element of area $dxdy$ of the disk,

$$d^2E = f(r)dxdy\,, \tag{3}$$

where $f(r)$ is the energy per unit area at a distance r from the center of the sun's disk. The intensity of the spectral line at a point distant y from the center of the spectrum line is proportional to

$$F(y) = \frac{dE}{dy} = 2\int_0^{(R^2-y^2)^{1/2}} f(r)\, dx\,. \tag{4}$$

Since $F(y)$ will be an even function, one can fit it empirically (for $-R < y < R$) with a series of the type

$$F(y) = (R^2 - y^2)^{1/2}\left[a + b\,\frac{(R^2-y^2)^{1/2}}{R} + \frac{c\,(R^2-y^2)}{R^2} + \ldots\right]. \tag{5}$$

The $f(r)$ which leads to the above series is

$$\begin{aligned} f(r) &= \frac{1}{\sqrt{\pi}}\left[\frac{\Gamma(3/2)}{\Gamma(1)}\,a + \frac{\Gamma(2)\,b\,(R^2-r^2)^{1/2}}{\Gamma(3/2)\,R} + \frac{\Gamma(5/2)\,c\,(R^2-r^2)}{\Gamma(2)\,R^2} + \ldots\right] \\ &= \frac{a}{2} + \frac{2}{\pi}\,b\cos\theta + \tfrac{3}{4}\,c\cos^2\theta + \ldots\,, \end{aligned} \tag{6}$$

where $\cos\theta = (1 - r^2/R^2)^{1/2}$. This gives the desired limb darkening in terms of the angle θ usually employed for such study.

To find the limb darkening of the sun in Lyman-α light, three densitometer tracings were made on each of the three spectrograms. One tracing was made from one end of the line to the other, down the center of the line over a strip corresponding to a width of 1.2 A in the line. The other two tracings to find the background were made parallel to the first tracing, just outside the line on each side. The average of these two tracings opposite a given point of the line was taken as the background density at this point. This background was assumed to be due to scattered white light, since spectrograms taken on the ground with the instrument gave substantially the same background. Curves relating Lyman-α intensity to film density for various white-light backgrounds were used to find the Lyman-α intensity at eighty equally spaced points on the lines from each of the three spectrograms. Functions of the form $a[1 - (y/R)^2]^{1/2} + b[1 - (y/R)^2]$ were fitted to these data by means of the least-squares method. The higher-order terms of the expansion equation (5) were dropped, since the accuracy of the data did not seem to be such as to justify carrying them. These functions were then converted to the form of equation (6) to give the limb-darkening equation.

For the lowest-altitude exposure the result was

$$I = 1 - (0.02 \pm 0.20)\cos\theta\,, \tag{7}$$

where the intensity of the limb is arbitrarily taken to be unity. The result for the intermediate altitude was

$$I = 1 - (0.35 \pm 0.13)\cos\theta\,, \tag{8}$$

and that for the highest altitude was

$$I = 1 + (4.0 \pm 2.2)\cos\theta\,. \tag{9}$$

The weighted average is

$$I = 1 - (0.06 \pm 0.32)\cos\theta\,. \tag{10}$$

The probable errors here were largely a result of fluctuations in density due to graininess. Other sources of error were much smaller in comparison. There seems to be a definite difference in limb darkening between successive exposures, greater than the probable errors involved. When one examines the densitometer tracings, these differences appear to be even more pronounced. The spectral line for the shortest exposure has definite peaks of intensity, equally spaced approximately four-tenths of the distance from the center to the end of the line and about one and one-half times the central intensity. The intensity of the intermediate exposure was more or less uniform until near the edge, while that of the longest exposure fell off continuously with increasing distance from the center of the line.

The foregoing analysis was done on the assumption that the intensity has circular symmetry with respect to the center of the sun. One can speculate that the differences between the three spectrograms might have arisen because this intensity is not circularly symmetric. An auxiliary white-light camera in the rocket indicated (but not conclusively) that the pointing mechanism did rotate through an appreciable angle about the center of the sun during the exposures. The assumption that Lyman-α radiation is more intense in the strong plage zones appearing around solar latitude ± 27° at the time is consistent with the foregoing results.

The authors are grateful for the help received from Mr. Adolph Jursa, project scientist of the Air Force Cambridge Research Center, and from Mr. Russell Nidey, Mr. Frank Stuart, and the many others of the Research Service Laboratories of the University of Colorado who contributed to the work.

REFERENCES

Byram, E. T., Chubb, T. A., Friedman, H., and Kupperion, J. 1956, *J. Opt. Soc. America*, **46,** 384.
Friedman, H., Lichtman, S. W., and Byram, E. T. 1951, *Phys. Rev.*, **83,** 1025.
Johnson, F. S., Purcell, J. O., Malitson, H. H., and Tousey, R. 1955, *Ap. J.*, **60,** 165.
Mitra, S. K. 1952, *The Upper Atmosphere* (2d ed.; Calcutta: Asiatic Society), p. 173.
Nidey, R. A., and Stacey, D. S. 1956, *Rev. Scient. Instr.*, **27,** 216.
Rense, W. A. 1953, *Phys. Rev.*, **91,** 299.
Stacey, D. S., Stith, G. A., Nidey, R. A., and Pietenpol, W. B. 1954, *Electronics*, **27,** 149.
Watanabe, K., Inn, E. C. Y., and Zelikoff, M. 1953, *J. Chem. Phys.*, **21,** 1026.

LYMAN-α AND THE STRUCTURE OF THE SOLAR CHROMOSPHERE*

R. G. Athay and R. N. Thomas
High Altitude Observatory and Harvard College Observatory

Received March 14, 1956

ABSTRACT

We investigate the range of chromospheric models compatible with present rocket observations of Lyman-α and conclude that it is considerable. We would require detailed observations of the line profile, with resolution better than one Doppler half-width, to be more specific on the actual model. We find a considerable difference between T_e and a radiation temperature defined by the line intensity, in conformity with earlier discussions of the non-equilibrium chromosphere by ourselves and by Giovanelli. A discussion of the relation of these results to the limb flare and SID correlations found by C. Warwick suggests a more extended investigation of the non-spherically symmetric model and its relation to the chromospheric opacity in Lyman-α.

I. INTRODUCTION

In our investigations of the solar chromosphere we have heretofore largely confined our discussion of the hydrogen lines to eclipse observations of integrated line intensities and to lines later than H10 in the Balmer series. By this restriction we have hoped to treat lines in which the chromosphere is not opaque and thus to separate self-absorption from non-equilibrium effects by the use of only integrated line intensities. On the other hand, to determine non-equilibrium effects from lines in which the chromosphere is opaque, one requires observations of profiles of the various lines and a knowledge of the relation between electron temperature, T_e, and excitation temperature, T_{ex}, for each line. The results of the analysis of the later Balmer lines (Thomas 1949, 1950; Athay and Thomas 1955; Matsushima 1955) made it clear that the chromosphere is opaque in the central regions of the early Balmer lines, as well, of course, as in the Lyman lines. Thus we might hope to supplement our analysis of the later Balmer lines with an investigation of the earlier lines.

Several analyses of the early hydrogen lines appear in the literature. With the notable exception of the papers by Giovanelli (1948), Jefferies (1953), and Jefferies and Giovanelli (1954), these analyses either do not discuss the relation between the inferred quantity, T_{ex}, and the desired quantity, T_e, or they imply $T_e = T_{ex}$. De Jager (1952) and Böhm-Vitense (1954) have applied disk observations of hydrogen-line profiles to determine the thermal structure of the upper photosphere and lower chromosphere. Most of de Jager's work sets $T_e = T_{ex}$; an important exception in his attempt to predict the behavior of Hα, using Giovanelli's computations of the non-equilibrium parameters. Böhm-Vitense presents all her work in terms of T_{ex}, assuming T_{ex} to be the same for all the Balmer lines. Although she carefully points out the probable presence of departures from local thermodynamic equilibrium in a discussion of the metallic lines, her graph of T_{ex} determined from the central intensities of the Balmer lines gives no guide to the relation of T_{ex} to T_e. Goldberg (1954) has interpreted rocket data on Lyman-α to suggest a model for the thermal structure of the chromosphere. Although he defines his temperature parameter as T_{ex}(Ly-α) when discussing the rocket data, he apparently assumes $T_{ex} = T_e$ in relating his model to the Woolley-Allen model chromosphere (1950) and to the upper-boundary temperature of the photosphere. Thus it is difficult to assess the actual

---

* This work was supported by the Air Force Cambridge Research Center, Geophysics Research Directorate, through Contract AF19(604)-146 with Harvard University.

physical differences between the various chromospheric models, particularly in the important transition region of the low chromosphere, and also those between results obtained from the earlier and later hydrogen lines.

In this and a following paper we attempt to discuss the data from the early hydrogen lines, particularly in terms of T_e and its relation to T_{ex} of the various lines, in the hope of clarifying this situation and resolving some of the problems encountered in analyzing the later hydrogen lines. As data we use eclipse and disk observations of early Balmer lines, and existing rocket data on Lyman-**α**. Recalling our discussion of an apparent variability of the chromosphere over the solar activity cycle (Athay and Thomas 1956*a*), we recognize that our data are not homogeneous. Thus we must attempt to differentiate between gross structural features that are invariant over the activity cycle and details of the structure which may vary. In this first paper we consider Lyman-**α**.

II. LYMAN-α

a) Rocket Observations and Their Implication for $T_e(h)$

Rocket observations of Lyman-**α** provide varying estimates of the total emission in the line, ranging from 0.4 erg/cm^2/sec incident on the earth's upper atmosphere (Tousey, Watanabe, and Purcell 1951), through 0.3(Pietenpol, Rense, Walz, Stacey, and Jackson 1953), to 0.1(Byram, Chubb, Friedman, and Gailar 1953). According to the last authors, more than 90 per cent of the energy in a 100 A band falls within ±0.5 A from the line center. Thus one ascribes an emission of some 0.01 erg/cm^2/sec to a 100 A strip of the continuum near Lyman-**α**. Johnson, Malitson, Purcell, and Tousey (1955) suggest a width of 0.3 A for the line itself; thus one expects the emission within the line to be concentrated in a region 0.3–1.0 A wide. If we estimate the intensity at the line center by assuming a rectangular profile and define a radiation temperature, $T_{\rm rad}$, by equating the intensity to a Planck function at $T_{\rm rad}$, the preceding data lead to the range of values

$$6000^\circ \lesssim T_{\rm rad} \lesssim 7500^\circ . \qquad (1)$$

Similarly, the intensity in the neighboring continuum corresponds to $T_{\rm rad} \lesssim 4600^\circ$. We ask, therefore, what information these data give on T_e in the chromosphere.

In an attempt to highlight the essential physical features of a high-temperature chromosphere, Giovanelli and Jefferies and Giovanelli have investigated the Lyman-**α** emission from a chromosphere having constant T_e and n_e above some specified level. Their results predict a Lyman-**α** profile well within the width set by the rocket data. Entering the tables calculated by Jefferies and Giovanelli with the range of $T_{\rm rad}$ given here, one infers the corresponding range in T_e to be about 13000°–19000°. On the other hand, from the limit of 1 A on the width of Lyman-**α**, Goldberg concludes that Lyman-**α** is formed in a region of the chromosphere in which the excitation temperature, T_{ex}, for Lyman-**α** increases rapidly with height. Implicitly, he sets $T_{ex} = T_e$. He suggests a chromospheric model of the Woolley-Allen type having T_e constant at the photospheric boundary value, which he takes from the continuum measures cited as 4600°, up to some height $\gtrsim$4000 km, from which the temperature rises to ~6000° near 6000 km. In essence, the Giovanelli-Jefferies results form a counter example to Goldberg's general conclusion that the rocket data require Lyman-**α** to be formed in a region where T_e, set equal to T_{ex}, increases rapidly with height.[1]

---

[1] C. de Jager has kindly sent to us prepublication results (1956) in which he combines the rocket data with earlier computations on the non-equilibrium configuration by Giovanelli (1948) to infer a value $T_e \sim 64000^\circ$ in the region of the chromosphere where the center of Lyman-**α** is formed.

The essential difference between the two results lies in the assumed source function, that is, in the general expression for the line profile:

$$I_\nu(0,\mu) = \int_0^\infty S_\nu e^{-\tau_\nu/\mu}\,\frac{d\tau_\nu}{\mu}. \tag{2}$$

Giovanelli and Jefferies note the importance of coherent scattering for this resonance line; hence they adopt

$$S_\nu = (1-\lambda)\langle I_\nu\rangle + s_{\nu_0}, \tag{3}$$

where $\langle I_\nu\rangle$ is I_ν averaged over direction and s_{ν_0} does not vary with frequency over the line profile. Goldberg uses as the source function the formal equivalent of the pure absorption model, defined in terms of the excitation temperature,

$$S_\nu = B_\nu\,[T_{ex}\,(\text{Ly-}\alpha)\,] = \frac{2h\nu_0^3}{c^2}\left[\frac{n_1}{n_2}\frac{\varpi_2}{\varpi_1} - 1\right]^{-1}, \tag{4}$$

where the n_i's are occupation numbers of the first and second quantum levels and the ϖ_i's are statistical weights. We proceed then to investigate two questions: (1) Which approach should one actually adopt to determine the implication of the rocket results? (2) If we have the correct approach, how much do the presently existing rocket data actually restrict the range of possible chromospheric models? Our discussion proceeds in three steps: (i) a specification of the form of the absorption coefficient for Lyman-α and a comment on the requirements for a narrow line profile; (ii) a discussion of the proper form for S_ν, particularly with respect to equations (3) and (4) and the assumptions underlying their validity; and (iii) a discussion of the physical process of the formation of Lyman-α.

(i) *The source of line broadening for Lyman-α.*—For Lyman-α, we expect Doppler broadening to predominate over all other forms of broadening in the region of interest. The Doppler half-width is $0.052[10^{-4}\,T_e]^{1/2}$ A, the damping coefficient is $\Gamma = A/4\pi = 3.7 \times 10^7$, so the parameter a entering the $H(a, v)$ function is $3.5 \times 10^{-4}[10^{-4}\,T_e]^{-1/2}$. Thus from Harris' (1948) tables of $H(a, v)$ we see that Doppler broadening predominates over natural broadening out to $\gtrsim 3$ Doppler widths for $T_e \gtrsim 4000°$, a lower limit for T_e in the chromosphere. Also, for $n_e < 10^{12}$, which is a safe limit for the chromosphere, Stark broadening is negligible for Lyman-α.

This extent of the Doppler core provides a rough measure of the criterion for a chromospheric model to be compatible with the rocket data on Lyman-α. For the absorption coefficient decreases by e^9 or 10^4 from the line center out to the point 3 Doppler widths; and, so long as $T_e < 10^5$, this Doppler width does not exceed 1 A. Thus, in terms of optical depth at the line center, τ_{ν_0}, this Doppler core of the line originates in the region $1 < \tau_{\nu_0} < 10^4$. Alternatively, if we define $N_1(h)$ as the number of first-quantum atoms above height h and note that α_{ν_0} for Lyman-α is $0.59 \times 10^{-13}(T_e \times 10^{-4})^{-1/2}$, the Doppler core arises in the region $10^{13} \lessapprox N_1(h) \lessapprox 10^{18}$. The extra order of magnitude comes from the range in α_ν due to uncertainty in T_e. If a particular chromospheric model is *not* to predict a line width less than 1 A, S_ν must not change by as much, say, as a factor e over this range in τ_{ν_0} or $N_1(h)$. In terms of the source function of equation (3), $\langle I_\nu\rangle$ must remain constant over h *and* over ν across the line profile to within a factor e. In terms of the source function of equation (4), T_{ex} must not vary by more than 200°–400°. Thus, to answer the question on the narrowness of profile and emission in the line, it is sufficient to restrict our discussion to the region of the chromosphere-corona falling within the above range in τ_{ν_0}, or $N_1(h)$.

(ii) *The form of* S_ν.—First, we note that the equation of transfer may be written in the form

$$\mu \frac{d I_\nu}{- a_{\nu_0} \rho d x} = I_\nu \left[\frac{n_1}{n_2} \frac{\varpi_2}{\varpi_1} - 1 \right] n_2 \phi_\nu + n_2 j_\nu \frac{2 h \nu_0^3}{c^2} , \tag{5}$$

provided that j_ν is left completely arbitrary in its dependence upon ν, direction, and occupation numbers of the various energy states. If $\phi_\nu = j_\nu$, the equation may be reduced to the standard form of the "pure absorption" model, with source function S_ν given by equation (4) (Milne 1930). If any appreciable coherent scattering exists, if natural or Stark broadening is comparable to Doppler broadening, etc., $\phi_\nu \neq j_\nu$, and we cannot use equation (4). For a recent discussion, see J. Warwick (1955).

Second, we note that equation (3) is not valid, as written, if the sole source of line broadening is Doppler. For the predominance of coherent scattering in a resonance line refers to the scattering frequency measured by an observer at rest with respect to the atom. To an observer at rest with respect to the atmosphere, the emitted frequency is fixed by the velocity component of the atom in the particular direction. This physical situation is, of course, precisely that implied when one neglects all sources of broadening other than Doppler, where the atom "thinks" it is always absorbing and emitting only at ν_0, while the actual absorption and emission profiles are fixed by the Doppler functions centered on ν_0. If the coherent scattering process, relative to the atom, is isotropic, then the emission and absorption profiles are identical. If the coherent scattering, relative to the atom, has an angular dependence, we will have a correction dependent on the radiative flux, which seems to be generally second order in the regions $\tau_\nu \sim 1$ and deeper. Compare, in Warwick's formulation, the case of completely incoherent scattering with that resulting from an angularly dependent scattering function. In the following, we assume that we may neglect the correction arising from this angular dependence, and so obtain $\phi_\nu = j_\nu$ *in the Doppler core*, to which we have restricted our discussion. We propose to return to this point, in greater detail, in another paper.

Third, we can evaluate $B_\nu(T_{e1})$ from the equation of statistically steady state for the first-quantum level, which is (Thomas 1948)

$$\begin{aligned} b_1 \left[\sum_{n=2}^{\infty,\,\kappa} Q_{1n} (1 + X_{1n}) \left(1 - \frac{b_n}{b_1} \right) e^{X_n} \right] &= \frac{2.85 \times 10^{20}}{n_e T_e^{1/2}} \left[\frac{g_{11}}{2} \frac{1}{X_1} \left\{ 1 - W_\kappa \frac{b_1 (X_1 / Y_1)\, e^{X_1} - (X_1 / [X_1 + Y_1])}{e^{Y_1} - 1} \right\} \right. \\ &\quad \left. + \sum_2^{\infty} b_n \frac{e^{X_n} g_{1n}}{n (n^2 - 1)} \left\{ 1 - W_{1n} \frac{(b_1 / b_n)\, e^{X_{1n}} - 1}{e^{Y_{1n}} - 1} \right\} \right] , \end{aligned} \tag{6}$$

where Q_{1n} is the dimensionless inelastic-collision cross-section ($Q_{12} \sim 1$; $Q_{13} \sim 0.18$, etc.; the g_{1n} are the Gaunt factors; X_n and Y_n are $h\nu_n / kT_e$ and $h\nu_n / kT_r$, respectively, and $X_{nm} = X_n - X_m$, etc.; and T_r and W_{ν_0} are defined by

$$\int_{\nu'} \phi_{\nu'} \langle I_{\nu'} \rangle d\nu' = W_{\nu_0} B_{\nu_0} (T_r) , \tag{7}$$

so that T_r may be chosen arbitrarily, leaving W to balance equation (6). Both exp Y_{12} and exp $X_{12} \gg 1$, and equation (6) may be rewritten in the form:

$$\begin{aligned}\frac{2h\nu^3}{c^2}\left(\frac{b_1}{b_2}\,e^{X_{12}}-1\right)^{-1} &= B_\nu\,(T_{ex}) \\ &= W_{\nu_0}B_\nu\,(T_r)\left[1+\sum_3^\infty \frac{6\,g_{1n}}{n\,(n^2-1)\,g_{12}}\,\frac{W_{1n}}{W_{12}}\,e^{-Y_{2n}}+\frac{3\,g_{11}\,e^{-Y_2}}{Y_1\,g_{12}}\,\frac{W_{1\kappa}}{W_{12}}\right]D^{-1} \\ &\quad + B_\nu\,(T_e)\left[\sum_2^\infty \frac{6Q_{1n}\,(1+X_{1n})\,(1-[b_n/b_1])\,e^{-X_{2n}}}{2.85\times 10^{20}n_e^{-1}T_e^{-1/2}g_{12}}\right]D^{-1}, \end{aligned} \tag{8}$$

$$D=\left[1+\sum_3^\infty \frac{b_n}{b_2}\,\frac{e^{-X_{2n}}6\,g_{1n}}{n\,(n^2-1)\,g_{12}}+\frac{3\,g_{11}\,e^{-X_2}}{g_{12}X_1 b_2}\right].$$

If $\langle I_\nu\rangle$ is Gaussian, then we can define T_r by $B_\nu(T_r)=\langle I_{\nu_0}\rangle$, and W becomes

$$W=\left[1+\left(\frac{\Delta\nu_D}{\Delta\nu_I}\right)^2\right]^{-1/2}, \tag{9}$$

where $\Delta\nu_I$ and $\Delta\nu_D$ are the "Doppler" widths of $\langle I_\nu\rangle$ and ϕ_ν, respectively. If $\langle I_\nu\rangle$ has a rectangular profile of extent greater than the Doppler core or if there is no line, $W=1$. Since we have shown that the line broadening is effectively pure Doppler over three Doppler widths, we expect the emergent profile of $\langle I_\nu\rangle$ to lie closer to a Doppler profile at T_e than to a rectangular profile of large extent. That is, $W\sim 2^{-1/2}$. Since $\Delta\nu_D \propto T_e^{1/2}$, W changes only slightly if $\Delta\nu_I$ does not correspond closely to T_e.

In order to obtain some feeling for the coefficients of $WB_\nu(T_r)$ and $B_\nu(T_e)$ in equation (8), consider the numerical value of the various terms and their physical implication.

The terms involving Σ_3.—These two terms, one occurring in the denominator of equation (8) and the other occurring in the numerator of the first number, would be identical if $(b_2/b_n)\exp X_{2n}=\exp Y_{2n}$ and $W_{1n}=W_{12}$. From the foregoing discussion, $W_{1n}\sim W_{12}$. For the other equality to be true, we would require $B_\nu[T_{ex}(2-n)]\sim\langle I_{\nu_0}\rangle(2-n)$. As we shall see in part iii, this last equality is essentially true for $\tau\sim 1$ for the Balmer lines, but in the higher atmosphere b_2/b_n decreases. Thus the term involving $\exp Y_{2n}$ is smaller than that involving $(b_2/b_n)\exp X_{2n}$. We can use the observed emergent intensity of the Balmer lines to set a generous upper limit on $\exp(-Y_{2n})$ as the value with $T_r=6000°$. (4000° would be more realistic, since the largest term corresponds to $n=3$.) For $T_r=6000°$, the term in the numerator is $\lesssim 0.007$, and the term in the denominator lies between 0.007 and the value ~ 0.25 obtained by setting $(b_2/b_n)\exp(X_{2n})=1$.

The terms involving exp $(-X_2)$ *and exp* $(-Y_2)$.—Again, the W ratio is ~ 1; and $b_2\exp X_2\sim\exp Y_2$ requires $B_\nu[T_{\text{ion}}(2)]\sim\langle I\rangle(\lambda\,3640)$. Both these terms are small compared with their respective Σ_3 terms. And the term containing $\exp(-Y)$ is always less than that containing $\exp(-X)$ because of the terms X_1 and Y_1.

Thus the coefficient of $WB_\nu(T_r)$ reduces to a value, $1-\epsilon$, lying between the limits

$$1-\frac{3\,e^{-X_2}}{b_2X_1}>1-\epsilon>0.75\,. \tag{10}$$

Under chromospheric conditions, the numerator of the coefficient of $B_\nu(T_e)$ on the right of equation (8) is always considerably less than unity. Thus we may neglect the infinitesimal departure from unity of the denominator in this term.

We see, then, that equation (8) has a certain formal resemblance to equation (2). The first member on the right represents the contribution to S_ν from $\langle I_\nu\rangle$; the second member represents the effect of inelastic collisions and thus the contribution of $B_\nu(T_e)$. In thermodynamic equilibrium, $b_n=1$, and the second member on the right of equation (8) vanishes. This second member depends only on the local conditions, while the first member represents the effect of the "visible environment." Thus the second term represents a local source or sink, being positive or negative as $b_n \gtrless b_{n+k}$, i.e., as $T_e \gtrless T_r$. With these results, we proceed to discuss the formation of Lyman-α.

(iii) *The formation of Lyman-α.*—We base the following discussion on equation (8). Clearly, in order to carry through a rigorous treatment of the expected form of Lyman-α, we must start with some definite chromospheric model and carry through a solution of the transfer equation, with proper boundary conditions, using equation (8) as the source function. Here, however, we are not so interested in the prediction from a particular chromospheric model as in asking what range of models is compatible with the Lyman-α rocket data.

Equation (8) makes clear the difficulty in the superficial procedure of explicitly identifying either $F_\nu(0)$ or $I_\nu(0)$ with $S_\nu(\tau_\nu \sim 1)$, then implicitly identifying S_ν with $B_\nu(T_e)$, to draw a conclusion on T_e at $\tau_\nu \sim 1$. The second member of equation (8), if it predominates, gives an S_ν much different from $B_\nu(T_e)$. If the first member predominates, we must investigate carefully the relation between $\langle I_\nu \rangle$ and $B_\nu(T_e)$.

Consider, then, the physical processes involved in the formation of an emission line in Lyman-α. Begin the consideration in the photosphere, somewhere below τ_ν(continuum) ~ 1. In this region we have a very close approach to thermodynamic equilibrium. The $b_n = 1$, and the coefficient of $B_\nu(T_e)$ in equation (8) vanishes. As we move up in the atmosphere, T_e decreases to T_0, the upper boundary temperature of the photosphere; $T_e \leq T_r$; and $b_n \leq 1$. The coefficient of $B_\nu(T_e)$ in equation (8) becomes negative or remains zero, and S_ν is constant or decreases. Since, at the point $\tau_\nu = t$,

$$\langle I_\nu \rangle (t) = \frac{1}{2}\left[\int_{-1}^{0} d\mu \int_{t}^{0} e^{-(\tau_\nu - t)/\mu} S_\nu \frac{d\tau_\nu}{\mu} + \int_{0}^{1} d\mu \int_{t}^{\infty} e^{-(\tau_\nu - t)/\mu} S_\nu \frac{d\tau_\nu}{\mu}\right], \qquad (11)$$

$\langle I_\nu \rangle$ decreases with S_ν; $\langle I_r \rangle$ approaches $B_\nu(T_0)$ but does not reach it; for in the case that $T_r \geq T_e$, $b_n \leq 1$ and $T_{ex} \geq T_e$. Now, when the mechanical source of energy which heats the chromosphere begins to provide a non-negligible source of energy per gram of chromospheric material, T_e starts to rise. The coefficient of $B_\nu(T_e)$ in equation (8) becomes positive, and S_ν increases. The question in the initial drop and later rise of S_ν and $\langle I_\nu \rangle$ is the size of the rise. Now, if the atmosphere has such a high local opacity that S_ν does not change appreciably over the region $|\tau_\nu - t| \underset{\sim}{<} 1$, then from equation (11), $\langle I_\nu \rangle \sim S_\nu$. Because of our discussion in §ii, we can write equation (8) in the form

$$S_\nu = B_\nu(T_{ex}) = \langle I_{\nu 0} \rangle \frac{W_{\nu 0}}{1+\epsilon} + \eta B_\nu(T_e), \qquad (12)$$

where ϵ is very small, $W_{\nu 0} \leq 1$, and $\eta < 1$, with their values given in §ii. Equation (12) and the result, $\langle I_{\nu 0} \rangle = S_\nu$, require

$$B_\nu(T_{ex}) = S_\nu = \langle I_{\nu 0} \rangle = B_\nu(T_e)\,\eta\,[1 - W(1-\epsilon)]^{-1}. \qquad (13)$$

From the manner of its derivation, this result represents an *upper limit* on S_ν. For other regions of the atmosphere, particularly those near $\tau_\nu \sim 1$, in which we are interested, we must compute S_ν in detail. We note two points which may at first sight cause concern. First, we have observed that η vanishes for thermodynamic equilibrium; so S_ν would appear to vanish in equation (13). However, in this situation $W = 1$, since there is no line and equation (8) shows $\epsilon = 0$. Also, if $T_r > T_e$, $b_n < 1$, and the signs in equation (13) are correct. We are, of course, interested here in the case $b_n > 1$. Second, if we have a rectangular line profile, wide relative to the Doppler core, $W \sim 1$, and it would appear from equation (13) that we would obtain a large increase in $B_\nu(T_{ex})$. We note, however, that our present interest lies in the emergent radiation, i.e., in $B_\nu(T_{ex})$ for those regions near $\tau_\nu \sim 1$. In this case, one readily shows that equation (11), with $t \sim 1$, leads to

$\langle I_\nu \rangle \sim S(t)[1 - a]$ rather than the value $\langle I_\nu \rangle \sim S(t)$ used in obtaining equation (13). And the factor $W[1 - a]$ rather than W enters equation (13). Here a has the value 0.15 at $t = 1$ for an atmosphere with constant S, and a larger value if S increases outward. Thus our uncertainty as to the precise value of W is not critical in evaluating $B_\nu(T_{ex})$ from equation (13).

In Table 1 we present T_{ex} computed from equation (14), which is equation (13) with $W = 2^{-1/2}$, $\epsilon = 0$, $(1 - b_2/b_1) = 1$, and using only the term for $n = 2$ in the numerator of η, since this term predominates by far. We have chosen a range of values for n_e and T_e which would appear to span the range of conditions under which Lyman-α is at all likely to be formed in the chromosphere, viz., $10^{11} < n_e < 10^9$; $5000° < T_e < 10^6$ ° K:

$$\exp\left(\frac{h\nu_{12}}{kT_{ex}}\right) = \frac{2.85 \times 10^{20}}{n_e T_e^{1/2}} \frac{1 - 2^{-1/2}}{6\,(1 + X_{1n})} \exp\left(\frac{h\nu_{12}}{kT_e}\right). \tag{14}$$

TABLE 1

T_{ex} FOR THE UPPER LIMIT ON SOURCE FUNCTION FOR LYMAN-α AND $n_1/n_e b_2$

n_e	T_e (° K)						
	5000	10^4	2×10^4	3×10^4	4.5×10^4	10^5	10^6
10^{11}	3400	5050	6650	7400	8000	8800	9900
10^{10}	3200	4600	5900	6450	6900	7500	8350
10^9	3000	4200	5250	5750	6100	6550	7150
$n_1/n_e b_2$....	4×10^8	30	5×10^{-3}	2.5×10^{-4}	2.5×10^{-5}	1.2×10^{-6}	6×10^{-9}

We wish here to reiterate the assumptions underlying equation (14) and Table 1 and to make very explicit the conditions under which conclusions may be drawn from them. In our discussion of the value of W, we emphasized that we are interested in the regions where $\tau_\nu \sim 1$ and that here the precise value of W is not too critical. If we go much deeper into the atmosphere, $\tau_\nu \gg 1$, then W may change very much from the assumed value, and T_{ex} computed from equation (14) may differ considerably from its correct value. Thus the results for the lowest values of T_e in Table 2 are useful only if we discuss a chromospheric model where $\tau_\nu \sim 1$ in chromospheric regions where T_e has such a low value. In the actual situation it would seem that $\tau_\nu \gg 1$ in these regions of low T_e, so the values of T_{ex} at these low T_e values do not mean much. In earlier work (Thomas 1952; Athay and Thomas 1956*b*) we have considered a limiting situation for $\tau_\nu \gg 1$.

To provide a basis for estimating the conditions under which we might expect the entries in Table 1 to correspond to $10^{13} < N_1(h) < 10^{18}$, we use equations (8) and (14), together with the non-equilibrium form of the Boltzmann-Saha equation:

$$n_n = 4 \times 10^{16} n_e^2 T_e^{-3/2} e^{X_1} \frac{\varpi_n}{2} b_n \tag{15}$$

to tabulate $n_1/n_e b_2$ in the last line of Table 1.

We have mentioned that equation (14) represents an upper limit for S_ν. We have also noted that equation (8) presents a formal resemblance to Giovanelli's equation (3), provided that we deal only with the frequency at the line center. We can therefore use Giovanelli's (1949) solution for the transfer problem to ask more precisely what value for S_ν we might infer observationally *at the line center*. As illustration, we adopt his approximation of an isothermal atmosphere. We make the formal identification, from Giovanelli's notation to ours, comparing equations (3) and (12):

$$1-\lambda \rightarrow W_{\nu 0} \qquad \text{and} \qquad \frac{\epsilon}{\alpha} \rightarrow \eta B_\nu (T_e)\ .$$

We note that $\eta \propto n_e$ and is not constant even for T_e = Constant. However, for constant T_e, $n_e \propto n_1 \propto \tau_\nu$, so that η and hence ϵ/α are linear in τ_ν, and the result is unchanged. Giovanelli's result gives, for $\langle I_\nu \rangle$ at the top of a chromosphere of optical thickness τ_1 at the line center,

$$\langle I_{\nu 0} \rangle = \frac{2}{\sqrt{3}} \frac{\epsilon}{\alpha \sqrt{\lambda}} \left[\frac{1-\exp(-2\tau_1 \sqrt{3\lambda})}{(1+\frac{2}{3}\sqrt{3\lambda})+(1-\frac{2}{3}\sqrt{3\lambda}) \exp(-2\tau_1 \sqrt{3\lambda})} \right], \tag{16}$$

which, in our notation. gives

$$\langle I_\nu \rangle \leq \frac{2}{\sqrt{3}} (1-W)^{-1/2} \eta B_\nu (T_e) \tag{17}$$

instead of the expression in equation (13). The result will decrease the values of T_{ex} in Table 1 by a few hundred degrees, which is not significant for our present purposes because the size of the effect is comparable with that introduced by our uncertainty in the value of W.

We regard Table 1 as a fair representation of the behavior of S_ν in the chromosphere, with the uncertainty being that corresponding to a factor of 2 or 3 change in $B_\nu(T_{ex})$. The present rocket data hardly warrant greater accuracy. It would appear evident from Table 1 that the rocket data do not place much restriction on a chromospheric model; only the entries for $T_e > 3 \times 10^4$ at $n_e \gtrsim 10^{11}$ would seem excluded by the presently existing data. Given a profile of Lyman-α, we can, of course, narrow the range considerably.

To apply the values of $n_1/(n_e b_2)$ in Table 1 to obtain $N_1(h)$, we need a value for b_2. In the region where $\tau_\nu < 1$ over most of Lyman-α, $b_2 \sim 10$, essentially independent of n_e and slowly varying with T_e (Thomas 1948). For $\tau_\nu \gg 1$ in Lyman-α, b_2 increases (Thomas 1949). Finally, to compute N_1 from n_1, we require an estimate for the scale height of n_1. While we cannot obtain a precise estimate of this scale height without going to a particular model, our discussion (Athay and Thomas 1956*b*) from stability considerations, on the general form of $T_e(h)$ for an arbitrary chromospheric model, serves as a partial guide.

We have shown that $T_e(h)$ behaves roughly as a step function, with the plateau part of each step corresponding to a region in which a particular atom is the dominant source of radiative dissipation for the mechanical energy heating the chromosphere and the steep rise between steps corresponding to the change from one source to another. Roughly, the region up to $T_e \sim 7000°$–$11000°$ finds hydrogen as the dissipative source, the hydrogen plateau; we expect an abrupt rise at these values of T_e up to $\sim 20000°$; a smooth rise up to $T_e \sim 25000°$–$45000°$, the helium plateau, where helium provides the dissipative source; and an abrupt rise to $T_e \sim 10^5$, where we are not certain whether free-free emission or emission from the highly ionized metals becomes predominant. Thus we cannot have a large scale height in the ranges $10^4 \lesssim T_e \lesssim 2 \times 10^4$ and $4.5 \times 10^4 \lesssim T_e \lesssim 10^5$; for the ranges of T_e lying on the plateaus, the scale height is fixed by the rate of mechanical-energy input and cannot be a priori specified.

With this information on scale height, $b_2 \gtrsim 10$, and $10^{11} > n_e > 10^{10}$, we see from Table 1 that any scale height $\gtrsim 1$ km gives $N_1(h) \gtrsim 10^{13}$ for $T_e \leq 3 \times 10^4$ and places the region of formation of the center of Lyman-α in the helium plateau. Further, if we taken $n_e \gtrsim 10^9$ and a 1000-km scale height, $N_1(h) > 10^{13}$ moves to the upper boundary of the helium plateau. Thus we conclude that the region producing the Doppler core of Lyman-**α**, 10^{13}–$10^{14} \lesssim N_1(h) < 10^{17}$–$10^{18}$, lies essentially entirely on the helium plateau, $2 \times 10^4 \lesssim T_e < 4.5 \times 10^4$, with the possibility that the center of Lyman-**α** may have some contribution from the region $T_e \sim 10^5$ ° K. If, for example, we place the center of the core at the top of the helium plateau and the edge at the bottom, we obtain a line that completely satisfies the rocket data.

For illustration only, and primarily to introduce a height scale, we may apply the preceding results to our empirical non-uniform model (Athay and Menzel 1956), composed of spciular and interspicular material. The spicular and interspicular material shows the step structure in T_e, but at different heights. Labeling by a, b, c, and d, respectively, the end of the hydrogen plateau, the beginning and end of the helium plateau, and the beginning of the highly ionized metal plateau, we represent the model schematically in Table 2. Clearly, the model satisfies the existing rocket data and places the region of formation of Lyman-**α** in the helium plateau.

TABLE 2

SCHEMATIC MODEL OF A TWO-COMPONENT CHROMOSPHERE AS APPLIED TO LYMAN-**α** EMISSION

	b	c	d	e
h(Km) spicule/interspicule	$\sim$4000 $\sim$1000	$\sim$4000 $\sim$1000	$\sim$12000 $\sim$4000	$\sim$12000 $\sim$4000
T_e	7000°–11000°	16000°–25000°	25000°–45000°	$>10^5$
n_e	5×10^{10}	5×10^{10}	10^{10}	$\sim10^9$
T_{ex}	4100°–5000°	5900°–6800°	6200°–6900°	>6600°
n_1	2×10^{16}–3×10^{12}	2×10^{10}–4×10^8	1×10^8–2×10^6	$<1\times10^4$
Scale height (cm)	10^6	10^8	10^6	$\sim10^9$
$N_1(h)$	2×10^{22}–3×10^{18}	2×10^{11}–4×10^{16}	1×10^{14}–2×10^{12}	$<1\times10^{13}$
T_{ion}	4300°–5400°	6400°–7400°	...	...

As a quick corollary to this computation of T_{ex} for Lyman-**α**, we may make the same sort of computation for the Lyman continuum. In an earlier criticism (Thomas 1952) of Woolley and Allen's (1950) use of $B_\nu(T_e)$ as the source function for the Lyman continuum, we pointed out that one should use, instead,

$$B_\nu(T_{\text{ion}}) = \frac{2h\nu^3}{c^2}\left[b_1 e^{h\nu/kT_e} - 1\right]^{-1} = \frac{2h\nu^3}{c^2}\left[2.5\times10^{15} n_1 T_e^{3/2} n_e^{-2} - 1\right]^{-1} \tag{18}$$

for the emission at the head of the Lyman continuum. For greater frequency, the emission decreases as $\exp[-(\nu - \nu_1)h/kT_e]$ times the expression in equation (18). Using corresponding values of n_e, T_e, and n_1 from the model in Table 2 and equation (18), we compute T_{ion} and tabulate it in the last row of Table 2. We note that the bound-free atomic absorption coefficient at ν_1 is 0.8×10^{-17}, so that only regions b and c have particular interest. Thus the emission from this model differs considerably from $B_\nu(T_e)$ and does not stand in any essential disagreement with inferences on emission in the Lyman continuum from ionospheric data. Again, we note that the calculation based on this particular model is for illustrative purposes only; the results are intended to show the generality of type of models giving the right range of results on $I_\nu(0)$ rather than to substantiate a particular model.

b) Lyman-α at the Solar Limb

In the preceding section we demonstrated that a range of chromospheric models would satisfy the presently existing Lyman-α rocket data. Thus any additional data which give information on $N_1(h)$ serve to restrict the range of possible models. Some observations on the correlation between the height of limb flares and the occurrence of SID's by C. S. Warwick (1955) provide indirect data. Mrs. Warwick's analysis of 39 limb flares shows that the great majority of those occurring above heights ~15000 km have associated SID's, while those below ~12000 km have essentially no associated SID's. She interprets these results as implying that Lyman-α is the SID-producing agent and thus that the "effective" optical depth for Lyman-α, in a tangential direction, reaches ~1 between 12000 and 15000 km. Let us estimate what this would mean in a model.

TABLE 3

NUMBER OF GROUND-STATE ATOMS IN LINE OF SIGHT AT ~10000 KM

T_e	2×10^4	4.5×10^4	10^5	3×10^5	10^6
N_1 (radial)	1×10^{17}	7×10^{14}	3×10^{13}	2×10^{12}	2×10^{11}
N_1 (tangential)	3×10^{18}	1×10^{16}	7.5×10^{14}	4×10^{13}	3×10^{12}

The average electron density along the tangential line of sight is well specified for the chromosphere in 1952 (Athay, Menzel, Pecker, and Thomas 1955), with the following values: $\bar{n}_e(6000\text{ km}) \sim 10^{9.9}$; $\bar{n}_e(10^4\text{ km}) \sim 10^{9.4}$; $\bar{n}_e(2\times10^4\text{ km}) \sim 10^{8.9}$. Mrs. Warwick's data cover the period 1951–1953, so the 1952 chromosphere should be fairly representative of the epoch. For a spherically symmetric chromosphere with $b_2 = 10$, a scale height of 10^9 cm, and $n_e = 10^{9.4}$, we obtain the values of N_1 in Table 3. Unless we are actually in a region of steep gradient in T_e, $H(n_1)$ is essentially the scale height of the electron density. In this case, $H(n_1) \sim 10^9$ cm, and the values of N_1 are as given in Table 3. If there is a steep gradient in T_e, H_1 might possibly drop to as low as 10^6 cm, and the values in the third row drop by a factor of 30.

In either event, the SID versus limb-flare results are incompatible with a spherically symmetric chromosphere having, near 10000 km height, either of the cases $4.5\times10^4 \gtrsim T_e \gtrsim 3\times10^5$. If we have a temperature plateau near $T_e = 1\times10^5$, we can produce the limb-flare results. If, on the other hand, we turn to a two-component model of the chromosphere, we might expect n_1 and, to a lesser extent, n_e to be higher in the spicules than in the surrounding medium, since we believe the spicules to be the colder. Spicule statistics show that a large majority of the spicules observed in Hα attain maximum heights in the range 10000–15000 km (Roberts and Rush 1954; Lippincott 1955). Since the apparent height for $\tau \sim 1$, as inferred from Mrs. Warwick's data, lies within this range of maximum spicule heights, it is tempting to ascribe the Lyman-α opacity mainly to the spicules. We note from Table 3, the second line, that for a single spicule, 1000 km thick, and $n_e \sim 10^{10}$, we obtain $\tau \gg 1$ anywhere on the helium plateau. Thus, so long as one spicule covers the flare, we might expect Mrs. Warwick's result. Unfortunately, one spicule *as seen in Hα* is much smaller than the apparent area of a flare, so we require a number of spicules side by side to produce the desired effect. Thus we must consider the spicule statistics in more detail before making a decision on the relative contribution of spicule and atmosphere to the Lyman-α opacity. We defer further discussion to the following paper, where we consider these spicule statistics relative to the observations of the early Balmer lines.

We are indebted to Dr. J. W. Warwick for extended discussions with us on this paper.

REFERENCES

Athay, R. G., and Menzel, D. H. 1956, *Ap. J.*, **123,** 285.

Athay, R. G., Menzel, D. H., Pecker, J. C., and Thomas, R. N. 1955, *Ap. J. Suppl.*, **1,** 505.

Athay, R. G., and Thomas, R. N. 1955, *Ap. J. Suppl.*, **1,** 491.

———. 1956*a*, *Ap. J.*, **123,** 299.

———. 1956*b*, *ibid.*, p. 309.

Böhm-Vitense, E. 1954, *Zs. f. Ap.*, **34,** 209.

Byram, E. T., Chubb, T., Friedman, H., and Gailar, N. 1953, *Phys. Rev.*, **91,** 1278.

Giovanelli, R. G. 1948, *Australian J. Sci.*, **1,** 275, 289, 305, 360.

———. 1949, *M.N.*, **109,** 298.

Goldberg, L. 1954, *Ap. J.*, **120,** 185.

Harris, D. L. 1948, *Ap. J.*, **108,** 112.

Jager, C. de. 1952, *Rech. Astr. Obs. Utrecht*, Vol. **13,** Part I.

———. 1956, in press.

Jefferies, J. T. 1953, *Australian J. Phys.*, **6,** 22.

Jefferies, J. T., and Giovanelli, R. G. 1954, *Australian J. Phys.*, **7,** 574.

Johnson, F. S., Malitson, H. H., Purcell, J. D., and Tousey, R. 1955, *A.J.*, **60,** 165.

Lippincott, S. 1955, paper read at meeting of American Astronomical Society at Troy, N.Y., *Pub. Smithsonian Ap. Obs.*, in press.

Matsushima, S. 1955, *Ap. J. Suppl.*, **1,** 479.

Milne, E. A. 1930, *Hdb. d. Ap.* (Berlin: Julius Springer), Vol. **3,** chap. ii.

Pietenpol, W. B., Rense, W. A., Walz, F. C., Stacey, D. S., and Jackson, J. M. 1953, *Phys. Rev.*, **90,** 156.

Roberts, W. O., and Rush, J. Q. 1954, *Australian J. Phys.*, **7,** 230.

Thomas, R. N. 1948, *Ap. J.*, **108,** 142.

———. 1949, *ibid.*, **109,** 480.

———. 1950, *ibid.*, **111,** 165.

———. 1952, *ibid.*, **115,** 550.

Tousey, R., Watanabe, K., and Purcell, J. D. 1951, *Phys. Rev.*, **83,** 792.

Warwick, C. S. 1955, *Ap. J.*, **121,** 385.

Warwick, J. W. 1955, *Ap. J.*, **121,** 190.

Woolley, R. v. d. R., and Allen, C. W. 1950, *M.N.*, **110,** 358.

MOTIONS OF PROMINENCES

Malcolm Correll, Martha Hazen, and John Bahng
Department of Physics, DePauw University, Greencastle, Indiana; University of Michigan Observatory, Ann Arbor, Michigan; Washburn Observatory, University of Wisconsin Madison, Wisconsin

Received March 2, 1956; revised June 6, 1956

ABSTRACT

The trajectories of luminous materials in active-region prominences frequently display patterns which are suggestive of the line-of-force configurations around a magnetic dipole. An attempt was made to fit an idealized field to an actual prominence, and a reasonably good correspondence between lines and trajectories was obtained. The results suggest that the dipole in this case is located at 0.2 solar radius beneath the surface of the sun.

I. INTRODUCTION

One of the most conspicuous features of active-region prominences is the movement of luminous materials as it is recorded by lapsed-time motion pictures with narrow-band filters or spectroheliographs, which are centered usually on Hα. The trajectories of these luminous materials have been considerably investigated. Accelerations, velocities, and paths have been determined in many instances. When the trajectories of prominence materials are recorded in this manner, they are, of course, seen in projection against the plane of the sky. Under these circumstances, it is frequently observed that several paths seem to converge upon, or diverge from, the same highly localized region near the limb of the sun. The similarity of such patterns to those of flux lines near magnetic poles has been pointed out by several investigators (e.g., Chapman 1943).

The gaseous matter of which prominences are constituted is in a highly ionized condition. The net charge density must be nearly zero (Alfvén 1950*a*). It is easily seen qualitatively that a plasma such as this will tend to migrate along any magnetic flux lines which thread through it; for when a gaseous ion moves within a magnetic field, the trajectory most generally is a helix which has a flux line for its axis. Positive and negative ions in the plasma will spiral in opposite senses as they advance along the lines. Electrostatic forces, however, will prevent any considerable separation of positives from negatives by this process. From a distance, only the gross motion of the cloud is apparent, and theory thus suggests that the shape of the local magnetic field and that of the prominence trajectory pattern are very closely related (Cowling 1953). It may be more rigorously shown from hydromagnetic theory that a body of plasma will migrate along lines of force which thread through it (Elsasser 1955).

The effects of perturbing forces on the mass motion of ionized gases may, in general, be ignored. Because of the conductivity of the medium, no appreciable electrostatic field can exist. And a gravitational field or a magnetic gradient normal to the magnetic field will cause opposite drifts of positive and negative ions whose resulting electrostatic fields will soon buck out the drift.

The problem of the present paper is to see to what degree well-defined prominence trajectories can be made to fit idealized magnetic-field patterns.

II. PROCEDURE

a) *The Composite Prominence Trajectory Diagram*

In order to prepare a suitable composite prominence-trajectory diagram, it is necessary that an extended, relatively uninterrupted sequence of lapsed-time motion pictures of a fairly active prominence be available. High Altitude Observatory film No. 309AB, taken February 26, 1946, provides such data. The prominence occurred at a heliographic position angle of about 65°. The photography proceeded almost without interruption from 21:44 to 24:30 U.T., with an exposure rate of three frames per minute. This film was projected onto a sheet of white paper at normal cinematographic speeds, in a projector specially built at the Observatory for this purpose. The motions of prominence knots and streamers were then traced directly on the paper. By repeated projections of the film onto the same paper, we obtained a composite trajectory diagram for all the major movements of the prominence.

This particular film is of great interest, since a large sunspot group was coming over the limb of the sun on this day. The heliographic position angle of the limb passage of the group was 65°. An additional reason for our initial interest in this film was the existence of High Altitude Observatory films Nos. 308 and 310 for February 24 and 26, 1946. Film No. 310, however, was too brief to yield a good composite trajectory diagram. Film No. 308 will be mentioned later.

b) The Idealized Magnetic Field

We assumed, as has previously been mentioned (Roberts 1955), that the fields most likely to be encountered would be satisfactorily represented by dipole formulae. The equation for a line of force from a dipole is well known and in a spherical co-ordinate system is

$$R = k \cos^2 \phi , \quad \lambda = \text{Const.}, \tag{1}$$

where k is a constant parameter for any given flux line and is the distance from the origin to the point where the line intersects the equatorial plane; ϕ is the latitudinal angle measured from the equatorial plane; λ is a longitudinal angle and is constant for any given flux line; and R is the radial distance from the origin to a point on a flux line of given k. It is assumed, of course, that the dipole is at the origin and is oriented normal to the equatorial plane (Alfvén 1950*b*).

If equation (1) be plotted for an arbitrarily selected k and for $\lambda = 0, \pm 15°, \pm 30°, \pm 45°, \pm 60°, \pm 75°$, and $\pm 90°$, one obtains a three-dimensional plot, which, when it is projected onto the plane of the paper ($\lambda = 0$), appears as in Figure 1.

A local solar dipole will not generally be oriented so that the equatorial plane $\phi = 0$ is parallel to our line of sight. Hence, most often, Figure 1 will need to be rotated about the x-axis so that the z-axis is tilted into or out of the paper. When three-dimensional families of curves of given k for a tilted dipole are projected onto the plane of the paper, the flux lines for $\lambda = \pm 15°, \pm 30°$, etc., are no longer coincident. Figure 2 shows all octants of such a family as they appear in projection.

For this study we prepared prototypes of Figure 2 for several different tilts of the dipole. We then made positive photographic transparencies of these field patterns, and, by means of an enlarger, we could produce images of different sizes corresponding to different values of the parameter k of equation (1). We projected such images onto the composite prominence-trajectory diagrams, in order to see whether a good correspondence between flux lines and prominence trajectories could be found.

In practice, one selects a certain transparency, which, of course, corresponds to a certain tilt of the dipole. Then, by trial and error, one attempts to find an orientation and position of the field pattern such that, ***by enlargement or reduction of the image alone***, one may make the field lines coincide with the prominence trajectories.

III. RESULTS

Figure 3 shows the fit of a dipole field of zero tilt, with the prominence streamers near heliographic position angle 65° for February 26, 1946. The fit is good, and it is strikingly better than any that may be obtained with a dipole field tilted ±15° or ±30° from the plane of the paper.

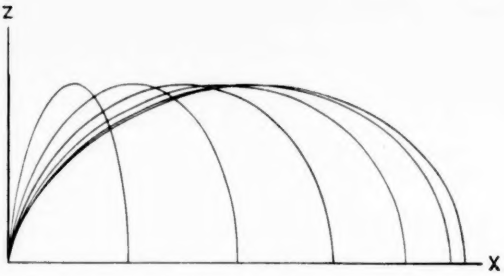

FIG. 1.—Projection, into the plane of the paper, of the dipole field lines $R = k \cos^2 \phi$, $\lambda = 0°, 15°, 30°, 45°, 60°, 75°$, and $90°$, as plotted in the first octant.

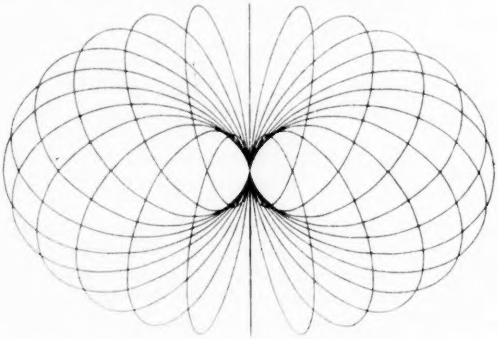

FIG. 2.—Projection, into the plane of the paper, of the field lines $R = k \cos^2 \phi$, $\lambda = n15°$ $(n = 1, 2, \ldots, 12)$ for a dipole tilted 30° toward or away from the observer.

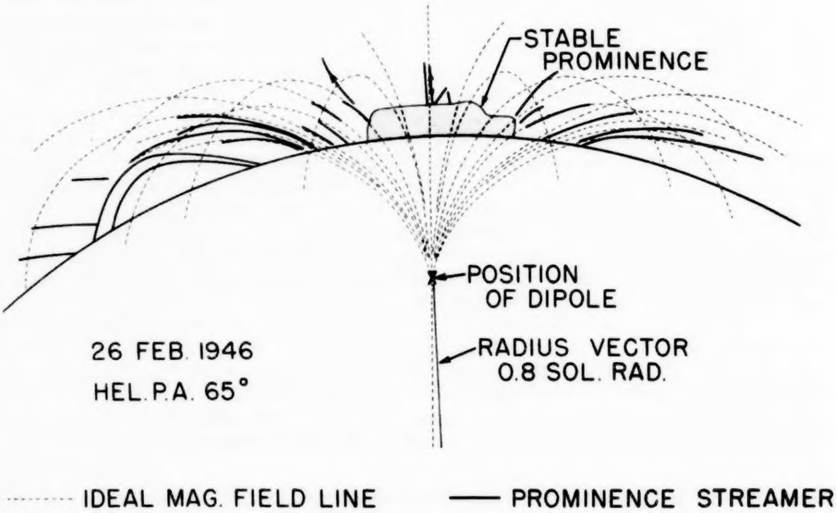
STABLE PROMINENCE
POSITION OF DIPOLE
RADIUS VECTOR 0.8 SOL. RAD.
26 FEB. 1946
HEL. P.A. 65°
IDEAL MAG. FIELD LINE
PROMINENCE STREAMER

FIG. 3.—Superposition of a dipole field pattern (0°—tilt) on prominence streamers

Probably the most significant observation to be made is that this dipole appears to be located about 0.2 solar radius below the surface of the sun. Since the phenomenon is viewed only as projected upon the plane of the sky, the dipole may be closer to the surface of the sun but somewhat before or behind the plane of the sun's limb, so far as the fitting process is concerned. There is good reason, however, from the prominence film No. 308 for February 24, 1946, to believe that in this case the dipole is essentially in the plane of the limb.

Film No. 308 was also taken at a heliographic position angle of 65°. At this heliographic latitude, 25° N., the sun rotates just slightly less than 14° per day. Hence the prominence that was photographed at the limb on the twenty-sixth would be from 28° to 30° behind the limb on the twenty-fourth. The film sequence of No. 308 was unusually good and yielded an excellent composite trajectory diagram. Unlike the diagram for film No. 309B, this one is not simple, and no single dipole pattern fits most of the major streamers. If, however, it is assumed that the dipole depicted in Figure 3 has approximately maintained its depth and its orientation with respect to the sun's radius, one finds that a dipole-field pattern tilted back 30° fits many of the streamers very nicely. It may then be assumed that the other streamers bear little relation to the field of this dipole and are perhaps accidentally associated with other prominences that are already in front of the plane of the limb. It seems reasonable to conclude, then, that there are trajectories that fit the field of a relatively stable dipole 0.2 radius below the surface of the sun. A more thorough study of film No. 308 is being undertaken, and discussion of this will be published later.

We recognize, of course, that there is a double infinity of flux lines around a dipole. Since field patterns have thus far been prepared for the longitude angles λ having increments of 15°, those streamers following lines lying in other longitude planes are not well fitted by any of the lines of the pattern. Moreover, the depth, orientation, and choice of tilt of the dipole are all dependent upon the judgment of the investigator, as is the projected size of the field pattern. Hence any fit is somewhat subjective. However, independent attempts by different observers to find a good fit agreed sufficiently well that this result may be regarded with confidence.

Undoubtedly, a knowledge of line-of-sight components of prominence-streamer motions should aid considerably in finding a proper fit and should appreciably reduce the subjective aspects of the method. Prominence records currently being obtained at other observatories can provide such data. We hope soon to examine such films and to compare their analyses with the present work.

The main portion of this study was carried on at the High Altitude Observatory during a stay made possible by a grant from the National Science Foundation, which is hereby gratefully acknowledged. Additional assistance was provided by the Geophysics Research Directorate, Air Force Cambridge Research Center, under High Altitude Observatory Contract AF 19(604)-969. The authors wish to thank Dr. W. O. Roberts, who suggested the problem and assisted in its analysis. We also thank the other members of the High Altitude Observatory staff, who generously made available their facilities, data, and advice for the conduct of the work.

REFERENCES

Alfvén, H. 1950*a*, *Cosmical Electrodynamics* (Oxford: Clarendon Press), p. 11.

———. 1950*b*, *ibid.*, p. 4.

Chapman, S. 1943, *M.N.*, **103,** 117.

Cowling, T. G. 1953, *The Solar System*, Vol. **1**: *The Sun*, ed. G. P. Kuiper (Chicago: University of Chicago Press), p. 535.

Elsasser, W. M. 1955, *Am. J. Phys.*, **23,** p. 590.

Roberts, W. O. 1955, *Proceedings of the Jodrell Bank Symposium on Radio Astronomy, August, 1955*, ed. H. C. van de Hulst.

SYNCHROTRON RADIATION IN THE SUN'S RADIO SPECTRUM*

U. E. KRUSE, L. MARSHALL, AND J. R. PLATT
Enrico Fermi Institute for Nuclear Studies, and Department of Physics, University of Chicago

Received October 2, 1956

ABSTRACT

It is suggested that synchrotron radiation by non-relativistic electrons in sunspots makes an important contribution to the sun's radio spectrum. In particular, those outbursts displaying simultaneous emission of two radio-frequency components, one at twice the frequency of the other, can be explained by the properties of synchrotron radiation from electrons moving in large magnetic fields. Assuming this mechanism, it is found that the velocity of the emitting electrons relative to the velocity of light lies between the limits $0.002 \leq \beta \leq 0.2$.

A significant part of the radio emission of the sun, correlated with large sunspots, consists of several double-frequency broadcasts reported by Wild, Murray, and Rowe (1953) and by Wild, Roberts, and Murray (1954), in which two frequencies differing by a factor of almost exactly 2 are emitted simultaneously.

In the present paper we propose that emission of synchrotron radiation by electrons traveling outward from sunspots is able to account for the magnitude and frequency doubling of these broadcasts. Previously, synchrotron radiation as a mechanism of the sun's radio emission has been briefly considered and dismissed (see, for example, Wild, Murray, and Rowe 1954) for the reason that it was apparently unable to escape from the sun's atmosphere. It was argued that synchrotron radiation was produced only in the so-called extraordinary mode, which, in order to leave the sun, had to pass through a region where the index of refraction was largely imaginary, a so-called stop band, and therefore where such radiation would be effectively absorbed.

We argue, instead, that, in general, synchrotron radiation propagates simultaneously in both the ordinary and the extraordinary mode. If frequency ω is produced in a region where the plasma frequency satisfies $\omega_0/\omega < 1$, that part of the synchrotron radiation propagating in the extraordinary mode in coming out from the sun encounters a stop band, but that part of synchrotron radiation propagating in the ordinary mode comes out without encountering a stop band.

To make this argument, we refer to Figures 36 and 39 in *Radio Astronomy* by Pawsey and Smerd (1955). In Figure 36 it is shown that the polarizations of both the ordinary and the extraordinary modes of propagation of frequency ω depend sensitively on the quantity ω_0/ω, which is a function of the medium. But the polarization of synchrotron radiation emitted by an electron depends only on the velocity of the electron and its orientation to the magnetic field. Then the polarization of the synchrotron radiation is independent of the surrounding medium, but the manner in which it propagates depends on the medium. It follows from this argument that the polarization of the emitted radiation can be expressed as a linear combination of the polarization of the extraordinary and ordinary modes of propagation for the appropriate value of ω_0/ω and ω_H/ω and that synchrotron radiation, in general, therefore propagates in both modes.

One sees from Figure 39 that, if $\omega_0/\omega < 1$, radiation in both modes of propagation can escape the sun only by traveling through regions of strong absorption. If, however, $\omega_0/\omega > 1$, this is still true for the extraordinary mode, but the ordinary mode travels out through regions where n^2 is always greaters than zero. We conclude, therefore, that part of the synchrotron radiation can escape from the sun without traveling through the stop bands.

---

* Research supported by a joint program of the U.S. Office of Naval Research and the U.S. Atomic Energy Commission.

Synchrotron radiation from electrons is apparently a ubiquitous phenomenon in the universe. It was demonstrated by Kiepenheuer in 1950 that cosmic-ray electrons of about 100 Mev, emitting synchrotron radiation as they traveled in galactic magnetic fields of around 10^{-6} gauss, could provide a radio spectrum which amply accounted for the observed intensity and spectral shape of the non-thermal radio noise of the Milky Way galaxy. Likewise, synchrotron radiation from electrons has been shown to be important in the Crab Nebula. Here the analysis made by Oort and Walraven (1956) shows that magnetic fields of about 10^{-3} gauss and electron energies of 10^{11} ev are required to explain the broad continuous spectra emitted in both the radio and the visible regions in terms of synchrotron radiation.

To demonstrate the importance of synchrotron radiation by electrons traveling up out of sunspots, we wish to discuss the double-frequency radio outbursts in particular. For example, as described by Wild and his colleagues, whose equipment can receive a frequency range of from 240 to 40 Mc, the disturbance of November 21, 1952, consisted of two emission bands, each about 10 per cent wide, whose frequency decreased with time, keeping a frequency ratio of between 1.90 and 1.99 and having approximately equal intensities. A detailed correspondence between various parts of the two bands led the authors to identify the bands as a fundamental and its second harmonic. Because the frequence ratio of the two bands was slightly less than 2 and because the intensity of the fundamental increased with decreasing frequency, they concluded that the fundamental was heavily absorbed as it traveled out from the sun and that the harmonic was much less so. The third harmonic was not observed and, the authors say, must have been at least ten times weaker than the second. This outburst swept down through the sensitive frequency range of the equipment in 10 minutes. Other outbursts having similar time-frequency dependences have been observed sometimes to have a second harmonic and sometimes to have none.

We propose to explain the double-frequency feature in terms of emission of synchrotron radiation by jets of electrons spiraling up out of sunspots around the magnetic lines of force. Magnetic fields in large sunspots (with which radio outbursts are strongly correlated) may be as large as 5000 gauss. In a field, for example, of 50 gauss above a sunspot, the fundamental cyclotron frequency $\nu = \omega_H/2\pi = (1/2\pi)\, eH/mc$ is 150 Mc/s, corresponding to the approximate center of the frequency range under discussion. An electron jet spiraling out of a sunspot through progressively decreasing magnetic fields emits a spectrum consisting of lines which are harmonics of the fundamental frequency, and all components of the line spectrum decrease in frequency as the magnetic field decreases. If the electron velocity is small compared with that of light, the intensity of the third harmonic can be made small compared with that of the first and second harmonics, to correspond with the observed intensities. For $\beta \ll 1$, the power radiated into the nth harmonic has been given by Schwinger (1949) for an electron moving with constant speed in a circular path in a magnetic field as

$$P_n = 2\omega_0 \frac{e^2}{R} \beta^{2n+1} F(n) , \tag{1}$$

where $\beta = (1/c) \times$ velocity component perpendicular to H and where

$$F(n) = (n+1) \frac{n^{2n+1}}{(2n+1)!} , \tag{2}$$

and $R = cp/eH = \beta\gamma c/\omega_H =$ radius of curvature in the magnetic field. Consequently, the dependence of P_n on β is given by

$$P_n = 2\omega_H^2 \frac{e^2}{\gamma c} \beta^{2n} F(n) . \tag{3}$$

That part of expression (3) which varies with the harmonic number n and with β is tabulated in Table 1 for pertinent values of β. The quantity $\beta = 0.0018$ corresponds to electrons at 10^4 degrees, the temperature attributed to the corona above a sunspot. This we take to be the velocity of electrons in surrounding plasma, through which the synchrotron radiation passes to escape from the sun. Consequently, we assume that the probabilities of absorption of the various harmonics, as they pass through the surrounding plasma, are proportional to the corresponding numbers for $\beta = 0.0018$ in Table 1. Roughly, according to Table 1, if the absorption coefficient for the second harmonic is an amount α, the absorption coefficient of the fundamental is $10^5\ \alpha$, in agreement with the conclusion of Wild *et al.* (1953) that the fundamental is more heavily absorbed than the second harmonic.

TABLE 1

$\beta^{2n}F(n) = {}^{2n}(n+1)n^{2n+1}/(2n+1)!$ VERSUS β

n	$\beta=0.0018$	$\beta=0.018$	$\beta=0.1$	$\beta=0.2$	$\beta=0.5$	$\beta=1$
1	1.1×10^{-6}	1.1×10^{-4}	3×10^{-3}	1.3×10^{-2}	0.083	0.33
2	0.84×10^{-11}	0.84×10^{-7}	0.8×10^{-4}	1.3×10^{-3}	.050	0.80
3	0.52×10^{-16}	0.52×10^{-10}	0.15×10^{-5}	0.97×10^{-4}	0.024	1.52

The fact that no third harmonic has been observed sets an upper limit on β. Specifically, we require $P_2/P_3 \geq 10$, and we ignore possible complications which may be introduced by an absorption of surrounding plasma differing for the two harmonics. The quantities in Table 1 demonstrate that β cannot be much larger than 0.2 in order for this requirement to be met. A correction for differential absorption increases the ratio of P_2 to P_3 at emission and so decreases the upper limit for β.

Again, an upper limit for β may be found from consideration of the ratio of intensities of the fundamental and second harmonic. This ratio is

$$\frac{P_1}{P_2} = \frac{0.33\beta^2}{0.8\beta^4}\,.$$

Wild and his colleagues have found this ratio to vary between $\frac{1}{2}$ and 10. Their data show a decrease in this ratio with increasing frequency, which they interpret as absorption of the fundamental. A possible explanation is that the ratio of fundamental to harmonic may be reduced by reabsorption of radiation into synchrotron motion by surrounding electrons. A second upper limit to β is determined from the largest ratio, namely,

$$10 \leq \frac{P_1}{P_2} \leq \frac{1}{2.4\beta^3}\,,$$

$$\beta \leq 0.2\,.$$

A lower limit for β is given, of course, by the temperature of the electrons in the corona above a sunspot, namely, 10^4 degrees (cf. Kiepenheuer 1953) corresponding to $\beta = 0.0018$. The experimental intensities of about 10^{-19} watt/meter^2 per unit frequency interval at 100 Mc can be accounted for on the synchrotron hypothesis. From formula (1) the radiation intensity is found to be $2 \times 10^{-12}\ \beta^2$ photons/cm of path per unit frequency interval per particle. The radio intensity received on the earth is given by

$$c\beta \times \frac{1}{4\pi r^2} \times \begin{pmatrix}\text{volume}\\ \text{of}\\ \text{electrons}\end{pmatrix} \times \begin{pmatrix}\text{density}\\ \text{of}\\ \text{electrons}\end{pmatrix} \times \begin{pmatrix}\text{energy}\\ \text{per}\\ \text{photon}\end{pmatrix} \times 2 \times 10^{-12}\beta^2\,,$$

where the distance from sun to earth, r, is 1.5×10^{11} meters. Assuming a volume of $(10^9\ \mathrm{cm})^3$ and an electron density of $10^9/\mathrm{cm}^3$ and converting to watts, one finds

$$\frac{3 \times 10^{10}}{25 \times 10^{22}} \times 10^{27} \times 10^{9} \times 6 \times 10^{-27} \times 10^{8} \times 2 \times 10^{-12} \beta^3 \times 10^{-7} ,$$

which is equal to $3 \times 10^{-14}\ \beta^3$ watt/meter^2 per unit frequency interval. For $\beta = 0.02$ the calculated intensity is 2×10^{-19} watt/meter^2 per unit frequency interval, in agreement with observation.

We are grateful for illuminating discussions with Nandor Balazs.

Postscript by L. Marshall.—I am grateful to J. A. Roberts for pointing out a mistake in a recent paper (*Ap. J.*, **124**, 469), in which it was incorrectly stated that Čerenkov radiation always travels in regions where $n^2 > 0$ on its way out from the sun's atmosphere. It is shown in Figure 39 of *Radio Astronomy* by Pawsey and Smerd (1955) that Čerenkov radiation, in traveling out from the sun, always encounters stop bands in which the index of refraction has a large imaginary component. But when its velocity vector is directed at a small angle to the magnetic field, Čerenkov radiation close to the plasma frequency can come out to the earth. This follows because for the ordinary mode of propagation, which is appropriate to Čerenkov radiation close to the plasma frequency, as the angle between photon momentum and direction of magnetic field approaches zero, the stop band becomes vanishingly narrow and propagation through the barrier becomes possible.

However, for the extraordinary mode, which applies to Čerenkov radiation at the cyclotron frequency, it appears that barrier penetration is more difficult. Probably most of the radiation energy emitted in this mode of propagation is reabsorbed in the stop-band regions and serves to heat the plasma.

REFERENCES

Kiepenheuer, K. O. 1950, *Phys. Rev.*, **79**, 738.
———. 1953, "Solar Activity" in *The Sun*, ed. G. P. Kuiper (Chicago: University of Chicago Press).
Marshall, L. 1956, *Ap. J.*, **124**, 469.
Oort, J. H., and Walraven, Th. 1956, *B.A.N.*, **12**, No. 462, 285.
Pawsey, J. L., and Smerd, S. F. 1955, *Radio Astronomy* (Oxford, England: Clarendon Press).
Schwinger, Julian. 1949, *Phys. Rev.*, **75**, 1912.
Sen, H. K. 1955, *Phys. Rev.*, **97**, 849.
Smerd, S. F. 1955, *Nature*, **175**, 297.
Wild, J. P. 1952, *Ap. J.*, **115**, 210.
Wild, J. P., Murray, J. D., and Rowe, W. C. 1953, *Nature*, **172**, 533.
———. 1954, *Australian J. Phys.*, **7**, 439.
Wild, J. P., Roberts, J. A., and Murray, J. D. 1954, *Nature*, **173**, 532.

INADEQUACY OF RECOMBINATION AS SOURCE OF RADIATION FROM METEORIC TRAINS*

ALLAN F. COOK AND GERALD S. HAWKINS
Harvard College Observatory, Cambridge, Massachusetts

Received April 28, 1956; revised June 25, 1956

ABSTRACT

The assumption is made that recombination of ions and free electrons produces the observed luminosity in meteoric trains. Available theoretical and observational results are used to establish an upper limit on the intensity of radiation from this source. This limit is compared with the threshold intensity at the observed epoch of disappearance of the train. Recombination is shown to fail, by at least two or three orders of magnitude, to account for the observed intensity.

I. INTRODUCTION

It is well known that a meteor in its passage through the atmosphere often leaves an afterglow or train (Trowbridge 1907, 1911). Radar observations show that the train must contain positive ions and electrons, and the suggestion has been made that the train luminosity is caused by a recombination process (Millman 1950*a*, *b*; Öpik 1955*a*, *b*). In this paper the suggestion is adopted as a hypothesis and treated on a quantitative basis.

II. THEORETICAL ESTIMATE OF LUMINOSITY DUE TO RECOMBINATION

a) Recombination along Meteor Trail

The column of ionization found behind the meteor diffuses in the atmosphere. The ion density, n_e, at a radial distance, r, from the axis of the trail and at a time, t, after the passage of the meteor, is well represented (Kaiser 1953) by the equation

$$n_e(r, t) = \frac{N_e}{4\pi Dt} \exp\left(\frac{-r^2}{4Dt}\right), \tag{1}$$

where N_e and D denote, respectively, the line density of electrons along the trail in inverse centimeters and the ambipolar diffusion coefficient for ions and electrons in square centimeters per second. The recombination rate is given by the expression

$$\frac{dn_e}{dt} = -\alpha_e n_e^2, \tag{2}$$

where α_e is the recombination coefficient. Substitution of n_e from equation (1) in equation (2) and integration over the entire plane perpendicular to the trail gives the equation

$$\frac{dN_e}{dt} = -\frac{\alpha_e N_e^2}{8\pi Dt}, \tag{3}$$

where dN_e/dt is the rate of change of the electron-line density due to recombination. In the deduction of equation (3) it has been assumed that N_e is effectively constant. This assumption will be verified later.

---

* This research was supported by the Massachusetts Institute of Technology, Lincoln Laboratory Contract No. AF19(122)-458, Sub-contract No. 57, and the Geophysics Research Directorate, Air Force Cambridge Research Center, Contract No. AF19(122)-482. Reproduction in whole or in part permitted for any purpose of the U.S. government.

The intensity of light, I_s, from 3.′5 of the trail, the resolving limit of the human eye, at a perpendicular distance of 100 km, is therefore given by the expression

$$I_s = 10^{-10} \frac{p\,\alpha_e N_e^2}{32\pi^2 Dt} \tag{4}$$

in ergs per square centimeter per second, where p is the luminous efficiency of a single recombination event. Since 3.′5 corresponds to 1.02×10^{-3} radian, the resolution of the human eye in equation (4) was taken to be 10^{-3} radian.

If the minimum range, R_0, of the trail, projected if necessary, differs from 100 km, the intensity from 3.′5 of the trail will be

$$I = 10^{-10} \frac{100}{R_0} \frac{p\,\alpha_e}{32\pi^2} \frac{N_e^2}{Dt} \tag{5}$$

in ergs per square centimeter per second, where R_0 is in kilometers. It should be remarked that, for constant p, α_e, N_e, D, and t along a trail, the observed intensity to the human eye would be constant along it, since the inverse-square law for intensity from a point source will be counteracted by two direct first powers of the distance factors, one occurring in the increase of the unresolved length for a perpendicular viewing with distance and the other occurring in the increase of unresolved length due to foreshortening. Thus the minimum range, R_0, is the distance which enters the expression for the intensity.

It is convenient to express the line density, N_e, in terms of the duration, τ_0, of a radar echo obtained with a transmitter operating at wave length λ (Kaiser 1953):

$$N_e = \frac{16\pi^2 D\tau_0}{1.124 \times 10^{-12}\lambda^2}. \tag{6}$$

Hence, from equation (5), the intensity from 3.′5 of the trail will be

$$I = 6.24 \times 10^{15} \frac{100}{R_0} \frac{p\,\alpha_e}{\lambda^4} \frac{D\tau_0^2}{t}. \tag{7}$$

In order to estimate the intensity from a meteor trail due to recombination, it is necessary to evaluate the constants of equation (7).

b) Possible Ionic Constituents of a Meteor Train

Millman (1950*b*) has published a spectrogram of a meteor train from which the main ionic constituents can be identified, if the lines are presumed to originate from recombination and subsequent cascade. The four lines of Fe I lasting less than 0.01 sec would indicate the presence of Fe II (a^6D), which is the ground state of that ion. The six lines lasting more than 0.05 sec due to Na I, Mg I, Ca I, and Fe I would indicate the presence of Na II (2^1S), Mg II (3^2S) and Ca II (4^2S), all in their ground states, and, finally, Fe II (a^4F), the first metastable state with an E.P. of 0.23 ev. Although not shown in the spectrogram, the ions Si II (3^2P^0) and O II (2^4S^0) would also be expected in meteor trains.

c) The Recombination Coefficient

Öpik (1955*a*) gives computed values for the recombination coefficients of the foregoing ions at a temperature of 781° K. An atmospheric temperature of 212° K is adopted for the train, and the coefficients are multiplied by a factor $(781/212)^{1/2}$, which, according to Öpik (1955*a*, eqs. [32] and [33]), is a good approximation for the temperature correction. The values found for the recombination coefficient range from 2.47×10^{-12} cm^3/sec for Na II to 2.80×10^{-12} cm^3/sec for Fe II (a^{6}D), with only that for O II being higher, at 3.18×10^{-12} cm^3/sec. The value $\alpha_e = 2.6 \times 10^{-12}$ cm^3/sec is adopted as being good to within ± 20 per cent.

The small range in values of the recombination coefficient is due to the predominance of recaptures to high, nearly hydrogenic, energy levels, which also makes possible a reasonably accurate estimate of the coefficient.

d) Luminous Efficiency

Öpik (1955*a*) gives computed luminous efficients both in line and in continuum radiation for recombinations of these ions. He assumes a rectangular sensitivity function or a pass band for visual light-quanta of energy from 2.23 to 2.65 ev (wave-length range 4680–5560 A). He computes values for different numbers of de-exciting collisions per second. Only the values corresponding to a minimum rate for such collisions will be used, because they should be quite rare except in the immediate neighborhood of the meteor. The upper limit of visual luminous efficiency, 0.94 ev per recombination, is attained by the assumption that all the ions are Fe II (a^{4}p), whence the luminous efficiency, p, will be less than, or equal to, 1.5×10^{-12} erg per recombination.

Öpik's luminous efficiencies for recombination and subsequent cascade should give something better than order-of-magnitude accuracy, since the rates of introduction of atoms into excited states can be estimated with some confidence for this process and since line emission by cascade predominates over continuous radiation by recombination.

e) Diffusion Coefficient

Greenhow and Neufeld (1955) have published an observed straight-line curve exhibiting log D against the height above sea level, H, in kilometers. This line is well represented by the formula

$$D = 10^4 \exp 0.1570\,(H - 83.5)\,. \tag{8}$$

III. ESTIMATE OF FAINTEST TRAIN DETECTABLE BY HUMAN EYE

While the human eye has a threshold on a transparent moonless night corresponding to detection of a star of apparent magnitude 6.5, Bobrov (1956) has shown that there is a gain in sensitivity for a line source of roughly a factor ten. Therefore, a train at its limit of visibility is regarded as though it were a succession of point sources of apparent magnitude 9, all spaced at the limit of angular resolution of the human eye, $3'.5$ or 0.00102 radian.

Cook and Millman (1955) give the following formula for the flux from an unreddened star of given apparent photovisual magnitude, spectral type, and luminosity class:

$$\log F_\lambda^* = (-8.425 - 0.4\Delta I_{pv}) + (\log F_\lambda - \log F_{5450}) - 0.4 I_{pv}\,, \tag{9}$$

where F_λ^* denotes the flux in ergs per angstrom per square centimeter per second from a star of apparent photovisual magnitude I_{pv} at wave length λ, F_λ denotes the flux in ergs per angstrom per square centimeter per second at the surface of the star, and ΔI_{pv} is a correction for obscuration by spectral lines. Milford (1950) has tabulated log F_λ and ΔI_{pv} as functions of spectral type and luminosity class. For a ninth-magnitude A0 V star, the flux through Öpik's (1955*a*) pass band is found to be

$$I_0 = \int_{4680}^{5560} F_\lambda^* \, d\lambda = 9.6 \times 10^{-10}\,\text{ergs/cm}^{-2}/\text{sec}^{-1}\,. \tag{10}$$

This is the flux from $3'.5$ of arc of a meteor train that is on the limit of visibility.

IV. OBSERVATIONAL DATA

The available observational data are given by Millman (1950*a*) in his Figure 2, which displays log t_0 against m_{vis} for the Leonid, Perseid, and Geminid showers deduced from 3700 meteors by Millman and Robins (1935). Here t_0 is the average observed duration of the train, and m_{vis} is the apparent visual magnitude of the meteors. Millman (1950*a*) also shows, on the same figure, log τ_0 against m_{vis}, where τ_0 is the mean duration of the radar echo at 9.1 meters wave length. Here the averages were taken for 700 meteors of the Perseid and Geminid showers. The observations show that a Perseid having an average observed visual train duration of 1 sec is of apparent visual magnitude -1.0, while a similar Geminid is of apparent visual magnitude -2.0. For both showers the corresponding average duration of the radar echo is $\tau_0 = 32$ sec. Millman (1950*a*) gives, for the average height of the Perseids, 102.6 km and, for the Geminids, 97.0 km, which are stated to correspond to a mean visual magnitude between $+1$ and $+2$. Meteors of magnitude -1.0 and -2.0 will occur at heights that are lower by a few kilometers, while the height at which maximum duration of trains occurs is about 96 km (Hughes and Cook 1956; Trowbridge 1907), so that 96 km may be adopted as the height in equations (7) and (8) without serious error.

An extreme situation tending to minimize R_0 and thus maximize I may be considered. This is the case of an observer with a region of attention consisting of a small circle with a radius of 0.2 radian, centered on the radiant. Millman and Robins' (1935) data presumably refer to the entire sky; so this assumption is extreme. The average value of sin θ, where θ is the angular distance from the radiant, over this area of attention is

$$\langle \sin\theta \rangle = \frac{2\pi \int_0^{0.2} \sin^2\theta d\theta}{2\pi \int_0^{0.2} \sin\theta d\theta} = 0.138 . \tag{11}$$

The corresponding value of the minimum range of the projected trail is $R\langle \sin\theta \rangle$, where R is the actual range of the train and cannot be less than the minimum height at which trains have been observed, 74 km (Hughes and Cook 1956). Thus $R_0 \geq 10.2$ km.

Substitution of the appropriate quantities in equations (8) and (7) gives

$$I(t_0) \leq 2.55 \times 10^{-11} \text{ ergs/cm}^{-2}/\text{sec}^{-1} \tag{12}$$

for both Perseids and Geminids with observed train duration, $t_0 = 1^{\mathrm{s}}.0$. This value is to be compared with the threshold for $3^{\mathrm{m}}.5$ of the train given by equation (10).

V. DISCUSSION

In writing equation (3) it has been assumed that $\Delta N_e \ll N_e$, where ΔN_e is the decrease in line density of the trail over the period of observation from t_0 to τ_0. This is valid, since

$$\Delta N_e = -\int_{t_0}^{\tau_0} \frac{dN_e}{dt} dt = \frac{a_e N_e^2}{8\pi D} \log_e \left(\frac{\tau_0}{t_0}\right) \ll N_e . \tag{13}$$

The inequality involves a factor of more than 500 for both Perseids and Geminids.

It can be seen that the estimated upper limit on the intensity is lower than the observed value, by a factor of about 38 or more, for both Perseid and Geminid trains. A more realistic value of R_0 is about five times the one used in finding this limit. Also average sky conditions should correspond to a stellar threshold at magnitude 5.0 rather than 6.5, which increases I_0 (cf. eq. [10]) by a factor four. The combined effects of these considerations remove the extreme values used except for the luminous efficiency and introduce a factor 20 into the discrepancies found above, i.e., recombination fails to produce the observed light from trains by a factor of roughly 800 for both Perseids and Geminids. An alternative method of storing energy other than ionization must be sought, therefore, together with a corresponding process for its release, e.g., formation of active nitrogen by interaction of the meteor and the atmosphere and subsequent excitation of parasitic radiation from *neutral atoms* in the train, possibly accompanied by nitrogen-band radiations (Whipple 1955). It may be noted that if Millman's spectrum (1950*b*) is assumed to be produced by recombination, then the Fe II (a^4F) state disappeared long before the Fe II (a^6D) state, while the recombination rates for these ions are approximately the same (2.8×10^{-12} and 2.53×10^{-2} cm^3/sec at 212° K, respectively). This is further evidence against the recombination hypothesis.

REFERENCES

Bobrov, M. S. 1956, *Astr. J. U.S.S.R.*, **33**, 164.
Cook, A. F., and Millman, P. M. 1955, *Ap. J.*, **121**, 250.
Greenhow, J. S., and Neufeld, E. L. 1955, *J. Atm. Terr. Phys.*, **6**, 133.
Hughes, R. F., and Cook, A. F. 1956, *Smithsonian Ap. Contr.*, in press.
Kaiser, T. R. 1953, *Adv. Phys.*, **2**, 495.
Milford, N. 1950, *Ann. d'ap.*, **13**, 243, 251.
Millman, P. M. 1950*a*, *J.R.A.S. Canada*, **44**, 209.
———. 1950*b*, *Nature*, **165**, 1015.
Millman, P. M., and Robins, J. A. 1935, *Pub. A.A.S.*, **8**, 147.
Öpik, E. J. 1955*a*, *Proc. R. Soc. London, A*, **230**, 463.
———. 1955*b*, *Special Suppl. J. Atm. Terr. Phys.*, **2**, 29.
Trowbridge, C. C. 1907, *Ap. J.*, **26**, 95.
———. 1911, *Phys. Rev.*, **32**, 129.
Whipple, F. L. 1955, *Trans. I.A.U.*, in press.

THE IMPACT OF LARGE METEORITES

J. J. GILVARRY* AND J. E. HILL
The RAND Corporation, Santa Monica, California

Received May 15, 1956

ABSTRACT

The impact of large meteorites on the moon or earth is discussed on the basis of a one-dimensional idealization of the flow problem, in which a plane shock wave is considered in both meteorite and impact surface. Conditions are discussed under which such a model can yield physically valid estimates of pressure and temperature generated on explosive impact of meteorites. Computations are carried out for an equation of state and internal energy from the statistical Thomas-Fermi atom model; departures from complete degeneracy are taken into account by means of results of a first-order perturbation with respect to temperature. It is assumed that the meteorite and impact surface are composed of the same pure element, taken as silicon, iron, and an average element (in a sense defined) for meteorites. The range of impact velocity considered goes up to the limit possible for meteorite origin in the solar system, which is well in excess of Whipple's estimates of mean atmospheric velocity for meteorite falls. Over this range, values of compression ratio, pressure, and temperature behind the shocks and of shock velocities are exhibited as functions of impact velocity; at the lowest and the highest velocities, results are only qualitative. Shock temperatures computed for iron agree reasonably with extrapolation of experimental data of Walsh and Christian for copper at lower pressures. The results yield pressures and temperatures of explosive magnitude behind the shock waves, in confirmation of the views of Gifford and Baldwin. Computed fusion temperatures behind the shocks show no inconsistency with Urey's mechanism of formation of lunar maria.

I. INTRODUCTION

The original suggestion that the craters of the moon were formed by explosions associated with the impact of large meteorites on the lunar surface can be credited to Gilbert (1893) and to Gifford (1924, 1930). In an extensive monograph Baldwin (1949) has put the hypothesis on a strong foundation. He presents powerful arguments against other modes of origin, such as vulcanism. Further, he demonstrates that the curve of diameter versus depth for the lunar craters shows a continuous variation through the analogous curve for the terrestrial meteoritic craters into the corresponding curve for explosion craters on the earth (due to artillery shells and bombs at low energy and accidental chemical explosions at high energy). The prescription, within a certain error, of diameter as a function of depth for all these craters by one analytic function, corresponding to the Baldwin curve, yields a strong argument for a common genesis in explosions.

To justify fully the empirical arguments of Gifford and Baldwin, it remains to show by direct computation from physical laws that the impact of large bodies on the moon or the earth with astronomically possible velocities actually produces temperatures and pressures of explosive magnitude. The explosion that forms a large lunar or terrestrial meteoritic crater arises from the high pressures and temperatures behind shock waves generated on meteorite impact. To solve the associated problem in shock hydrodynamics to any approximation, it is necessary to assume an equation of state (and a corresponding form of the internal energy) for the material of the meteorite and the impact surface. Gold (1955) has made computations based on an equation of state corresponding to an ideal gas of dissociated nuclei and electrons. However, the compressions and temperatures one expects (at least for the lower impact velocities) are such that the electron gas should be relatively degenerate, since this gas is strongly degenerate in a metal under standard conditions. The purpose of this paper is to present computations of the pressures and temperatures attained in the impact of large meteorites, based on an equation of state (Gilvarry 1954*a;* Gilvarry and Peebles 1955) obtained from the statistical Thomas-Fermi model of the atom. In this equation of state, departure of the electrons

---

[*] Now at Research Laboratories, Allis-Chalmers Manufacturing Co., Milwaukee, Wisconsin.

from complete degeneracy is taken into account by means of a first-order perturbation with respect to temperature; provided that the absolute temperature is less than a certain degeneracy limit, the model should be physically applicable for pure elements if the pressure exceeds a limit in the order of megabars. A preliminary description (Gilvarry and Hill 1956) of results has been given. Previous discussions (Baldwin 1949; Urey 1952; Kuiper 1954) of the impact of large meteorites have ignored shock formation in any analytic treatment given.

For simplicity, the meteorite and the lunar surface will be assumed to be composed of the same pure element. As reasonable average values of atomic number, $Z = 14$ (silicon) and $Z = 26$ (iron) have been selected, corresponding to stone and iron meteorites, respectively. A hypothetical element "averagium" can be defined by determining the average atomic number of the elements, weighted by their gross relative abundance by mass over the silicate, sulfide, and metal phases of meteorites. From data of Brown (1949), the atomic number of averagium is 18.5. Results are presented for this element in some cases also. Conclusions for averagium should be representative in some average sense, since thermodynamic functions on the Thomas-Fermi model scale with, and thus vary smoothly as, the atomic number Z. Note that thermodynamic functions on this model are insensitive to the physical state of the uncompressed material (presumably pumice-like in the case of the moon).

As a gross simplification to reduce the problem to one-dimensional form, the meteorite will be considered as a right cylinder whose base impinges upon the surface of the moon or earth. A plane shock wave enters the cylinder along its axis, and a plane shock wave enters the surface of the moon or earth. This idealized model will apply to the impact of a large meteorite of roughly spherical shape, for a time sufficiently short that the distances traversed by the shocks in the meteorite and impact surface are small compared to a linear dimension of the impinging mass. For times sufficiently long that the shock in the meteorite reaches the rear surface (from which a rarefaction wave arises in this case), the idealization loses physical validity, since appreciable lateral motion of the meteoritic material can exist, and the shock wave can no longer be regarded as plane. A basic assumption which will be made is that the shock pressure exceeds the yield stress of the material, so that the colliding masses can be treated as fluid. The validity of this assumption is borne out by the experimental work of Walsh and Christian (1955) and of Minshall (1955) on shock waves in metals.

The maximum velocity of a meteorite before impact on the moon or earth will be taken as the sum of the heliocentric parabolic limit (42.2 km/sec), corresponding to the mean distance of the earth-moon system, and the orbital velocity (29.7 km/sec) of the earth-moon system about the sun, or about 72 km/sec. In the case of the earth, this figure neglects the small accelerating effect (contributing about 1 km/sec) of the earth's gravitational field and the decelerating effect of the atmosphere; in the case of the moon, it neglects the effect of the moon's gravitational field and its orbital velocity about the earth. The limit in question is in agreement with the general results (Lovell 1954) of measurements of meteor velocities in the earth's upper atmosphere by photographic and radio techniques. If the bodies that caused the lunar and terrestrial meteoritic craters were members of the solar system, it follows that this approximate figure represents the maximum possible selenocentric or geocentric velocity; this limit may be reduced substantially if it is established that meteorites are essentially different from the bodies that produce meteors and come from orbits similar to those of the observed minor planets (Whipple 1955). The choice made here of an upper limit on the velocity carries no implication on the mean value. In the absence of an atmosphere the minimum velocity for impact normal to the surface is the escape velocity (2.4 and 11.2 km/sec for the moon and earth, respectively). The effects of atmospheric retardation for the earth and of obliquity of impact for both moon and earth reduce the lower limit on the normal velocity. In what follows, the impact will be assumed to correspond to a normal plane shock.

It should be emphasized that the results presented here are valid only when shock formation is the dominant mechanism of energy transfer, that is, for relatively large velocities of impact. To obtain an idea of a possible lower limit on velocity, one can note that Allen, Rinehart, and White (1952) have accelerated steel pellets with masses of a few grams to velocities of 6 km/sec by a shaped-charge technique; they observed severe deformation of the impinging pellets but no certain evidence of explosive impact, in agreement with previous results (Rinehart 1950; Rinehart and White 1952) at somewhat lower velocities. The figure of 6 km/sec noted seems to be the upper limit on velocity obtained to date under laboratory conditions for small solid projectiles. For the same velocity, however, experiments with pellets may not necessarily be representative of conditions for impact of the large masses responsible for production of the larger craters. An efficiency question may enter for smaller bodies, in the sense that the instantaneous pressure generated on impact may not have sufficient time to overcome the inertia of the material and explode the body before the pressure is relieved by rarefactions from the rear and sides. For plane shocks obtained by an explosive lens system, Walsh and Christian (1955) determined particle velocities of the order of 1 km/sec for shock pressures up to about 500 kilobars; thus impact velocities of this order may be sufficient for explosive impact if the meteorite is large enough to yield a sustained plane shock.

The most one can say, therefore, is that the lower limit on impact velocity for validity of the treatment given lies possibly between 1 and 10 km/sec and may depend on meteorite size; one can note that the velocity at which the kinetic energy per unit mass equals the energy release (about 5×10^{10} ergs/gm) of TNT is about 3 km/sec. Consequently, collision of a meteorite with the surface of the earth does not necessarily result in an explosion, since geocentric velocities down to low values are possible as a result of atmospheric deceleration. A continuous gradation must exist from energy transfer by shock formation at the higher velocities to transfer by plastic yield or elastic strain at the lower velocities (Whiffen 1948; Minshall 1955). The likelihood of a meteoroid's surviving the atmosphere and impinging with low fractional mass loss at high velocity must be strongly favored by large initial size, since the decelerating, melting, volatilizing, and ablating effects of the atmosphere vary as the surface area, while the mass and energy vary as the volume.[1]

II. EQUATION OF STATE

On the first-order temperature-perturbed Thomas-Fermi model for a pure element, the pressure P and internal energy U per atom for a volume v of the atom are

$$P = p[1 + \tfrac{5}{2}(\sigma + 2\tau)\zeta(kT)^2], \tag{1a}$$

$$U = u + \tfrac{15}{2}pv(\sigma + 2\tau + 3\omega)\zeta(kT)^2, \tag{1b}$$

respectively, where the leading terms p and u are the corresponding values for the volume v at zero value of the absolute temperature T. Values of p and u depend on the solutions of the zero-temperature Thomas-Fermi equation and can be obtained as a function of v from fitted functions given by Gilvarry (1954*a*). In the temperature-perturbation terms of order T^2, k is Boltzmann's constant, and ζ is a quantity having dimensions of the reciprocal square of an energy and depending only on the atomic number Z. The perturbation parameters σ, τ, and ω depend on the solutions of the first-order temperature-perturbed and the zero-temperature Thomas-Fermi equations, and they can be obtained in terms of v from fitted functions given by Gilvarry and Peebles (1955). For this temperature-perturbed Thomas-Fermi model to have validity, the absolute temperature T must satisfy $T \ll T_0$, where the degeneracy limit T_0 is a function of v defined in terms of the Thomas-Fermi variables ϕ_b and x_b by

---

[1] The large fractional mass losses predicted for *large* meteorites by computations (Thomas and Whipple 1951) based on values of the coefficient of heat transfer corresponding to an accommodation coefficient of the order of unity should be accepted only with hesitation. A meteoroid large enough to survive the domain of long mean free path enters a region in which hydrodynamic flow sets in and a detached shock (head wave) forms in front of the body. The hot compressed air behind the head wave furnishes an additional sink for the energy, which, in the domain of long mean free path, is largely absorbed by the meteoroid. This effect can reduce the coefficient of heat transfer and the resulting mass loss by orders of magnitude, as shown by C. Gazley, Jr. (unpublished), and Lees (1956).

$$Z^{-4/3}\frac{kT_0}{R} = 8\left(\tfrac{2}{9}\pi^2\right)^{1/3}\frac{\phi_b}{x_b}, \tag{2}$$

in which R is the Rydberg constant. The quantity kT_0 is the chemical potential of the atom at zero temperature. Perturbation terms of higher order can be included by means of a general perturbation method (Gilvarry 1954*a*, *b*), to permit correspondingly greater relaxation of the condition $T \ll T_0$.

As will appear, the parameter which characterizes to a large extent the effect of the first-order temperature-perturbation terms in the shock transition is

$$\gamma_e = \frac{1}{3}\,\frac{\sigma + 2\tau}{\sigma + 2\tau + 3\omega}, \tag{3}$$

which is a function only of the volume v of the atom. From equations (1), one obtains

$$U - u = \gamma_e^{-1}(P - p)v \tag{4}$$

as a relation connecting the energy and pressure which is independent of the temperature.

On the Thomas-Fermi model, the atom showing zero pressure at its boundary has an infinite radius. Hence the value v_0 of the volume v per atom corresponding to normal density implies a fairly high pressure p_0. The values of v_0 taken were 19.3 and 11.8 A^3 for $Z = 14$ and $Z = 26$, respectively,[2] from densities given by Forsythe (1954); the corresponding values of p_0 are 0.71 and 4.0 megabars for $Z = 14$ and $Z = 26$, respectively. One could remove this artificial feature of the Thomas-Fermi model by fairing the pressure-volume curve into that corresponding to the equation of state of Bridgman (1949) at low pressure. In this paper, however, the pressure p_0 implied by the Thomas-Fermi model at normal density will be taken as the initial pressure of the material (at temperature $T = 0$) before shock; for consistency, the internal energy for the atom at the normal volume v_0 will be taken as the Thomas-Fermi value u_0. Thermodynamic quantities behind the shock will be computed on this basis, except that the final curve for the pressure below $5p_0$ will be corrected by extrapolating it into the value zero for zero impact velocity. Pressures greater than $5p_0$ are high enough to make thermodynamic variables behind the shock approximately independent of the choice of initial pressure and correspond roughly to the range of high pressure for which the Thomas-Fermi model is physically valid.

III. SHOCK DYNAMICS

On the one-dimensional idealization made, the analytic description of the impact is equivalent to that for the normal collision of two plane slabs, which are semi-infinite in opposing directions. Behind the shock in each slab, the flow pattern and the distribution of pressure and temperature are uniform up to the interface between material of the two slabs. Continuity of flow velocity at the interface requires the flow velocity to be constant in the region between the two shocks, and continuity of pressure at the interface for the same composition of the two slabs implies that thermodynamic functions are the same behind both shocks. If one slab (referred to as the "impact surface") is at rest, and the other (referred to as the "meteorite") possesses the velocity V, a Galilean transformation from a frame in the impact surface to one located in the interface at time of impact shows that, in this frame, the interface remains at rest and the particle velocity behind the shock in each slab vanishes, by virtue of the symmetry. By transforming back to the frame fixed in the impact surface, one obtains the result that the particle velocity behind the shock wave in the impact surface and in the meteorite is $V/2$ (directed into the impact surface in both cases), which likewise is the velocity of the interface between meteoritic material and that of the impact surface. The velocity C' (directed away from the impact surface) of the shock wave in the meteorite is related in magnitude by the equation

---

[2] For averagium, an average v_0 and an average mass per atom for silicon and iron were taken; curves of compression ratio, pressure, and temperature given for this case by Gilvarry and Hill (1956) differ somewhat from those given here because of a slightly different choice of v_0.

$$C' = C + V , \tag{5}$$

with the velocity C (directed into the impact surface) of the shock wave in the impact surface; C also represents the speed of the shock wave in the meteorite with respect to the undisturbed material of the meteorite ahead of it.

Since thermodynamic variables are the same behind the shocks in both media, it is necessary to satisfy the Rankine-Hugoniot equations explicitly only for the shock wave in the impact surface, which moves with velocity C into undisturbed material and imparts to it a velocity $V/2$. The Rankine-Hugoniot equations (Courant and Friedrichs 1948) corresponding to conservation of mass, momentum, and energy at this shock front are

$$\frac{C - V/2}{v} = \frac{C}{v_0}, \tag{6a}$$

$$(P - p_0)\, v_0 = \tfrac{1}{2}\, mCV , \tag{6b}$$

$$U - u_0 = \tfrac{1}{2}\,(P + p_0)\,(v_0 - v) , \tag{6c}$$

respectively, where m is the mass of an atom. The initial state ahead of the shock corresponds to $T = 0$ and $v = v_0$, with the initial pressure and energy per atom chosen as the values p_0 and u_0, respectively, as discussed previously. The final state behind the shock corresponds to a volume v per atom, a pressure P, and an energy U per atom which are connected with the non-vanishing temperature T behind the shock by the Thomas-Fermi equations (1).

The mechanical shock conditions, equations (6*a*) and (6*b*), yield

$$C^2 = m^{-1} v^2 \frac{P - p_0}{v_0 - v} \tag{7}$$

as an expression for the shock velocity and also provide the relation

$$(P - p_0)(v_0 - v) = \tfrac{1}{4} m V^2 , \tag{8}$$

in which the shock velocity and energy U per atom do not enter. In addition to the last equation, conjunction with the thermodynamic shock condition (6*c*) of the constitutive equation (4) from the Thomas-Fermi model yields a second relation in which the shock velocity and the energy U per atom do not enter. The eliminant of these two relations with respect to P is

$$Q(v) = \tfrac{1}{4} m V^2 , \tag{9}$$

where

$$Q = \frac{(p - p_0)\,(v_0 - v) + \gamma_e\,[p_0\,(v_0 - v) - (u - u_0)\,]\,(v_0 - v)\,/\,v}{1 - \frac{1}{2}\gamma_e\,(v_0 - v)\,/\,v} . \tag{10}$$

In addition to dependence on thermodynamic variables v_0, p_0, and u_0 associated with the initial state, Q depends on the final state behind the shock only through v, p, u, and

γ_e, which are all functions only of v; hence equation (9) fixes the volume v per atom behind the shock uniquely as a function of impact velocity V.

The method of solution of the shock equations used in this paper is to plot $Q(v)$ from equation (10) for a particular atomic number Z against the volume v per atom. The value of v behind the shock for a particular impact velocity V is obtained graphically as the one satisfying equation (9). The corresponding temperature T behind the shock is determined by

$$\zeta\,(kT)^2 = \tfrac{2}{5}\,(\sigma + 2\tau)^{-1}\left[\frac{Q}{p\,(v_0 - v)} + \frac{p_0}{p} - 1\right], \qquad (11)$$

which follows from equations (8) and (9) with the use of equation (1*a*) for P. With the temperature known, the pressure P behind the shock is fixed by the Thomas-Fermi equation (1*a*), and relation (8) is available as a check.

IV. NUMERICAL RESULTS

On the basis of the preceding theory, the corresponding compression ratio $\eta = v_0/v$ is shown in Figure 1 for $Z = 14$, 18.5, and 26 as a function of meteorite velocity V up to the maximum value 72 km/sec noted previously. The pressure P (in megabars) behind the shocks is shown likewise; the dashed portions of the curves (for pressures below $5p_0$) were extrapolated into the origin. For comparison with P, values of p obtained in the course of solution of the shock equations are shown (*dot-dashed*) in Figure 1 for $Z = 14$ and $Z = 26$; p is the pressure which the material behind the shock would have at the corresponding compression ratio if its temperature were zero. It is clear from the order of magnitude of the pressures shown in Figure 1 that the yield stresses of the materials are exceeded by a wide margin, in general.[3]

The absolute temperature T behind the shocks is shown in Figure 2 as a function of impact velocity for $Z = 14$, 18.5, and 26. The degeneracy limit T_0 of equation (2), relative to which T must be small for validity of the temperature-perturbed Thomas-Fermi model, is shown likewise. It is seen that the condition $T \ll T_0$ is satisfied reasonably well at the lower impact velocities but that T tends to become comparable to T_0 at the higher velocities. No reason exists, however, to believe that the pressures of Figure 1 and the temperatures of Figure 2 shown for the region of higher impact velocity are not qualitatively correct, as follows from a comparison (Latter 1955) of results of the temperature-perturbed theory with numerical results of the Thomas-Fermi theory as generalized to arbitrary temperatures by Feynman, Metropolis, and Teller (1949). The comparison shows that pressures from the temperature-perturbed theory are qualitatively correct so long as the total pressure P does not exceed about twice the zero-temperature pressure p; one notes from Figure 1 that this criterion is met reasonably for the cases $Z = 14$ and $Z = 26$ where p is given.

As a check on the computed shock temperatures, the only experimental data available are those of Walsh and Christian (1955) on aluminum, copper, and zinc for shock pressures up to about 500 kilobars. The curve of shock temperature versus pressure for copper ($Z = 29$) should be reasonably close to that for iron ($Z = 26$) in the range of very high pressure where the Thomas-Fermi model becomes physically valid, since thermodynamic functions on this model scale with atomic number Z (which differs only by about 10 per cent for the two cases in question). At low pressure, the coefficients a and b in Bridgman's (1949) isothermal equation of state, $-(v - v_0)/v_0 = aP - bP^2$, are roughly the same for the two metals (Slater 1949). Thus the curve of shock temperature versus pressure for copper should be close to that of iron at the lower pressures, since values of the density, the volume coefficient α of thermal expansion, the parameter $(\partial P/\partial T)_v = \alpha/a$, and the heat capacities, which enter (Walsh and Christian 1955) in determining the difference between the isothermal equation of state and the Hugoniot relation, are approximately the same for the two metals under normal conditions (Forsythe 1954). Hence one expects the data of Walsh and Christian for copper, when extrapolated, to fair smoothly into the computed curve of shock temperature for iron; Figure 3 shows that such is actually the case when the extrapolation is carried out against pressure. The dashed line through the data points of Walsh and Christian has been

---

[3] Whiffen (1948) finds a pressure of about 6.4 kilobars for the dynamic compressive yield stress of mild steel, and Minshall (1955) reports comparable values.

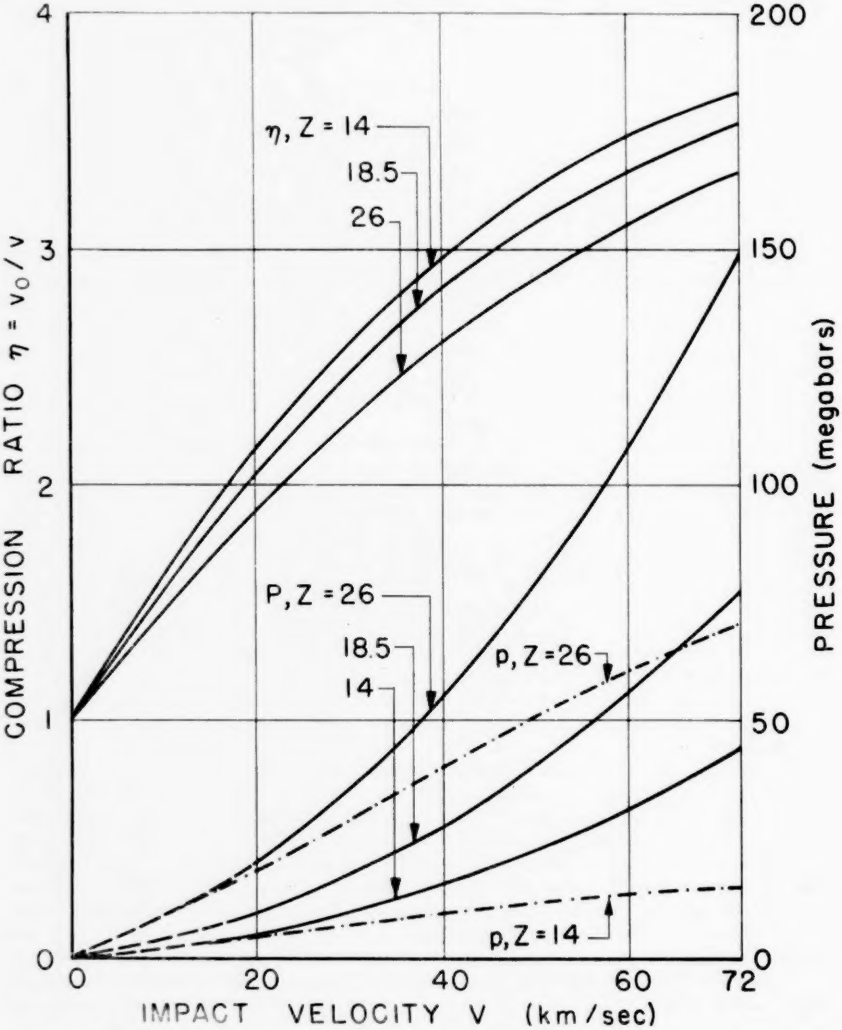

FIG. 1.—Compression ratio η and pressure P behind the shock waves as a function of the impact velocity of the meteorite. The quantity p is the pressure that the material behind the shock would have at the corresponding compression ratio if its temperature were zero.

terminated in a point of tangency on the curve (*full*) of computed shock temperature, at a pressure of $5p_0$. To determine the curve of shock temperature for iron down to the low temperatures shown, it was necessary to extrapolate temperatures given by equation (11) into those given by Taylor expansion at small compression.

The velocities C and C' of the shock wave in the impact surface and the meteorite, as defined by equations (7) and (5), respectively, are shown in Figure 4 for $Z = 14$ and $Z = 26$ as a function of impact velocity V. Both shock velocities are of the same order of magnitude as the impact velocity. The sonic speed c behind the shock is shown (*dashed*) in Figure 4 for $Z = 14$ and $Z = 26$; the values are determined by

$$c = \left(\frac{\epsilon_0 p v}{m}\right)^{1/2} \left\{ 1 + \tfrac{5}{2}\left[\epsilon_0^{-1}\gamma_e(\sigma + 2\tau) - \tfrac{1}{2}\epsilon_0^{-1}\frac{d\sigma}{d\ln v} + \tfrac{1}{2}\sigma + \tfrac{1}{5}\tau\right]\zeta(kT)^2 \right\}, \tag{12}$$

where ϵ_0 is defined (Gilvarry 1954*a*) as $-d\ln p/d\ln v$. On the Thomas-Fermi theory, the value c_0 of c at $V = 0$ represents the sound speed in the undisturbed material ahead of the shock; the values of c_0 shown are roughly of the correct order of magnitude for sound

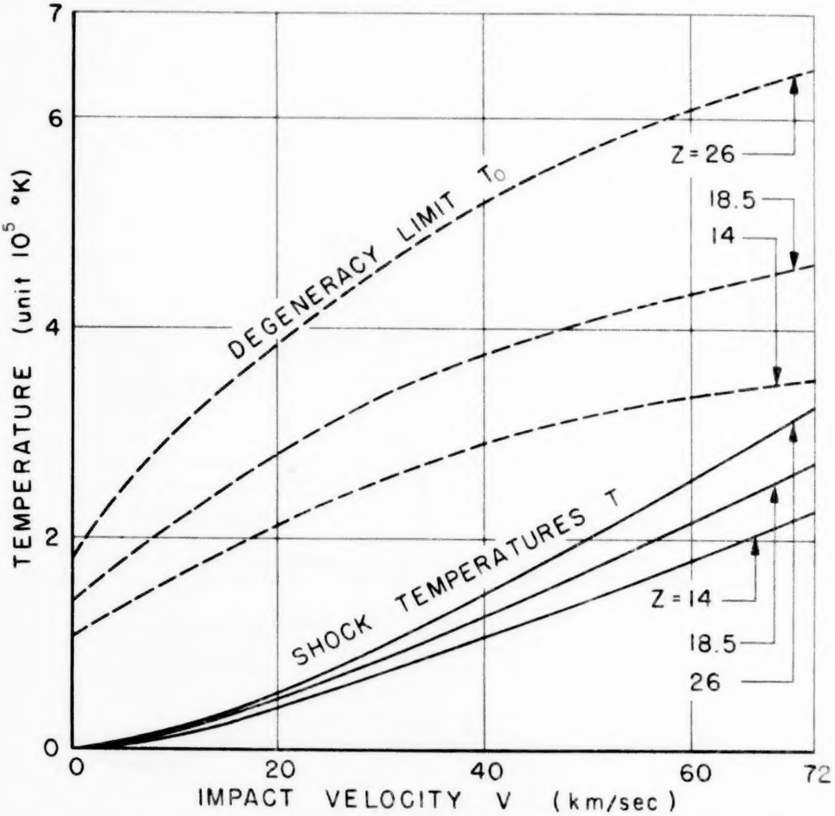

FIG. 2.—Absolute temperatures behind the shock waves as a function of impact velocity, with the degeneracy limit for comparison.

speeds in solids under normal conditions.[4] One notes that $C > c_0$ for $V > 0$, so that the material velocity relative to the shock front is correctly supersonic ahead of the shock in both the impact surface and the meteorite, as demanded by the Bethe-Weyl conditions (Courant and Friedrichs 1948).

V. DISCUSSION AND CONCLUSIONS

It is clear from the preceding discussion that the results obtained are merely qualitative for the region of high impact velocity, because of the poor approximation entailed in this domain by the first-order temperature-perturbed theory. If one takes a difference between P and p of $p/3$ as corresponding to a tolerable validity of the temperature-perturbed model, the pressures and temperatures of Figures 1 and 2, respectively, should be reasonably valid below an impact velocity of about 27 km/sec for $Z = 14$ and 37 km/sec for $Z = 26$. The range of lower velocity for a pressure behind the shock of less

---

[4] Thus c_0 for iron is 11 km/sec from the data of Fig. 4, as against a sound speed of about 5.9 km/sec measured by Minshall (1955) in steel.

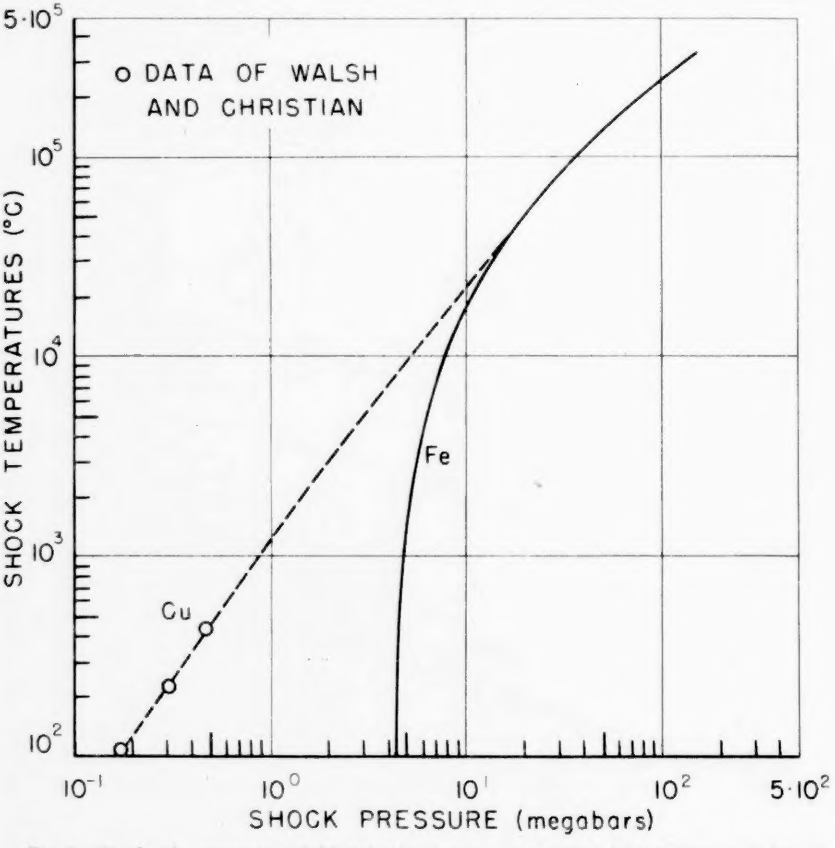

FIG. 3.—Centigrade temperatures behind the shock wave as a function of shock pressure for iron, as compared to extrapolation of the data of Walsh and Christian for copper.

than $5p_0$ corresponds to $V < 16$ and $V < 20$ km/sec for $Z = 14$ and $Z = 26$, respectively; in this region the results are subject to uncertainties arising from incipient departure of the model from physical validity. Thus only a relatively narrow range exists, from extremes depending on Z of 16–37 km/sec in impact velocity, over which the results are relatively unqualified. However, this range includes the values estimated by Whipple (1955) of 16.5 (from his own data) and 21.3 km/sec (from data of Astapovich) for the mean atmospheric velocity of meteorite falls and of 32.2 km/sec for the atmospheric velocity of the minor planet (1566) Icarus if this planet encountered the earth. In any event, the orders of magnitude obtained permit one to draw significant conclusions on the premises of Gifford (1924, 1930) that the impacts are explosive and that they yield circular craters, even when oblique.

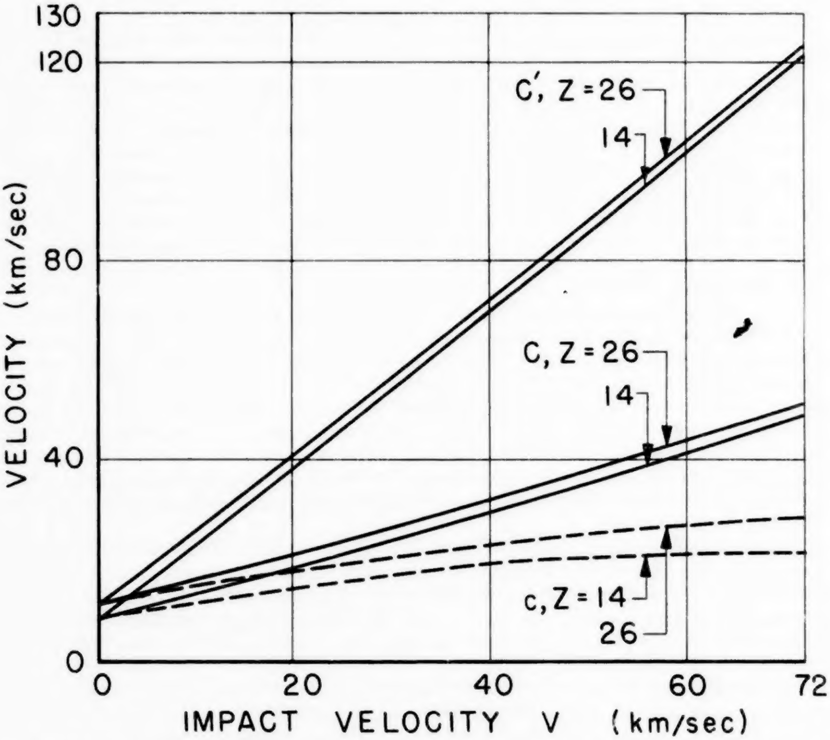

FIG. 4.—Velocities C and C' of the shock wave in the impact surface and the meteorite, respectively, as a function of impact velocity; c is the corresponding sound speed for the material behind the shock.

One sees immediately from Figure 1 that the highest pressures possible are over 100 megabars; in general, the pressures attained are of the order of those reached in the explosion of an atomic bomb (Glasstone 1950). Similarly, the higher temperatures shown in Figure 2 reach values larger than 100000° C, but they are below the value (1000000° C) estimated by Gold (1955); in general, the temperatures shown are above the range (of the order of 5000° C) corresponding to a chemical explosion but are below the range (of the order of 10000000° C or higher) attained in an atomic explosion (Brickwedde 1955).

For the mean atmospheric velocities given by Whipple, the pressures and temperatures are clearly of explosive magnitude. The possibility of such high pressures and temperatures stems from the fact, of course, that the kinetic energy per unit mass of a body moving at the higher speeds considered is far in excess of the explosive energy per unit mass of TNT, as stressed by Gifford (1924). As further emphasis, one can note that a method (Hill and Gilvarry 1956) of scaling dimensions of explosion craters on the earth from that of a prototype crater of known energy release yields an energy expenditure for the Arizona crater of about 2×10^{23} ergs, or about 4 megatons of TNT equivalent, which is comparable with that possible from a thermonuclear explosion.

Initially, these pressures and temperatures subsist in a volume which is of the order of the initial volume of the impinging meteorite, if one takes into account the volume swept out by the shock wave in the impact surface, noting the values of compression ratio indicated in Figure 1. The explosive release of the energy initially confined in this volume blasts out the lunar crater. Gifford's conclusion that oblique impacts can yield circular craters then follows if the flow velocities generated by the explosive release exceed any component of velocity parallel to the impact surface which the material may have acquired as a consequence of oblique impact. The initial phase of the release is intractable to calculation because the process occurs at an interface between two different media; as an added difficulty, the results of Figure 2 show that the material is relatively degenerate initially, but the equation of state will tend to approach that of an ideal gas under adiabatic release.

Since Figure 4 shows that the velocity C of the shock wave in the meteorite relative to the meteorite itself is of the order of the impact velocity, it follows that the explosive pressures and temperatures are created in a time of the order of that required for the impinging mass to traverse a distance equal to its diameter. Hence the effective center of the explosion must lie within a depth below the impact surface of the order of a linear dimension of the impinging mass. This fact is of importance in a practical application made (Hill and Gilvarry 1956) of the Baldwin crater relation to the scaling of dimensions of explosion craters in the earth as a function of energy release. As emphasized by Gifford and Baldwin, the original volume of the exploding material will be small relative to the volume of the crater.

By means of a reformulation (Gilvarry 1956*a*) of the Lindemann law of melting, a method of estimating the fusion temperature at high pressure has been given by Gilvarry (1956*b*). The method depends on the assumption that the critical ratio of root-mean-square amplitude of thermal vibration to nearest-neighbor distance in the solid at fusion is a constant independent of pressure. On this basis, Figure 5 exhibits as a function of impact velocity the melting temperature T_m behind the shock corresponding to the compression ratio η of Figure 1, for $Z = 14$ and $Z = 26$; also shown is the melting temperature T_m' behind the shock corresponding to the pressure P of Figure 1.[5] One notes that the shock temperatures shown exceed the fusion temperatures corresponding to either the same compression or the same pressure. This method of estimating the melting temperature does not permit any reliability at the lower impact velocities, because of the uncertainties arising from use of the Thomas-Fermi model. However, the corresponding extrapolation (shown dashed below a velocity corresponding to a pressure of $5p_0$ behind the shock) of the fusion-curves shows no inconsistency with the postulated mechanism of Urey (1952) for formation of the lunar maria, by large planetesimals impinging with normal components of velocity low enough that the temperature of the material merely reaches the fusion temperature. Although this result lends some plausibility to Urey's mechanism, different impact processes have been suggested by Baldwin (1949) and Kuiper (1954), and the possibility of a subsidence mechanism has been stressed by Alter (1956).

---

[5] The parameter Ω appearing in the equation for the melting temperature given by Gilvarry (1956*b*) was assigned the average value 0.012 justified in that paper.

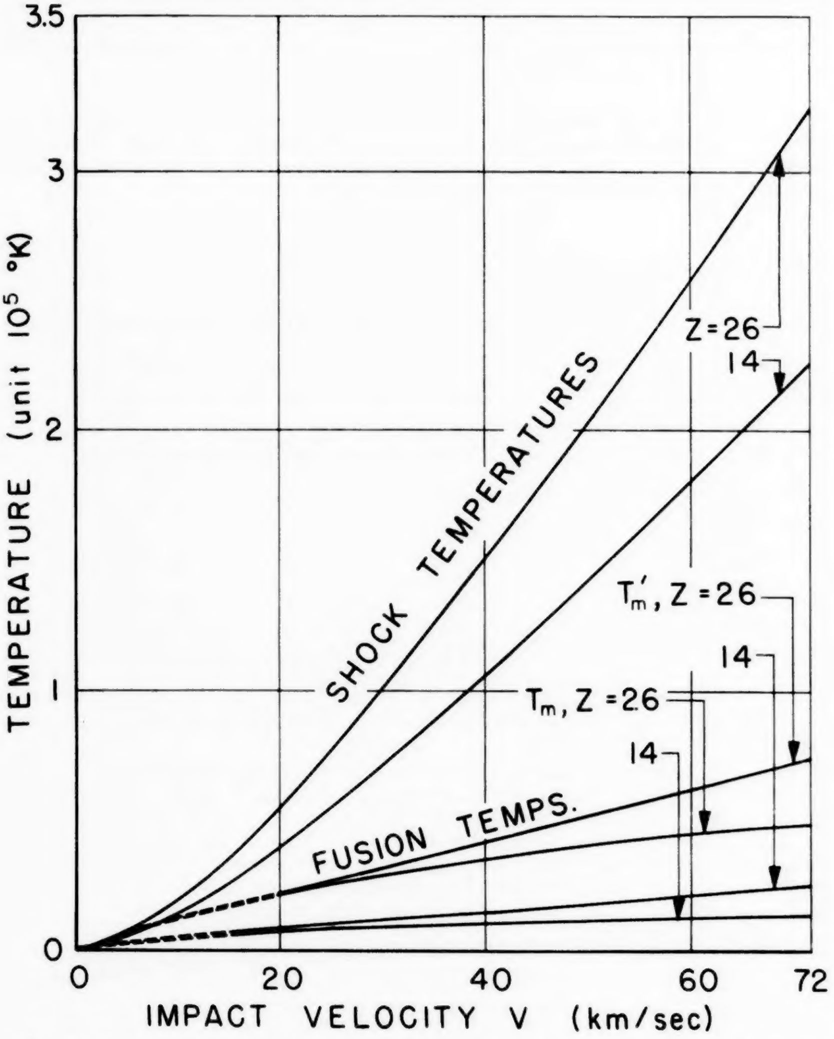

FIG. 5.—Shock temperatures as a function of impact velocity, for comparison with the fusion temperatures T_m and T'_m corresponding to the compression ratio and pressure, respectively, of Fig. 1.

In this paper the explosive nature of meteorite impacts at high velocity has been shown from the laws of hydrodynamics and quantum statistical mechanics rather than by the empirical considerations of Gifford and Baldwin. In spite of their qualitative nature, the results bear out the fundamental correctness of the picture of the origin of lunar and terrestrial meteoritic craters, as given by Gifford and Baldwin.

The authors wish to acknowledge valuable discussions of this problem with Dr. R. B. Baldwin, and with Dr. A. Latter, Dr. W. G. McMillan, and Dr. C. Gazley. Thanks are due Dr. H. K. Kallman and particularly Dr. F. R. Gilmore for critical discussion of the manuscript, and Miss E. Force for the computational work.

REFERENCES

Allen, W. A., Rinehart, J. S., and White, W. C. 1952, *J. Appl. Phys.*, **23**, 132.
Alter, D. 1956, *Pub. A.S.P.*, **68**, 38.
Baldwin, R. B. 1949, *The Face of the Moon* (Chicago: University of Chicago Press).
Brickwedde, F. G. 1955, *Temperature*, Vol. **2**, ed. H. C. Wolfe (New York: Reinhold Publishing Corporation).
Bridgman, P. W. 1949, *The Physics of High Pressure* (London: G. Bell & Sons, Ltd.), p. 169.
Brown, H. 1949, *Rev. Mod. Phys.*, **21**, 625.
Courant, R., and Friedrichs, K. O. 1948, *Supersonic Flow and Shock Waves* (New York: Interscience Publishers, Inc.), pp. 121, 141.
Feynman, R. P., Metropolis, N., and Teller, E. 1949, *Phys. Rev.*, **75**, 1561.
Forsythe, W. E. 1954, *Smithsonian Physical Tables* (Washington: Smithsonian Institution), pp. 145, 155, 291.
Gifford, A. C. 1924, *New Zealand J. Sci. Tech.*, **7**, 129.
———. 1930, *ibid.*, **11**, 319.
Gilbert, G. K. 1893, *Bull. Phil. Soc. Washington*, **12**, 241.
Gilvarry, J. J. 1954*a*, *Phys. Rev.*, **96**, 934.
———. 1954*b*, *ibid.*, p. 944.
———. 1956*a*, *ibid.*, **102**, 308.
———. 1956*b*, *ibid.*, p. 317.
Gilvarry, J. J., and Hill, J. E. 1956, *Pub. A.S.P.*, **68**, 223.
Gilvarry, J. J., and Peebles, G. H. 1955, *Phys. Rev.*, **99**, 550.
Glasstone, S. (ed.). 1950, *The Effects of Atomic Weapons* (Washington: Combat Forces Press), p. 25.
Gold, T. 1955, public lecture, University of California, Los Angeles.
Hill, J. E., and Gilvarry, J. J. 1956, *J. Geophys. Res.* (in press).
Kuiper, G. P. 1954, *Proc. Nat. Acad. Sci.*, **40**, 1096.
Latter, R. 1955, *Phys. Rev.*, **99**, 1854.
Lees, L. 1956, *Jet Propulsion*, **26**, 259.
Lovell, A. C. B. 1954, *Meteor Astronomy* (Oxford: Clarendon Press), chaps. xi, xii.
Minshall, S. 1955, *J. Appl. Phys.*, **26**, 463.
Rinehart, J. S. 1950, *Pop. Astr.*, **58**, 458.
Rinehart, J. S., and White, W. C. 1952, *Amer. J. Phys.*, **20**, 14.
Slater, J. C. 1940, *Phys. Rev.*, **57**, 744.
Thomas, R. N., and Whipple, F. L. 1951, *Ap. J.*, **114**, 448.
Urey, H. C. 1952, *The Planets* (New Haven: Yale University Press), pp. 26–39.
Walsh, J. M., and Christian, R. H. 1955, *Phys. Rev.*, **97**, 1544.
Whiffen, A. C. 1948, *Proc. R. Soc. London, A*, **194**, 300.
Whipple, F. L. 1955, *Meteors*, ed. T. R. Kaiser (London: Pergamon Press).

DIAMONDS, METEORITES, AND THE ORIGIN OF THE SOLAR SYSTEM

Harold C. Urey
Department of Chemistry and Enrico Fermi Institute for Nuclear Studies
University of Chicago

Received August 27, 1956

ABSTRACT

In order to explain the chemical composition and physical structures of meteorites, it is proposed that two sets of objects of asteroidal and lunar size were accumulated and destroyed during the history of the solar system. These are referred to as the "primary" and "secondary" objects. Since diamonds occur in meteorites, some of the objects must have been of lunar mass or greater; but it is not possible to be certain as to whether this occurred in the primary or secondary objects. The ages of the meteorites require that the primary objects accumulated about 4.5×10^9 years ago, were heated by some means to the melting point of silicates and iron, were then cooled to $\sim 500^\circ$ C for 10^7–10^8 years, and subsequent to this were broken into fragments of less than centimeter and millimeter sizes. The secondary objects accumulated from these about 4.3×10^9 years ago, and they were at least of asteroidal size. These objects were broken up at some time or times during the last 4.5×10^9 years, and the fragments are the meteorites. These collisional processes occurred during the formation of the solar system. The primary objects must have antedated the time of active formation of the system.

Solid objects appeared early during the formation of the system and played an important physical role during the formation of the planetary system and possibly in the formation of the sun. It is suggested that the solar nebula consisted of a disk of gas and solid objects and that the dissipation of the gases and some of the solids took place from this disk. Protoplanets in the sense of large masses of gas and dust of solar composition did not occur, at least in the case of the terrestrial planets, and not until much dissipation of the gases and dust had occurred.

Two problems relative to the origin of the solar system have been a source of much thought and speculation on the part of the author during the last six years. One has been the origin of the heating process which melted the metal and silicates of the meteorites, and the other the process by which a considerable fractionation of the silicate and metallic fractions of solar material occurred, as indicated by the varying densities of the planets. It has been assumed that these two processes were related to each other.

Chamberlain and Moulton first suggested that solid objects of considerable mass were an important feature of the origin of the solar system. Jeans and Jeffreys were not too definite about this point but introduced the concept of gas spheres formed by gravitational instability in a filament of gas which had been produced by tidal disruption of the sun. Eucken (1944) discussed the condensation of the planets by condensation of liquids from gases within Emden gas spheres. Von Weizsäcker (1944) proposed that the sun acquired a disk-shaped nebula during its early history and that this nebula broke up into a system of regular vortices and that the planets accumulated in secondary eddies between these vortices. Kuiper (1951) modified the previous discussions by assuming gravitational instability within a disk-shaped solar nebula as a source of gaseous spheres, which he called "protoplanets." Urey (1951) discussed the chemical problems associated with these models and tried to fit the chemical evidence into the protoplanet model. Throughout his discussion, these problems of the fractionation of the silicate and metallic constituents, the high-temperature melting of the silicate and metallic phases in meteorites, without any important fractionation of the more volatile from the less volatile elements, have been predominant. In fact, his arguments constitute the only, or at least the most compelling, argument for the existence of massive solid objects sufficiently large to be able to preserve the more volatile elements through some kind of high-temperature melting process during the early history of the solar system.

Recently Kuiper (1954) has proposed that the solar system originated about 5×10^9 years ago, that insulated objects formed at this time, and that they melted some 5×10^8 years later because of radioactive heating by potassium, uranium, and thorium. It was assumed that after the melting process the radioactive elements became concentrated at the surfaces of these objects during a solidification process. Kuiper does not account for the conglomerate structures of the chondritic meteorites, which have not lost their A^{40} during the last 4.3×10^9 years.

Urey (1955) discussed radioactive heating but pointed out that the structures of chondrites would require a very vigorous breakup of the originally melted materials to form the chondrites which must have occurred some 4.5×10^9 years ago and that presumably this was part of the process of formation of the solar system. Radioactive heating then requires a long time, some $0.5–1.0 \times 10^9$ years, for the melting process *prior* to the time of active formation of the system. Thus Kuiper's time schedule does not meet the conditions unless some vigorous collisional process occurred some $0.5–1.0 \times 10^9$ years after the formation of the system. In order to avoid this unlikely event, Urey suggested that radioactive heating due to short-lived radioactive elements took place, e.g., Al^{26}.

Recently Donn and the writer (Donn and Urey 1956; Urey and Donn 1956) in two brief papers pointed out that chemical heating due to reactions of condensed free radicals or to thermodynamically unstable compounds with satisfied valencies derived from free radicals could be the source of explosions in comets and heating in a lunar-type object at the time of the origin of the solar system and that such heating melted the silicates and metal of the meteorites. This offers a very plausible explanation of the first of the problems mentioned above, but, as stated by them, it does not solve the problem of variable planetary densities. It is the purpose of this note to point out a solution to the second problem by an extension of their line of argument.

Urey and Donn (1956) assumed that objects of lunar mass grew by accretion of dust at low temperatures until considerable masses of silicates and free radicals, e.g., OH, CH, CH_2, CH_3, NH, NH_2, etc., or molecules formed from them, e.g., H_2O_2, C_2H_2, etc., had accumulated. Then reaction was started by some chance excitation, and this produced high temperatures, reduced iron to metal and melted it, and melted the silicates. These cooled to about 500° C, and the process was repeated until an object of lunar mass was formed. Uhlig (1955) has argued that high pressures were required for the formation of iron-nickel phases of the iron meteorites, and this conclusion was accepted in the previous paper. A reconsideration of this question leads to some doubt as to the necessity of high pressures for this purpose; in fact, the older interpretation of the formation of the two iron-nickel phases at low pressures is preferable. This requires some revision of the previous discussion.

Urey (1954) suggested that large objects may have accumulated before the time of the origin of the solar system in the primitive dust and gas clouds, that such objects were captured by the sun, and that superficial heating of these objects occurred as they moved through gases in the neighborhood of the sun. If such objects exist, such heating might occur in a number of ways. Thus a gas sphere with a radius of 40 A.U. and solar mass would have a central temperature of about 3700° K. Objects of asteroidal or lunar mass could move through such a body of gas and be superficially heated, and thus a mechanism for melting the minerals of the meteorites and the fractionation of the silicate and metal phases may have occurred by evaporation methods, as previously suggested by the writer. It is well to search for evidence to guide us in these problems.

THE PRIMARY AND SECONDARY OBJECTS

In order to account for the structure and other properties of meteorites, it is necessary to assume at least two sets of objects from asteroidal to lunar mass. These will be referred to as the "primary" and "secondary" objects, and it will be shown that the primary objects were at least partly broken up to form particles ranging from dust to meteorites in size. These were reaccumulated into the secondary objects, which, it is supposed, were of the same type as the present asteroids. The breakup of these secondary objects supplied the meteorites. Evidence for this series of events is supplied by the structures, chemical composition, and ages of the meteorites, as outlined below.

1. Certain properties of the meteorites show that the primary objects existed and give information in regard to the mass and thermal history of these objects and the time schedule of events.

The chondritic meteorites are conglomerates of silicate minerals and the two iron-nickel phases, kamacite (α-phase) and taenite (γ-phase). The silicate minerals were formed under other conditions than those in which they are now found, and the mixture of minerals is inconsistent with solidification from a melt. The compositions of some achondrites are consistent with an origin by crystallization from a melt, but those of others are not, and in some cases they are conglomerates also. This has been recognized for many years by students of meteorites. The two iron-nickel phases exist as small bits of metal mixed with the silicates, and they did not crystallize in the positions in which they are now found.[1] The formation of these minerals from any cosmic mixture requires the material to have been melted at one time, and this would necessitate a temperature of 1500° C or higher. This must have occurred in a gravitational field perhaps of the magnitude of that of Ceres ($\sim$40 dynes) or greater, in order that separation of phases could occur. We assume that the large metal masses of the iron meteorites were made in this process. Also fairly large masses of nearly pure silicate minerals occur in the achondritic meteorites. Thus one stone of the Norton County achondrite has a mass of 1 ton, and the object that entered the atmosphere was probably much larger and consisted of nearly pure $MgSiO_3$. The crystallization of such large masses would require a substantial gravitational field, so that crystals would settle from a liquid or convection could be established. The exact size is difficult to estimate, but this writer would suggest a field more nearly that of the moon (165 dynes) than that of Ceres.

The kamacite and taenite are present in the Holbrook, Beardsley, Richardton, Forest City, and LaLande (Beck *et al.* 1951) meteorites. The average nickel content of the iron phase is known for three of these, and by means of the iron-nickel phase diagram (Owen and Liu 1949)[2] it is possible to estimate the temperature at which these phases were produced. It is also possible to estimate roughly the relative proportions of the kamacite and taenite phases from the intensities of the X-ray diffraction patterns or the relative numbers of metal particles of the two kinds as viewed under the microscope. Studies of this kind have been much too sporadic,[3] but some conclusions can be drawn. The metal of Holbrook contains 16.5 per cent nickel (Foote 1912), and the ratio of kamacite to taenite is about 2 from X-ray diffraction patterns. This indicates that the separation of the phases was arrested at about 450° C. The metal of Forest City contains

---

[1] At the writer's suggestion, observations on Holbrook, Beardsley, and Forest City were made by Mrs. B. Nielson and Miss Ann Plettinger. Professor W. Zacharieson interpreted the X-ray diffraction patterns. C. W. Beck, R. G. Stevenson, and L. La Paz (1951) report these two phases in LaLande.

[2] Since the reference may not be readily available to many readers, the equilibrium percentages of nickel in the two phases are given below:

	T (° C)								
	300	350	400	450	500	550	600	700	800
Kamacite (α)	7.5	6.9	6.3	5.7	5.0	4.4	3.7	2.5	1.2
Taenite (γ)	56.0	48.5	41.5	34.3	27.5	22.2	17.3	9.4	3.8

[3] This has been due to lack of time on the part of the writer and to lack of sufficient other personnel in his laboratories.

6.2 per cent nickel (Kunz 1890). Below 400° C, only kamacite would exist if equilibrium were established. The presence of only small amounts of taenite again indicates a temperature of about 500° C. Because of lack of analytical data on the others, no quantitative estimates can be made. The kamacite crystals of these meteorites run up to 1 or 2 mm, and the diffusion times to be discussed below show that the kamacite phase of this dimension would require some 10^8 years or possibly somewhat less for its formation. Holbrook and Forest City have ages of 4.3×10^9 and 4.2×10^9 years, respectively, from the K^{40}-A^{40} method.[4] This means that the metal in these objects was melted at ~1500° C, cooled to 450°–600° C, and maintained at this temperature for a time of the order of 10^8 years during a period before the ages given. This indicates that the pools of metal in the primary objects were highly insulated and probably not located on the surfaces of the objects.

The stony irons consist of approximately equal volumes of metal and silicates, and the two phases are dispersed in each other, each being physically continuous. It appears that partial crystallization of a liquid occurred, with the crystals forming a loose structure within the liquid, and that the liquid was then displaced by liquid iron. The gravitational field was surely not so great as that of the earth; for, had this been the case, the silicate minerals would have floated on the iron and been more compacted than they are in some cases. Prior's catalogue (Prior and Hey 1953) records twelve observed falls of stony irons and forty-two observed falls of irons. Since the stony irons are evidently the result of contact between the silicate phases and the metal phase, this argues that the surface regions were large and that the iron masses were not. A large iron core would be inconsistent with this evidence. Localized pools of metal would provide sizable surface areas of the kind required.

The Pb^{206}-Pb^{207} ages record the time elapsed since the lead of the iron meteorites became separated from uranium, most plausibly interpreted as the time of melting in a gravitational field. This time is estimated by Patterson (1955) as about 4.5×10^9 years. Also the Rb^{87}-Sr^{87} ages secured by Schumacher (1956) record the time since the strontium of the Pasamonte meteorite became separated from rubidium, which again is 4.5×10^9 years and is interpreted as the time of crystallization of the silicate minerals. Both these dates have a probable error of some hundreds of millions of years. Within this limit, they date the time of melting in the primary objects. Thus the materials of the meteorites were melted 4.5×10^9 years ago and had cooled to about 500° C and been incorporated into the Holbrook and Forest City stones 4.3×10^9 years ago, as shown by the K^{40}-A^{40} ages. (The dates have probable errors of 2 or 3×10^8 years.) It is very difficult to heat objects of the magnitudes here considered and cool them to the required temperatures within these time limits. This was discussed by Urey and Donn (1956), and Allan and Jacobs (1956) arrive at the same conclusion. The former authors have suggested the chemical heating mechanism in order to account for this required series of events.

2. Some of the properties of the meteorites give evidence in regard to the properties of the secondary objects.

The chondrites are often very compact objects of strength comparable to that of terrestrial rocks without gross flaws. This indicates that the secondary objects had substantial gravitational fields. The pressure at the center of Ceres is about 2500 atmospheres and decreases with radius proportional to $[1 - (r^2/a^2)]$, where r/a is the fraction of the radius at the point considered. When r/a equals 0.9, the pressure is about 500 atmospheres.[5]

---

[4] All potassium-argon dates in this paper are calculated using 1.27×10^9 years as a half-life and a branching ratio of 0.124. The dates given disagree sometimes with those in the literature because of the choice of constants.

[5] Urey and Craig (1953) proposed a different model, in which compaction was assumed to occur during high pressures during a collision. This model has been criticized on the ground that collisions would always shatter the object. This criticism seems to be a valid one.

The chondrules secured their round and often nearly spherical form while falling as liquid drops, according to suggestions made many years ago. Some of them still contain some glass, and hence the secondary objects were formed at low temperatures, for otherwise rapid crystallization would have taken place. Both the space was cold, since the drops were chilled quickly, and the conditions of accumulation were cold, at least in some regions, since complete crystallization has not occurred. On the other hand, considerable evidence for reheating exists and is generally recognized (Perry 1947; Smith 1950). This is most likely due to radioactive heating in insulated objects. Small objects would be highly insulated because they would be loosely compacted, and large objects would have high insulation because of size. Without more data, no conclusion can be drawn.

Dating of chondrites by the K^{40}-A^{40} method gives dates ranging from 4.3×10^9 years to some 0.7×10^9 years (Gerling and Rik 1955; Wasserburg and Hayden 1955). Errors due to uncertainty of the constants used may be some hundreds of millions of years, and the maximum date may be the same as those given above for the Pb^{206}-Pb^{207} and Rb^{87}-Sr^{87} dates. These K^{40}-A^{40} dates are the times since the meteoritic material last lost its argon. Since slow leaks over long periods of time could occur because of mild heating—400° C or less, according to Geiss (1956)—or because of the fine structure of the feldspar or other crystals in which the potassium is held, these are minimum ages. The oldest meteorite, according to measurements in the Chicago laboratories by Wasserburg and Hayden and Geiss and Hess, is the Holbrook chondrite, which is described as a "crystalline spherical hypersthene-chondrite" whose chondrules break with the matrix. It is a very compact strong stone, and, because it has retained its argon for 4.3×10^9 years, its materials have not been reheated in this time. Its compactness indicates that it was subjected to substantial pressures but hardly pressures greater than those available in an object as large as Ceres.

Other chondrites have K^{40}-A^{40} ages, which are definitely not in agreement with an age near 4.5×10^9 years, and it is most probable that reheating before the breakup of the secondary objects to form the meteorites occurred in these cases. The ages of some achondrites also are low, and the same explanation may apply to them.

3. Certain properties of meteorites may have been acquired in either the primary or the secondary object.

The Widmanstätten figures of the octahedrite group of iron meteorites consist of plates of kamacite (α-iron phase) bounded by thin layers of taenite (γ-iron phase) arranged parallel to the faces of the octahedron. The structure is often more complicated than this. The separation of these two phases with the observed percentages of nickel in the two phases would require temperatures between about 450° and 600° C for the different meteorites, if the pressures were low.[6] Uhlig (1954) summarized formulae for the diffusion of nickel in kamacite (α-phase) and taenite (γ-phase). The rate of diffusion in the former is some thousand times more rapid than diffusion in the latter. However, kamacite layers in the coarse octahedrites are from ten to a hundred times as thick as taenite, and, since times for diffusion are given by the equation $t = l^2/2D$, the diffusion times are comparable (l is the thickness and D the coefficient of diffusion). In the fine octahedrites the kamacite plates are thinner, and then diffusion in the taenite may be controlling, but the times may be about the same as those for the coarse octahedrites. Table 1 gives some calculated diffusion times. The data used are approximate, and this is especially true for the thickness of the taenite. The nickel concentration of the taenite of some octahedrites is sometimes as low as 13 or 14 per cent, but the analyses are very old and are probably unreliable. An analysis of Casas Grandes gives 16.7 per cent nickel; from the phase diagram this is the equilibrium value at 600° C. The taenite of Canyon Diablo contains from 27.7 to 34.6 per cent nickel, according to different analyses, indicating temperatures of from 500° to 450° C. An analysis on Cranbourne or Beaconfield taenite would indicate a temperature of 355° C, but this disagrees markedly with another analysis and is probably in error. Thus temperatures for the formation of these phases in the octahedrites run from 450° to 600° C and hence are in the same range as the more uncertain range estimated for the chondrites. If the analysis on Beaconfield is correct, a time comparable to the age of the solar system is required, and hence these phase separations occurred in the secondary objects. Otherwise they could have formed in times from 10^5 to 10^8 years and thus may have formed in the primary objects, as is necessarily true for the kamacite and taenite of the chondrites, Forest City, Beardsley, Richardton, LaLande, and Holbrook. Since diffusion coefficients decrease rapidly with increased pressure, high pressures would increase the required times very greatly. Also increased pressures cause a shift of the entire phase diagram to lower temperatures—by 200° C for a pressure of 10^5 atmospheres, according to Uhlig (1955). It is evident from Table 1 and the general effect of pressure that the kamacite and taenite of the iron meteorites could not have formed under such pressures during the whole of geologic time. Other iron meteorites require other conditions. The hexahedrites contain about 5.5 per cent nickel and consist of large crystals of kamacite, while the nickel-poor ataxites have the same composition but the crystals are very small. Perry (1944) believes that the hexahedrites crystallized at about 450° and the nickel-poor ataxites are reheated hexahedrites. This may have occurred in the secondary objects. Many points of the history of these meteorites are obscure, and probably several possible histories could be devised for them.

---

[6] See Farrington (1915, pp. 132 and 134) for these analyses.

TABLE 1[*]

DIFFUSION TIME FOR NICKEL IN KAMACITE AND TAENITE

T (° C)		Kamacite ($l = 0.2$ cm)	Taenite ($l = 0.007$ cm)
300	D	1.5×10^{-22}	8.1×10^{-27}
	t	4.2×10^{12}	9.5×10^{13}
400	D	3.2×10^{-19}	5.5×10^{-23}
	t	2.0×10^{9}	1.4×10^{10}
450	D	6.5×10^{-18}	1.8×10^{-21}
	t	9.7×10^{7}	4.3×10^{8}
500	D	9.1×10^{-17}	3.8×10^{-20}
	t	6.4×10^{6}	2.1×10^{7}
600	D	7.2×10^{-15}	5.7×10^{-18}
	t	8.8×10^{4}	1.3×10^{6}

[*] Time in years; D in cm^2/sec.

Diamonds have been observed in the Canyon Diablo and Magura octahedrites. So far as we know, diamonds cannot be produced except under fairly high temperatures and high pressures. Using thermodynamic data (Kelley 1949; Rossini, Wagman, Evans, Levine, and Jaffe 1952) and the densities of graphite (2.26 gm/cm^3) and diamond (3.51 gm/cm^3), the required minimum pressures at 1000° and 1200° K are 31000 and 37000 bars, respectively. The pressure at the center of the moon is 46000 bars, and hence we see that at least *one* of the primary or secondary objects was of lunar mass or greater. Since both Canyon Diablo and Magura are octahedrites and have well-developed Widmanstätten figures, we conclude, in view of the preceding paragraph, that they did not acquire both the kamacite and taenite of these figures and diamonds at the same time under the same conditions of temperature and pressure. Canyon Diablo contains some graphite and Magura large nodules of graphite, which appears to have crystallized at low pressures. They contain diamonds, which means that they were subsequently subjected to high pressures. Finally, Magura and some other irons contain graphite pseudomorphs of diamonds, so that they were again subjected to low pressures. All these processes occurred at least at moderate temperatures, for no crystallization of carbon into either graphite or diamonds will take place at ordinary temperatures (Farrington 1915). Diamonds and pseudomorphs of diamonds have been observed only in coarse octahedrites, with the exception of Toluca, which is a medium octahedrite. The rate of diffusion of carbon in iron is much greater than that of nickel (West 1950), and hence no problem of diffusion times exists.

The Urey and Donn model for chemical heating of the primary objects of lunar mass would supply the conditions for the formation of graphite at low pressures and diamond at high pressures, and radioactive heating in the secondary objects would provide conditions for the conversion of diamonds to graphite at low pressures. Under the last conditions the Widmanstätten figures could have been formed. However, the process is an involved one, and it can hardly be unique. The writer has devised other hypothetical processes, though none that seems as satisfactory as that mentioned.

Diamonds have been reported in the Carcote crystalline bronzite chondrite (von Sandberger 1889) but not from any other chondrite. Also they are reported in Novo Urei by Jerofejeff and Latschinoff, which was confirmed by Kunz (Jerofejeff and Latschinoff 1888; Kunz 1888). This is a rare type of achondrite, of which three are known. Neither of these has been dated by the K^{40}-A^{40} method, and both are not available to this laboratory. If diamonds are definitely shown to be present in chondrites of maximum age, the primary objects must have been of lunar mass or greater. In order that half the volume of an object of density 3.34 may be subject to a pressure of 37000 bars, it is necessary that its radius be 1.5 times the moon's radius.

4. The Urey-Donn heating mechanism by reactions of free radicals requires that the primary objects be of considerable size, in order that it may be an acceptable method for producing molten pools of silicates and metal. If the gravitational field is too low, the heated materials will be blown completely away from the object by the escaping gases, and, even if the field is sufficient to retain the gases and suspended liquids, they might be raised to high altitudes, be cooled, and the condensed phases would fall back as solids to the surface and thus supply no pools of liquids. The free radical heating process resembles physically and chemically a blast-furnace operation in which iron ore, limestone, and coke have gases passing through them and out at the top and liquid iron and melted silicates flow out at the bottom. A blast furnace would operate with great difficulty on the moon, for there would be a very great tendency for all products to leave at the top of the apparatus. We emphasize the qualitative problem but can draw no quantitative conclusions.

The superficial heating of objects would not provide any method for the formation of diamonds, since no high-pressure regions would be established.

Radioactive heating in objects formed some 10^9 years before the history under discussion could have supplied the melted iron and silicates and the kamacite and taenite if the primary objects were of asteroidal size. However, they could not have done this if they were large, because of the time required for cooling, as Urey and Donn point out; thus diamonds could not have formed in the primary objects if melting was due to radioactive heating either by potassium, uranium, and thorium or by short-lived nuclides.

The achondritic meteorites have less potassium and sodium than the chondrites. This is particularly striking in the case of those achondrites having a chemical composition similar to basalt, except that the concentrations of alkalies are much too low. (The mineral compositions differ from those of basalts, and hence their histories are not the same in all details.) The Pasamonte meteorite illustrates the similarity in chemical composition very well (see Table 2). The Nuevo Laredo meteorite belongs to the

Howardites, as does Pasamonte. Uranium and barium have higher concentrations and the alkalies lower concentrations in this meteorite than in the chondrites (Turkevich, Reed, and Hamaguchi 1956). Thus the differences shown in Table 2 extend to the minor constituents. The free-radical heating method would account for these facts; for partial melting of the primitive silicates should produce a basaltic liquid and the escape of gases should volatilize the alkalies and not the other constituents, as is well known from laboratory experience on melting silicates. The volatilized alkalies and other volatile elements would condense as dust and fall back to the surface, but the silicate melts would be deficient in alkalies, as is observed. The Urey mechanism of heating by the fall of these objects through gases at high velocity would supply superficial heating and volatilization of the alkalies from silicates. In this case the materials at the center of the object would not be heated and fractionated in this way; these materials supplied the higher concentrations of these elements in the chondrites. There is no evident process by which radioactive heating could have produced the loss of alkalies. On the basis of this argument, the achondrites generally are relics of the primary objects and do not owe their *chemical composition* to reheating in the secondary objects, even though such reheating may account for the loss of A^{40} and hence lower observed ages for some of them. (Both the Pasamonte and the Frankfort K^{40}-A^{40} ages are 3.3–3.5 × 10^9 years [Geiss and Hess, unpublished], and an estimate of the radioactive heating in highly insulated objects indicates a 500° or 600° C rise in temperature quite sufficient to remove argon during the times considered.) Schumacher's Rb^{89}-Sr^{89} age of 4.5 × 10^9 years for Pasamonte shows that the removal of rubidium occurred very early and supports the view that this took place in the primary objects.

TABLE 2*

COMPOSITION OF TERRESTRIAL BASALTS, THE PASAMONTE METEORITE, AND THE SILICATES OF THE CHONDRITES (IN PERCENTAGES)

	Pasamonte	Average Basalts	Average Silicate of Chondrites
SiO_2	48.20	49.06	47.04
MgO	6.47	6.17	29.48
FeO	17.04	6.37	15.40
Fe_2O_3	0	5.38	0.00
Al_2O_3	13.91	15.70	3.09
CaO	10.24	8.95	2.41
Metal	2.64	0.00	....
FeS	0.19	0.13	....
Na_2O	0.54	3.11	1.11
K_2O	0.066	1.52	0.122
Rb_2O	0.63 p.p.m.	70 p.p.m.	5.3 p.p.m.

* The average of the basalts is taken from Rankama and Sahama (1950), except for the rubidium, which is taken as 1/200 of the potassium, since Ahrens, Pinson, and Kearns (1952) have established by recent work that this ratio is nearly constant. The Pasamonte analysis is by W. Foshag (1938) except for the sodium and potassium analyses, which are by Edwards (1955), and the rubidium analysis, which is by Schumacher (1956). The analysis of the silicate phases of chondrites is taken from Urey and Craig (1953), except that the sodium and potassium values are from Edwards (1955) and that rubidium is a single value for the Forest City meteorite from Schumacher (1956).

Our conclusions from this discussion are as follows: Both the primary and secondary objects existed, and either one group or the other or both were sufficiently massive to produce diamonds. The primary objects collected, were heated to above 1500° C, and cooled to 450° or 600° C. After remaining at this temperature for some 10^8 years, they were broken up mostly into fine particles, though some of the fragments were fairly large and supplied fragments like the achondrites and iron meteorites. These fragments were accumulated into the secondary objects within a time of the order of 10^8 years. These secondary objects have collided with each other from time to time during the last 4.5×10^9 years, and the fragments are the meteorites. Arguments that the primary objects were of lunar mass are inconclusive; but, independently of the question of the time and place at which the diamonds were formed, the arguments indicate that the primary objects were of asteroidal dimensions or larger.

APPLICATION TO THE ORIGIN OF THE SOLAR SYSTEM

The foregoing outline of events leads to an interesting conclusion. First, a quiet period of accumulation of the primary objects and a resting period of considerable time are required. Second, a period of violent collisions must have occurred. Third, a period of reaccumulation into asteroidal bodies is required. If these events occurred under the same physical conditions during a short period of time, then it would appear that the meteorites are the result of a series of events of low probability. It is more reasonable to assume that these processes occurred under different physical conditions.

It is the purpose of this paper to explore a possible course of events in which it is assumed that the intense collisional process occurred during the formation of the solar system and that these collisions were an important and not merely an incidental part of the physical processes. In this case the accumulation of the primary objects preceded the active and energetic processes involved in the formation of the system. This reasoning indicates that these objects may have accumulated in the primitive dust cloud before the sun was formed or that they were captured by the sun from such a dust cloud. Any preceding condition consistent with the accumulation of these objects and the formation of their characteristic minerals would be satisfactory to the present discussion. The chemical heating process would supply heat regardless of the presence of a star or of adiabatically compressed gases, which are the usually assumed sources of heat.

POSTULATED MODEL FOR THE ORIGIN OF THE SOLAR SYSTEM

In this paper it is suggested that objects of considerable size and mass accumulated in a dust cloud at low temperatures. Intermittent chemical heating may have produced molten silicate and metal phases. After some period of time, millions or tens of millions of years, these objects fell rapidly toward a gravitation center, and the sun was formed with a disk of residual gas and these objects. Melting of the silicate and metallic materials may have occurred during this process. In this process intense collisions occurred which reduced the solid material to fragments varying from micron sizes and smaller to the sizes of the materials of the chondritic meteorites and iron meteorites. The gas and dust were dissipated from the disk by solar light-pressure and turbulent gases, and some of the solid material was removed by the Poynting-Robertson effect. The planets and asteroids accumulated during this time. Protoplanets in the sense of masses of gas and solids of solar composition did not occur, at least in the case of the terrestrial and minor planets, or, if protoplanets were present at all, they did not form until the permanent gases were removed and the fractionation of the silicate and metallic phases was complete, and hence they did not have the mean solar composition. The satellite systems of the major planets were formed by analogous processes.

The problem of the accumulation of large objects in interstellar dust clouds is a difficult one for which no mathematical discussions are available. We know that the clouds as we observe them today contain micron-sized or smaller particles in great numbers (Platt 1956). Also comets appear to be objects which formed in regions of very low densities of matter, so that some accumulation of solid matter does occur even under these conditions. Small solid objects in a gas present a very unstable situation, since these objects will fall toward a region of higher density and convert their kinetic and potential energy into heat. Such processes are thermodynamically irreversible. Passing stars must concentrate dust in their wakes, and such concentrations of gas and dust will fall toward any other high-density centers. It is easily seen that these processes are very complicated. However, it is evident that the accumulation will be a rapidly accelerating process as any object grows, and, if objects of lunar mass once were formed, rapid sweeping up of smaller objects should occur.

Also, a gas mass containing lunar-sized objects and probably more of smaller mass would be highly unstable, because the objects would fall rapidly toward any region of increased density. The smaller objects, in particular, would be decelerated by the gas and would increase the gravitational field, thus increasing the movement of gases toward such a center. In fact, such effects might produce an almost implosive origin of stars. Such objects, not subject to the hydrodynamic behavior of gases, would substantially stabilize the process of star formation. Altogether, such effects might make certain features of the formation of stars more understandable, as, for example, the formation of the O stars within quiet clouds, as discussed by Oort and Spitzer (1955) and Strömgren (1954). The "non-volatile" fraction of solar matter could supply some 10^5 moons. Some of the gas and solid objects would not become part of the sun, and it can be reasonably postulated that the gases formed a gaseous-disk nebula in the plane of the ecliptic, as had been assumed previously, and the primary objects which first plunged through this collided with one another and finally moved within the disk. Indeed, the debris would accumulate fairly close to the median plane if the gases were not too turbulent. While the mass of the earth distributed in the neighborhood of the earth's orbit within a ring 0.4 A.U. wide and 0.15 A.U. thick would supply a density of solid particles of only some 5×10^{-12} gm/cm^3, this same material concentrated in a plane amounts to some 10 gm/cm^2, and the total solid material in this region may have been many times the present earth mass at the time that we are considering. This concentrating effect would promote many collisions. The chondritic meteorites testify definitely and conclusively to the existence of such collisional processes during a period about 4.5×10^9 years ago.

The meteorites are assumed to be members of the asteroidal belt of objects. The total mass of the asteroids is estimated as $0.002\ M_{\oplus}$, while the mass of the moon is $0.0123 M_{\oplus}$. The history we are outlining requires at least two large objects, in order that there may be at least one effective collision and thus about twelve times the mass now present in this region. Again the total material at the time being considered may have been many times this amount. However, the varying densities of the planets (Urey 1952) and the existence of two prominent groups of meteorites with different iron-to-silicate ratios (Urey and Craig 1953) require that some material be lost and that this loss result in variable proportions of the more and less dense fractions of "non-volatile" constituents. This is precisely what must be expected on the basis of the present model. Assuming that the sun acquired its present luminosity at the period under consideration or at any previous time, several effects would dissipate the solar nebula, namely: (1) gases and very small-sized dust would be lost from the disk-shaped solar nebula because of radiation pressure driving them away from the sun; (2) somewhat larger particles would move toward the sun because of the Poynting-Robertson effect; and (3) particles would be lost by the dissipation of the solar nebula through the mechanism of loss of turbulent gases from the system, as von Weizsäcker and ter Haar (1946) have maintained. Part of the gases and solids would move into the sun and part to greater distances and probably some to an infinite distance. All these processes favor the removal of the smaller and lower-density particles. In collisions the weaker and more easily shattered silicates, as compared to metallic iron-nickel, would be broken into smaller particles; hence these would be removed preferentially, leaving residues enriched in metallic iron-nickel. The solids approaching the sun would be volatilized and at least partially driven away from the sun again, so that the total material entering the sun may have been small. In this case no especially high-temperature sun is required to produce this fractionation, though a somewhat more luminous sun would accelerate the process. Thus the second problem mentioned in the opening paragraph of this paper is solved quite naturally by this model.

The rate at which objects move toward the sun because of the Poynting-Robertson effect is proportional to the light-intensity and inversely proportional to the product of the density and radius of the particle (Wyatt and Whipple 1950). Elementary calculations show that the energy required for the removal of solid objects by this effect is fairly large. Thus the energy received by a spherical black body of radius s and distance a from the sun is

$$\frac{L_\odot}{4}\frac{s^2}{a^2}\,dt\,,$$

where $L_\odot$ is the energy per second radiated by the sun. Substituting for dt from the equation for the Poynting-Robertson effect for a circular orbit, namely,

$$dt = -\frac{8}{3L_\odot}\,\pi c^2 s \rho a\,da\,,$$

dividing by $\frac{4}{3}\pi\rho s^3$, and integrating gives $c^2/2$ in a_0/a for the energy per gram. Using 3 A.U. and 10^6 km as reasonable limits for a_0 and a gives 2.7×10^{21} ergs/gm. This is a very large energy requirement, which could be supplied only by the sun during times much greater than 10^9 years if masses of the order of the terrestrial mass or greater are to be removed and if only the energy from a narrow region of the sun is available. The Poynting-Robertson effect would furnish only an auxiliary mechanism for removal of solids.

The removal of dust particles by light-pressure under the conditions being considered, namely, mixtures of dust and gas, is a most involved process. Calculations based on simple models would be of most doubtful value. This is even more true for particle radiation, since we know so little about the mechanism by which high-velocity particles are produced by the present sun. Bierman (1951) estimates concentrations of 10^3–10^5 protons and electrons per cubic centimeter near the earth and velocities of 10^8 cm/sec. The high concentrations exist for only short periods of time. Using the lower number, the pressure produced by stopping these particles, ρv^2, is 1.6×10^{-5} dyne/cm^2, as compared to a solar light-pressure of 4.5×10^{-5} dyne/cm^2.

High-velocity particles are capable of accelerating individual atoms of high atomic weight to high velocities, though the probability of effective collisions of this kind is very small. Bierman finds that the material of comet tails is accelerated by particle radiation instead of light-pressure, and the dissipation of comet tails from a region of a low local gravitational field is very similar to the process considered in this paper for the dissipation of the solar nebula. However, to the extent that such dissipative processes were effective, they would carry away the smaller and lower-density silicate particles to a greater degree than the higher-density metallic particles.

Small dust particles would move with any hydrodynamic movement of the gas. The Reynolds' number is defined as $\rho v d/\eta$, where ρ is the density; v the velocity of flow, which is approximately the orbital velocity; d an appropriate linear dimension; and η the viscosity; the gas flow becomes turbulent when this number exceeds 100,000. With v equal to 3×10^6, d equal to 1 A.U. or 1.5×10^{13} cm, and η equal to 10^{-4} poise, the critical density is 2.5×10^{-19} gm/cm^3, and hence, until this density is reached, turbulent flow of gas will result. Ter Haar (1946) has discussed the turbulent dissipation of the solar nebula and estimates the time required as 1000 years, which, as he observes, seems to be very much too low. It should be noted that the presence of solid objects of such mass that they would not move with the gas would decrease the value of d by many orders of magnitude, and hence the loss of gas would not be so complete as estimated above. Ter Haar remarks that "the condensation into planets started at a time when there was a strong interaction between the solar envelope and the surrounding interstellar gas, so that the dissipation process was counteracted by a replenishing of matter from the surrounding interstellar medium." Although we tend to describe these processes in successive stages, the actual course of events was continuous, and hence dissipation began before the solar nebula was formed. Chandrasekhar (1946) shows that small dust particles will move with turbulent gases and thus be carried with high velocity to large objects not moving with the gas. He estimates that the time of accretion of planetary bodies may be some 10^7 years. Chandrasekhar's mechanism might apply to the accumulation of comets and the primary objects discussed here. For our present purposes, we note that the turbulent gases would also carry off the particles of lower density and smaller size and hence would remove silicate rather than metallic particles as the gas was moved toward the sun or to infinity, as postulated in the discussions on the turbulent gas nebula.

Many factors might have occurred which would influence the rate of removal of debris from the solar-disk nebula, such as (1) the intensity of sunlight as influenced by the luminosity of the sun and absorption by intervening materials, (2) the size of the particles and their densities, and (3) the condensation of water or other low-density substances on the more dense particles. Such condensation would have occurred at great distances from the sun, and the density of such condensed materials may have been very low indeed. Also the planets were presumably growing, and a competition among these processes must have taken place. If the suggestion of this paper is correct, the distribution of mass among the planets and the asteroidal belt very probably was influenced in an important way by these dissipative processes.

Maxwell discussed the stability of the rings of Saturn in a classical paper. He considered no forces which would degrade energy to heat and found that the rings would be stable. If gas were present or if the particles contained metal and thus were magnetic and conductors and a solar magnetic field existed, frictional forces would be present, and under these conditions the rings would probably not be stable and the particles would eventually touch one another. Within the Roche limit they would separate again unless the physical strength of the body was sufficient to prevent disruption by tidal forces. Thus the rings of Saturn would be stable, i.e., the particles would not coalesce, but similar rings outside the Roche limit would most probably agglomerate. It is often suggested that a satellite or satellites moved within the Roche limit and broke up to form the rings. Is it not possible that the satellites outside this limit accumulated from fine material and that the rings represent the more primitive situation? It is this latter possibility which is being considered here. The carbonaceous chondrites contain appreciable quantities of water, and collisions between such objects would produce gases. Thus a continuous production of gases and their removal would provide frictional forces and at the same time sweep out the inert gases from the region of the terrestrial planets.

For a number of years the writer has been troubled by difficulties in securing a satisfactory model for the problems discussed in this paper using the Kuiper (1951) protoplanet model. The problems briefly are as follows: (1) the removal of the inert gases, especially xenon, from the earth requires that gases be removed while the mass of the earth was distributed over a large volume and thus solid masses must have been distributed in this way within the protoplanet; (2) in order to secure a high temperature so that some of the silicates were volatilized, namely, some 2500° K at the center of the protoplanet, the ratio of mass to radius must have been one-quarter the present ratio for the earth, as is easily calculated from Emden's tables for a sphere of polytropic index 2.5, i.e., hydrogen gas; (3) the escape energy for this sphere is one-quarter that of the earth, and it is not evident that there is any feasible way for removing xenon from its surface, while the removal of silicate dust presents an even greater problem; and (4) the process must have been accomplished quickly in order that the high temperatures did not completely volatilize the solid planetesimals within which the more volatile elements were assumed to have been preserved (Urey 1954). It is difficult to prove that some possible combination of events could not have met these conditions. Perhaps gases and solids were lost in some way because of rotation, but surely no convincing discussion has been presented. A high-temperature sun of great luminosity for a brief period of time due to the early thermonuclear reaction of deuterium or helium of atomic weight 3 has often been thought of by the writer as a possible solution to these problems. The writer has found it necessary to retain the protoplanet model because no other source of high temperature for producing the minerals of the meteorites had been suggested, even though this model had these serious difficulties. However, the model suggested in this paper does not present these difficult problems, since it postulates the removal of gas and solids before any protoplanet structure was formed.

It has been evident to all students from Galileo to the present that the satellite systems of the major planets are very similar in structure to the solar system and that it seems reasonable to expect that a similar mechanism of formation should apply. Jeans (1929) says: "Each of these small systems is so exact a replica in miniature of the solar system that no suggested origin for the main system can be accepted unless it can account equally for the smaller planetary systems; any hypothesis which assigned different origins to the main system and the subsystems would be condemned by its own artificiality." Yet he proposes a gravitational instability of a gaseous medium as the mechanism for the formation of the planets and concludes that the asteroids and the satellites of Saturn must have been liquid or solid from birth; thus he used quite different mechanisms for the solar and satellite systems. The protoplanet hypothesis of Kuiper cannot be applied to these small satellites of the major planets because their masses are much too small to retain any gaseous envelope and hence their nearly circular orbits and the regular spacing cannot have been produced by a protosatellite mechanism. On the other hand, the writer sees no compelling objection at the present time to the possibility of applying the ideas presented in this paper to the planets and asteroids as well as to the satellites of the major planets.

Herbig (1954) has made an intensive study of the T Tauri stars in recent years and has pointed out that some of these stars are probably associated physically with the ζ Persei cluster of B-type stars which Blaauw (1952) has shown are not over 1.3×10^6 years old. These T Tauri stars are G to M dwarf-type stars imbedded in dust clouds and may well be the type of star being considered here. If this is the case, we are witnessing the dispersal of the solar nebulae of these stars. The bright-line spectra extend to considerable distances from these stars and show the bright lines of H I, Ca II, O II, and S II, indicating that some of the "non-volatile" elements, such as calcium, are dispersed as atoms and at least not entirely as dust particles.

The present suggested events for the origin of the solar system are not satisfactory in a number of ways. This model does not explain the presence of only one planet at each distance from the sun. This is the basis of the protoplanet model, but that model does not explain the spacings of the satellite systems. Also there is no satisfactory theory for the accumulation of either small or large objects in interstellar dust clouds, though the mechanisms involving turbulent gases as discussed by Chandrasekhar (1946) might be applicable. Also the turbulent gas mechanisms as oulined for the solar nebula by ter Haar and von Weizsäcker may furnish adequate mechanisms for the accumulation of satellites, asteroids, and planets.

Kuiper (1953) has proposed a mechanism for the accumulation of asteroids and satellites of the major planets other than the protoplanet mechanism. First, he assumes that objects some 50 km in radius accumulated by molecular condensation of silicate gas. (His only specification is a molecular weight of 50.) Then these objects accumulated, by some mechanism not further described, into objects of asteroidal dimensions. The first part of this proposal was first presented by Hoyle (1947). The condensation of supersaturated silicate gas on a few limited centers, some ten perhaps or even a hundred in the asteroidal belt, during 10^7 years is an impossible physical process. Supersaturated gases, except under very special conditions, condense to clouds of micron-sized particles in a fraction of a second. In no known way could supersaturated gases persist for long periods of time, especially in the presence of radioactive substances at the densities assumed. Dust is observed in interstellar space even at much lower densities. What we need is a mechanism for the accumulation of micron-sized dust particles into the primary objects and of the fragments present in the chrondrites into the secondary objects.

Schmidt (1944) has postulated solid objects as part of his theory for the formation of the solar system, though the theory of capture of objects by the sun was based on incorrect celestial mechanics. His formula for the accumulation of the planets has recently been derived again by Safranov (1954), who assumes that solid dust particles would behave like a gas, with the particles moving with random mean velocities of 10^5 cm/sec. Micron-sized silicate particles moving with such velocities would require the temperature to be 10^{14} °K. This makes this theory quite unacceptable. Yet the school of O. J. Schmidt has quite independently maintained for years that solids were an important part of the early history of the solar system, and with this general point of view this writer agrees. He has been aware of these suggestions, and yet, aside from the fundamental difficulties outlined above, he has not accepted them because they not only fail to account in any way for the properties of the meteorites but also in no way attempt to do so. Chemical substances and minerals have much more detailed properties than a mean molecular weight or a mean density, and these properties are often very informative and also very limiting as to postulates which can be made concerning their origins. I can think of no possible way to modify these suggestions to account for the properties of the meteorites except by a completely new approach to the problem, based on observational data, such as is attempted in this paper, rather than on simple theoretical calculations.

CONCLUSIONS

A series of events during the origin of the solar system has been postulated which accounts for at least some of the characteristics of meteorites and for the varying densities of the planets. It is suggested that objects of about asteroidal or lunar mass accumulated early in the history of the solar system. Two possible heating mechanisms are considered by which the minerals and metal phases of meteorites were produced, namely, chemical heating by free-radical reactions or heating by the fall of objects through gases. These primary objects were broken up in collisions and partially reaccumulated into secondary objects, probably of a class with the present asteroids. During the process of breakup and reaccumulation, fractionation of the silicate and metal phases occurred, with a preferential loss of silicate phases in varying degrees. This variable loss accounts for the variation in densities of the planets. The reaccumulation process probably was part of the general process of planet formation.

I am indebted to Professors J. E. Mayer, M. Goeppert Mayer, John Marshall, and Leona Marshall for reading the manuscript of this paper in several stages of preparation and for making very constructive suggestions in regard to it. I am indebted to Dr. T. Massalski for many informative discussions on the problems of the iron-nickel phases. I am also indebted to Miss Ann Pletinger for the X-ray investigation of the kamacite and taenite of the meteorites and to Mrs. Betty Nielson for the microscopic observations on this same material.

REFERENCES

Ahrens, L. H., Pinson, W. H., and Kearns, M. M. 1952, *Geochim. et cosmochim. acta*, **2**, 229.
Allen, D. W., and Jacobs, J. A. 1956, *Geochim. et cosmochim. acta*, **9**, 256–272, esp. 270.
Beck, C. W., Stevenson, R. G., and LaPaz, L. 1951, *Pop. Astr.*, **59**, 88.
Bierman, L. 1951, *Zs. f. Ap.*, **29**, 274.
Blaauw, A. 1952, *B.A.N.*, **11**, 405.

Chandrasekhar, S. 1946, *Rev. Mod. Phys.*, **18,** 94.

Donn, B., and Urey, H. C. 1956, *Ap. J.*, **123,** 339.

Edwards, G. 1955, *Geochim. et cosmochim. acta*, **8,** 285.

Edwards, G., and Urey, H. C. 1955, *Geochim. et cosmochim. acta*, **7,** 154.

Eucken, A. 1944, *Nachr. Akad. d. Wiss., Göttingen, Math.-phys. Kl.*, No. 1, pp. 8, 9.

Farrington, O. C. 1915, *Meteorites* (Chicago: The author).

Foote, W. M. 1912, *Am. J. Sci.*, **34,** 437.

Foshag, W. F. 1938, *Am. J. Sci.*, **35,** 374.

Geiss, J. 1956, unpublished data.

Gerling, E. K., and Rik, K. G. 1955, *Doklady Akad. Nauk, U.S.S.R.*, **101,** 433.

Haar, D. ter, 1950, *Ap. J.*, **111,** 179.

Henderson, E. P., and Perry, S. H. 1954, *Geochim. et cosmochim. acta*, **6,** 221–241.

Herbig, G. H. 1954, *Pub. A.S.P.*, **66,** 19; *Ap. J.*, **119,** 483.

Hoyle, F. 1947, *M.N.*, **106,** 406.

Jeans, J. 1949, *Astronomy and Cosmogony* (Cambridge: At the University Press), p. 406.

Jerofejeff, M., and Latschinoff, P. 1888, *Verk. Russ. Min. Gesellsch. St. Petersburg*, **24,** 263.

Kelley, K. K. 1949, *Contributions to Data on Theoretical Metallurgy* (Bur. of Mines Bull. 476).

Kuiper, G. P. 1951, *Astrophysics*, ed. J. A. Hynek (New York: McGraw-Hill Book Co.), chap. viii.

———. 1953, *Proc. Nat. Acad. Sci.*, **39,** 1159.

———. 1954, *ibid.*, **40,** 1101.

Kunz, G. F. 1888, *Science,* **11,** 118.

———. 1890, *Am. J. Sci.*, **40,** 318.

Oort, J. H., and Spitzer, L., Jr. 1955, *Ap. J.*, **121,** 6.

Owen, E. A., and Liu, Y. H. 1949, *J. Iron and Steel Inst.*, **163,** 132–137.

Patterson, C. C. 1955, *Geochim. et cosmochim. acta*, **7,** 151. This work was first presented at a conference on the abundances of elements at Williams Bay, Wisconsin, September, 1953.

Perry, S. H. 1944, U.S. Nat. Museum Bull. 184.

Platt, J. R. 1956, *Ap. J.*, **123,** 486.

Prior, G. T., and Hey, M. H. 1953, *Catalogue of Meteorites* (London: British Museum).

Rankama, K., and Sahama, Th. G. 1950, *Geochemistry* (Chicago: University of Chicago Press), p. 159.

Rossini, F. D., Wagman, R. D., Evans, W. H., Levine, S., and Jaffe, I. 1952, *Selected Values of Chemical Thermodynamic Properties* (Nat. Bur. Standards Circ. 500).

Safranov, W. S. 1954, *Astr. J. U.S.S.R.*, **31,** 499.

Sandberger, F. von 1889, *Neues Jahrb. Min.*, **2,** 173.

Schmidt, O. J. 1944, *Rept. Acad. Sci. U.S.S.R.*, **45,** 245–249, and a number of later papers. See "Les Particles solides dans les astres," *6th Liège Colloquim, Mem. Soc. Roy. des Sci d'Liège*, 4th Ser., **15,** 638.

Schumacher, E. 1956, *Helvet. chim. acta*, **39,** 531, 538; *Zs. f. Naturforsch.*, **11a,** 206.

Smith, W. Campbell. 1950, *Adv. Sci.*, **7,** 143–153.

Strömgren, B. 1954, *Mem. Soc. Roy. des Sci. Liège*, 4th Ser., **15,** 624.

Turkevich, A., Reed, G., and Hamaguchi, H. 1956, private communication.

Uhlig, H. H. 1954, *Geochim. et cosmochim. acta*, **6,** 282.

———. 1955, *ibid.*, **7,** 34.

Urey, H. C. 1952, *The Planets* (New Haven: Yale University Press).

———. 1954, *Ap. J. Suppl.*, **1,** 147–173.

Urey, H. C., and Craig, H. 1953, *Geochim. et cosmochim. acta*, **4,** 36–82.

Urey, H. C., and Donn, B. 1956, *Ap. J.*, **124,** 307.

Wasserburg, J. G., and Hayden, R. J. 1955, *Phys. Rev.*, **97,** 86.

Weizsäcker, C. F. von. 1944, *Zs. f. Ap.*, **22,** 319.

West, C. A. 1950, *Phys. Rev.*, **79,** 601.

Wyatt, S. P., Jr., and Whipple, F. L. 1950, *Ap. J.*, **111,** 134.

NOTE ON THE HIGH RELIEF OF THE LUNAR MARIA

E. R. DuFresne
Department of Chemistry, University of Chicago

Received October 30, 1955; revised May 24, 1956

ABSTRACT

Contemporary statistical methods have been applied to older determinations of absolute elevations of numerous points on the lunar surface. Analysis shows that there is an unexpected component of variability in the marine points which appears to be an actual relief or undulation of the surface of the maria rather than observational error. The over-all marine relief is found to be probably equal to, or greater than, the upland relief.

Baldwin (1949) has brought forward as part of a larger work an analysis of data obtained by Franz (1889) and Saunder (1905) on the height of the "tidal bulge" of the moon. These data he expressed as altitudes relative to a fictitious spherical surface, plotted against the fractional radius of the moon projected on the plane of the sky. The height of the bulge was determined from those curves, corrected for ellipticity, which best fitted the plotted data. Baldwin found that the scatter of the data could be markedly reduced by discriminating between sea and land points and referring them to separate curves. However, as Baldwin notes, the scatter of the maria points about their curve is much greater than the deviation of the land points from their own. Indeed, there are many maria points lying above the mean of the land data and one maria point which is higher than any of the land elevations.

To test the hypotheses (I) that the bulge values result from a chance combination of observational errors and (II) that there is no essential difference between the errors of and information provided by the land and sea data, the writer made a statistical analysis of the data as presented in the original literature. As a simplification, linear regression and correlation techniques were employed, terms of higher order not being justified by the precision of the data. Certain points, such as Ptolemaeus A (a crater within a crater) and Laplace *A* (the grand peak on Prom. Laplace) were discarded for obvious topographic reasons. All points were checked against maps and photographs for suitability. The main work was concentrated on the Franz (1889) data, Saunder's data being scanty and confined to a limited region of the moon's surface. Pooling of the data does, however, give results substantiating the analysis of the Franz data alone.

When the least-squares or Gaussian "best" lines for the graphs of altitude versus map radius are determined for Franz's land and maria data, it is found that the slopes differ markedly, the slope for the land being roughly double that for the maria. The equations are

$$E_L = 143.1 - 179.6\rho \quad \text{and} \quad E_M = 14.07 - 95.77\rho ,$$

where E stands for elevation in units of 10^{-5} lunar radii, measured from the same base sphere, and ρ stands for projected or map radius in units of one lunar radius, measured from the center of the visible disk. The probability that these slopes could have arisen by the null or chance hypothesis (I above) can be evaluated from the calculated values of Pearson's correlation coefficient, r, which are -0.6151 for the land areas and -0.1808 for the marine, the number of data being twenty-seven and thirty-one, respectively. The two-tailed test with Fisher's z-transformation shows that there is less than one chance in a thousand that the land value would arise purely by random error, while the marine value might be expected to arise so three times in ten in the long run.

As a check on the appropriateness of correlation methods in this case, the problem may be treated as one in regression, and confidence limits for slope constructed. If symmetrical limits are chosen with a 95 per cent probability of finding the true slope values between them, they are found to be

$$\text{Land: } -274.4 \text{ and } -84.6; \quad \text{Maria: } -294.3 \text{ and } +102.5 .$$

Thus a line with slope = 0 runs well within the confidence limits for the maria regression line, yet outside the limits for the land.

This astonishing difference in the precision of the slope estimates calls for a test of the hypothesis (II) that the observational situation is the same in both cases. The scatter of the data, when expressed as the variance (mean-square deviation), may be partitioned into two fractions, one corresponding to the interdependency of elevation and map radius, the other to the perturbing factors (expressed as the vertical scatter about the "best" line). The total variance is the sum of these two, variances being additive. The variances due to perturbing factors may then be compared in Snedecor's F-test by taking the ratio $F = \mathrm{Var}_{(\mathrm{maria})}/\mathrm{Var}_{(\mathrm{land})}$. This equals 2.670, with 29 and 25 degrees of freedom, respectively; such a large ratio would arise less than 1 per cent of the time in a large number of comparable sets of observations if the perturbing factors were closely similar.

Large observational error alone cannot create this effect. If the observational error is roughly the same in both cases, then

$$\frac{\mathrm{Var}_{(\mathrm{maria})} - \mathrm{Var}_{(\mathrm{obs})}}{\mathrm{Var}_{(\mathrm{land})} - \mathrm{Var}_{(\mathrm{obs})}}$$

will increase over the observed ratio as $\mathrm{Var}_{(\mathrm{obs})}$ is increased from zero, giving correspondingly higher levels of significance. The larger the error, the stronger the real effect must be, to show through the curtain of poor observation.

If it could be shown that the observational component of variance is larger for the maria or could be expected to be so on a priori grounds, the foregoing would have little force. Franz unfortunately gives his data in the form of averages for each location rather than as individual observations, so that it seems impossible at this late date to get direct estimates of the observational variance on a comparable scale. Fortunately, an indirect estimate is possible, since some of Saunder's locations are coincident with locations observed by Franz in a later study (1901). There are fourteen such pairs of averages of observations, six in marine territory, seven on land, and one to be omitted. Both sets of pairs are susceptible to the technique called "two-way analysis of variance without replication," which sieves out systematic sources of variance, to yield a residual error variance. This residual is ideally the sum of a $\mathrm{Var}_{(\mathrm{obs})}$ and an interaction variance; however, it is a common practice in such cases to make the assumption that the interaction variance is negligible. This procedure gives two estimates in the ratio: $\mathrm{Var}_{(\mathrm{res,\ land})}/\mathrm{Var}_{(\mathrm{res,\ maria})} = 4.952$, with 6 and 5 degrees of freedom, a result which would arise only once in twenty times on the chance hypothesis. It may be concluded with some confidence that the maria data have been obtained with substantially *greater* precision than the land data, from which it follows that the unevenness of the marine surfaces is probably both real and large.

The estimates so obtained are essentially pooled averages of the errors of both Franz and Saunder rather than Franz's errors alone; so, although the result of the ratio test is pertinent, the analysis properly should not be carried to the point of estimating the scatter due to true relief. Yet it is possible to say qualitatively that the marine true relief is probably greater than the land true relief, or at least as large, and that the smoothness of marine surfaces conceals a hill-and-valley structure much too great to be explained by such ridges and steps as can be detected by shadows. Baldwin's hypothesis of intermarine variation in level can account for a part of the relief variance but seemingly cannot include more than a fraction; the intramarine remainder may take the form of "bosses" of such superficial smoothness as to make detection by shadows difficult. The maria thus do not necessarily represent the absence of features but features swamped by an imperfectly fluid, masking substance.

Urey (1956) has brought forward a modification of the very interesting and significant theory of Gold, who considers the maria to be primarily dust formations. Gold's idea that the dust is still unconsolidated and capable of large-scale movements under small forces is incompatible with the high relief found in this study; however, the relief is consonant with Urey's proposed alternative. If the marine material has been pulverized by the explosive collision of a planetesimal with the moon and deposited in the presence of a temporary atmosphere of water vapor released by the collision, as Urey suggests, the explanation of the relief is straightforward. The idea that older features have been covered unevenly with dust of substantial thickness is much more likely in the light of the results here presented than is the notion that the maria represent lava flows only. In his excellent work, Baldwin (1949, p. 213) develops the lava theory quantitatively in such a way as to show that a relatively high fluidity is required. Highly fluid lava, like fluid dust, is inconsistent with the apparent magnitude of the relief, as it would wipe out the intramarine fraction of variance.

A seeming contradiction here is that the level of the maria is lower than that of the land, while a planetesimal collision suggests the addition of material. Certain points need to be kept in mind: In the presence of the differences in scatter and slopes of the curves, confidence limits for the difference in levels cannot be estimated with accuracy. Also, the maria data may themselves represent two types of locations, on Urey's hypothesis—those from the marine areas covering the explosion pits and those peripheral zones where features surviving the collision have been partially buried. The areas over explosion pits may be sufficiently low to bring down the marine average when the data are scanty and possibly selected with a bias in favor of the clearly marine character of locations near mare centers.

But even if the difference in levels is taken at face value, another explanation is possible. The violent release of energy involved in a mare-forming collision and the high temperatures of the steam produced suggest that the "cloud" rising from the explosion did not necessarily settle *in toto* but that a substantial portion may have escaped from the moon altogether. The collision may thus represent a net removal of material. Such an explanation requires no aid from hypothetical isostatic readjustments and hence avoids the problem of why the "tidal" bulge failed to sink at the time readjustments supposedly took place. Indeed, the moon may never have been warm enough for the fluid or plastic deformations necessary to isostasy; although the bulge exists, it is not plainly tidal in origin and may be merely the result of uneven accretion. A bulge so produced would eventually be pointed toward the earth regardless of the original orientation of the moon.

It is submitted that the problems posed by this analysis would justify a new attempt to collect data, with the advantages of contemporary instrumental and statistical techniques. If such observations are made, it is suggested that precautions be taken with respect to number of observations, randomization of location, reporting of repeated observations, and size of features studied, to insure that information is not needlessly thrown away. With the proper precautions, a modern study might well supply us with a substantiated theory of lunar origins.

The writer wishes to thank Mr. K. A. Brownlee, of the Committee on Statistics, for several very helpful suggestions and especially to express his deep indebtedness to Professor H. C. Urey for his encouragement, guidance, and criticism.

REFERENCES

Baldwin, R. B. 1949, *The Face of the Moon* (Chicago: University of Chicago Press), pp. 185 ff.; lava theory, pp. 213 ff.

Franz, J. 1889, *Die Konstanten der physischen Libration des Mondes* ("Astr. Beob. U.-Sternw. z. Königsberg," Abt. 38 [Königsberg: Leupold]).

———. 1901, *Mitt. Königl. U.-Sternw. zu Breslau*, Vol. 1 (Breslau). This comprises a study of measurements on 150 locations, but these were not reduced to elevations by Franz himself. Saunder (1905) reduced and reported the figures on 14 of these.

Saunder, S. A. 1905, *M.N.*, **65**, 458.

Urey, H. C. 1956, "The Origin of the Moon's Surface Features," *Sky and Telescope*, Vol. **15**, Nos. 3 and 4.

APPENDIX

TABLE 1

ALTITUDES AS GIVEN BY FRANZ (1889)

NAME (FRANZ)	NAME (NEISON)*	LOCATION		TYPE†	ALT.‡	MAP RADIUS§
		λ	β			
Grimaldi A		−71°	− 5°	L	− 41	0.95
Damoiseau D		−62	− 7	L	−110	.89
Grimaldi f	(Hermann)	−57	− 1	M	−147	.84
Pythagoras A	(in Babbage)	−53	+58	L	−112	.95
Fourier C		−51	−29	L	+ 47	.83
Flamsteed d		−45	− 3	M	−299	.71
Gassendi z		−43	−16	L	− 43	.71
Sharp A		−43	−48	L	−109	.87
Encke E		−40	0	M	−144	.64
Mare Humorum J	(Gassendi I)	−37	−22	M	+ 81	.67
Weigel A		−35	−57	L	+ 20	.90
Landsberg A		−31	0	M	−134	.52
Landsberg d		−30	− 3	M	−136	.50
Landsberg		−26	0	M	− 40	.44
Laplace *A*		−25	+45	Omit	−182	.77
Lubiniezky C	(G)	−20	−16	M	+115	.43
Gambert A	(Gambart A)	−19	+ 1	M	− 32	.33
Heinsius A		−16	−40	L	+129	.68
Parry A		−16	− 9	M	+124	.31
Mare Imbrium D	(Carlini D)	−16	+33	M	−171	.59
$\lambda = -15.5^\circ$, $\beta = 20^\circ$		−15	+20	M	−102	.42
Gambert B	(Gambart B)	−12	+ 2	M	−121	.21
Lalande A		−10	− 7	M	+ 17	.21
Thebit B		− 9	−22	M	+ 60	.40
Mösting c		− 8	− 2	M	−119	.14
Mösting A		− 5	− 3	L	+ 3	.11
Alphonsus *A*		− 3	−13	Omit	+ 61	.23
Herschel c		− 3	− 5	L	+130	.10
Bode		− 2	+ 7	L	+177	.12
Bode A		− 2	+ 9	L	+ 84	.16
Ptolomaeus A	(Ptolemaeus A)	0	− 9	Omit	− 20	.16
Sinus Medii B	(Bruce)	0	0	M	+ 1	.00
Triesnecker A	(Murchison A)	+ 1	+ 4	M	+ 47	.07
Airy Randkrater		+ 5	−18	L	+ 43	.32
Rhäticus A		+ 5	+ 1	M	− 91	.10
Hipparchus E		+ 7	− 3	L	+127	.13
Hyginus		+ 7	+ 8	M	+ 65	.17
Manilius D		+ 7	+13	M	− 13	.25
Boscovich A		+11	+ 9	L	+193	.25
Linné e		+11	+30	M	− 38	.53
Linné		+12	+27	M	−201	.50
Silberschlag a		+13	+ 7	L	− 1	.25
Dionysius A	(Cayley)	+15	+ 4	L	+131	.27
Menelaus		+15	+16	Omit	− 30	.38
Bessel e		+15	+20	M	− 74	.42
Sacrobosco A		+16	−24	L	+129	.48
Buch γ		+18	−40	L	+123	.68
Büsching C		+20	−37	L	+ 59	.66
Ross A	(Maclear)	+20	+10	M	+120	0.39

---

* Names from Neison's *The Moon* have been given whenever it seemed that the discrepancy was greater than could be accounted for by language differences. There are typographical errors both in this column and in the location column of the source; these last are always in the sign, but not in the magnitude, of the co-ordinates and have been corrected here.

† The decisions represented by this column were made by the writer while studying photographs, without regard to their effect on the analysis.

‡ Franz's figures in units of 10^{-5} lunar radii.

§ In units of 1 lunar radius as computed from the location figures.

TABLE 1—*Continued*

NAME (FRANZ)	NAME (NEISON)*	LOCATION		TYPE†	ALT.‡	MAP RADIUS§
		λ	β			
Taquet A.		+20	+14	M	+172	0.41
"Bergspitze"		+23	−47	L	+ 56	.78
Lacus Mortis B	(Bürg B)	+23	+43	L	+ 14	.74
Nicolai A.		+24	−42	L	+ 95	.73
Plinius A.	(Dawes)	+27	+17	M	− 91	.52
Jansen		+28	+11	M	+107	.52
Baily A.		+30	+49	M	+ 18	.82
Mare Tranquillitatis A.	(Cauchy)	+38	+10	M	+172	.63
Macrobius a		+40	+20	L	− 91	.69
Fabricius K		+42	−46	L	+ 28	.86
"Anonymus"		+45	−53	L	− 22	.90
Burckhardt G.		+47	+27	L	− 33	.79
Taruntius A.		+50	+ 8	M	+ 1	0.77

TABLE 2*

INTEROBSERVER COMPARISON AS GIVEN BY SAUNDER (1905)

Name (Saunder)	ξ	η	S	F	S−(F−170)	Type
Thebit A	−0.079	−0.368	− 11	+115	+ 44	M
Lalande D	− .119	− .097	−127	+171	−128	L
Hipparchus G	+ .129	− .088	− 18	+279	−127	L
Triesnecker B	+ .007	+ .020	+ 98	+193	+ 75	M
Triesnecker	+ .063	+ .073	+ 28	+247	− 49	M
Bode B	− .053	+ .152	+ 59	+148	+ 81	L
Archimedes A	− .098	+ .470	− 70	+189	− 89	L
Murchison A	+ .020	+ .070	+ 53	+160	+ 63	M
Ptolemaeus A	− .048	− .158	−148	+ 55	− 33	Omit
Herschel c	− .055	− .087	+ 54	+258	− 34	L
Mösting A	− .090	− .056	− 56	+105	+ 9	M
Rhäticus A	+ .091	+ .030	+ 24	+222	− 28	M
Bode	− .042	+ .117	+160	+136	+194	L
Bode A	−0.020	+0.156	+ 25	+172	+ 23	L

* All columns but the last have been copied from Saunder (1905). The last column shows decisions made on the same basis as before. S = Saunder's results; F = Franz's results reduced by Saunder. The figure 170 represents Saunder's a posteriori estimate of the difference in the reference spheres used by the two observers. The column "S − (F − 170)" may be used to form estimates of interobserver variance for land and sea, by the pooling method. Assuming these estimates proportional to the observational error variances, their ratio may be used as an approximation to the observational error variance ratio. However, the figure 170 may be challenged, and a reduction by one in the number of degrees of freedom for the pooled estimates seems called for.

The estimate ratio so calculated is $\text{Var}_{(\text{i obs, land})}/\text{Var}_{(\text{i-obs, maria})} = 5.00$ with $(7 - 1 = 6)$ and $(6 - 1 = 5)$ degrees of freedom, corresponding to a probability on the chance hypothesis of less than one in twenty. This may be compared with the result from the analysis of variance quoted in the present paper, bearing in mind that only the assumptions involved are apparently independent, not the data.

ON THE MOTIONS OF STARS IN AN ELLIPSOIDAL STELLAR SYSTEM*

GEORGE CONTOPOULOS
Laboratory of Astronomy of the University of Athens

Received February 17, 1956; revised May 1, 1956; revised August 8, 1956

ABSTRACT

The gravitational field and the motions of individual stars are studied for stellar systems in which the equidensity surfaces are similar ellipsoids, with the density varying according to a given law. The equations of motion are solved by the method of undetermined coefficients as well as by using a class of approximate osculating orbits. The variations of these osculating orbits are studied by the method of the "variation of constants."

INTRODUCTION

Many authors (Hubble 1930; Redman and Shirley 1938; Oort 1940; de Vaucouleurs 1948; Evans 1951) have noted that the isophotal curves of an elliptical nebula are ellipses having a common center and almost the same axis ratio. We therefore assume that the equidensity surfaces of the elliptical nebulae are also similar ellipsoids. Then the density of a nebula is a function of only one parameter, which defines the position of every star layer of equal density. The law which gives the variation of the density is taken to be an arbitrary function of this parameter. There are only a few restrictions for this function, derived from general considerations: namely, that the density is strongest at the center and diminishes outward, tending toward zero at great distances from the center. This distribution has the important property that it is projected into an elliptical distribution, whatever the density law (Contopoulos 1956).

When the density law is given, it is possible to derive the potential function of the nebula and the motions of stars in it. The most important case is when the equidensity surfaces are similar spheroids, a case which is believed to represent fairly well the forms of the elliptical nebulae.

A more general model would be composed of two or more superimposed ellipsoidal distributions of mass, with the same centers but different eccentricities, as in Oort's model of the Galaxy (Oort 1941), where as many as eleven homogeneous spheroids are considered, in addition to a "central mass." We shall not discuss this model, although it may be treated in a similar way.

THE POTENTIAL FUNCTION

Let the equidensity ellipsoids be similar to a basic ellipsoid with axes a, b, and c. If α, β, and γ are the axes of any equidensity ellipsoid, then

$$\frac{\alpha}{a}=\frac{\beta}{b}=\frac{\gamma}{c}=\sqrt{K}\,.$$

The density ρ will be a finite, continuous, and decreasing function of K for every $K > 0$; $\rho(K)$ may even be increasing or discontinuous, but it must be integrable from 0 to any $K > 0$.

---

* Published with the aid of a grant from the American Astronomical Society.

The components X, Y, and Z of the attracting force are the partial derivatives of the potential function.

$$U = -\pi G m a b c \int_0^\infty \frac{ds}{Q} \int_\infty^K \rho(K)\, dK \,, \tag{1}$$

where

$$K = \frac{x^2}{a^2+s} + \frac{y^2}{b^2+s} + \frac{z^2}{c^2+s} \tag{2}$$

and

$$Q^2 = (a^2+s)(b^2+s)(c^2+s) \,.$$

The integral $\int_\infty^K \rho(K)dK$ converges uniformly if the mass of the system is finite. Equation (1), already known in some special cases (Moulton 1935; Perek 1950, 1954), gives U as a continuous function of x, y, and z, provided that ρ is a continuous, or at least an integrable, function of K.

If $\rho(K)$ can be developed in a Taylor series we have

$$\rho(K) = \rho_0 + \rho_1 K + \ldots + \frac{\rho_\nu}{\nu!} K^\nu + \ldots \,. \tag{3}$$

Hence we derive

$$\begin{aligned} U - U_0 = -\pi G m \Big\{ & \rho_0 \left[A_{100}(x^2 - x_0^2) + A_{010}(y^2 - y_0^2) + A_{001}(z^2 - z_0^2) \right] \\ & + \ldots + \frac{\rho_{\nu-1}}{\nu!} \Sigma \frac{\nu!}{\kappa!\lambda!\mu!} A_{\kappa\lambda\mu}(x^{2\kappa} y^{2\lambda} z^{2\mu} - x_0^{2\kappa} y_0^{2\lambda} z_0^{2\mu}) + \ldots \Big\} \,, \end{aligned} \tag{4}$$

where

$$\kappa + \lambda + \mu = \nu \qquad \text{and} \qquad A_{\kappa\lambda\mu} = a b c \int_0^\infty \frac{ds}{Q(a^2+s)^\kappa (b^2+s)^\lambda (c^2+s)^\mu} \,.$$

It can easily be shown that U converges in at least the same region as $\rho(K)$.

If ρ = Constant (homogeneous ellipsoid), then

$$U - U_0 = -\pi G m \rho [A_{100}(x^2 - x_0^2) + A_{010}(y^2 - y_0^2) + A_{001}(z^2 - z_0^2)] \,, \tag{5}$$

and the equipotential surfaces are the ellipsoids

$$A_{100}x^2 + A_{010}y^2 + A_{001}z^2 = \text{Const.}, \tag{6}$$

with constant axis ratios

$$\sqrt{\left(\frac{A_{100}}{A_{010}}\right)} \quad \text{and} \quad \sqrt{\left(\frac{A_{100}}{A_{001}}\right)} .$$

In the case of an attracting mass consisting of different superimposed ellipsoids, as in Oort's model of the Galaxy, U is the sum of the potential functions corresponding to each ellipsoid. To calculate $A_{\kappa\lambda\mu}$ we use Jeans's (1928) relation,

$$A_{\kappa\lambda\mu} = \frac{1}{(a^2 - b^2)} [A_{\kappa-1,\lambda,\mu} - A_{\kappa,\lambda-1,\mu}] \,.$$

By successive reductions, the calculation of $A_{\kappa\lambda\mu}$ is reduced to A_{K00}, $A_{0\Lambda0}$, A_{00M} and, by partial integration, to the integrals A_{000}, A_{100}, A_{010}, and A_{001}. Mineur (1939) gives the values of $b_1' = 2A_{100}$, $b_2' = 2A_{010}$, and $b_3' = 2A_{001}$ for different ratios b/a and b/c.

When the ellipsoid is reduced to a spheroid ($a = b > c$), the foregoing formulae become

$$K = \frac{r^2}{a^2 + s} + \frac{z^2}{c^2 + s}$$

and

$$U - U_0 = -\pi G m \Big\{ \rho_0 \left[A_{10} (r^2 - r_0^2) + A_{01} (z^2 - z_0^2) \right] + \ldots + \frac{\rho_{\nu-1}}{\nu!} \Sigma \frac{\nu!}{m!n!} A_{mn} (r^{2m} z^{2n} - r_0^{2m} z_0^{2n}) + \ldots \Big\}, \tag{7}$$

where $m + n = \nu$ and

$$A_{mn} = a^2 c \int_0^{\infty} \frac{d s}{(a^2 + s)^{m+1} (c^2 + s)^{n+1/2}}. \tag{8}$$

TABLE 1

VALUES OF $a^2 A_{20}$, $a^2 A_{11}$, $c^2 A_{02}$ AS FUNCTIONS OF c/a

	c/a										
	0.0	0.1	0.2	0.3	0.4	0.5	0.6	0.7	0.8	0.9	1.0
$a^2 A_{20}$. . .	0.000	0.100	0.174	0.230	0.272	0.306	0.333	0.355	0.373	0.388	0.400
$a^2 A_{11}$. . . .	2.000	1.598	1.304	1.081	.910	.775	.668	.581	.509	.450	.400
$c^2 A_{02}$. . . .	0.667	0.656	0.632	0.602	0.570	0.537	0.506	0.477	0.449	0.424	0.400

We proceed to calculate A_{mn} in the same way as $A_{\kappa\lambda\mu}$. The result is

$$A_{mn} = \sum_{\nu=0}^{n-1} \frac{(-1)^{\nu}}{(a e)^{2(m+\nu)}} C_{m+\nu-1}^{\nu} A_{0,\, n-\nu} + (-1)^{n} \sum_{\nu=0}^{m-1} \frac{1}{(a e)^{2(n+\nu)}} C_{n+\nu-1}^{\nu} A_{m-\nu,\, 0},$$

where

$$A_{0\mathrm{N}} = \sum_{\nu=0}^{\mathrm{N}-1} (-1)^{\nu} \frac{2}{2\mathrm{N} - 2\nu - 1} \cdot \frac{1}{a^{2\nu} e^{2\nu+2} c^{2\mathrm{N}-2\nu-2}} + (-1)^{\mathrm{N}} \frac{2c}{a^{2\mathrm{N}-1} e^{2\mathrm{N}+1}} \sin^{-1} e$$

and

$$A_{\mathrm{M}0} = \frac{2c}{a^{2\mathrm{M}-1} e^{2\mathrm{M}+1}} \int_{c/ae}^{\infty} \frac{d\phi}{(1 + \phi^2)^{\mathrm{M}+1}}.$$

This last integral is easily expressed in terms of $\sin^{-1} e$, where $e = \sqrt{[(a^2 - c^2)/a^2]}$ is the eccentricity of the spheroid. For example,

$$A_{00} = \frac{2ac}{e} \sin^{-1} e, \qquad A_{10} = \frac{c}{a e^3} \sin^{-1} e - \frac{c^2}{a^2 e^2}, \qquad A_{01} = \frac{2}{e^2} - \frac{2c}{a e^3} \sin^{-1} e,$$

and so on. The values of $2A_{00}/a^2$, $2A_{10}$, and $2A_{01}$ for various c/a are given by Mineur (1939). Table 1 gives the values of $a^2 A_{20}$, $a^2 A_{11}$, and $c^2 A_{02}$ for some values of c/a.

If c/a is small (in Oort's spheroids c/a varies from 0.05 to 0.3), so that higher powers of c/a can be neglected, the foregoing formulae reduce to

$$A_{\mathrm{M}0} = \frac{c\pi}{a^{2\mathrm{M}-1}} \cdot \frac{(2\mathrm{M} - 1) \ldots 3.1}{2\mathrm{M} \ldots 4.2}, \quad A_{0\mathrm{N}} = \frac{2}{(2\mathrm{N} - 1)\, c^{2\mathrm{N}-2}}, \quad A_{mn} = \frac{2}{(2n - 1)\, a^{2m} c^{2n-2}}$$

or

$$A_{00} = a c \pi, \qquad A_{10} = \frac{c\pi}{2a}, \qquad A_{01} = 2, \qquad \text{etc.}$$

EQUATIONS OF MOTION

If we denote by $W = U/m$ the potential function per unit mass, the energy integral takes the form

$$v^2 = 2W(r, z) + H, \qquad \text{where} \qquad H = v_0^2 - 2W(r_0, z_0).$$

Since $W(\infty) = 0$, we know that if $H \geq 0$, the orbit extends to infinity, whereas if $H < 0$, it remains within a limited space.

If the system is spheroidal, the projection of the attracting force on the plane of symmetry is radial. Therefore, using cylindrical co-ordinates r, θ, and z, we find

$$r^2 \frac{d\theta}{dt} = C, \tag{9}$$

$$\frac{C^2}{r^2} + \left(\frac{dr}{dt}\right)^2 + \left(\frac{dz}{dt}\right)^2 = 2W(r, z) + H, \tag{10}$$

$$\frac{d^2 z}{dt^2} = \frac{\partial W}{\partial z}, \tag{11}$$

where C is the constant of areas of the projected motion.

The initial conditions for $t = 0$ are

$$\theta_0,\ r_0,\ \left(\frac{dr}{dt}\right)_0 = R_0,\ z_0, \qquad \text{and} \qquad \left(\frac{dz}{dt}\right)_0 = Z_0.$$

If we find the solution $r = r(t)$ and $z = z(t)$ of system (10) and (11), the equations of the orbit will be given by the formulae

$$\theta - \theta_0 = \int_{r_0}^{r} \frac{C\,dt(r)}{r^2} \qquad \text{and} \qquad z = z[t(r)],$$

where $t(r)$ is the inverse function of $r(t)$.

SOLUTION OF SYSTEM (10) AND (11)

If the potential function can be written as the sum of two functions of r and z, respectively, i.e., if $W = W_1(r) + W_2(z)$, the z-motions are independent of the motions parallel to the plane of symmetry. In this case

$$\frac{d^2 z}{dt^2} = \frac{dW_2(z)}{dz}.$$

Then

$$\left(\frac{dz}{dt}\right)^2 - Z_0^2 = 2W_2(z) - 2W_2(z_0);$$

hence

$$t = \int_{z_0}^{z} \frac{dz}{\sqrt{[2W_2(z) - 2W_2(z_0) + Z_0^2]}}.$$

Let the solutions of the equation $2W_2(z) - 2W_2(z_0) + Z_0^2 = 0$ be $\pm z_{\max}$ (W_2 is an even function of z, because it is symmetrical with respect to the plane Oxy). Then the period of oscillation, T, is given by

$$T = 2\int_{-z_{\max}}^{+z_{\max}} \frac{dz}{\sqrt{[2W_2(z) - 2W_2(z_0) + Z_0^2]}}.$$

If we make the approximation (Trumpler and Weaver 1953)

$$W_2(z) = W_2(0) + W_2''(0)\frac{z^2}{2!},$$

then

$$z_{\max}^2 = -\frac{Z_0^2}{W_2''(0)} \qquad [W_2''(0) < 0, z_0 = 0],$$

and

$$z = z_{\max} \sin\{ t \sqrt{[-W_2''(0)]} \}.$$

We also find that

$$T = 2\pi \sqrt{\left[\frac{-1}{W_2''(0)}\right]}$$

and

$$\frac{C^2}{r^2} + \left(\frac{dr}{dt}\right)^2 = 2W_1(r) + h,$$

where $h = H + 2W_2(z_0) - Z_0^2$. Thus the projection of the orbit on the plane of symmetry is a known curve (Contopoulos 1954). It must be noted, however, that the assumption that $W(r, z)$ is the sum of a function of r and a function of z holds only as an approximation for small values of z and nearly circular orbits.

The accurate solution of system (10) and (11) can be obtained by the method of successive approximations (Goursat 1949) or by the method of undetermined coefficients. We will follow this second method here.

Let r and z be given by the series

$$r = r_0 + R_0 t + r_2 t^2 + \ldots \quad \text{and} \quad z = z_0 + Z_0 t + z_2 t^2 + \ldots .$$

The equations of motion are then written as follows:

$$\begin{aligned}\left(-\frac{2C^2R_0}{r_0^3} + 4R_0 r_2 + 4Z_0 z_2\right) t + \Big[\frac{C^2}{r_0^4}(3R_0^2 - 2r_0 r_2)& \\ + 6R_0 r_3 + 4r_2^2 + 6Z_0 z_3 + 4z_2^2\Big] t^2 + \ldots& \\ = -2\pi G \Big\{ \rho_0 [A_{10}(2r_0R_0t + \ldots) + A_{01}(2z_0Z_0t + \ldots)] + \frac{\rho_1}{2}[A_{20}(4r_0^3R_0t + \ldots)& \\ + 2A_{11}\{2(r_0z_0^2R_0 + r_0^2z_0Z_0)t + \ldots\} + A_{02}(4z_0^3Z_0t + \ldots)] + \ldots \Big\}&\end{aligned} \tag{12}$$

and

$$\begin{aligned}&2z_2 + 6z_3t + 12z_4t^2 + \ldots \\ &\quad = -2\pi G(z_0 + Z_0t + z_2t^2 + \ldots)\Big\{\rho_0 A_{01} + \frac{\rho_1}{2}[2A_{11}(r_0^2 + 2r_0R_0t + \ldots) \\ &\qquad + 2A_{02}(z_0^2 + 2z_0Z_0t + \ldots)] + \ldots\Big\}.\end{aligned} \tag{13}$$

From these two equations we find

$$z_2 = -\pi G z_0 [\rho_0 A_{01} + \rho_1 (A_{11} r_0^2 + A_{02} z_0^2) + \ldots]$$

$$r_2 = \frac{C^2}{2r_0^3} - \pi G r_0 [\rho_0 A_{10} + \rho_1 (A_{20} r_0^2 + A_{11} z_0^2) + \ldots]$$

$$z_3 = -\frac{\pi G}{3}\,[Z_0\{\rho_0 A_{01} + \rho_1 (A_{11} r_0^2 + A_{02} z_0^2) + \ldots\}$$

$$+ 2\rho_1 z_0 (A_{11} r_0 R_0 + A_{02} z_0 Z_0) + \ldots] , \qquad \text{etc.}$$

so that

$$r = r_0 + R_0 t + \left(\frac{C^2}{2 r_0^3} - \pi G \rho_0 A_{10} r_0 + \ldots\right) t^2 + \ldots \tag{14}$$

and

$$z = z_0 + Z_0 t - \pi G z_0 (\rho_0 A_{01} + \ldots) t^2 + \ldots . \tag{15}$$

Whenever $z_0 = 0$, we also have $z_2 = 0$, which expresses the known fact that for $z_0 = 0$ the force in the z-direction is zero. Under these conditions,

$$z_3 = -\frac{\pi G}{3} Z_0 (\rho_0 A_{01} + \rho_1 A_{11} r_0^2 + \ldots) , \qquad \text{etc.},$$

and

$$z = Z_0 t - \frac{\pi G}{3} Z_0 (\rho_0 A_{01} + \ldots) t^3 + \ldots .$$

We notice that the coefficients r_2, z_2, r_3, and z_3 can be calculated approximately by means of the initial conditions (r_0, R_0, z_0, Z_0) and the constants ρ_0, ρ_1, and $A_{ij}(i + j = 1, 2)$. Thus, if the coefficients ρ_0 and ρ_1 are known, we can, by means of Mineur's tables and Table 1 of this paper, calculate the motion of the star with an accuracy of at least the third order in t.

In our Galaxy the following data have been used: $a = 15$ kpc, $c = 2.5$ kpc, $c/a = 0.17$, $A_{10} = 0.21$, $A_{01} = 1.57$, $a^2 A_{20} = 0.15$, $a^2 A_{11} = 1.40$, and $c^2 A_{02} = 0.66$. We also take $\rho_0 = 22.4 \times 10^{-24}$ gm/cm^3 and $\rho_1/a^2 = \lim \Delta\rho/(r^2 - r_0^2) \simeq -0.25 \times 10^{-24}$ gm/cm^3/kpc^2 (cf. Kwee, Muller, and Westerhout 1954).

APPROXIMATE ORBITS

Instead of this general method for the determination of the orbits, another method can be used, when the z-motions are relatively small. We may call it the "method of the approximate orbits." The equations,

$$\frac{C^2}{r^2} + \left(\frac{dr}{dt}\right)^2 + Z_0^2 = 2W(r, z_0) + H \qquad \text{and} \qquad r^2 \frac{d\theta}{dt} = C \tag{16}$$

define the osculating orbit, i.e., for $t = 0$, the two orbits are tangential and have the same initial velocities.

Let $r = r_a(t)$ be the solution of this equation (Contopoulos 1954). The difference between this solution and the true solution $r(t)$ is of the third order in t:

$$r(t) - r_a(t) = -\tfrac{2}{3}\pi G \rho_1 A_{11} r_0 z_0 Z_0 t^3 + \ldots . \tag{17}$$

This difference is negligible when the z-co-ordinate and velocity are small. If $r_0 = 8.2$ kpc, $z_0 = 0.5$ kpc, and $Z_0 = 10$ km/sec, it is

$$\Delta r(t) \simeq 2 \times 10^{-21} t^3 \text{ pc} ,$$

where t is measured in years. In 10^7 years this difference is only $\Delta r \simeq 2$pc.

Whenever $z_0 = 0$, the difference is of the fourth order, and

$$r(t) - r_a(t) = -\tfrac{1}{6}\pi G \rho_1 A_{11} r_0 Z_0^2 t^4 + \ldots . \tag{18}$$

For $r_0 = 8.2$ kpc and $Z_0 = 10$ km/sec, we have

$$\Delta r\ (t) \simeq 8 \times 10^{-30} t^4 \text{ pc},$$

i.e., in 10^7 years this difference becomes $\Delta r = 0.08$ pc.

If the approximate value $r = r_a(t)$ is now inserted in equation (11), we find an approximate solution $z = z_a(t)$ for z, accurate to the fourth order in t. The difference between $z(t)$ and $z_a(t)$ is

$$z\ (t) - z_a\ (t) = \tfrac{2}{15} \pi^2 G^2 \rho_1^2 A_{11}^2 r_0^2 z_0^2 Z_0 t^5 + \ldots . \tag{19}$$

For $r_0 = 8.2$ kpc, $z_0 = 0.5$ kpc, and $Z_0 = 10$ km/sec,

$$\Delta z\ (t) \simeq 10^{-37} t^5 \text{ pc},$$

and in 10^7 years $\Delta z \simeq 0.01$ pc.

Whenever $z_0 = 0$, the difference is of the seventh order:

$$z\ (t) - z_a\ (t) = \tfrac{1}{63} \pi^2 G^2 \rho_1^2 A_{11}^2 r_0^2 Z_0^3 t^7 + \ldots . \tag{20}$$

For these data, $\Delta z(t) \simeq 6 \times 10^{-55}\ t^7$ pc, and in 10^7 years this difference is only $\Delta z \sim 6 \times 10^{-6}$ pc.

If a higher approximation is desired, we may insert the expression $z = z_a(t)$ instead of $z = z_0$ in equation (12), and we will have a solution for r accurate to at least the fourth order in t, and so on.

Let us now compare these results with the approximation obtained by Oort (Oort 1932; Smart 1938) in his study of the z-motions of the stars near the sun. Oort assumes $r = r_0$; in this case equation (11) is easily integrated. Let $z = z_b(t)$ be the solution of this equation. It can be shown that this solution is generally accurate only to the second order in t, and the difference between this solution and $z(t)$ is

$$z(t) - z_b(t) = -\tfrac{2}{3} \pi G \rho_1 A_{11} r_0 z_0 R_0 t^3 + \ldots . \tag{21}$$

If $r_0 = 8.2$ kpc, $z_0 = 0.5$ kpc, and $Z_0 = 10$ km/sec, then

$$\Delta z(t) \simeq 2 \times 10^{-21}\ t^3 \text{ pc},$$

i.e., $\Delta z \simeq 2$ pc in 10^7 years.

If $z_0 = 0$, the difference is of the fourth order in t:

$$z(t) - z_b(t) = -\tfrac{1}{3} \pi G \rho_1 A_{11} r_0 R_0 Z_0 t^4 + \ldots . \tag{22}$$

For $r_0 = 8.2$ kpc and $R_0 = Z_0 = 10$ km/sec, this gives $\Delta z \simeq 0.2$ pc in 10^7 years.

If $R_0 = 0$, the difference is again of the fourth order:

$$z(t) - z_b(t) = -\tfrac{1}{3} \pi G \rho_1 A_{11} r_0 z_0 r_2 t^4 + \ldots . \tag{23}$$

For $r_0 = 8.2$ kpc, $z_0 = 0.5$ kpc, and $\Theta_0 = 250$ km/sec, it is $C = r_0 \Theta_0 = 2 \times 10^3$ kpc/km/sec, $r_2 \simeq 2 \times 10^{-28}$ pc/sec^2, and $\Delta z(t) \simeq 2 \times 10^{-29}\ t^4$ pc, i.e., $\Delta z \simeq 0.2$ pc in 10^7 years. It is only when $z_0 = R_0 = 0$ that the difference is of the fifth order:

$$z(t) - z_b(t) = -\tfrac{1}{5} \pi G \rho_1 A_{11} r_0 r_2 Z_0 t^5 + \ldots . \tag{24}$$

For the foregoing data $\Delta z(t) \simeq 2.5 \times 10^{-37}\ t^5$ pc. In 10^7 years $\Delta z \simeq 0.025$ pc. Therefore, this method always gives a better approximation than Oort's for the orbits of the stars in a galaxy.

PERTURBATIONS

The theory of perturbations of planetary orbits can be extended to cases where the osculating orbit is not a conic but a curve of another special family. In this paper the osculating orbit is defined by equations (16), where z_0 and Z_0 are the position and velocity at a given moment. The osculating orbit is tangent to the projection of the real orbit and has the same initial velocity; it coincides quite closely with the projection of the star's orbit and osculates as the ordinate z and the velocity Z vary with the time.

For computing the rate of change of the osculating orbit, we can use the method of "variation of constants" of the theory of perturbations. The canonical constants of the plane motion are (Chazy 1953)

$a_1 = -h$ (h = energy per unit mass); $a_2 = C$ (constant of areas) ;

$b_1 = \tau$ (perigalacticon transit time); $b_2 = g$ (longitude of perigalacticon) .

This equation of the osculating orbit is

$$\frac{C^2}{r^2}+\left(\frac{dr}{dt}\right)^2 - 2W_0 = H - Z_0^2 = 2h\,,$$

where we have substituted W_0 for $W(r, z_0)$. If we let R be the perturbation function,

$$R = W(r, z) - W(r, z_0)\,, \tag{25}$$

we have the following equations (Chazy 1953):

$$\frac{d(-h)}{dt} = \frac{\partial R}{\partial \tau}, \qquad \frac{dC}{dt} = \frac{\partial R}{\partial g}, \qquad \frac{d\tau}{dt} = -\frac{\partial R}{\partial(-h)}, \qquad \frac{dg}{dt} = -\frac{\partial R}{\partial C}, \tag{26}$$

and, as the perturbing force

$$F = \frac{dW(r, z)}{dr} - \frac{dW(r, z_0)}{dr} \tag{27}$$

is central, equations (26) become

$$\frac{dh}{dt} = -F\frac{\partial r}{\partial \tau}, \qquad \frac{dC}{dt} = F\frac{\partial r}{\partial g}, \qquad \frac{d\tau}{dt} = F\frac{\partial r}{\partial h}, \qquad \frac{dg}{dt} = -F\frac{\partial r}{\partial C}. \tag{28}$$

But

$$t - \tau = \int_{r_1}^{r} \frac{r\,dr}{\sqrt{\phi(r)}}\,,$$

where

$$\phi(r) = (2W_0 + 2h)r^2 - C^2\,, \tag{29}$$

i.e., r is a function of the constants τ, h, and C but not of g. Therefore,

$$\frac{\partial r}{\partial \tau} = -\frac{dr}{dt} = -\frac{\sqrt{\phi(r)}}{r}\,, \qquad \frac{\partial r}{\partial g} = 0\,, \quad \text{etc.},$$

and, finally,

$$\frac{dh}{dt} = F\frac{\sqrt{\phi(r)}}{r}\,, \qquad \frac{dC}{dt} = 0\,, \qquad \text{etc.} \tag{30}$$

As C is constant, the ellipticity of the system has no effect upon the constant of areas of the projected motion.

We also have

$$F = \frac{\partial (W - W_0)}{\partial r} + \frac{\partial (W - W_0)}{\partial z} \frac{d z}{d r},$$

where z is replaced by the approximate value $z = z_a[t_a(r)]$, $t_a(r)$ being the inverse function of $r_a(t)$. Since

$$\frac{d z}{d r} = \frac{d z / dt}{d r / dt} = \frac{Z_0 + 2 z_2 t + \ldots}{R_0 + 2 r_2 t + \ldots},$$

we may write

$$F = -2\pi G \frac{Z_0}{R_0} z_0 \rho_0 A_{01} + \ldots . \tag{31}$$

It is now possible to calculate the variation of the constants of the osculating orbit by means of equations (30) and (31), thus finding a better approximation for the motions of the stars in the system.

The perturbations which we have considered here are of a special kind. They are due to the ellipticity of the system, i.e., its departure from the spherical shape. There are many other kinds of perturbations; the encounters between stars, resistance of the interstellar material, etc. These must be treated separately.

REFERENCES

Chazy, Z. 1953, *Mécanique céleste* (Paris: Presses Universitaires), pp. 185–226.
Contopoulos, G. 1954, *Zs. f. Ap.*, **35**, 67.
———. 1956, *ibid.*, **39**, 126.
Evans, D. S. 1951, *M.N.*, **110**, 526.
Goursat, E. J. B. 1949, *Cours d'analyse mathématique*, **2** (7th ed.; Paris: Gauthier Villars).
Hubble, E. P. 1930, *Ap. J.*, **71**, 231.
Jeans, J. H. 1929, *Astronomy and Cosmogony* (2d ed.; Cambridge: At the University Press).
Kwee, K. K., Muller, C. A., and Westerhout, G. 1954, *B.A.N.*, **12**, 211.
Mineur, H. 1939, *Ann. d'ap.*, **2**, 1.
Moulton, F. R. 1935, *An Introduction to Celestial Mechanics* (2d ed.; New York: Macmillan Co.).
Oort, J. H. 1932, *B.A.N.*, **6**, 249.
———. 1940, *Ap.J.*, **91**, 273.
———. 1941, *B.A.N.*, **9**, 185.
Perek, L. 1950, *B. A. Czech.*, **2**, 75.
———. 1954, *Contr. Astro. Inst. Brno*, Vol. **1**, No. 13.
Redman, R. O., and Shirley, E. G. 1938, *M.N.*, **98**, 613.
Smart, W. 1938, *Stellar Dynamics* (Cambridge: At the University Press).
Trumpler, R. J., and Weaver, H. F. 1953, *Statistical Astronomy* (Berkeley and Los Angeles: University of California Press), pp. 613–615.
Vaucouleurs, G. de. 1948, *Ann. d'ap.*, **11**, 247.

AN F/2 CASSEGRAIN CAMERA*

A. B. MEINEL
Yerkes Observatory

Received June 22, 1956

ABSTRACT

A Cassegrain camera system to provide prime-focus performance at the Cassegrain focus has been constructed. Utilization of this camera with the 82-inch McDonald telescope and the 40-inch Yerkes refractor would indicate that this camera system could be used with advantage on many existing telescopes.

Many research programs in astronomy requiring direct photography are difficult to perform. The reasons for this arise from several different sources. In some cases it is a requirement of a large field of good definition. Large Schmidt telescopes provide excellent field characteristics combined with high optical speed; however, even the largest Schmidts suffer from a limited scale. In some cases the requirement is set by the desire to use small spectral ranges, such as for interference photography. In this case one is confronted by the necessity of using a filter of small size, up to about 6 inches in maximum diameter. If it is to be used with a large-scale telescope, then the filter must be in the converging beam of the telescope. For interference filters the shift in position of the transmission bands varies with inclination to the incident ray; consequently, the permissible *f*-ratio of the telescope is limited.

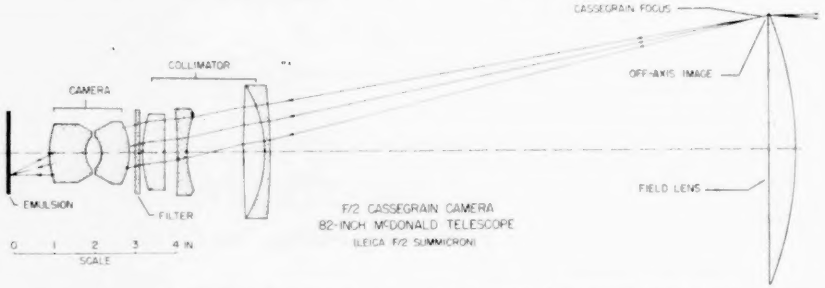

FIG. 1.—Diagram of the *F*/2 Cassegrain camera used on the 82-inch telescope. The Leica Summicron lens is schematically shown.

In the last few decades the prime-focus position has become popular; yet this popularity does not seem to be justified by a careful examination of the facts. The argument of efficiency and optical speed would be correct under idealized circumstances. It is necessary to note, however, that the prime focus cannot be used in practice without the addition of corrective systems. The small *f*-ratio of the prime focus results in a negligibly small field of good definition. To increase this field, a Ross-type corrector is generally employed, although other corrective systems can be substituted (Meinel 1953). The corrective systems, being made up of refractive elements, yield chromatic errors in both focus and geometrical aberration terms. Therefore, whenever positional accuracy is required, as in offset photometry, the corrector system must be used to give optical defini-

---

* This research has been supported in part by a grant from the Perkin-Elmer Corporation for research in optics.

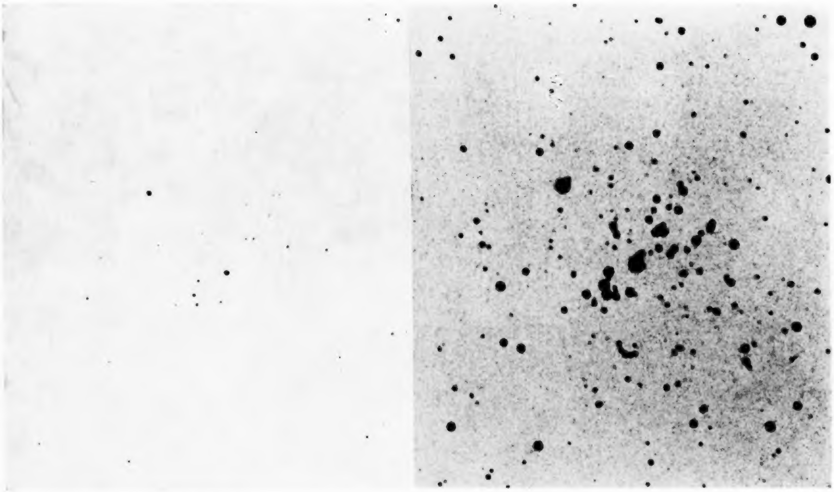

H PERSEI
1.0 min – 103*a*-G
Yerkes 40-inch
F/18

H PERSEI
1.0 min – 103*a*-G
Yerkes 40-inch
F/3

FIG. 2.—Comparative exposures on H Persei with the Yerkes 40-inch telescope at effective speeds of *F*/18 and *F*/3. For the same number of quanta the *F*/3 exposure reaches a much fainter limiting magnitude.

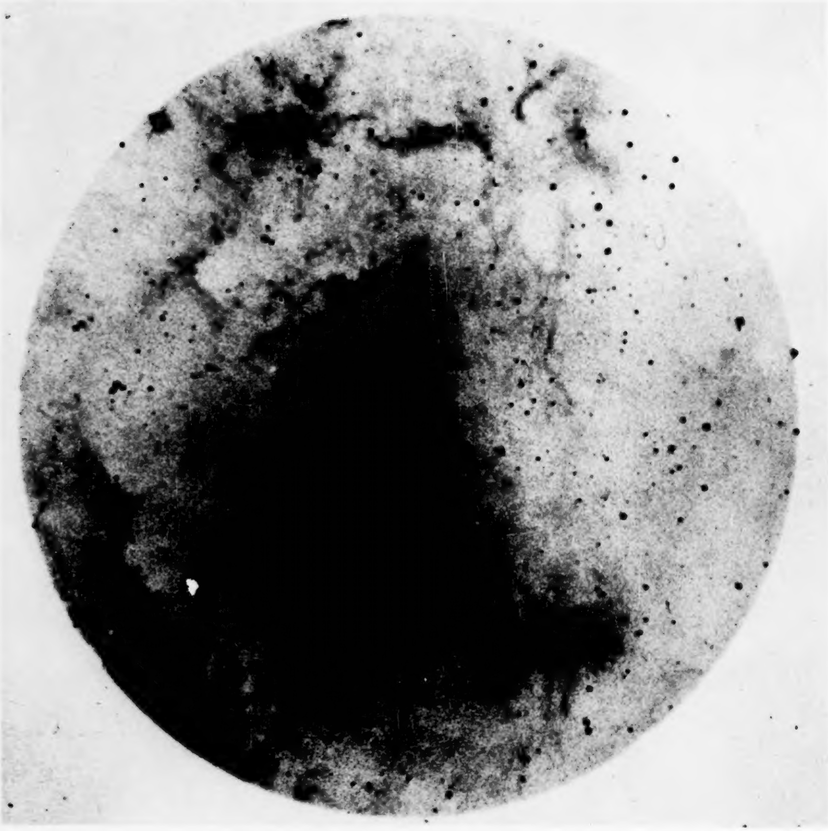

FIG. 3.—A 15-minute exposure, 103*a*-E + RG-2, on H II region 17^h16^m, $-34°8'$, by H. A. Abt with the 82-inch telescope at *F*/2, June 11/12, 1955.

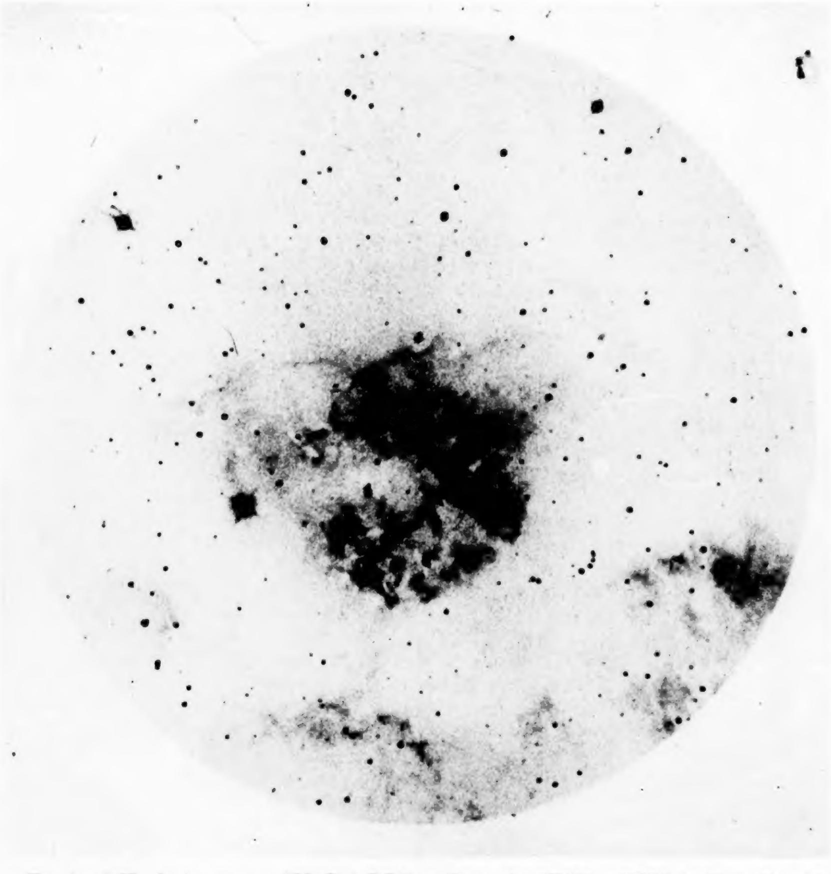

FIG. 4.—A 25-minute exposure, 103*a*-E + RG-2, on H II region 17^h22^m, $-34°20'$, by H. A. Abt with the 82-inch telescope, June 11/12, 1955.

tion for the field stars and to reproduce the same errors that were present in the reference photograph. The last requirement is only one of convenience, however, since H. L. Johnson has utilized 200-inch telescope plates for offset work at the 82-inch Cassegrain focus after applying correction terms for the field errors in the 200-inch photographs.

The other chief disadvantages to the prime focus are also consequences of the large angular convergence of the beam. In the case of spectrographs it is possible to obtain large-beam diameters with small collimator lengths, but the *f*-ratio makes it necessary to utilize a Newtonian collimator system, so that the reflective efficiency drops back to exactly the same value as if the Cassegrain focus of the telescope, with its less stringent space limitations, had been used. In the case of photoelectric photometry the large angular convergence makes it difficult to form an exit pupil point on the cathode of any tube other than end-on cathode tubes. Supplementary optical systems to modify the beam characteristics are then required for the 1P21 or the Lallemande multipliers.

As a consequence of the independence of the final efficiency of the telescope upon the *f*-ratio of the telescope, as has been discussed previously by Weaver (1948) and by Bowen (1952), a decision was made at the Yerkes Observatory to investigate the use of the Cassegrain focus for those direct photographic operations now associated with the prime focus. A solution to the foregoing problems has been found for the case where fields up to 1° are adequately large and where the large aperture and scale of existing telescopes can be readily utilized with only small investment in new equipment.

A general theorem in optics is that the first-order optical performance of an optical system is dependent solely upon the solid angle of radiation at the final focus and the initial aperture of the system. In other words as long as the final solid angle is that of an *F*/2 system, the 82-inch McDonald telescope would have the scale and speed of an 82-inch *F*/2 telescope, regardless of the size of the optical elements interposed between the 82-inch mirror and the final focus. Astronomers are well acquainted with the speed of spectrographs depending solely upon the *f*-ratio of the camera, but the extension to direct photography has not been generally realized. The simplest camera system, in fact, consists of no more than a spectrograph without a dispersive element.

The *F*/2 camera system designed for use at the 82-inch Cassegrain focus is shown in Figure 1. The size of the field lens placed at the Cassegrain focus determines the angular size of the field. When used with the 82-inch telescope, the field is 20′, and, when used with the 40-inch Yerkes refractor (at *F*/3), the field is 30′. The location of the field lens at the focus was a matter of convenience, since a field lens at this position introduces minimum aberrations. Displacement of the field lens away from the focus adds color terms and coma. In a more elaborate system these aberrations can be used to correct telescope aberrations and balance aberrations in the camera system. At the Cassegrain, however, the telescope aberrations are almost negligible. The coma, for instance, is dependent upon the Cassegrain *f*-ratio and independent of the telescope mirror *f*-ratio and is equal to the coma of the telescope mirror of the same *f*-ratio as the effective Cassegrain *f*-ratio.

The field lens of the Cassegrain camera provides an exit pupil image of the 82-inch mirror at the aperture stop of the camera, so that the entire beam of the 82-inch telescope passes through the *F*/2 camera for all points of the field. As a matter of convenience, the power system of this camera consists of a Tessar collimator and an *F*/2 Leica Summicron lens. The region of parallel light between these two elements is utilized for filters or dispersive elements in the case of objective spectroscopy.

While the light beam is parallel between the collimator and camera for all field positions, enabling use of interference filters, the parallel bundles for off-axis positions are inclined. As a consequence, the field is limited by the characteristics of the interference filter and the *f*-ratio of the field lens. The beam size of 1 inch for the 82-inch *F*/2 Cassegrain camera and an arbitrary limit of *F*/2 on the field lens yielded a field-lens diameter of $6\frac{1}{2}$ inches.

The optical performance of the 82-inch $F/2$ Cassegrain camera is not perfect. The camera has been made as simple as possible, utilizing essentially standard components, to illustrate that such components can render the Cassegrain focus as useful as the prime focus. Numerous refinements can be made in specially designed systems to yield high performance.

The $F/2$ Cassegrain camera has been used extensively for a period of more than a year. The high gain in speed accorded by the exceedingly small images, along with no effective loss in resolution—since the resolution is still limited by the diameter of the seeing disk—enabled this camera to be used with the 40-inch Yerkes refractor for a systemic survey of early-type multiple systems by D. Crawford. The effective speed with the 40-inch is $F/3$. An example of the improvement of efficiency when the same number of star quanta is focused in a smaller image is shown in Figure 2. The photographs were taken in immediate succession with the same exposure time and development time. The difference in limiting magnitude is 2.3. For 30-minute photographs the difference is almost 4 mag.

The second program for which this camera has been used is with the 82-inch McDonald telescope for a survey of H II regions with large scale. Figures 3 and 4 show several regions. The exposures were made with 103*a*-E plates and an RG-2 filter with the moon at first-quarter phase. During the dark of the moon, exposures of 1 hour with this combination can be made with only moderate sky fog.

The results obtained with this type of optical system on both refractors and reflectors would indicate that the addition of this type of system to existing telescopes could make possible research programs that are at present impossible. The possibility of changing the final *f*-ratio and scale merely by changing a small camera element should prove attractive on small research budgets where direct photography and objective spectroscopy of faint objects is required.

REFERENCES

Bowen, I. S. 1952, *Ap. J.*, **116**, 1.
Meinel, A. B. 1953, *Ap. J.*, **118**, 335.
Weaver, H. F. 1948, *Pub. A.S.P.*, **60**, 79.

ON THE POSSIBLE PRESENCE OF He^3 IN THE MAGNETIC STAR 21 AQUILAE*

E. MARGARET BURBIDGE
Kellogg Radiation Laboratory, California Institute of Technology
AND
G. R. BURBIDGE
Mount Wilson and Palomar Observatories
Carnegie Institution of Washington, California Institute of Technology

Received October 22, 1956

ABSTRACT

Measurements of the helium lines in the spectrum of the magnetic star 21 Aquilae reveal a wavelength shift between the singlet and triplet lines. Although some part of this shift may be due to Stark effect, comparison with the laboratory measures of isotope shifts between lines of He^3 and He^4 suggests that there is a reasonable probability that the major part of the shift may be due to the presence of He^3 in the star's atmosphere in an amount comparable with that of He^4. Theoretical arguments suggest that the acceleration of protons in the stellar atmosphere will lead to the production of neutrons and deuterons and thence to some synthesis of He^3 through the $H(d, \gamma)He^3$ reaction.

I. INTRODUCTION AND OBSERVATIONS

Among the peculiar A stars there are a few in which the strength of the He I lines is slightly greater than would be consistent with type A0; the Si II lines are usually anomalously strong at the same time. The star 21 Aquilae is one of these; it has been classified as type B8 on the basis of its He I lines, and there is also a line due to C II 4267, yet the Si II lines are very strong.

The star HD 124224 is a spectrum variable (Deutsch 1952) in which the strengths of He I and Si II vary oppositely in phase and would indicate different temperatures at the time each reaches maximum; yet the star hardly varies in light. When He I is at maximum, it has a strength corresponding to that in a B5 dwarf. Deutsch has attempted to explain the variation by means of a temperature gradient in the stellar atmosphere which is different in the two hemispheres, the *effective* temperature remaining constant and the two hemispheres being viewed alternately due to stellar rotation. It is hard to see, however, how such a variation in gradient could arise as to allow different depths in the atmosphere to be seen, where spectrum lines characteristic of different temperatures would be formed and yet for the effective temperature of the photosphere to remain almost constant. An alternative possibility is that we are dealing with real anomalies in the abundances of helium and silicon in the stellar atmosphere, possibly localized on the surface. Other stars similar to HD 124224 are 56 Ari and HD 34452 (Deutsch 1947*a*, *b*).

The observational material available on 21 Aql consists of one coudé spectrogram (dispersion $8\frac{1}{2}$ A/mm) obtained by the authors at the McDonald Observatory and four coudé spectrograms (dispersion $4\frac{1}{2}$ A/mm) obtained by Dr. H. W. Babcock at the Mount Wilson Observatory for magnetic-field measurements. These latter plates have been measured by Miss Sylvia Burd, and we are indebted both to Dr. Babcock and to Miss Burd for making the plates and the measures available to us. The star has a surface magnetic field which varies from $H_p = +500$ to $H_p = -1900$ gauss (Babcock and Cowling 1953). There does not appear to be a radial-velocity variation, and, although Morgan (1932, 1935) thought the star was a spectrum variable, this is still not confirmed.

---

* Supported in part by the joint program of the Office of Naval Research and the U.S. Atomic Energy Commission.

Until equivalent-width measures of the spectrum lines have been made and analyzed, we cannot say whether abundance anomalies are present. However, very qualitatively we may say, in view of previous work on the magnetic stars α^2 CVn and HD 133029 (G. R. and E. M. Burbidge 1955; E. M. and G. R. Burbidge 1955), that silicon is probably overabundant and helium may be present in slightly increased abundance over the normal.

As will be shown in the later discussion, the identification of 21 Aql as a magnetic star has suggested to us that some of the helium present in the atmosphere may be He^3. The spectrum of He^3 I has been studied in the laboratory by Fred, Tomkins, Brody, and Hamermesh (1951), and an unsuccessful attempt to detect lines of this isotope in the solar atmosphere was made by Greenstein (1951). The lines which can be measured in 21 Aql are λλ 4471.51 ($2^3P^0-4^3D$), 4120.86 ($2^3P^0-5^3S$), 4026.22 ($2^3P^0-5^3D$), and, on one plate, 3867.53 ($2^3P^0-6^3S$), where these wave lengths are the weighted means of the pairs of lines, and λλ 4387.93 ($2^1P^0-5^1D$), 4143.76 ($2^1P^0-6^1D$), and 4009.27 ($2^1P^0-7^1D$). These are the wave lengths arising from the He^4 isotope. In Table 1 we give the isotope shifts, $\lambda(He^3)-\lambda(He^4)$, measured in the laboratory by Fred *et al.* and converted to angstroms and listed by Greenstein. It will be seen that there is a systematic shift of the singlet lines relative to the triplet lines, in the value of $\lambda(He^3)-\lambda(He^4)$. If He^3 were present in a stellar atmosphere in an amount comparable with the He^4 normally present, one would expect that it might be detectable by means of an observed shift between the singlet and the triplet lines of He I, and the effect should therefore be capable of being disentangled from any relative Doppler shifts between lines of different elements, such as is present, for example, in the spectrum of α^2 CVn.

TABLE 1

ISOTOPE SHIFTS IN He I LINES

$\lambda(He^4)$ (A)	$\Delta\lambda_I=\lambda(He^3)-\lambda(He^4)$ (A)	$\lambda(He^4)$ (A)	$\Delta\lambda_I=\lambda(He^3)-\lambda(He^4)$ (A)
4471.51	+0.07	4026.22	+0.08
4387.93	+ .28	4009.27	+ .25
4143.76	+ .26	3867.53	+0.08
4120.86	+0.07		

II. RESULTS AND CONCLUSIONS

In Table 2 we give the differences between λ_{obs}, the observed wave lengths of the He I lines in 21 Aql, and $\lambda(He^4)$, the laboratory He^4 wave lengths. Most of the measures on the Mount Wilson plates were made by Miss Burd, incidentally to the measurement of these plates for the determination of the magnetic field in 21 Aql. Her values were supplemented by some measures by us where certain He I lines had not been measured by her. The McDonald plate was measured by us. The line λ 4009 was weak, and both it and λ 3868 were measured on only one plate each. When we measured the Mount Wilson plates, we included some of the other lines measured by Miss Burd, as a check, and found good agreement. The mean difference, λ(Burbidge) − λ(Burd), having regard to sign, was +0.007 A, and the average deviation was ±0.017 A. The values in Table 2 have been corrected for the observer's velocity with respect to the sun. In the first column, "T" and "S" denote triplet and singlet lines, respectively.

As Table 2 shows, there is indeed a systematic shift in four of the five plates between the triplet and singlet lines, and it is in the same sense as would be expected if an appreciable fraction of the helium in the star's atmosphere consisted of He^3. If the abundance ratio $\mathrm{He}^3/He^4 = R$ and if the two lines are blended without self-absorption or saturation, then we have (Greenstein 1951)

$$\lambda_{\mathrm{obs}} - \lambda\,(\mathrm{He}^4) = \frac{\lambda}{c}\,v + \frac{R}{1+R}\,\Delta\lambda_I\,, \tag{1}$$

where v is the total velocity causing a Doppler shift, including any differential velocity given by one element relative to another.

TABLE 2

VALUES OF $\lambda_{\mathrm{obs}} - \lambda(\mathrm{He}^4)$ IN 21 AQL

LINE	PLATE AND DATE				
	Ce 4705 May 31, 1947	Ce 4892 Oct. 1, 1947	Ce 5184 May 20, 1948	Ce 5669 June 9, 1949	McD May 11, 1953
4472 (T)	−0.112 (B)*	−0.058 (B)	−0.097 (B)	−0.083 (B)	+0.02
4388 (S)	− .083	+ .026 (B)	+ .005 (B)	− .042	+ .15
4144 (S)	− .065	+ .098	+ .060	+ .051	+ .15
4121 (T)	− .057 (B)	− .061 (B)	− .145 (B)	− .061 (B)	− .02
4026 (T)	−0.056 (B)	− .056 (B)	− .041 (B)	−0.080 (B)	+0.04
4009 (S)	....	+0.120	....	....	....
3868 (T)	....	....	−0.091 (B)	....	....

* (B) = Miss Burd's measure.

TABLE 3

DETERMINATION OF P AND v

	PLATE				
	Ce 4705	Ce 4892	Ce 5184	Ce 5669	McD
P	0.02±0.07	0.71±0.11	0.67±0.12	0.40±0.13	0.72±0.07
v (km/sec)	−5.6 ±1.0	−7.8 ±1.6	−10.5 ±1.5	−7.4 ±1.6	−2.9 ±0.8
v (km/sec) (Burd: all lines)	−7.0 ±0.3	−5.9 ±0.5	−6.9 ±0.3	−5.6 ±0.3	....
v (km/sec) (Burd: He I)	−5.3	−2.7	−5.3	−5.5	....

For each plate we have either five or six of these equations, which we have solved by least squares for v and P, where $P = R/(1 + R) = \mathrm{He}^3/(\mathrm{He}^3 + \mathrm{He}^4)$. The results are given in Table 3, together with their probable errors; we also give Miss Burd's determinations of the mean velocity from the lines of all elements and the mean velocity from He I alone. The determination of P yields a significant non-zero value on all plates except Ce 4705, and this value appears to vary from plate to plate. We now ask whether this may be interpreted as being due to the presence in the stellar atmosphere of the He^3 isotope in amounts comparable with the He^4 present or whether it could be due to some other cause.

All Doppler shifts have been included in the determination of v. The only effect which might lead to a differential effect between singlet and triplet lines of He I is the Stark effect, due either to transient electric fields arising through the magnetic fields or to the usual interionic effect in stellar atmospheres. The latter can be investigated in two ways, either by considering the theoretical Stark effect or by comparing our wave lengths with those found empirically in normal stellar spectra.

Mrs. Krogdahl (1947) has predicted approximate values of the shifts for some He I lines for the B0 star τ Sco. They are: λ 4472 = +0.04 A, λ 4388 = +0.28 A, λ 4121 = +0.01 A, and λ 4026 = +0.12 A. From these values it would appear that the only triplet-singlet pair of lines available would give a relative shift of the same size and sign as the predicted isotope shift. However, Miss Underhill's (1948) measures in the B2 star γ Peg do not agree very well with the predicted values; there is a small positive shift for all lines, but it is no larger for λ 4388 than for the others. Wave-length shifts derived by Merrill and Adams (1943) for τ Sco are similarly small, and that for λ 4388 is +0.04 A instead of the predicted +0.28 A. This may be connected with the well-known puzzle that the forbidden line at λ 4469.9, which should appear in the presence of an electric field but should be shifted to the violet proportionately to the field strength, does indeed appear in B-type stars but always at the zero-field wave length.

Petrie (1953) has empirically deduced wave lengths for radial-velocity determinations of B-type stars. They give the following shifts with respect to λ(He^4): λ 4472 = −0.18 A, λ 4388 = 0.00 A, λ 4121 = −0.02 A, and λ 4026 = −0.08 A, where we have taken his values for main-sequence stars for λ 4472 and λ 4026. Thus the only lines which show an effect are λ 4472 and λ 4026, and they both have violet shifts. These lines, however, on medium-to-low dispersion or in broad-lined stars are complicated by blending with the forbidden lines just to the violet of the permitted ones. If we consider the lines λ 4388 and λ 4121 alone, Petrie's relative wave-length shift between the two is only +0.02 A, while the relative isotope shift is +0.21 A, and the measured shift on three of our five plates is appreciable.

The forbidden line at λ 4469.9 is not visible on inspection of our plates, although there may be a very weak depression on microphotometer tracings of them. It is possible that on occasion this line has reached considerable strength (Morgan 1933), but it still appeared at the zero-field position, as in spectra of normal B-type dwarfs, and not at the shifted position both predicted and found experimentally in the case of macroscopic stationary electric fields.

Qualitatively, we may say that the measured shifts in γ Peg and τ Sco agree with the expected shifts for interionic Stark effect, and also they are in the same sense as, although much smaller than, isotope shifts. Although these stars are of early B type and 21 Aql is somewhat cooler, we deduce that a small part of the shift in 21 Aql may be due to Stark effect, so that possibly the values of P given in Table 3 should be reduced by values <0.1. The total wave-length shifts on plates Ce 4892, Ce 5184, and McD are definitely too large to be attributed to interionic Stark effect.

Large-scale electric fields of the same order of magnitude as the interionic fields, i.e., about 10^3 volts/cm, arising and being maintained over large areas of the stellar surface would seem to be extremely improbable. Diagrams by Foster (1927) indicate that such fields would be demanded to explain the shift of λ 4388 relative to λ 4471.

We conclude that there is a reasonable probability that the major part of the numerical values of P given in Table 3 may actually be due to the presence of He^3 in 21 Aql. If this is the case, then the amounts of He^3 and He^4 are comparable. The normal He^4 abundance relative to hydrogen is still rather uncertain. However, it may be put ~ 10, so that the H/He^3 ratio may also be ~ 10.

An explanation of the presence of He^3 in the atmosphere of this star is possible on the basis of previous work carried out on the synthesis of elements through nuclear reactions on the surfaces of magnetic stars (Fowler, Burbidge, and Burbidge 1955; Burbidge, Burbidge, and Fowler 1956). In the most recent of these papers we have modified our earlier models, and it now appears that synthesis must take place following the production of neutrons by (p, n) reactions on the light nuclei, the capture of these neutrons by the hydrogen to form deuterium, and the reacceleration of the deuterium in a proton gas in which the following reactions will predominate:

$$H(d, \gamma)\,He^3\,, \qquad H(d, n)\,2H\,, \qquad N_Z^A(n, \gamma)\,N_Z^{A+1}\,.$$

It appears that the activity takes place in bursts, with a duration of about 1 second, and that the particles which are accelerated may be similar to those which give rise to radio bursts of type III in the sun (Wild, Roberts, and Murray 1954). The production of the deuterium, for example through the $N^{14}(p, n)O^{14}$ reaction, followed by the capture of the neutrons by protons will take place if a flux of protons having energies $\geq \sim 6$ Mev, the threshold for the $N^{14}(p, n)O^{14}$ reaction, is accelerated. Following the production of deuterium, the reacceleration of the gas to rather low energies, below the threshold for further neutron production, will result in the production of He^3 through the $H(d, \gamma)$-He^3 reaction by the fraction of the protons having energy below the energy (~ 2.2 Mev) necessary to free the neutrons from deuterium. The fraction of deuterons and protons accelerated to energies above this threshold will result in the release of the neutrons and their eventual capture either by hydrogen again or by the iron group, which eventually leads to the synthesis of the heavy elements. Calculations which have been carried out for different assumed particle-energy spectra suggest that, in order that the heavy-element abundances may be built to ~ 1000 times their normal values corresponding to the abundances in some magnetic stars (G. R. and E. M. Burbidge 1955; E. M. and G. R. Burbidge 1955), an amount of He^3 comparable to the normal amount of He^4 will also be produced. If only very low-energy (< 2 Mev) fluxes are available, after deuterium has been produced by higher-energy particles, then *only* He^3 will be produced in appreciable quantities. This may be the situation in 21 Aql. On the other hand, some He^3 may always be present in stars where the heavy-element anomalies are present, but it may not be detectable, owing to temperature conditions in stars like α^2 CVn and HD 133029.

In conclusion, we wish to thank Dr. H. W. Babcock for his kindness in lending us the Mount Wilson spectrograms of 21 Aql, and Dr. Babcock and Miss Sylvia Burd for making Miss Burd's wave-length measures available to us. We are also indebted to many colleagues for helpful and critical discussions and, in particular, to Drs. J. L. Greenstein, P. W. Merrill, and William A. Fowler.

REFERENCES

Babcock, H. W., and Cowling, T. G. 1953, *M.N.*, **113,** 357.
Burbidge, E. M., and Burbidge, G. R. 1955, *Ap. J.*, **122,** 396.
Burbidge, E. M., Burbidge, G. R., and Fowler, W. A. 1956, Stockholm Symposium on Cosmical Magnetism (in press).
Burbidge, G. R., and Burbidge, E. M. 1955, *Ap. J. Suppl.*, **1,** 431.
Deutsch, A. J. 1947*a*, *Ap. J.*, **105,** 283.
———. 1947*b*, *ibid.*, p. 503.
———. 1952, *ibid.*, **116,** 536.
Foster, J. S. 1927, *Proc. R. Soc. London, A*, **117,** 137.
Fowler, W. A., Burbidge, G. R., and Burbidge, E. M. 1955, *Ap. J. Suppl.*, **2,** 167.
Fred, M., Tomkins, F. S., Brody, J. K., and Hamermesh, M. 1951, *Phys. Rev.*, **82,** 406.
Greenstein, J. L. 1951, *Ap. J.*, **113,** 531.
Krogdahl, M. K. 1947, *Ap. J.*, **105,** 327.
Merrill, P. W., and Adams, W. S. 1943, *Ap. J.*, **97,** 98.
Morgan, W. W. 1932, *Ap. J.*, **76,** 275.
———. 1933, *ibid.*, **77,** 226.
———. 1935, *Pub. Yerkes Obs.*, **7,** 133.
Petrie, R. M. 1953, *Pub. Dom. Ap. Obs. Victoria*, **9,** 297.
Underhill, A. B. 1948, *Ap. J.*, **107,** 337.

NOTES

21-CM LINE EMISSION FROM THE COMA CLUSTER

Observations have been made of 21-cm line emission from neutral hydrogen in the Coma cluster of galaxies ($\alpha = 12^{\rm h}57^{\rm m}.5$; $\delta = +28^\circ.3$). The observations were made with the 24-foot radio telescope at Agassiz Station, which has a beam width of 2°. Figure 1 shows an original record, taken with the antenna at a fixed position and the receiver tuned to a frequency of 1386.85 Mc/s. The record displays the variation of the difference in antenna temperature at two frequencies separated by 3.5 Mc/s as the source moves through the antenna pattern. The results reported in this note were derived from eighty such drift-curves at various frequencies.

Figures 2 and 3 show the results of the observations. In Figure 2 each point is the mean of sixteen measurements obtained from drift-curves such as that of Figure 1. The probable error of a mean point is $\pm 0^\circ.2$. The solid line of Figure 3 shows the line profile, built up from drift-curves at different frequencies. The shape of this profile is strongly influenced by the characteristics of the radiometer. The comparison radiometer used for these observations measures the difference in antenna temperature in two frequency bands, one 2 Mc/s, the other 0.2 Mc/s broad. A curve like that of Figure 3 results when the true line profile is broader than the separation of the two bands. It is difficult in this case to derive a profile free of instrumental effects. Unequal width in the two bands compounds the difficulty. The dashed curve of Figure 3 represents the line profile, after a rough correction for this instrumental effect. The data presented here are all derived from this corrected profile and hence contain the uncertainties in the correction.

The radial velocity of the Coma cluster is, on the basis of these observations, +7000 km/sec, with an estimated uncertainty of ± 200 km/sec. The optically determined radial velocity is +6680 km/sec (Schwarzschild 1954). In view of the large uncertainty in both the radio and the optical values, the agreement between the two is satisfactory.

The dispersion in radial velocity of neutral hydrogen within the cluster is 500 km/sec, with an estimated uncertainty of ± 200 km/sec. This dispersion may result from three motions: the peculiar motion of individual galaxies containing hydrogen; the internal motion of the hydrogen within these galaxies; and the peculiar motion of any neutral hydrogen in the intergalactic regions of the cluster. The optically determined dispersion in radial velocity of galaxies in the cluster is 825 km/sec, with an estimated uncertainty of ± 30 per cent (Schwarzschild 1954). The lower value obtained for hydrogen would, if real, be significant, but the uncertainties in both values are too large to warrant any discussion of the difference at present.

Schwarzschild (1954) has derived a total mass for the Coma cluster of $3 \times 10^{14} M_\odot$. An estimate of the mass of neutral hydrogen may be made if it is assumed that the line is not saturated. The temperature in the line, then, is

$$\Delta T(v) = \tau_v T ,$$

where τ_v is the optical depth in the line and T is the kinetic temperature of the hydrogen. If we assume the usual expression for τ_v (Heeschen 1955), this becomes

$$\Delta T(v) = 5.44 \times 10^{-14} N_H f(v) ,$$

where N_H is the number of neutral hydrogen atoms per square centimer along the line of sight and $f(v)$ is the distribution function of radial velocities. Setting $f(v) = \Delta v^{-1} =$

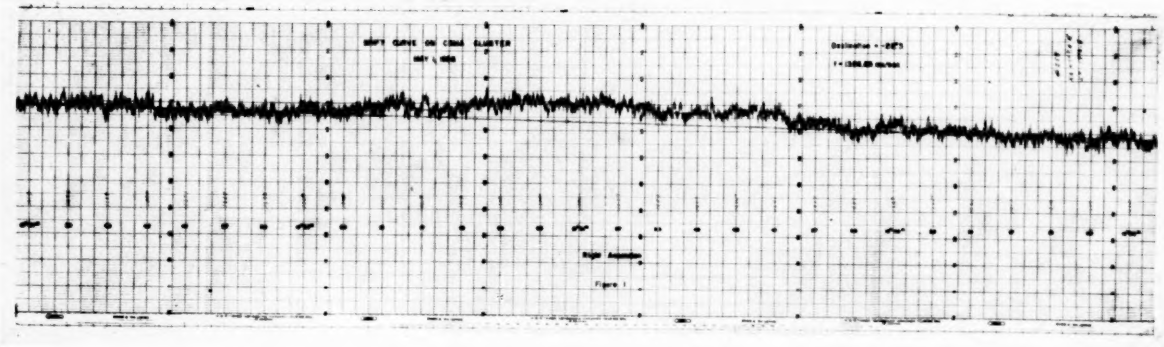

FIG. 1.—A record of the passage of the Coma cluster through the antenna pattern

$(10^8 \text{ cm/sec})^{-1}$ and $\Delta T = 2°$ gives $N_H = 3.7 \times 10^{21}/\text{cm}^2$. If we take the distance of the cluster as 2.5×10^7 parsecs (Schwarzschild 1954) and the diameter, from Figure 2, as 5°, this value of N_H gives a total mass of neutral hydrogen of $0.8 \times 10^{14} M_\odot$.

This result may be uncertain by as much as a factor of 2. The large uncertainty arises from several causes:

1. The extreme weakness of the signal makes it difficult to determine Δv and the diameter of the cluster.
2. The correction of the observed profile for instrumental effects may introduce considerable error into both Δv and ΔT.

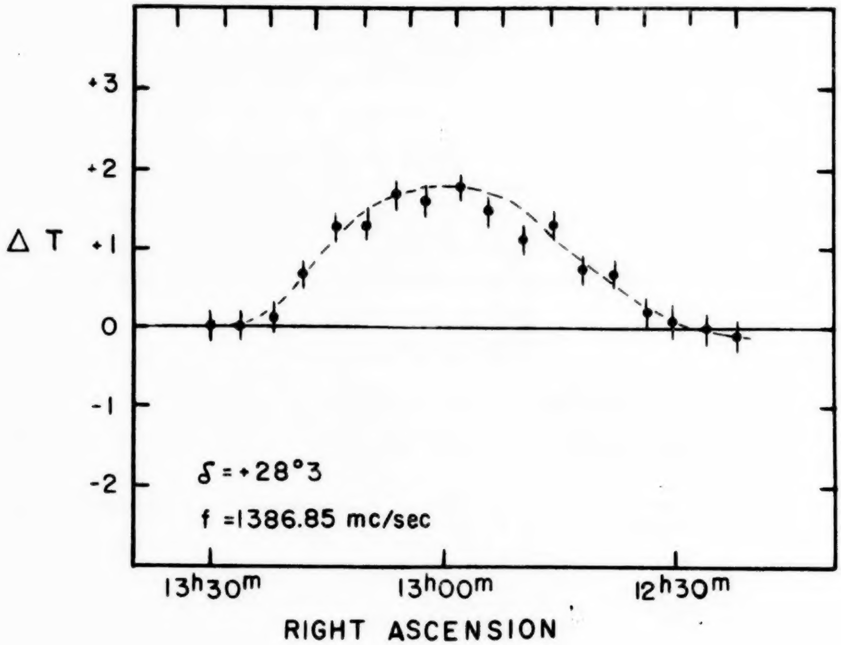

FIG. 2.—The mean of sixteen drift-curves

3. At the frequency of these observations the radiometer calibration is less certain than at the normal hydrogen-line frequency.
4. The approximation $f(v) = \Delta v^{-1}$, e.g., a rectangular profile, may introduce some error. If the true profile were more accurately known, the area under it should yield a better determination of N_H.
5. The assumption of low optical depth may be incorrect.

The foregoing results, based as they are on low-resolution observations, must be considered very preliminary and qualitative. Observations with larger antennae may be expected to provide considerably improved accuracy for the Coma cluster and for other clusters of galaxies. The present observations demonstrate the existence of an appreciable quantity of neutral hydrogen in the Coma cluster and show that 21-cm line observations of clusters of galaxies are feasible and may yield valuable results.

DAVID S. HEESCHEN

G. R. AGASSIZ STATION
HARVARD COLLEGE OBSERVATORY

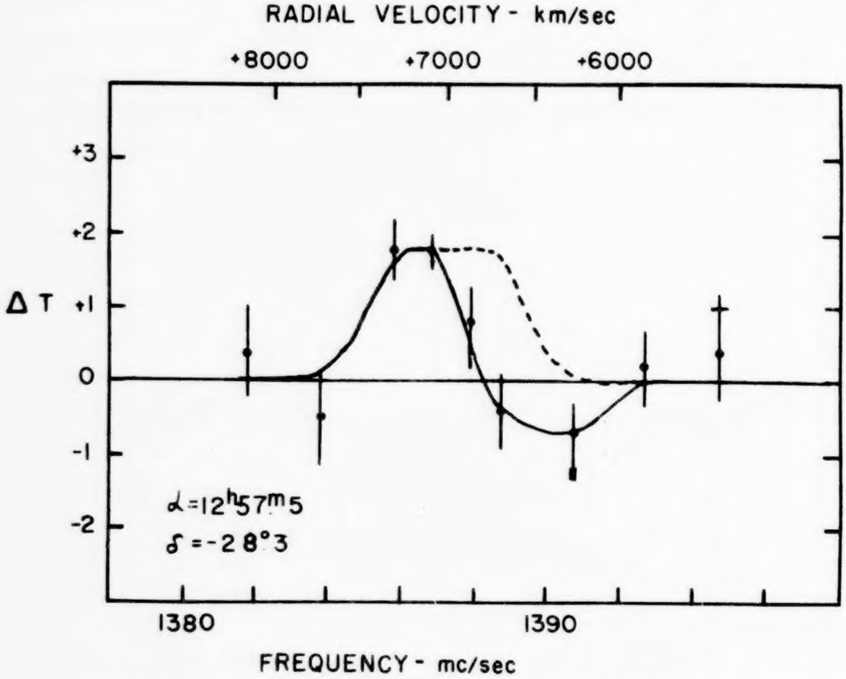

FIG. 3.—The solid curve is the observed line profile. The dashed curve is the profile after correction for instrumental effects.

REFERENCES

Heeschen, D. S. 1955, *Ap. J.*, **121**, 569.
Schwarzschild, M. 1954, *A.J.*, **59**, 273.

EXCITATION IN NEBULAE: ELECTRON-HYDROGEN INELASTIC COLLISIONS IN A RADIATIVE H II REGION

The excitation of hydrogen by inelastic electron collisions plus dilute stellar radiation was discussed earlier (Chamberlain 1953, Sec. V; referred to hereafter as "Paper I") for negligible absorption of the Lyman continuum between the star and nebula. It is of interest, however, to estimate the possible effects of collisional excitation in planetary nebulae. Toward the outer boundary of a Strömgren (1939) sphere, the number of neutral H atoms could conceivably become sufficiently abundant for collisions to be appreciable in exciting the Balmer lines.

The population of the nth level is expressed in terms of a parameter b_n, which is essentially a correction factor to the combined excitation-ionization formula for hydrogen that takes account of departures from thermodynamic equilibrium (Paper I, eq. [4]). We introduce another parameter, $\mathfrak{H}$, defined in terms of the ionization equilibrium by Paper I, equations (34) and (24):

$$\frac{N_1}{N_e} = \mathfrak{H}\left(\frac{N_1}{N_e}\right)_{\text{coll}}, \tag{1}$$

where $(N_1/N_e)_{\text{coll}}$ is the ratio of neutral atoms to electrons (with the latter postulated equal to the density of ionized atoms) for pure collisional excitation. Then, in the general case, b_n is conveniently related to the ionization ratio by

$$b_n = (1 - \mathfrak{H})b_n\ (\text{rad.}) + \mathfrak{H}b_n\ (\text{coll.})\ , \tag{2}$$

where b_n(rad.) and b_n(coll.) represent the known solutions for purely radiative and collisional excitation, respectively. Since b_n(coll.) is considerably greater than the b_n(rad.) for Baker and Menzel's (1938) cases A_2 and B, the Balmer lines are enhanced as collisions increase and radiative ionizations decrease (i.e., as $\mathfrak{H}$ goes progressively from 0 to 1). Considering absorption of the ionizing radiation as well as the geometrical dilution factor, $W = R^2/4s^2$, in the generalized ionization equation (Paper I, eq. [28]), we find

$$\frac{1 - \mathfrak{H}}{\mathfrak{H}} = \frac{(2\pi m k)^{3/2} K}{N_e \alpha_\kappa h_3} \int_{y_1}^{\infty} \frac{W \bar{g}\, e^{-\tau_\nu}}{y\,(e^y - 1)}\, d y\ , \tag{3}$$

where $y_1 = h\nu_1/kT_*$ and $\tau_\nu = \int_0^s N_1(s)a_1(\nu)ds$. Here s is the distance from the star, $a_1(\nu)$ is the absorption coefficient for the ground orbit, ν_1 is the frequency at the Lyman limit, and the remaining notation is as defined in Paper I. For small optical thicknesses, the solution is

$$\frac{1 - \mathfrak{H}}{\mathfrak{H}} = \frac{(2\pi m k)^{3/2} K}{h^3 N_e \alpha_\kappa} \frac{R^2}{4 s^2}\left[E_1\,(y_1) - a_1\,(\nu_1)\,E_4\,(y_1) \int_0^s N_1\,(s)\, d s + \ldots\right], \tag{4}$$

where E_n, the incomplete gamma function, is

$$E_n\,(y_1) = y_1^{n-1} \int_{y_1}^{\infty} \frac{e^{-y} d y}{y^n}\,. \tag{5}$$

Equations (4) and (1) may be solved numerically and simultaneously for the ionization equilibrium and $\mathfrak{H}$. Very near s_0, the distance from the star of the H II boundary, equation (4) is not valid, since the optical thickness will require higher-order terms in the expansion. But a more severe difficulty is that the temperature as well as the ionization must fall off rapidly near s_0, whereas for this solution we take T_e and N_e as effectively constant. Also it should be noted that if and when collisions become important, T_e will decrease, other conditions remaining constant; but to ascertain the possible importance of collisions, a few sample calculations have been made with the above formulation.

When α_κ, the rate coefficient for collisional ionizations, is assumed negligible, the generalized ionization equation is identical to that used by Baker, Menzel, and Aller (1938), and it may be shown that it is essentially equal to the ionization equation used by Strömgren (1939).

It is well known from Strömgren's work that the ionization decreases quite suddenly at the distance s_0 from the star, where the ionizing radiation is depleted by absorption, This distance is virtually unaffected by the inclusion of collisions. Moreover, numerical examples for T_* between 40000 and 160000° K indicate that collisions will not add appreciably to the Balmer intensities in a nebula as cool as 20000° K, which is probably an upper limit for T_e in planetary nebulae. On the other hand, if T_e could be kept high (say, of the order of T_*), collisional excitation would be important at a considerable distance shortward of s_0, in spite of the relatively small number of neutral hydrogen atoms present. For the hotter stars the ionization cutoff at s_0 is relatively sharper than for cooler ones; therefore, for a given T_e, collisions will be less likely to exert an influence when T_* is large.

To summarize, it should be noted from equation (1) that $\mathfrak{H}$, which measures the importance of collisions, is dependent not merely on the amount of ionization but also on the electron temperature or $(N_1/N_e)_{\text{coll}}$. For very hot stars, such as are probably encountered in planetary nebulae, collisions can have appreciable effects away from the H II boundary only if the electron temperature is much greater than 20000° K. In any particular case, a quick estimate of the importance of collisions can be obtained by neglecting Lyman absorption, as in Paper I, and finding the position of the broad transition region, where $\mathfrak{H}$ changes from 0 to 1, relative to the distance s_0 determined by Strömgren's paper. If this region is within, or only slightly outside, s_0, the foregoing equations may be used for more precise calculations. Otherwise it is safe to conclude that collisions are negligible except at the H II boundary and only then if sufficient mechanical energy is supplied to keep T_e fairly high as hydrogen becomes neutralized.

JOSEPH W. CHAMBERLAIN

YERKES OBSERVATORY
June 20, 1956

REFERENCES

Baker, J. G., and Menzel, D. H. 1938, *Ap. J.*, **88**, 52.
Baker, J. G., Menzel, D. H., and Aller, L. H. 1938, *Ap. J.*, **88**, 422.
Chamberlain, J. W. 1953, *Ap. J.*, **117**, 387.
Strömgren, B. 1939, *Ap. J.*, **89**, 526.

ON ROHRLICH'S DISCUSSION OF THE CALCIUM XV PROBLEM

Rohrlich (1956) has recently criticized certain relatively minor aspects of my paper on the identification of the yellow coronal line (Layzer 1954). As this problem has been a source of confusion in the past, it seems worth while to try to set the record straight.

Rohrlich's principal criticism concerns my procedure for evaluating a certain parameter Φ, one of eight that enter into my theoretical formulae. Rohrlich describes and comments on this procedure in the following terms: "This low value [for Φ] was obtained by applying a formula for the level separation $^3P_1(2p^4)-{}^3P_1(2s^22p^2)$ to the only observed $^3P_1(2p^4)$ levels, viz., those for $q = 2$, 3, 4, and 5, and by extrapolating the result for $q = 14$, assuming a linear variation of L and Φ. We regard this to be a rather daring procedure."

Actually, I used an entirely different procedure to evaluate Φ (line 29, p. 698, of the paper cited above): "From (3.11 *a*, *b*) [equations which give the values of certain parameters L, SD, and F_2 in Ca XV] and (3.7) [a relation between these parameters and Φ that is valid only for highly ionized atoms] we obtain $\Phi = 101310$ cm^{-1} in Ca XV."

Rohrlich goes on to suggest that, since one cannot accurately evaluate Φ by what he supposes to be my procedure, one should replace it by a different parameter that has no direct connection with the problem at hand but which can be determined accurately from the available data and which, on theoretical grounds, ought not to differ very much from

Φ. It turns out that this parameter exceeds Φ by about 10 per cent, from which Rohrlich concludes that my value of Φ is too low by this amount.

The main objectives of my paper on Ca XV were, in the first place, to sketch the broad outlines of a theory that enables one to take explicit account of the major effects of configuration mixing in highly ionized atoms and, in the second place, to show that this theory removes the small discrepancies that exist between Garstang's analysis, based on a less precise theory, and observation. Rohrlich appears to agree that my theory does in fact remove these discrepancies. But he argues that my own analysis of the numerical data is not "careful" enough to establish this conclusion, mainly, I gather, because I have merely guessed at the errors instead of estimating them in some objective way. Now it seems to me that the major sources of error in the problem under discussion arise from the approximate nature of the underlying theory and from gaps and errors of unknown magnitude in the experimental data. Under these circumstances I believe that one must rely primarily on judgment, experience, and common sense rather than on any objective criterion for estimating errors. As it happens, independent guesses as to the magnitude of the errors involved, by Garstang (1952), Edlén (1954), and myself, all agree pretty well, and all are considerably higher than Rohrlich's "objective estimates."

DAVID LAYZER

HARVARD COLLEGE OBSERVATORY

REFERENCES

Edlén, B. 1954, *M.N.*, **114**, 700–703.
Garstang, R. H. 1952, *Ap. J.*, **115**, 569–570.
Layzer, D. 1954, *M.N.*, **114**, 692–699.
Rohrlich, F. 1956, *Ap. J.*, **123**, 521–531.

A NOTE ON THE COLOR-MAGNITUDE ARRAY OF THE WHITE DWARFS. I*

Recently Humason and Zwicky (1947) and Luyten (1953, 1954) have discovered a number of faint blue stars, some of which are recognized as white dwarfs, though the majority are very likely members of the galactic halo population. As these stars are apparently very faint, they are difficult to observe spectroscopically except with the very largest telescopes, and it appeared worthwhile to see whether the stars could be classified photometrically. The three-color observations of several classical white dwarfs published by Johnson and Morgan (1953) indicated that, for stars with $B - V$ less than 0.4 mag., the white dwarfs could be distinguished from unreddened normal stars. Therefore, it was decided to extend the three-color observations to all the known white dwarfs north of $-20°$ declination, to the stars discovered by Humason and Zwicky, and to early-type subdwarfs. Although the program is not yet completed as far as the fainter stars are concerned, it appears desirable to report on the results so far obtained for those stars whose membership in the Hyades cluster or whose trigonometric parallaxes assure that they are white dwarfs.

The photometric observations on the U, B, V system are listed in Tables 1 and 2, where the asterisks following the number of observations indicate stars for which Johnson and Morgan's observations have been incorporated in the means. For the trigonometric parallaxes we have followed the suggestion of Schilt (1954) and reduced the relative parallaxes to absolute, omitting the systematic corrections included in the 1952 Yale Catalogue of Trigonometric Parallaxes. For the Hyades we have used the mean distance modulus of $3^{m}03$ derived by van Bueren (1952), as the existing proper motions are not sufficiently accurate to determine individual distances.

---

* *Contributions from the McDonald Observatory*, No. 271.

The color-absolute-magnitude array shown in Figure 1 is quite similar to that given by Luyten (1952) and needs little comment other than to note that the scatter cannot be entirely accounted for by errors of observation. The four open circles refer to stars in Table 1 whose absolute magnitudes are uncertain by more than ±0.5.

The bluest white dwarf so far observed is H-Z 14 in the Hyades with a $B - V$ color of only −0.15 mag. The great majority of the white dwarfs appear to have colors between −0.15 and +0.40 mag. and confirm the results of Johnson and Morgan, in that they can be distinguished from unreddened main-sequence stars. They are also easy to distinguish from A- and F-type subdwarfs, which have much smaller ultraviolet colors; but it should be noted that reddened OB stars, as well as DQ Herculis and UX Ursae Majoris (Walker 1956), would be mistaken for white dwarfs from the three-color observations alone. For white dwarfs with colors greater than +0.5 mag., the separation of the various types of stars does not appear to be feasible from three-color observations alone: for example, v Ma 2 has a color almost identical with that of an F9 V star.

TABLE 1

COLORS AND MAGNITUDES OF THE NEAREST WHITE DWARFS

Yale No.	Name	V (mag.)	$B-V$ (mag.)	$U-B$ (mag.)	n	π_t	M_v (mag.)	P.E. (mag.)
160...	v Ma 2	12.36	+0.56	+0.04	4*	0″238 (5)	14.2	±0.1
....	L 870-2	12.84	+ .34	− .50	4	.066 (13)	11.9	±0.4
462...	h Per 1166	13.63	− .10	− .91	6*	.027 (8)	10.8	±0.6
791...	W 219	15.20	+ .30	− .52	4	.071 (11)	14.5	±0.3
945...	40 Eri B	9.50	+ .03	− .70	4	.203 (5)	11.0	±0.1
1579...	He 3	12.03	− .06	− .90	4	.058 (6)	10.8	±0.2
1813...	L 745-46 A	(13.04	+ .32	− .63)	1	.173 (9)	14.2	±0.1
2312...	SA 29-130	13.32	+ .07	− .54	4	.040 (12)	11.3	±0.7
2642...	R 627	14.24	+ .31	− .52	3	.084 (13)	13.9	±0.3
2976...	W 457	(15.90	+ .64	− .09)	1*	.081 (11)	15.4	±0.3
3081...	BD−7°3632	12.33	+ .06	− .62	4	.062 (9)	11.3	±0.3
3112...	W 489	14.68	+ .96	+ .37	2*	.134 (12)	15.3	±0.2
3124...	G+70°5824	12.79	− .09	− .84	4	.029 (12)	10.1	±0.9
4440...	G+70°8247	13.19	+ .05	− .85	4*	.066 (6)	12.3	±0.2
4709...	L 997-21	13.69	+ .27	− .55	3	.079 (12)	13.2	±0.3
4895...	W 1346	11.54	− .07	− .87	5*	.074 (5)	10.9	±0.2
5191...	LDS 749 B	14.68	− .05	− .91	4	.021 (10)	11.3	±1.0
....	G+82°3818	13.02	−0.02	−0.72	4	0.050 (11)	11.5	±0.5

TABLE 2

COLORS AND MAGNITUDES OF THE HYADES WHITE DWARFS

Name	V (mag.)	$B-V$ (mag.)	$U-B$ (mag.)	n	M_v (mag.)
H-Z 4........	14.47	+0.15	−0.67	4	11.4
H-Z 7........	14.18	− .03	−0.89	4	11.2
H-Z 9........	13.95	+ .33	−0.69	4	10.9
H-Z 14.......	13.83	− .15	−1.04	4	10.8
VR 7........	14.29	− .02	−0.84	4	11.3
VR 16.......	14.02	−0.09	−0.97	4	11.0

It is a pleasure to acknowledge the assistance of Dr. Luyten, who provided charts for the identification of the stars, and to Dr. Johnson, who provided the sensitive photoelectric equipment needed to measure the fainter stars.

D. L. HARRIS III

YERKES OBSERVATORY

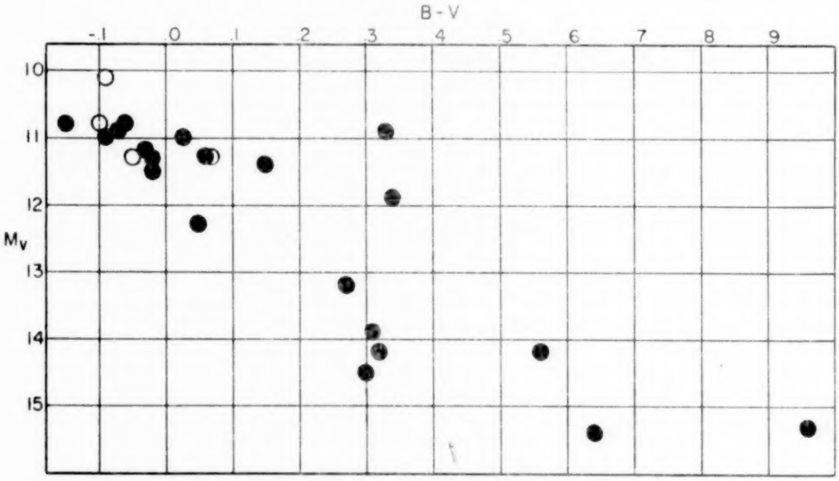

FIG. 1.—Color-magnitude array of the white dwarfs

REFERENCES

Bueren, H. G. van. 1952, *B.A.N.*, **11**, 385.
Humason, M. L., and Zwicky, F. 1947, *Ap. J.*, **105**, 85.
Johnson, H. L., and Morgan, W. W. 1953, *Ap. J.*, **117**, 313.
Luyten, W. J. 1952, *Ap. J.*, **116**, 283.
———. 1953, *A.J.*, **58**, 75.
———. 1954, *ibid.*, **59**, 224.
Schilt, J. 1954, *A.J.*, **59**, 55.
Walker, M. F. 1956, *Ap. J.*, **123**, 68.

ABSTRACTS OF ASTROPHYSICAL JOURNAL SUPPLEMENT SERIES

Supplement No. 23, Volume II

STUDIES OF EXTREMELY YOUNG CLUSTERS. I. NGC 2264

MERLE F. WALKER
Mount Wilson and Palomar Observatories
Carnegie Institution of Washington, California Institute of Technology

Although considerable observational work has now been done upon the problem of the later evolution of stars away from the main sequence, almost no observational investigations of the very early stages of stellar evolution have been made. Recent theoretical work has indicated that in a group of stars which is only a few million years old the fainter members of the cluster will still be in the process of contracting gravitationally from the prestellar medium. In the contraction stage a star moves nearly horizontally toward higher temperatures in the color-magnitude diagram. Since the rate of contraction varies with the mass of the configuration, the color-magnitude diagram for an extremely young cluster of stars should consist of a normal main sequence for the brightest stars. Below some point which depends upon the age of the cluster, the stars should lie above the main sequence.

Three-color photoelectric and photographic observations of NGC 2264 have been obtained to $V = 17$ in order to investigate the color-magnitude diagram of an extremely young cluster of stars. This cluster was chosen for observation for the following reasons: (1) the presence of OB stars in the cluster show it to be very young; (2) the cluster consists of a well-defined clustering of both bright and faint stars, seen projected against a dark cloud, so that a large proportion of the fainter stars are physical members of the group; (3) the cluster is relatively near, so that intrinsically faint members are within reach of observation; (4) the amount of emission nebulosity is small; and (5) the reddening of the cluster is small and uniform.

The color-magnitude diagram of the cluster consists of a normal main sequence extending from O7 to A0, below which the stars fall above the main sequence The reality of this effect has been confirmed by spectroscopic observations. The shape of the color-magnitude diagram thus agrees approximately with that predicted theoretically for an extremely young cluster whose fainter stars are still in the process of contracting gravitationally from the prestellar medium. The age of the cluster given by the point at which the cluster stars depart from the main sequence is about 3×10^6 years.

In addition to luminosity effects, the spectra of the stars which lie above the main sequence show a number of peculiarities. One of the most outstanding is that, later than F8, the rotational velocity of the stars appears to increase, suggesting that these stars have not yet had time to dissipate the original angular momentum of the material from which they have condensed.

NGC 2264 is known to contain about ninety T Tauri stars, of which forty-two were discovered in this investigation. The occurrence of T Tauri stars in the cluster and their location in the color-magnitude diagram indicate that stars of this type are extremely young and are still in the gravitational contraction state. Whether the T Tauri phenomenon represents a necessary stage in the gravitational contraction of all newly formed stars cannot be determined from the present observations.

The luminosity function of the cluster is complete to $M_v = +8$ and appears to have a maximum at $M_v = +6$. Brighter than $M_v = +3$, the observed function agrees with the luminosity function which would be observed in the solar neighborhood had no evolution of stars away from the main sequence taken place.

Supplement No. 24, Volume II

PHOTOMETRIC, POLARIZATION, AND SPECTROGRAPHIC OBSERVATIONS OF O AND B STARS

W. A. Hiltner
Yerkes and McDonald Observatories

This *Supplement* consists primarily of a catalogue of O and B stars for which polarization, color, magnitude, and spectroscopic observations were made principally with the 82-inch reflector of the McDonald Observatory. The stars were selected from the various lists of O and B stars.

The polarization measurements were made with a photoelectric photometer in which Polaroid was used as the analyzer. The observations are given in magnitude for the amount of polarization, and the position angle of the electric vector is given in both equatorial and galactic co-ordinates. The magnitudes and colors are on the U, B, V system (see Johnson 1955). In all cases two or more observations were obtained for each star.

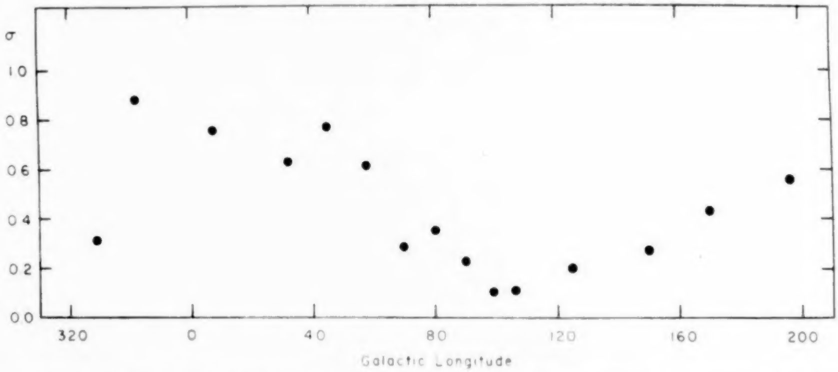

FIG. 1.—The relationship of the standard deviation, σ, of the electric vector alignment and the galactic longitude. Note the minimum at $l = 102°$, which probably represents the longitude at which the spiral arm is observed normal to the axis of the arm.

The spectral classifications are on the two-dimensional MK system. When available, the classifications made by Morgan on Yerkes slit spectrograms were used. Otherwise, slit spectrograms were obtained with the 82-inch reflector. These spectrograms were classified principally by Morgan and the remaining ones by the author. In addition to the direct observational data, the positions in both galactic and equatorial co-ordinates, the interstellar absorption, the distance modulus, and the ratio of polarization to absorption are given. The interstellar absorption was computed on the accepted value of 3.0 for the ratio of total to selective absorption (Hiltner and Johnson 1956).

Diagrams showing the alignment of the electric vector in galactic co-ordinates are given. The variation of alignment with galactic longitude is shown in Figure 1, which is a reproduction of Figure 23 in the *Supplement*. In this figure the standard deviation of the electric vector from the mean value for each longitude interval is plotted against galactic longitude. This figure fully illustrates the presence of a minimum at longitude 102°. This minimum may be interpreted as that longitude at which the line of sight is nearly perpendicular to the axis of the spiral arms. This value is in fair agreement with

110° from O-association data (Morgan, Whitford, and Code 1953) but differs significantly from 135° from H I data (van de Hulst, Muller, and Oort 1954).

Attention has been given to the evaluation of a maximum value for the ratio of interstellar polarization to absorption. From a consideration of the distribution of the individual values of p/A_v, where p is the polarization and A_v is the total visual absorption, the relationship of σ and p/A_v, where σ is the standard deviation of the planes of vibration for a longitude interval, and the relationship of A_v and p/A_v, a value for $p/A_v = 0.060$ is given as the upper limit of the ratio for the Cas-Per region where the observed ratio is highest. This value is about 40 per cent larger than that previously considered.

REFERENCES

Hiltner, W. A., and Johnson, H. L. 1956, *Ap. J.*, **124**, 367.
Hulst, H. C. van de, Muller, C. A., and Oort, J. H. 1954, *B.A.N.*, **12**, 117.
Johnson, H. L. 1955, *Ann. d'ap.*, **18**, 292.
Morgan, W. W., Whitford, A. E., and Code, A. D. 1953, *Ap. J.*, **118**, 318.

THE ASTROPHYSICAL JOURNAL SUPPLEMENT SERIES

These *Supplements* are intended to provide a medium for the publication of extensive investigations, such as wave-length lists of stars of special interest, photometric data, results of numerical integrations pertaining to stellar interiors, model stellar atmosphere calculations, and original memoirs.

Supplement No. 22

"Catalogues of Hα-Emission Stars and Nebulae in the Magellanic Clouds." KARL G. HENIZE

"A Photometric Catalogue of Emission Nebulosities in the Large Magellanic Cloud." LOWELL DOHERTY, KARL G. HENIZE, and LAWRENCE H. ALLER

The first paper contains accurate coordinates, finding charts, qualitative estimates of line and continuum intensity, line sharpness, stellar magnitudes, nebular dimensions and form, for 236 Hα-Emission stars and 532 nebulae in the Magellanic Clouds. The second paper gives absolute surface brightnesses and simplified cross-section profiles in Hα for parts of selected nebulosities in the Large Magellanic Cloud. The position of each of 285 microphotometer tracings is shown on accompanying charts.

Price, $3.00

Supplement No. 23

"Studies of Extremely Young Clusters. I. NGC 2264." MERLE F. WALKER

Photometric and spectroscopic observations of stars in NGC 2264 are presented. The color-magnitude diagram of the cluster suggests that the group has an age of about 3×10^6 years and that the fainter stars in the cluster are still in the process of contracting gravitationally from the pre-stellar medium.

Price, $1.25

Supplement No. 24

"Photometric, Polarization, and Spectrographic Observations of O and B Stars." W. A. HILTNER

A catalogue and discussion of 1259 O and B stars for which photoelectric interstellar polarization observations, photoelectric magnitude and color observations on the U, B, V system, and spectroscopic classifications on the MK system were made at McDonald Observatory.

Price, $3.00

An abstract of each supplement will be published in THE ASTROPHYSICAL JOURNAL. The *Supplements* will appear irregularly and may be purchased separately or by subscription. Each volume of *Supplements* will consist of approximately 500 pages.

Subscriptions

$8.00 per current volume
Canada, $8.75. Foreign, $9.50.
To members of the American Astronomical Society, $6.00 per current volume.

Orders now accepted.

THE UNIVERSITY OF CHICAGO PRESS
5750 ELLIS AVENUE **CHICAGO 37, ILLINOIS**

A NEW account of . .

GENERAL RELATIVITY AND COSMOLOGY

By G. C. McVITTIE, *University of Illinois*. This work is the first published in English in 20 years that presents general relativity in the light of the accumulated data obtained with the 100″ and 200″ telescopes. It also covers the work done in this period on interpretation and elucidation of the meaning of Einstein's theory. The author explores the possibilities of general relativity as a method in mathematical physics and astronomy and as a means of interpreting data supplied by observation. Many of the theoretical formulae are presented in forms suitable for the numerical computation of the parameters they contain, as and when more complete observational data become available. *1956. 198 pages. $9.00.*

GASEOUS NEBULAE

By L. H. ALLER, *University of Michigan*. Correlates and summarizes much of the extensive theoretical material hitherto scattered throughout the world literature. Offers a concise and critical review of astrophysical theory and provides a quantum mechanical treatment of forbidden line radiation that is more complete than in any other book. Analysis of observations made at the Mt. Wilson and Palomar Observatories is featured. *1956. 322 pages. $11.00.*

These volumes are publications in the International Astrophysics Series.

Send for examination copies.

JOHN WILEY & SONS, Inc. · 440 Fourth Ave., New York 16, N.Y.

AVAILABLE NOW

For

Theoretical Physicists
Physical Chemists
Astrophysicists

Tables for the Variational Determination of Atomic Wave Functions

PHILIP M. MORSE *and* HUSEYIN YILMAZ

10 × 12, 86 pp. pamphlet-bound
$2.50

Technology Press
Massachusetts Institute of Technology
CAMBRIDGE 39, MASS.

from Chicago

BOOKS IN PHYSICS

ANALYTICAL EXPERIMENTAL PHYSICS

Second Revised Edition

By Michael Ference, Jr., Harvey B. Lemon, and Reginald J. Stephenson

Significant features of this new edition are use of the meter-kilogram-second, or mks, system of units throughout—but retaining the cgs and British Engineering systems; a gradual increase of calculus during the course of the book; a discussion of modern rockets; an account of the Coriolis force; increased emphasis on the fundamental aspects of wave motion in the sections on light and sound; and up-to-date material in the discussions of quantum, atomic, and nuclear physics, electricity, heat, and thermodynamics. *$8.00*

ELECTRONS (+ and −), PROTONS, PHOTONS, NEUTRONS, MESOTRONS, AND COSMIC RAYS

Second Edition

By Robert A. Millikan

A veritable education in modern atomic progress. A brilliant survey of the advances made in physics in the last half-century. *$9.00*

FROM GALILEO TO THE NUCLEAR AGE

By Harvey Brace Lemon

Text edition, $5.00; Regular edition, $7.00

THE UNIVERSITY OF CHICAGO PRESS

5750 ELLIS AVENUE · CHICAGO 37 · ILLINOIS

BOOKS FROM CHICAGO

THE SOLAR SYSTEM

Edited by Gerard P. Kuiper

Vol. I. *The Sun.* $12.50
Vol. II. *The Earth as a Planet.* $12.50

FOR LATER PUBLICATION:

Vol. III. *Planets and Comets,* Part I: Planets and Satellites.

Vol. IV. *Planets and Comets,* Part II: Minor Planets, Meteorites, Comets, Origin of the Solar System.

The most authoritative and comprehensive treatment of our knowledge of the solar system. A monumental series that will give the solar physicist all he can reasonably expect in the way of an advanced text for many years to come.

THE ATMOSPHERES OF THE EARTH AND PLANETS

Edited by Gerard P. Kuiper $8.50

THE FACE OF THE MOON

By Ralph B. Baldwin $5.00

PRINCIPLES OF METEOROLOGICAL ANALYSIS

By Walter J. Saucier $10.00

THE UNIVERSITY OF CHICAGO PRESS
5750 ELLIS AVENUE CHICAGO 37, ILLINOIS